AERMOD Model Formulation and Evaluation

EPA-454/ R-17-001
May, 2017

AERMOD Model Formulation and Evaluation

U.S. Environmental Protection Agency
Office of Air Quality Planning and Standards
Air Quality Assessment Division
Research Triangle Park, NC

Notice

The original document, AERMOD: Description of Model Formulation, was published in September, 2004, with the EPA document number EPA-454/R-03-004. This version of the document has several revisions, including a new title (AERMOD Model Formulation and Evaluation), the new model formulations added to the model since the original publication in 2004, a model evaluation based on the latest version of the model (version 16216 of AERMOD and AERMET), and minor changes to the formatting and supplemental content to make it appropriate according to current EPA document publication standards.

This report has been reviewed by the Office of Air Quality Planning and Standards, U.S. Environmental Protection Agency, and has been approved for publication. Mention of trade names or commercial products does not constitute endorsement or recommendation for use.

Acknowledgments

This project was made possible through the continued support of Mr. Joe Tikvart, of EPA's Office of Air Quality Planning and Standards (OAQPS), and Mr. Frank Schiermeier, of NOAA's Atmospheric Sciences Modeling Division. The authors are particularly grateful to Dr. Gary Briggs, and Mr. John Irwin, of NOAA's Atmospheric Sciences Modeling Division, for their thorough and constructive review of an earlier version of this document. Finally, we would like to thank the many scientists who participated in peer reviews and beta testing.

This report was compiled primarily by Alan J. Cimorelli, Steven G. Perry, Akula Venkatram, Jeffrey C. Weil, Robert J. Paine, Robert B. Wilson, Russell F. Lee, Warren D. Peters, Roger W. Brode, James O. Paumier, and James Thurman

Table of Contents

Figures

Figure **Page**

Tables

Table **Page**

1. Introduction

1.1 Background

In 1991, the American Meteorological Society (AMS) and the U.S. Environmental Protection Agency (EPA) initiated a formal collaboration with the designed goal of introducing current planetary boundary layer (PBL) concepts into regulatory dispersion models. A working group (**A**MS/**E**PA **R**egulatory **M**odel **I**mprovement **C**ommittee, **AERMIC**) comprised of AMS and EPA scientists was formed for this collaborative effort.

In most air quality applications one is concerned with dispersion in the PBL, the turbulent air layer next to the earth's surface that is controlled by the surface heating and friction and the overlying stratification. The PBL typically ranges from a few hundred meters in depth at night to 1 - 2 km during the day. Major developments in understanding the PBL began in the 1970's through numerical modeling, field observations, and laboratory simulations; see Wyngaard (1988) for a summary. For the convective boundary layer (CBL), a milestone was Deardorff's (1972) numerical simulations which revealed the CBL's vertical structure and important turbulence scales. Major insights into dispersion followed from laboratory experiments, numerical simulations, and field observations (e.g., see Briggs (1988), Lamb (1982) and Weil (1988a) for reviews). For the stable boundary layer (SBL), advancements occurred more slowly. However, a sound theoretical/experimental framework for surface layer dispersion and approaches for elevated sources emerged by the mid 1980's (e.g., see Briggs (1988) and Venkatram (1988)).

During the mid-1980's, researchers began to apply this information to simple dispersion models for applications. This consisted of eddy-diffusion techniques for surface releases, statistical theory and PBL scaling for dispersion parameter estimation, a new probability density function (pdf) approach for the CBL, simple techniques for obtaining meteorological variables (e.g., surface heat flux) needed for turbulence parameterizations, etc. Much of this work was reviewed and promoted in workshops (Weil 1985), revised texts (Pasquill and Smith 1983), and in short courses and monographs (Nieuwstadt and van Dop 1982; Venkatram and Wyngaard 1988). By the mid 1980's, new applied dispersion models based on this technology had been

developed including PPSP (Weil and Brower 1984), OML (Berkowicz et al. 1986), HPDM (Hanna and Paine 1989), TUPOS (Turner et al. 1986), CTDMPLUS (Perry et al. 1989); later, ADMS developed in the United Kingdom (see Carruthers et al. (1992)) was added as well as SCIPUFF (Sykes et al. 1996). AERMIC members were involved in the development of three of these models - PPSP, CTDMPLUS and HPDM.

By the mid-to-late 1980's, a substantial scientific base on the PBL and new dispersion approaches existed for revamping regulatory dispersion models, but this did not occur. In a review of existing or proposed regulatory models developed prior to 1984, Smith (1984) reported that the techniques were many years behind the state-of-the-art and yielded predictions that did not agree well with observations. Similar findings were reported by Hayes and Moore (1986), who summarized 15 model evaluation studies. The need for a comprehensive overhaul of EPA's basic regulatory models was clearly recognized. This need, including a summary of background information and recommendations, was the focus of an AMS/EPA Workshop on Updating Applied Diffusion Models held 24-27 January 1984 in Clearwater, Florida (see Weil (1985) and other review papers in the November 1985 issue of the Journal of Climate and Applied Meteorology.

In February 1991, the U.S. EPA in conjunction with the AMS held a workshop for state and EPA regional meteorologists on the parameterization of PBL turbulence and state-of-the-art dispersion modeling. One of the outcomes of the workshop was the formation of AERMIC. As noted above, the expressed purpose of the AERMIC activity was to build upon the earlier model developments and to provide a state-of-the-art dispersion model for regulatory applications. The early efforts of the AERMIC group are described by Weil (1992). In going through the design process and in considering the nature of present regulatory models, AERMIC's goal expanded from its early form. In addition to improved parameterization of PBL turbulence, other problems such as plume interaction with terrain, surface releases, building downwash and urban dispersion were recognized as needing attention.

The new model developed by AERMIC is aimed at short-range dispersion from stationary industrial sources, the same scenario handled by the EPA Industrial Source Complex Model, ISC3 (U.S. Environmental Protection Agency, 1995). This work clearly has benefitted

from the model development activities of the 1980's especially in the parameterization of mean winds and PBL turbulence, dispersion in the CBL, and the treatment of plume/terrain interactions. Techniques used in the new model for PBL parameterizations and CBL dispersion are similar to those used in earlier models. Turbulence characterization in the CBL adopts "convective scaling" as suggested by Deardorff (1972) as is included in most of the models mentioned above (e.g., PPSP, OML, and HPDM). Algorithms used in these earlier models were considered along with variants and improvements to them. In addition, the developers of OML met with AERMIC to discuss their experiences. Thus, much credit for the AERMIC model development is to be given to the pioneering efforts of the 1980s.

1.2 The AERMIC focus: a replacement for the ISC3 model

AERMIC's initial focus has been on the regulatory models that are designed for estimating near-field impacts from a variety of industrial source types. EPA's regulatory platform for near-field modeling, during the past 25 years has, with few exceptions, remained fundamentally unchanged. During this period, ISC3 was the workhorse regulatory model (used in the construction of most State Implementation Plans, new source permits, risk assessments and exposure analysis for toxic air pollutants) with code structure that is conducive to change. Therefore, AERMIC selected the EPA's ISC3 Model for a major overhaul. AERMIC's objective was to develop a complete replacement for ISC3 by: 1) adopting ISC3's input/output computer architecture; 2) updating, where practical, antiquated ISC3 model algorithms with newly developed or current state-of-the-art modeling techniques; and 3) insuring that the source and atmospheric processes presently modeled by ISC3 will continue to be handled by the AERMIC Model (AERMOD), albeit in an improved manner.

The AERMOD modeling system consists of two pre-processors and the dispersion model. The AERMIC meteorological preprocessor (AERMET) provides AERMOD with the meteorological information it needs to characterize the PBL. The AERMIC terrain pre-processor (AERMAP) both characterizes the terrain, and generates receptor grids for the dispersion model (AERMOD).

AERMET uses meteorological data and surface characteristics to calculate boundary layer parameters (e.g. mixing height, friction velocity, etc.) needed by AERMOD. This data, whether measured off-site or on-site, must be representative of the meteorology in the modeling domain. AERMAP uses gridded terrain data for the modeling area to calculate a representative terrain-influence height associated with each receptor location. The gridded data is supplied to AERMAP in the format of the Digital Elevation Model (DEM) data (USGS 1994). The terrain preprocessor can also be used to compute elevations for both discrete receptors and receptor grids.

In developing AERMOD, AERMIC adopted design criteria to yield a model with desirable regulatory attributes. It was felt that the model should: 1) provide reasonable concentration estimates under a wide variety of conditions with minimal discontinuities; 2) be user friendly and require reasonable input data and computer resources as is the case with the ISC3 model; 3) capture the essential physical processes while remaining fundamentally simple; and, 4) accommodate modifications with ease as the science evolves.

Relative to ISC3, AERMOD currently contains new or improved algorithms for: 1) dispersion in both the convective and stable boundary layers; 2) plume rise and buoyancy; 3) plume penetration into elevated inversions; 4) computation of vertical profiles of wind, turbulence, and temperature; 5) the urban nighttime boundary layer; 6) the treatment of receptors on all types of terrain from the surface up to and above the plume height; 7) the treatment of building wake effects; 8) an improved approach for characterizing the fundamental boundary layer parameters; and 9) the treatment of plume meander.

1.3 Model development process

A seven step model development process, followed by AERMIC, resulted in the promulgation of a regulatory replacement for the ISC3 model, AERMOD. The process followed is as follows: 1) initial model formulation; 2) developmental evaluation; 3) internal peer review and beta testing; 4) revised model formulation; 5) performance evaluation and sensitivity testing; 6) external peer review; and 7) submission to EPA's Office of Air Quality Planning and Standards (OAQPS) for consideration as a regulatory model.

The initial formulations of AERMOD are summarized in Perry et al. (1994) and Cimorelli et al. (1996). Once formulated, the model was tested (developmental evaluation) against a variety of field measurements in order to identify areas needing improvement. The developmental evaluation provided a basis for selecting formulation options.

This developmental evaluation was conducted using five data bases. Three consisted of event-based tracer releases, while the other two each contain up to a full year of continuous SO_2 measurements. These data bases cover elevated and surface releases, complex and simple terrain, and rural and urban boundary layers. A description of the early developmental evaluation is presented in Lee et al. (1995) and in a later report by Lee et al. (1998). Additionally, a comprehensive peer review (U.S. Environmental Protection Agency, 2002) was conducted. Many revisions to the original formulation have resulted from this evaluation and comments received during the peer review, beta testing, and the public forum at EPA's Sixth Conference on Air Quality Modeling (in 1995). Lee et al. (1998) describe the developmental evaluation repeated with the current model (i.e., revisions based on the developmental evaluation and peer review).

In addition, AERMOD underwent a comprehensive performance evaluation (Brode 2002) designed to assess how well AERMOD's concentration estimates compare against a variety of independent data bases and to assess the adequacy of the model for use in regulatory decision making. That is, how well does the model predict concentrations at the high end of the concentration distribution? AERMOD was evaluated against five independent data bases (two in simple terrain and three in complex terrain), each containing one full year of continuous SO_2 measurements. Additionally, AERMOD's performance was compared against the performance of four other applied, regulatory models: ISC3 (U.S. Environmental Protection Agency, 1995), CTDMPLUS (Perry 1992), RTDM (Paine and Egan 1987), and HPDM (Hanna and Paine 1989; Hanna and Chang 1993). The performance of these models against AERMOD has been compared using the procedures in EPA's "Protocol for Determining the Best Performing Model" (U.S. Environmental Protection Agency, 1992).

On 21 April 2000 EPA proposed[1] that AERMOD be adopted as a replacement to ISC3 in appendix A of the Guideline on Air Quality Models (Code of Federal Regulations 1997). As such, upon final action, AERMOD would become EPA's preferred regulatory model for both simple and complex terrain. Furthermore, on 19 May 2000 EPA announced[2] its intention to hold the Seventh Conference on Air Quality Modeling on 28-29 June 2000. The purpose of this conference was to receive comments on the April 2000 proposal. At the Seventh Conference, results of the performance evaluation and peer review were presented and public comments were received. Based on these comments AERMOD was revised to incorporate the PRIME algorithms for building downwash, to remove the dependency on modeling domain in AERMOD's complex terrain formulation, and a variety of other less significant issues. A description of the fully revised model is presented here and in Cimorelli et al. (2004) and Perry et al. (2003). Performance of the final version of AERMOD is documented in Perry et al. (2003) and Brode (2002).

1.4 Purpose of the document

The purpose of this document is to provide a comprehensive, detailed description of the technical formulation of AERMOD and its preprocessors. This document is intended to provide many of the details that are not included in the published journal articles (Cimorelli et al. 2004; Perry et al. 2003).

This document does not include information related to model performance. As mentioned above, a description of the performance of the model that is described in this document can be found in Perry et al. (2003) and Brode (2002).

---

[1]40 CFR Part 51 pages 21506-21546

[2]Federal Register on May 19, 2000 (Volume 65, Number 98)

2. Model overview

This section provides a general overview of the most important features of AERMOD. With the exception of treating pollutant deposition, AERMOD serves as a complete replacement for ISC3. However, it is the intention of AERMIC to incorporate both dry and wet particle and gaseous deposition as well as source or plume depletion. Once this is accomplished this report will be revised to include a description of the deposition formulation. Thus, the AERMOD model described here is applicable to rural and urban areas, flat and complex terrain, surface and elevated releases, and multiple sources (including, point, area and volume sources). Every effort has been made to avoid model formulation discontinuities wherein large changes in calculated concentrations result from small changes in input parameters.

AERMOD is a steady-state plume model. In the stable boundary layer (SBL), it assumes the concentration distribution to be Gaussian in both the vertical and horizontal. In the convective boundary layer (CBL), the horizontal distribution is also assumed to be Gaussian, but the vertical distribution is described with a bi-Gaussian probability density function (pdf). This behavior of the concentration distributions in the CBL was demonstrated by Willis and Deardorff (1981) and Briggs (1993). Additionally, in the CBL, AERMOD treats "plume lofting," whereby a portion of plume mass, released from a buoyant source, rises to and remains near the top of the boundary layer before becoming mixed into the CBL. AERMOD also tracks any plume mass that penetrates into the elevated stable layer, and then allows it to re-enter the boundary layer when and if appropriate. For sources in both the CBL and the SBL AERMOD treats the enhancement of lateral dispersion resulting from plume meander.

Using a relatively simple approach, AERMOD incorporates current concepts about flow and dispersion in complex terrain. Where appropriate the plume is modeled as either impacting and/or following the terrain. This approach has been designed to be physically realistic and simple to implement while avoiding the need to distinguish among simple, intermediate and complex terrain, as required by other regulatory models. As a result, AERMOD removes the need for defining complex terrain regimes. All terrain is handled in a consistent and continuous manner while considering the dividing streamline concept (Snyder et al. 1985) in stably-stratified conditions.

One of the major improvements that AERMOD brings to applied dispersion modeling is its ability to characterize the PBL through both surface and mixed layer scaling. AERMOD constructs vertical profiles of required meteorological variables based on measurements and extrapolations of those measurements using similarity (scaling) relationships. Vertical profiles of wind speed, wind direction, turbulence, temperature, and temperature gradient are estimated using all available meteorological observations. AERMOD is designed to run with a minimum of observed meteorological parameters. As a replacement for the ISC3 model, AERMOD can operate using data of a type that is readily available from National Weather Service (NWS) stations. AERMOD requires only a single surface measurement of wind speed (measured between $7z_o$ and 100m - where z_o is the surface roughness height), wind direction and ambient temperature. Like ISC3, AERMOD also needs observed cloud cover. However, if cloud cover is not available (e.g. from an on-site monitoring program) two vertical measurements of temperature (typically at 2 and 10 meters), and a measurement of solar radiation can be substituted. A full morning upper air sounding (rawinsonde) is required in order to calculate the convective mixing height throughout the day. Surface characteristics (surface roughness, Bowen ratio, and albedo) are also needed in order to construct similarity profiles of the relevant PBL parameters.

Unlike existing regulatory models, AERMOD accounts for the vertical inhomogeneity of the PBL in its dispersion calculations. This is accomplished by "averaging" the parameters of the actual PBL into "effective" parameters of an equivalent homogeneous PBL.

Figure 1 shows the flow and processing of information in AERMOD. The modeling system consists of one main program (AERMOD) and two pre-processors (AERMET and AERMAP). The major purpose of AERMET is to calculate boundary layer parameters for use by AERMOD. The meteorological INTERFACE, internal to AERMOD, uses these parameters to generate profiles of the needed meteorological variables. In addition, AERMET passes all meteorological observations to AERMOD.

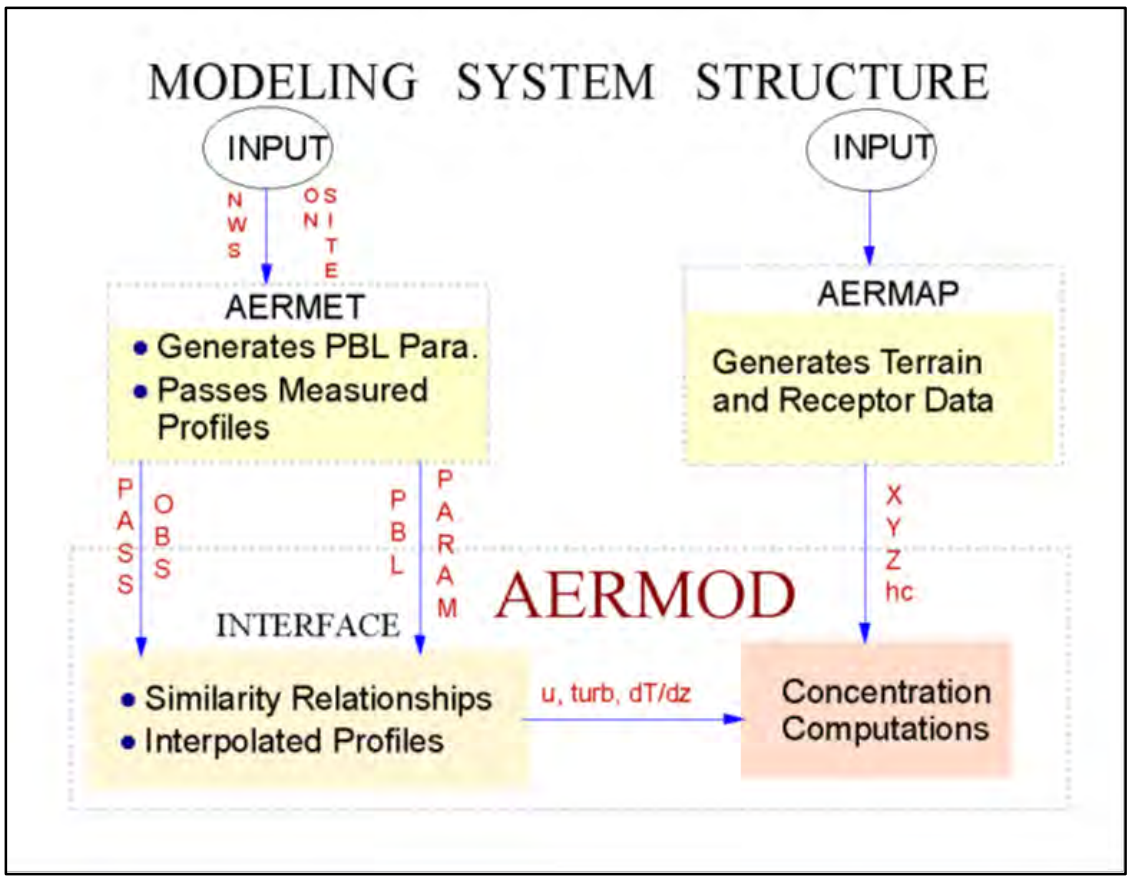

Figure 1. Data flow in the AERMOD modeling system

Surface characteristics in the form of albedo, surface roughness and Bowen ratio, plus standard meteorological observations (wind speed, wind direction, temperature, and cloud cover), are input to AERMET. AERMET then calculates the PBL parameters: friction velocity (u_*), Monin-Obukhov length (L), convective velocity scale (w_*), temperature scale (θ_*), mixing height (z_i), and surface heat flux (H). These parameters are then passed to the INTERFACE (which is within AERMOD) where similarity expressions (in conjunction with measurements) are used to calculate vertical profiles of wind speed (u), lateral and vertical turbulent fluctuations (σ_v, σ_w), potential temperature gradient ($d\theta/dz$), and potential temperature (θ).

The AERMIC terrain pre-processor AERMAP uses gridded terrain data to calculate a representative terrain-influence height (h_c), also referred to as the terrain height scale. The terrain height scale h_c, which is uniquely defined for each receptor location, is used to calculate the dividing streamline height. The gridded data needed by AERMAP is selected from Digital

Elevation Model (DEM) data. AERMAP is also used to create receptor grids. The elevation for each specified receptor is automatically assigned through AERMAP. For each receptor, AERMAP passes the following information to AERMOD: the receptor's location (x_r, y_r), its height above mean sea level (z_r), and the receptor specific terrain height scale (h_c).

A comprehensive description of the basic formulation of the AERMOD dispersion model including the INTERFACE, AERMET, and AERMAP is presented in this document. Included are: 1) a complete description of the AERMET algorithms that provide quantitative hourly PBL parameters; 2) the general form of the concentration equation with adjustments for terrain; 3) plume rise and dispersion algorithms appropriate for both the convective and stable boundary layers; 4) handling of boundary layer inhomogeneity; 5) algorithms for developing vertical profiles of the necessary meteorological parameters; 6) a treatment of the nighttime urban boundary layer; 7) treatment of building downwash (incorporation of PRIME); and 8) enhancement of lateral dispersion due to plume meander. The model described here represents the 02222 versions of AERMOD, AERMET and AERMAP. In addition, all of the symbols used for the many parameters and variables that are referred to in this document are defined, with their appropriate units, in the section titled "List of Symbols."

3. Meteorological preprocessor (AERMET)

The basic purpose of AERMET is to use meteorological measurements, representative of the modeling domain, to compute certain boundary layer parameters used to estimate profiles of wind, turbulence and temperature. These profiles are estimated by the AERMOD interface which is described in Section 0.

While the structure of AERMET is based upon an existing regulatory model preprocessor, the Meteorological Processor for Regulatory Models (MPRM) (Irwin et al. 1988), the actual processing of the meteorological data is similar to that done for the CTDMPLUS (Perry 1992) and HPDM (Hanna and Paine 1989; Hanna and Chang 1993) models. The growth and structure of the atmospheric boundary layer is driven by the fluxes of heat and momentum which in turn depend upon surface effects. The depth of this layer and the dispersion of pollutants within it are influenced on a local scale by surface characteristics such as surface roughness, reflectivity (albedo), and the availability of surface moisture. The surface parameters provided by AERMET are the Monin-Obukhov Length (L), surface friction velocity (u_*), surface roughness length (z_o), surface heat flux (H), and the convective scaling velocity (w_*). AERMET also provides estimates of the convective and mechanical mixed layer heights, z_{ic} and z_{im}, respectively. AERMET defines the stability of the PBL by the sign of H (convective for $H > 0$ and stable for $H < 0$). Although AERMOD is capable of estimating meteorological profiles with data from as little as one measurement height, it will use as much data as the user can provide for defining the vertical structure of the boundary layer. In addition to PBL parameters, AERMET passes all measurements of wind, temperature, and turbulence in a form AERMOD needs.

3.1 Energy balance in the PBL

The fluxes of heat and momentum drive the growth and structure of the PBL. To properly characterize the PBL, one first needs a good estimate of the surface sensible heat flux (H) which depends on the net radiation (R_n) and surface characteristics such as the available surface moisture (described in the form of the Bowen ratio (B_o)). In the CBL, a simple energy balance approach, as in Oke (1978), is used to derive the expression, used in AERMET, to

calculate the sensible heat flux, *H*. We begin with the following simple characterization of the energy balance in the PBL:

$$H + \lambda E + G = R_n \qquad \textbf{(1)}$$

where *H* is the sensible heat flux, λE is the latent heat flux, *G* is the soil heat flux, and R_n is the net radiation. To arrive at an estimate of H simple parameterizations are made for the soil and latent heat flux terms; that is $G=0.1\ R_n$ and $\lambda E = H / B_o$, respectively. Substituting these expressions into eq. **(1)** the expression for surface heat flux becomes

$$H = \frac{0.9\ R_n}{(1 + {}^{1}/_{B_o})}. \qquad \textbf{(2)}$$

3.1.1 Net radiation

If measured values for R_n are not available, the net radiation is estimated from the insolation and the thermal radiation balance at the ground following the method of Holtslag and van Ulden (1983) as

$$\frac{R_n = (1 - r\{\varphi\})\ R + c_1\ T_{ref}^6 - \sigma_{SB}\ T_{ref}^4 - c^2\ n}{1 + c_3}, \qquad \textbf{(3)}$$

where $c_1 = 5.31 \times 10^{-13}$ W m^{-2} K^{-4}, $c_2 = 60$ W m^{-2}, $c_3 = 0.12$, σ_{SB} is the Stefan Boltzman constant (5.67×10^{-8} W m^{-2} K^{-4}), T_{ref} is the ambient air temperature at the reference height for temperature and R_n is the net radiation. The albedo is calculated as

$$\{\varphi\} = r' + (1 - r')\exp(a\varphi + b),$$

where $a = -0.1$, $b = -0.5(1-r')$, and $r' = r\{\varphi\text{-}90°\}$. Note, braces, {}, are used throughout this report to denote the functional form of variables.

Solar radiation, *R*, corrected for cloud cover, is taken from Kasten and Czeplak (1980) as

$$R = R_o\,(1 - 0.75n^{3.4})\,, \qquad \textbf{(4)}$$

where n is the fractional cloud cover and Ro is the clear sky insolation which is calculated as R_o = 990(sin φ) - 30, and $\varphi(=(\varphi\{t_p\}+\varphi\{t\})/2)$ is the solar elevation (tp and t are the previous and present hours, respectively(1975). Note that when observations of cloud cover are unavailable a value of 0.5 is assumed in eq. **(3)** and measurements of solar radiation are required.

3.1.2 Transition between the CBL and SBL

When the PBL transitions from convective to stable conditions the heat flux changes sign from a positive to a negative value. At the point of transition the heat flux must therefore vanish, implying that the net radiation is equal to zero. By setting R_o equal to zero in eq. **(3)**, and solving for sin φ, the critical solar elevation angle, φ_{crit}, corresponding to the transition point between the CBL and the SBL can be determined from

$$\sin(\varphi_{crit}) = \frac{1}{990}\left[\frac{-c_1T^6 + \sigma_{SB}T^4 - c_2n}{(1 - r\{\varphi\})(1 - 0.75n^{3.4})} + 30\right]. \qquad \textbf{(5)}$$

Therefore, AERMET defines the point of transition between the CBL and SBL (day to night) as the point in time when the solar elevation angle $\varphi = \varphi_{crit}$. On average, for clear and partly cloudy conditions, the transition from stable to convective conditions occurs when φ reaches approximately 13°; for overcast conditions φ_{crit} increases to about 23° (Holtslag and van Ulden 1983).

However, if solar radiation measurements are available AERMET determines φ_{crit} from an estimate of cloud cover rather than the actual observations themselves. In eq. **(5)** the cloud cover (n) is replaced with an equivalent cloud cover (n_{eq}) that is calculated from eq. **(4)** such that

$$n_{eq} + \left(1 - \frac{R/Ro}{0.75}\right).$$

3.2 Derived parameters in the CBL

3.2.1 Friction velocity (u_*) & Monin Obukhov length (L) in the CBL

In the CBL, AERMET computes the surface friction velocity, u_*, and the Monin-Obukhov length, L, using the value of H estimated from eq. **(2)**. Since the friction velocity and the Monin Obukhov length depend on each other, an iterative method, similar to that used in CTDMPLUS (Perry 1992), is used. AERMOD initializes u_*, and L by assuming neutral conditions (i.e., L=∞). The final estimate of $u*$ and L is made once convergence is reached through iterative calculations (i.e., there is less than a 1% change between successive iterations). The expression for u_* (e.g., Panofsky and Dutton (1984)) is

$$u_* = \frac{k\, u_{ref}}{\ln(z_{ref}/z_0) - \Psi_m\{z_{ref}/L\} + \Psi_m\{z_0/L\}}, \qquad \textbf{(6)}$$

where k is the von Karman constant (= 0.4), u_{ref} is the wind speed at reference height, z_{ref} is the reference measurement height for wind in the surface layer, and z_o is the roughness length. The stability terms (Ψ_m's) in eq. **(6)** are computed as follows:

$$\Psi_m\left\{\frac{z_{ref}}{L}\right\} = 2\ln\left(\frac{1+\mu}{2}\right) + \ln\left(\frac{1+\mu^2}{2}\right) - 2\tan^{-1}\mu + \pi/2$$

$$\Psi_m\left\{\frac{z_0}{L}\right\} = 2\ln\left(\frac{1+\mu_0}{2}\right) + \ln\left(\frac{1+\mu_0^2}{2}\right) - 2\tan^{-1}\mu_0 + \pi/2 \qquad \textbf{(7)}$$

where $\mu = (1 - 16z_{ref}/L)^{1/4}$ and $\mu_0 = (1 - 16z_0/L)^{1/4}$.

The initial step in the iteration is to solve eq. **(6)** for $u*$ assuming that $\psi_m = 0$ (neutral limit) and setting $u = u_{ref}$. Having an initial estimate of $u*$, L is calculated from the following definition (e.g., see Wyngaard (1988)):

$$L = \frac{\rho\, c_p\, T_{ref} u_*^3}{k\, g\, H} \qquad \textbf{(8)}$$

where g is the acceleration of gravity, c_p is the specific heat of air at constant pressure, ρ is the density of air, and T_{ref} is the ambient temperature representative of the surface layer. Then u_* and L are iteratively recalculated using eqs. **(6)**, **(7)** and **(8)** until the value of L changes by less than 1%.

The reference heights for wind speed and temperature that are used in determining the friction velocity and Monin-Obukhov length are optimally chosen to be representative of the surface layer in which the similarity theory has been formulated and tested with experimental data. Typically, a 10 m height for winds and a temperature within the range of 2 to 10 m is chosen. However, for excessively rough sites (such as urban areas with z_o can be in excess of 1 m), AERMET has a safeguard to accept wind speed reference data that range vertically between $7z_o$ and 100 m. Below 7 z_o (roughly, the height of obstacles or vegetation), measurements are unlikely to be representative of the general area. A similar restriction for temperature measurements is imposed, except that temperature measurements as low as z_o are permitted. Above 100 m, the wind and temperature measurements are likely to be above the surface layer, especially during stable conditions. Therefore, AERMET imposes an upper limit of 100 meters for reference wind speed and temperature measurements for the purpose of computing the similarity theory friction velocity and Monin-Obukhov length each hour. Of course, other US EPA guidance for acceptable meteorological siting should be consulted in addition to keeping the AERMET restrictions in mind.

3.2.2 Convective velocity scale (w_*)

AERMOD utilizes the convective velocity scale to characterize the convective portion of the turbulence in the CBL. Field observations, laboratory experiments, and numerical modeling studies show that the large turbulent eddies in the CBL have velocities proportional to the convective velocity scale (w_*) (Wyngaard 1988). Thus in order to estimate turbulence in the CBL, an estimate of w_* is needed. AERMET calculates the convective velocity scale from its definition as:

$$w_* = \left(\frac{g\ H\ z_{ic}}{\rho\ c_p\ T_{ref}} \right)^{1/3}, \qquad \textbf{(9)}$$

where z_{ic} is the convective mixing height (see Section 0).

3.3 Derived parameters in the SBL

In this section the parameters used to characterize the SBL are discussed along with their estimation methods. During stable conditions the energy budget term associated with the ground heating component is highly site-specific. During the day, this component is only about 10% of the total net radiation, while at night its value is comparable to that of the net radiation (Oke 1978). Therefore, errors in the ground heating term can generally be tolerated during the daytime, but not at night. To avoid using a nocturnal energy balance approach that relies upon an accurate estimate of ground heating, AERMIC has adopted a much simpler semi-empirical approach for computing u_* and L.

3.3.1 Friction velocity (u_*) in the SBL

The computation of u_* depends on the empirical observation that the temperature scale, θ_* defined as

$$\theta_* = -H/\rho\ c_p\ u_*\ , \qquad \textbf{(10)}$$

varies little during the night. Following the logic of Venkatram (1980) we combine the definition of L eq. **(8)** with eq. **(10)** to express the Monin-Obukhov length in the SBL as

$$L = \frac{T_{ref}}{k\ g\ \theta_*}\ u_*^2 \qquad \textbf{(11)}$$

.

From (Panofsky and Dutton 1984) the wind speed profile in stable conditions takes the form

$$u = \frac{u_*}{k}\left[\ln\left(\frac{z}{z_0}\right) + \frac{\beta_m z_{ref}}{L}\right], \qquad \textbf{(12)}$$

where $\beta_m = 5$ and z_{ref} is the wind speed reference measurement height. Substituting eq. **(11)** into eq. **(12)** and defining the drag coefficient, C_D, as $k / ln(z_{ref}/z_0)$ (Garratt 1992), results in

$$\frac{u}{u_*} = \frac{1}{C_D} + \frac{\beta\, z_{ref}\, g\, \theta_*}{T_{ref}\, u_*^2}. \qquad \textbf{(13)}$$

Multiplying eq. **(13)** by $C_D\, u_*^2$ and rearranging yields a quadratic of the form

$$u_*^2 - C_D u\, u_* + C_D u_0^2 = 0 \qquad \textbf{(14)}$$

where $u_0^2 = \beta_m\, z_{ref}\, g\, \theta_* / Tref$. As is used in HPDM (Hanna and Chang 1993) and CTDMPLUS (Perry 1992) this quadratic has a solution of the form

$$u_* = \frac{C_D\, u_{ref}}{2}\left[-1 + \left(1 + \left(\frac{2\, u_0}{C_D^{\frac{1}{2}}\, u_{ref}}\right)^2\right)^{1/2}\right] \qquad \textbf{(15)}$$

Equation **(15)** produces real-valued solutions only when the wind speed is greater than or equal to the critical value $u_{cr} = \left[4\, \beta_m\, z_{ref}\, g\, \theta_* / T_{ref} C_D\right]^{1/2}$. For the wind speed less than the critical value, u* and θ_* are parameterized using the following linear expression:

$$u_* = u_*\{u = u_{cr}\}\left(\frac{u}{u_{cr}}\right) \qquad for\ u < u_{cr}$$

$$\theta_* = \theta_*\left(\frac{u}{u_{cr}}\right) \qquad for\ u < u_{cr}$$

These expressions approximate the u_* verses θ_* dependence found by van Ulden and Holtslag (1983).

In order to calculate u_* from eq. **(15)** an estimate of $\theta_*$is needed. If representative cloud cover observations are available, the temperature scale in the SBL is taken from the empirical form of van Ulden and Holtslag (1985) as

$$\theta_* = 0.09\,(1 - 0.5\,n^2)\,, \qquad \textbf{(16)}$$

where n is the fractional cloud cover. However, if cloud cover measurements are not available, AERMET can estimate θ_* from measurements of temperature at two levels and wind speed at one level. This technique, known as the Bulk Richardson approach, starts with the similarity expression for potential temperature (Panofsky and Dutton 1984), that is,

$$\theta\{z\} - \theta_0 = \frac{\theta_*}{k}\left(ln\frac{z}{z_0} + \beta_m\frac{z}{L}\right), \qquad \textbf{(17)}$$

where $\beta_m \approx 5$ and k (= 0.4) is the von Karman constant. Applying eq. **(17)** to the two levels of temperature measurements and rearranging terms yields

$$\theta_* = \frac{k(\theta_2 - \theta_{1)}}{\left[\left(ln\frac{z_2}{z_1}\right) + \beta_m\frac{(z_2 - z_1)}{L}\right]}. \qquad \textbf{(18)}$$

Since both $u*$ (eq.**(12)**) and $\theta*$ (eq. **(18)**) depend on L, and L (eq. **(11)**) in turn depends on $u*$ and $\theta*$, an iterative approach is needed to estimate $u*$. First $u*$ and $\theta*$ are found by assuming an initial value for L and iterating among the expressions for $u*$, $\theta*$ (eq. **(18)**) and L (eq. **(11)**) until convergence is reached. The expression used for $u*$, in the iteration, is taken from (Holtslag 1984) and depends on atmospheric stability. For situations in which $z/L < 0.5$ is estimated using eq. **(12)**, otherwise (for more stable cases) $u*$ is calculated as follows:

$$u_* = \frac{ku}{\left[\ln\frac{z}{z_o} + 7\ln\frac{z}{L} + \frac{4.25}{(z/L)} - \frac{0.5}{(z/L)^2} + \frac{\beta_m}{2} - 1.648\right]}. \qquad \textbf{(19)}$$

3.3.2 Sensible heat flux (H) in the SBL

Having computed u_* and θ_* for stable conditions, AERMET calculates the surface heat flux from eq. **(10)** as

$$H = \rho\, c_p u_* \theta_* \,. \qquad \textbf{(20)}$$

AERMET limits the amount of heat that can be lost by the underlying surface to 64 W m^{-2}. This value is based on a restriction that Hanna (1986) placed on the product of θ_* and u_*. That is, for typical conditions Hanna found that

$$[\theta_* u_*]_{max} = 0.05 ms^{-1}\, K \,. \qquad \textbf{(21)}$$

When the heat flux, calculated from eq. **(20)**, is such that $\theta_*\, u_* > 0.05$ m s^{-1} K, AERMET recalculates u_* by substituting $0.05/u_*$ into eq. **(15)** for θ_* (u_o in eq. **(15)** is a function of θ_*).

3.3.3 Monin-Obukhov length (L) in the SBL

Using the sensible heat flux of eq. **(20)** and u_* from eq. **(15)**, the Monin-Obukhov Length, for the SBL is calculated from eq. **(8)**.

3.4 Mixing height

The mixing height (z_i) in the CBL depends on both mechanical and convective processes and is assumed to be the larger of a mechanical mixing height (z_{im}) and a convective mixing height (z_{ic}). Whereas, in the SBL, the mixing height results exclusively from mechanical (or shear induced) turbulence and therefore is identically equal to z_{im}. The same expression for calculating z_{im} is used in both the CBL and the SBL. The following two sections describe the procedures used to estimate z_{ic} and z_{im}, respectively.

3.4.1 Convective mixing height (z_{ic})

The height of the CBL is needed to estimate the profiles of important PBL variables and to calculate pollutant concentrations. If measurements of the convective boundary layer height are available they are selected and used by the model. If measurements are not available, z_{ic} is calculated with a simple one-dimensional energy balance model (Carson 1973) as modified by Weil and Brower (1983). This model uses the early morning potential temperature sounding (prior to sunrise), and the time varying surface heat flux to calculate the time evolution of the convective boundary layer as

$$z_{ic}\theta\{z_{ic}\} - \int_0^{z_{ic}} \theta\{z\}dz = (1+2A)\int_0^t \frac{H\{t'\}}{\rho\, c_p}dt, \qquad \textbf{(22)}$$

where θ is the potential temperature, A is set equal to 0.2 from Deardorff (1980), and t is the hour after sunrise. Weil and Brower found good agreement between predictions and observations of z_{ic}, using this approach.

3.4.2 Mechanical mixing height (z_{im})

In the early morning when the convective mixed layer is small, the full depth of the PBL may be controlled by mechanical turbulence. AERMET estimates the heights of the PBL during convective conditions as the maximum of the estimated (or measured if available) convective boundary layer height (z_{ic}) and the estimated (or measured) mechanical mixing height. AERMET uses this procedure to insure that in the early morning, when z_{ic} is very small but considerable mechanical mixing may exist, the height of the PBL is not underestimated. When measurements of the mechanical mixed layer are not available, z_{im} is calculated by assuming that it approaches the equilibrium height given by Zilitinkevich (1972) as

$$z_{ie} = 0.4\left({u_* L}/{f}\right), \qquad \textbf{(23)}$$

where z_{ie} is the equilibrium mechanical mixing height and f is the Coriolis parameter.

Venkatram (1980) has shown that, in mid-latitudes, eq. **(23)** can be empirically represented as

$$z_{ie} = 2300\, u_*^{3/2}, \qquad \textbf{(24)}$$

where z_{ie} (calculated from eq. **(24)**) is the unsmoothed mechanical mixed layer height. When measurements of the mechanical mixed layer height are available they are used in lieu of z_{ie}.

To avoid estimating sudden and unrealistic drops in the depth of the shear-induced, turbulent layer, the time evolution of the mechanical mixed layer height (whether measured or estimated) is computed by relaxing the solution toward the equilibrium value appropriate for the current hour. Following the approach of Venkatram (1982)

$$\frac{dz_{im}}{dt} = \frac{(z_{ie} - z_{im})}{\tau}. \qquad \textbf{(25)}$$

The time scale, τ , governs the rate of change in height of the layer and is taken to be proportional to the ratio of the turbulent mixed layer depth and the surface friction velocity (i.e. $\tau = z_{im} / \beta_\tau\, u_*$). AERMOD uses a constant β_τ value of 2. For example, if u_* is of order 0.2 m s^{-1}, and z_{im} is of order 500 m, the time scale is of the order of 1250 s which is related to the time it takes for the mechanical mixed layer height to approach its equilibrium value. Notice that when $z_{im} < z_{ie}$, the mechanical mixed layer height increases to approach its current equilibrium value; conversely, when $z_{im} > z_{ie}$, the mechanical mixed layer height decreases towards its equilibrium value.

Because the friction velocity changes with time, the current smoothed value of $z_{im}\{t+\Delta t\}$ is obtained by numerically integrating eq. **(25)** such that

$$z_{im}\{t + \Delta t\} = z_{im}\{t\}\left(e^{-\Delta t/\tau}\right) + z_{ie}\{t + \Delta t\}\left[1 - \left(e^{-\Delta t/\tau}\right)\right] . \qquad \textbf{(26)}$$

where $z_{im}\{t\}$ is the previous hour's smoothed value. For computing the time scale in eq. **(26)**, z_{im} is taken from the previous hour's estimate and u$_*$ from the current hour. In this way, the time

scale (and thus relaxation time) will be short if the equilibrium mixing height grows rapidly but will be long if it decreases rapidly.

Although eqs. **(24)** and **(26)** are designed for application in the SBL, they are used in the CBL to ensure a proper estimate of the PBL height during the short transitional period at the beginning of the day when mechanical turbulence generally dominates. The procedure, used by AERMET, guarantees the use of the convective mixing height once adequate convection has been established even though the mechanical mixing height is calculated during all convective conditions. Since AERMET uses eq. **(26)** to estimate the height of the mixed layer in the SBL, discontinuities in z_i from night to day are avoided.

In AERMOD, the mixing height z_i, has an expanded role in comparison to how it is used in ISC3. In AERMOD the mixing height is used as an elevated reflecting/penetrating surface, an important scaling height, and enters in the w_* determination found in eq. **(9)**. The mixing height z_i for the convective and stable boundary layers is therefore defined as follows:

$$\begin{aligned} z_i &= MAX\left[z_{ic};\ z_{im}\right] \qquad for\ \ L<0\ \ (CBL) \\ z_i &= z_{im} \qquad\qquad\qquad\quad for\ \ L<0\ \ (SBL) \end{aligned} \tag{27}$$

Since algorithms used for profiling differ in the SBL and CBL, the stability of the PBL must be determined. For this purpose the sign of L is used by AERMET; if $L < 0$ then the PBL is considered to be convective (CBL) otherwise it is stable (SBL).

3.5 Adjustment for the low wind speed/stable conditions in AERMET

An option has been incorporated in AERMET to address issues associated with model overpredictions under low-wind/stable conditions. The ADJ_U* option is available in AERMET by specifying ADJ_U* on the METHOD STABLEBL keyword in the Stage 3 AERMET input file.

The ADJ_U* option can be specified with or without the Bulk Richardson Number option in AERMET, which utilizes delta-T measurements. The Bulk Richardson Number option in AERMET is selected by specifying BULKRN on a separate METHOD STABLEBL keyword in the Stage 3 AERMET input file. The formulation for the ADJ_U* option without the BULKRN option is based on Equation 26 of Qian and Venkatram (2011). The formulation for the ADJ_U* option with the BULKRN option is based on Equations 22, 23, and 25 of Luhar and Rayner (2009), with a critical value of z/L of 0.7.

4. Vertical structure of the PBL - AERMOD'S meteorological interface

The AERMOD interface, a set of routines within AERMOD, uses similarity relationships with the boundary layer parameters, the measured meteorological data, and other site-specific information provided by AERMET to compute vertical profiles of: 1) wind direction, 2) wind speed, 3) temperature, 4) vertical potential temperature gradient, 5) vertical turbulence (σ_w) and 6) lateral turbulence (σ_v).

For any one of these six variables (or parameters), the interface (in constructing the profile) compares each height at which a meteorological variable must be calculated with the heights at which observations were made and if it is below the lowest measurement or above the highest measurement (or in some cases data is available at only one height), the interface computes an appropriate value from selected PBL similarity profiling relationships. If data are available both above and below a given height, an interpolation is performed which is based on both the measured data and the shape of the computed profile (see Section 0). Thus the approach used for profiling, simultaneously takes advantage of the information contained in both the measurements and similarity parameterizations. As will be discussed, at least one level of measured wind speed, wind direction, and temperature is required. However, turbulence profiles can be parameterized without any direct turbulence measurements.

The following sections provide a comprehensive description of AERMOD's profiling equations and how these estimated profiles are used to extract pertinent layer-averaged meteorology for AERMOD's transport and dispersion calculations. Also, example profiles (one typical of the CBL and one typical of the SBL) for the various parameters have been constructed for illustration. The CBL case assumes that z_i = 1000 m, L = -10 m and z_o = 0.1 m (i.e., $z_o = 0.0001 z_i$ and $L = -0.01 z_i$). The SBL case assumes that z_i = 100 m, L = 10 m and z_o = 0.1 m (i.e., $z_o = 0.001\ z_i$ and $L = 0.1\ z_i$).

4.1 General profiling equations

4.1.1 Wind speed profiling

The AERMOD profile equation for wind speed, has the familiar logarithmic form:

$$
\begin{aligned}
u &= u\{7z_o\}\left[\frac{z}{7z_o}\right] && \text{for} \quad z < 7z_o \\
u &= \frac{u_*}{k}\left[\ln\left(\frac{z}{z_o}\right) - \Psi_m\left\{\frac{z}{L}\right\} + \Psi_m\left\{\frac{z_o}{L}\right\}\right] && \text{for} \quad 7z_o \le z \le z_i \\
u &= u\{z_i\} && \text{for} \quad z > z_i
\end{aligned}
\qquad \textbf{(28)}
$$

At least one wind speed measurement, that is representative of the surface layer, is required for each simulation with AERMOD. Since the logarithmic form does not adequately describe the profile below the height of obstacles or vegetation, eq. **(28)** allows for a linear decrease in wind speed from its value at $7z_o$.

For the CBL, the Ψ_m*'s* are evaluated using eq. **(7)** with z_{ref} replaced by z, and during stable conditions they are calculated from van Ulden & Holtslag (1985) as

$$
\begin{aligned}
\Psi_m\left\{\frac{z}{L}\right\} &= -17\left[1 - \exp\left(-0.29\frac{z}{L}\right)\right] \\
\Psi_m\left\{\frac{z_o}{L}\right\} &= -17\left[1 - \exp\left(-0.29\frac{z_o}{L}\right)\right].
\end{aligned}
\qquad \textbf{(29)}
$$

For small z/L ($<<1$) and with a series expansion of the exponential term, the first equation in (29) reduces to the form given in eq. **(12)**, i.e., $\psi_m = \beta_m\, z/L$ with $\beta_m = 5$. However, for large z/L (>1) and heights as great as 200 m in the SBL, the ψ_m given by eq. **(29)** is found to fit wind observations much better than the ψ_m given by eq. **(12)** (van Ulden and Holtslag 1985). Using the example case parameter values Figure 2 and Figure 3 were constructed to illustrate the form of the wind profiles used by AERMOD in the layers above and below $7z_o$.

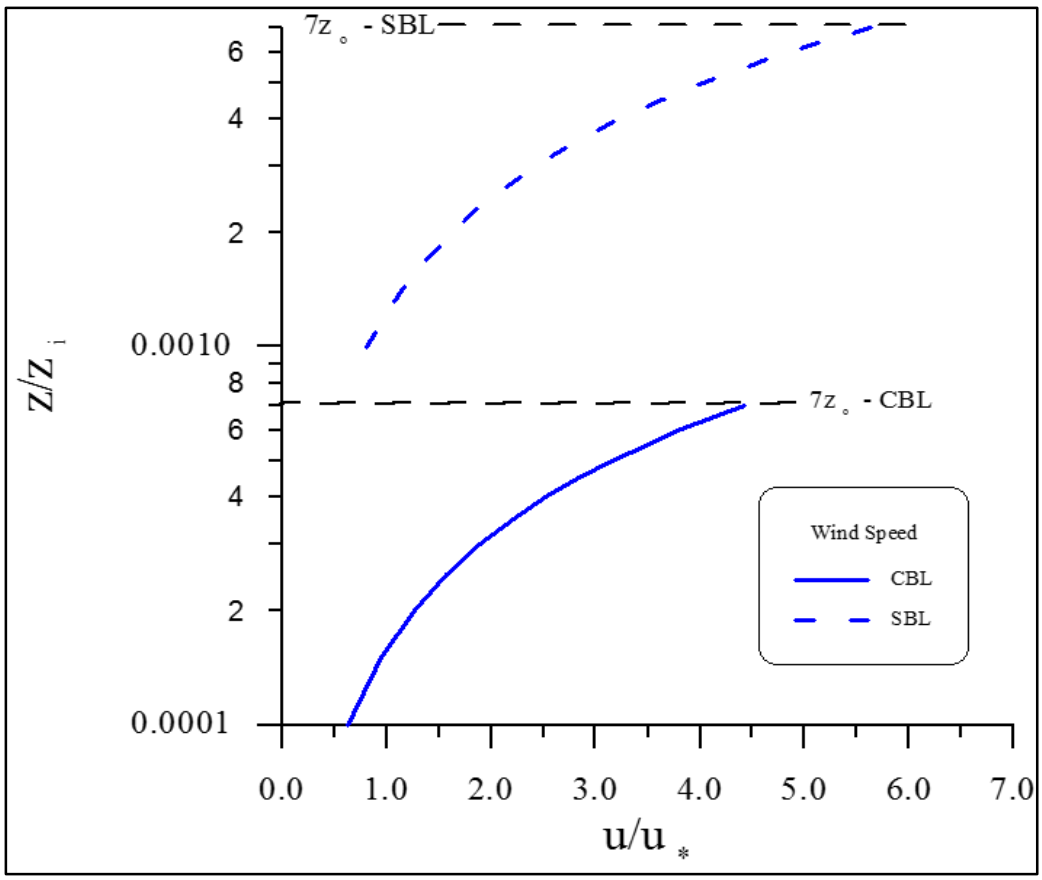

Figure 2. Wind speed profile, for both the CBL and SBL, in the region below 7z0

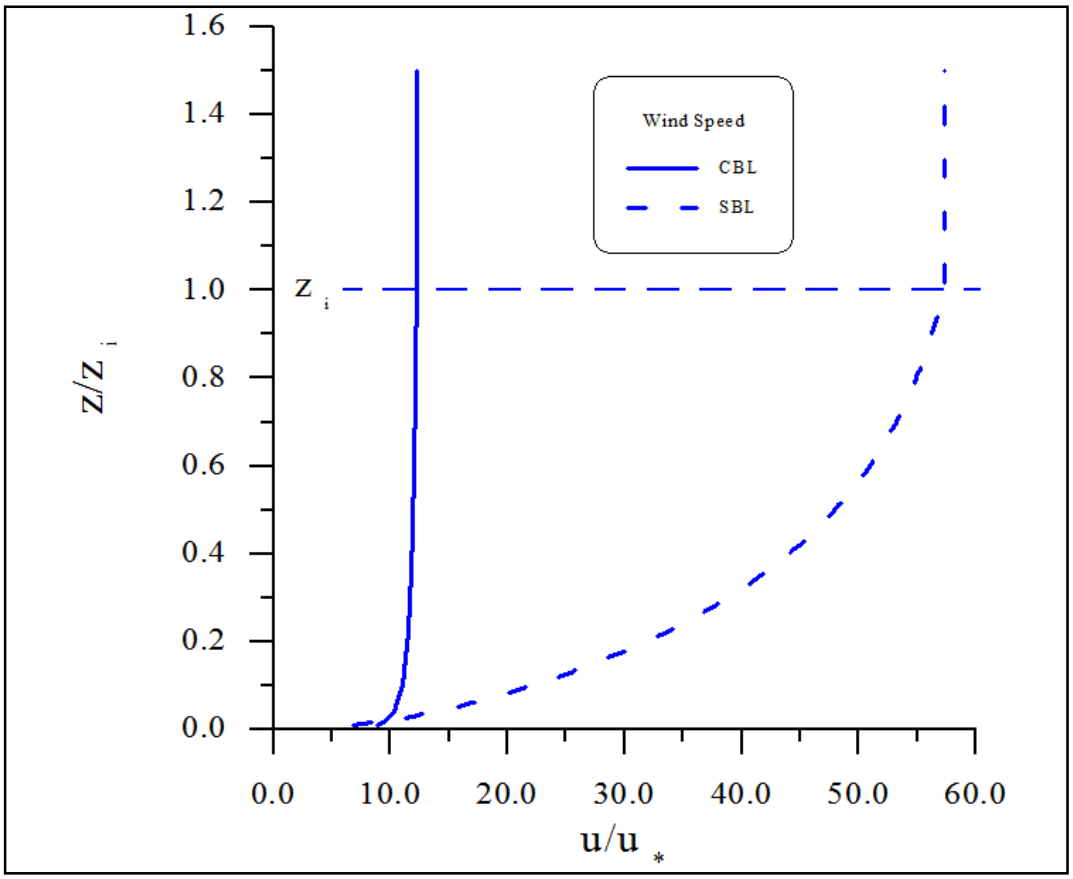

Figure 3. Wind speed profiling, for both the CBL and SBL, in the region above 7z0

4.1.2 Wind direction profiles

For both the CBL & SBL wind direction is assumed to be constant with height both above the highest and below the lowest measurements. For intermediate heights, AERMOD linearly interpolates between measurements. At least one wind direction measurement is required for each AERMOD simulation.

4.1.3 Profiles of the potential temperature gradient

Above the relatively shallow superadiabatic surface layer, the potential temperature gradient in the well mixed CBL is taken to be zero. The gradient in the stable interfacial layer just above the mixed layer is taken from the morning temperature sounding. This gradient is an important factor in determining the potential for buoyant plume penetration into and above that

layer. Above the interfacial layer, the gradient is typically constant and slightly stable. Although the interfacial layer depth varies with time, for the purposes of determining the strength of the stable stratification aloft, AERMET uses a fixed layer of 500 m to insure that a sufficient layer of the morning sounding is sampled. A 500 m layer is also used by the CTDMPLUS model (Perry 1992) for this same calculation. This avoids strong gradients (unrealistic kinks) often present in these data. For a typical mixed layer depth of 1000 m an interfacial layer depth of 500 m is consistent with that indicated by Deardorff (1979). A constant value of 0.005 K m^{-1} above the interfacial layer is used as suggested by Hanna and Chang (1991). Using the morning sounding to compute the interfacial temperature gradient assumes that as the mixed layer grows throughout the day, the temperature profile in the layer above z_i changes little from that of the morning sounding. Of course, this assumes that there is neither significant subsidence nor cold or warm air advection occurring in that layer. Field measurements (e.g. Clarke et al. (1971)) of observed profiles throughout the day lend support to this approach. These data point out the relative invariance of upper level temperature profiles even during periods of intense surface heating.

Below 100 m, in the SBL, AERMOD uses the definition of the potential temperature gradient suggested by Dyer (1974) as well as Panofsky and Dutton (1984). That is,

$$\begin{aligned} \frac{\partial\theta}{\partial z} &= \frac{\theta_*}{k(2)}\left[1+5\frac{(2)}{L}\right] \qquad for \;\; z \le 2m \\ \frac{\partial\theta}{\partial z} &= \frac{\theta_*}{k\,z}\left[1+5\frac{z}{L}\right] \qquad for \;\; 2m < z \le 100m. \end{aligned} \tag{30}$$

Eq. **(30)** is similar to that of Businger et al. (1971). Above 100 m the form of the potential temperature gradient, taken from Stull (1983) and van Ulden & Holtslag (1985) is

$$\frac{\partial\theta}{\partial z} = \frac{\partial\theta\{z_{mx}\}}{\partial z}\exp\left[-\frac{(z-z_{mx})}{0.44z_{i\theta}}\right] \tag{31}$$

where z_{mx} = 100 m, $z_{i\theta}$ = max[z_{im}; *100m*], and the constant 0.44 within the exponential term of eq. **(31)** is inferred from typical profiles taken during the Wangara experiment (Andre and Mahrt 1982). For all z, $\partial\theta/\partial z$ is limited to a minimum of 0.002 K m^{-1} (Paine and Kendall 1993).

In the SBL if $d\theta/dz$ measurements are available below100 m and above z_o, then θ_* is calculated from eq. **(30)** using the value of $\partial\theta/\partial z$ at the lowest measurement level and z_{Tref} replaced by the height of the $\partial\theta/\partial z$ measurements. The upper limit of 100 m for the vertical temperature gradient measurements is consistent with that imposed by AERMET for wind speed and temperature reference data used to determine similarity theory parameters such as the friction velocity and the Monin-Obukhov length. Similarly, the lower limit of z_o for the vertical temperature gradient measurements is consistent with that imposed for reference temperature data. If no measurements of $\partial\theta/\partial z$ are available, in that height range, then θ_* is calculated by combining eqs. **(8)** and **(20)**. θ_* is not used in the CBL.

Figure 4 shows the inverse height dependency of $\partial\theta/\partial z$ in the SBL. To create this curve we assumed that: Z_{im}=100 m; and therefore, $Z_{i\,\theta}$ = 100 m; L = 10 m; u_* = .124, which is consistent with a mixing height of 100 m; T_{ref} = 293 K; and therefore based on eq. **(11)** θ_* = 0.115 K. These parameter values were chosen to represent a strongly stable boundary layer. Below 2 m $\partial\theta/\partial z$ is persisted downward from its value of 0.228 K m^{-1} at 2m. Above 100 m $\partial\theta/\partial z$ is allowed to decay exponentially with height.

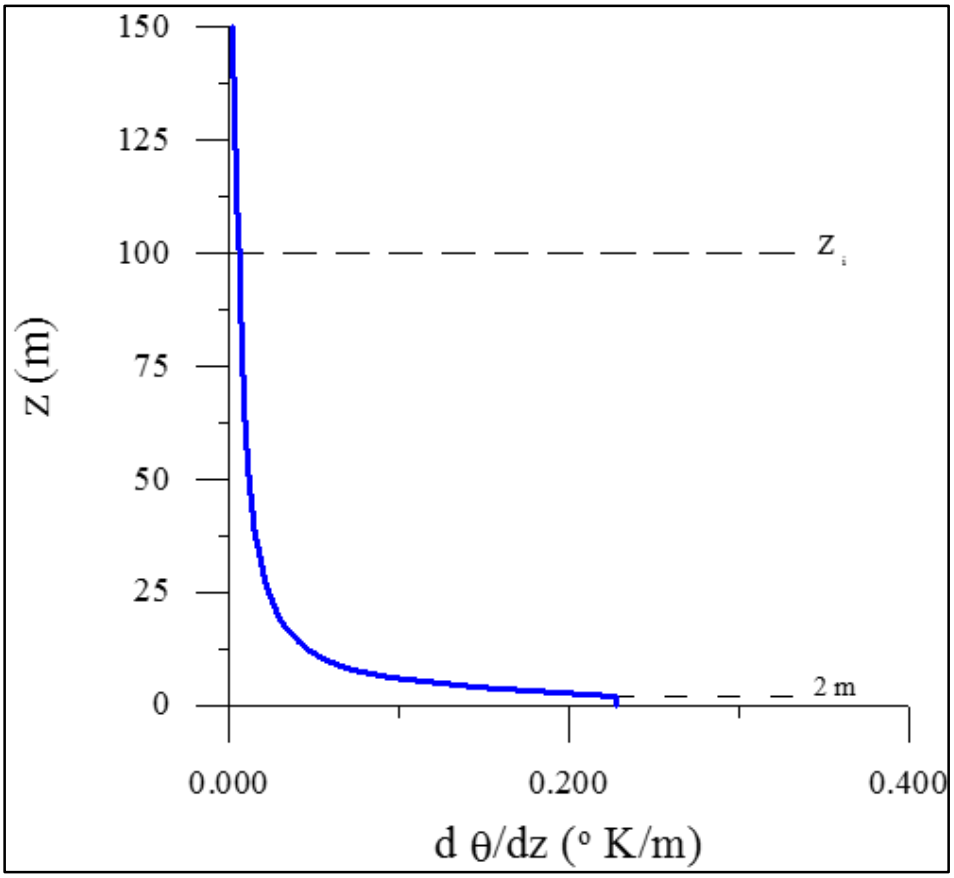

Figure 4. Profile of potential temperature gradient for the SBL

4.1.4 Potential temperature profiling

For use in plume rise calculations, AERMOD develops the vertical profile of potential temperature from its estimate of the temperature gradient profile. First, the model computes the potential temperature at the reference height for temperature (i.e., z_{Tref}) as

$$\theta\{z_{Tref}\} = T_{ref} + \frac{g\, z_{msl}}{c_P}, \qquad \textbf{(32)}$$

where $z_{msl} = z_{ref} + z_{base}$ is the user specified elevation for the base of the temperature profile (i.e., meteorological tower). Then for both the CBL and SBL the potential temperature is calculated as follows:

$$\theta\{z+\Delta z\} = \theta\{z\} + \left.\frac{\partial\theta}{\partial z}\right|_{\bar{z}} \Delta z \qquad \textbf{(33)}$$

where $\overline{\partial\theta}/_{\partial z}$ is the average potential temperature gradient over the layer Δz. Note that for $z < z_{Tref}$, Δz is negative.

4.1.5 Vertical turbulence calculated

In the CBL, the vertical velocity variance or turbulence (σ_{wT}^2) is profiled using an expression based on a mechanical or neutral stability limit ($\sigma_{wm} \propto u_*$) and a strongly convective limit ($\sigma_{wc} \propto w_*$). The total vertical turbulence is given as:

$$\theta\{z+\Delta z\} = \theta\{z\} + \left.\frac{\partial\theta}{\partial z}\right|_{\bar{z}} \Delta z \qquad \textbf{(34)}$$

This form is similar to one introduced by Panofsky et al. (1977) and included in other dispersion models (e.g., Berkowicz et al. (1986), Hanna and Paine (1989), and Weil (1988a)).

The convective portion (σ^2_{wc}) of the total variance is calculated as:

$$\begin{aligned}
\sigma_{wc}^2 &= 1.6\left(\frac{z}{z_{ic}}\right)^{2/3} \cdot w_*^2 && for\ \ z \le 0.1 z_{ic} \\
\sigma_{wc}^2 &= 0.35 w_*^2 && for\ \ 0.1 z_{ic} < z \le z_{ic} \qquad \textbf{(35)} \\
\sigma_{wc}^2 &= 0.35 w_*^2 \exp\left[-\frac{6\left(z - z_{ic}\right)}{z_{ic}}\right] && for\ \ z > z_{ic}
\end{aligned}$$

where the expression for $z \le 0.1\ z_{ic}$ is the free convection limit (Panofsky et al. 1977), for $0.1 z_i < z \le z_{ic}$ is the mixed-layer value (Hicks 1985), and for $z > z_{ic}$ is a parameterization to connect the mixed layer σ^2_{wc} to the assumed near-zero value well above the CBL. An example profile of convective vertical turbulence described in eq. **(35)** is presented in Figure 5.

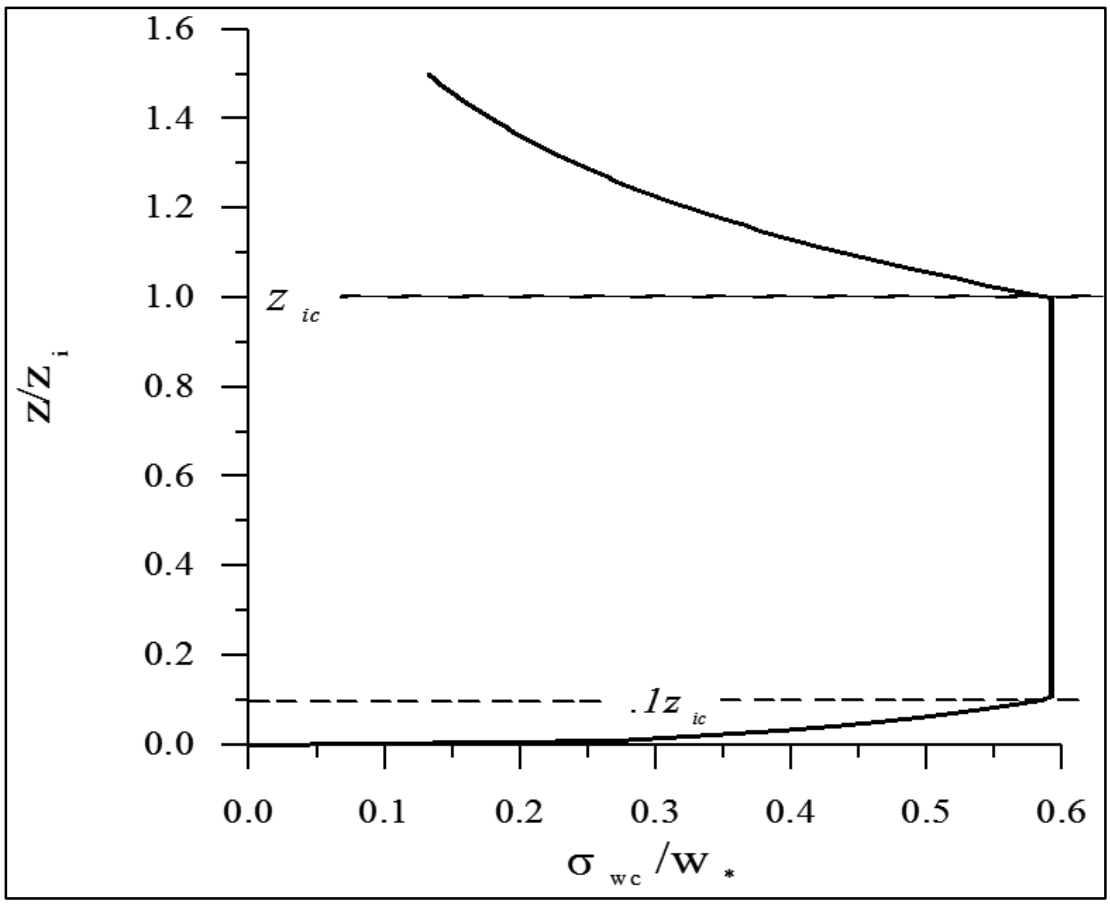

Figure 5. Convective portion of the vertical turbulence in the CBL

The mechanical turbulence (σ_{wm}) is assumed to consist of a contribution from the boundary layer (σ_{wml}) and from a "residual layer" (σ_{wmr}) above the boundary layer ($z > z_i$) such that,

$$\sigma_{wm}^2 = \sigma_{wml}^2 + \sigma_{wmr}^2 . \qquad \textbf{(36)}$$

This is done to satisfy the assumed decoupling between the turbulence aloft ($z > z_i$) and that at the surface in the CBL shear layer, and to maintain a continuous variation of σ^2_{wm} with z near $z = z_i$. The expression for σ_{wml} following the form of Brost et al. (1982) is

$$\sigma_{wml} = 1.3u_* \left(1 - \frac{z}{z_i}\right)^{1/2} \qquad for \;\; z < z_i \tag{37}$$

$$\sigma_{wml} = 0.0 \qquad for \;\; z \geq z_i$$

where the $\sigma_{wml} = 1.3u_*$ at $z = 0$ is consistent with Panofsky et al. (1977).

Above the mixing height σ_{wmr} is set equal to the average of measured values in the residual layer above z_i. If measurements are not available, then σ_{wmr} is taken as the default value of 0.02 $u\{z_i\}$. The constant 0.02 is an assumed turbulence intensity i_z ($= \sigma_{wm} / u$) for the very stable conditions presumed to exist above z_i (Briggs 1973). Within the mixed layer the residual turbulence (σ_{wmr}) is reduced linearly from its value at z_i to zero at the surface. Figure 6 presents the profile of the mechanical portion of the vertical turbulence in the CBL. The effect of combining the residual and boundary layer mechanical turbulence (eq. **(36)**) can be seen in this figure.

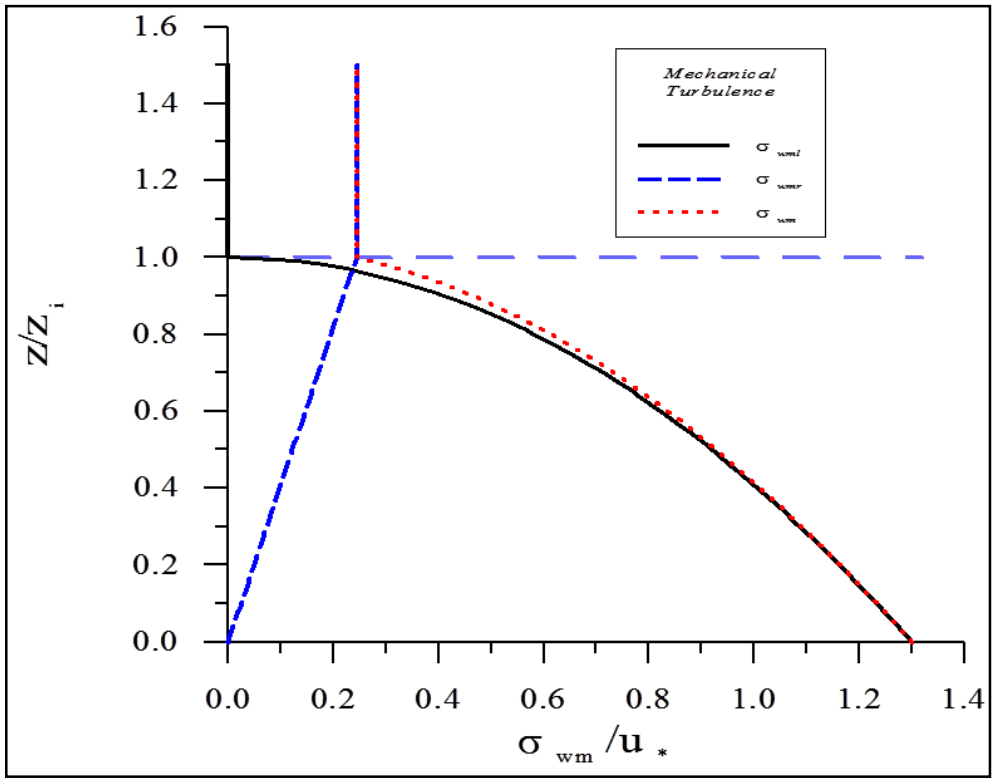

Figure 6. Mechanical portion of the vertical turbulence in the CBL

In the SBL the vertical turbulence contains only a mechanical portion which is given by eq. **(36)**. The use of the same σ^2_{wm} expressions for the SBL and CBL is done to ensure continuity of turbulence in the limit of neutral stability. Figure 7 illustrates AERMOD's assumed vertical turbulence profile for the SBL. This is similar to the profile for the CBL except for a notable increase in the value of σ_{wmr}. Since values for σ_{wmr} are based on the magnitude of the wind speed at z_i, the differences in the two figures stem from setting $z_o = 0.0001z_i$ in the CBL example case while for the SBL case $z_o = 0.001z_i$.

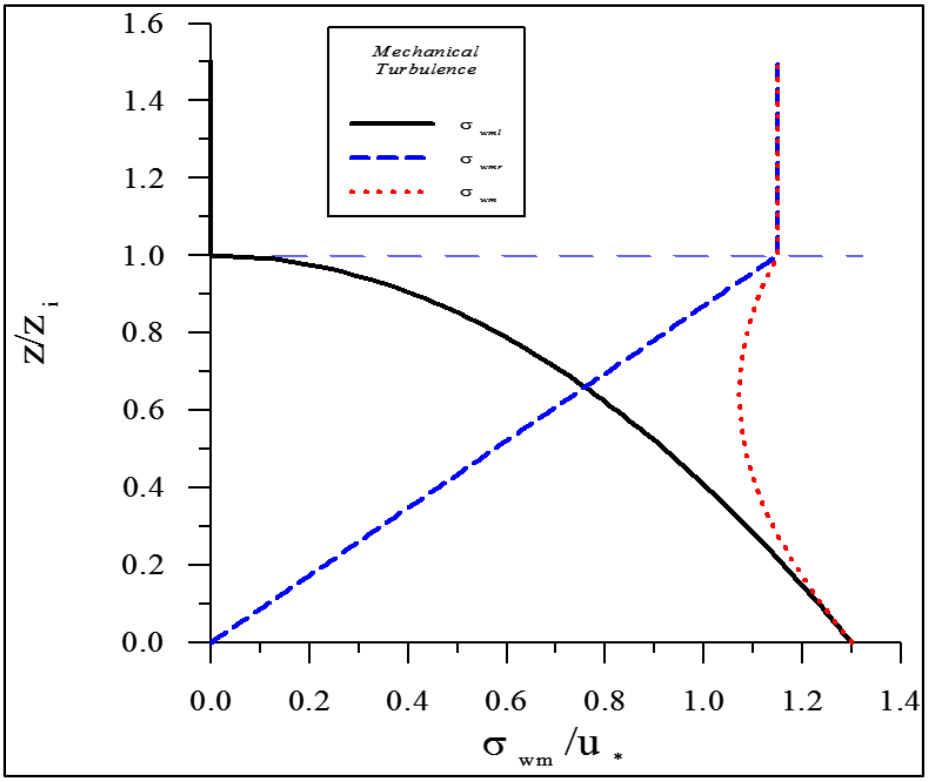

Figure 7. Profile of vertical turbulence in the SBL

4.1.6 Lateral turbulence calculated by the interface

In the CBL the total lateral turbulence, σ^2_{vT}, is computed as a combination of a mechanical (σ_{vm}) and convective (σ_{vc}) portions such that

$$\sigma^2_{vT} = \sigma^2_{vc} + \sigma^2_{vm}. \qquad \textbf{(38)}$$

In the SBL the total lateral turbulence contains only a mechanical portion. AERMOD, uses the same σ_{vm} expression in the CBL and SBL. This is done to maintain continuity of σ_{vm} in the limit of neutral stability. A description of mechanical and convective profiles of lateral turbulence follows.

4.1.6.1 Mechanical portion of the lateral turbulence

The variation with height of the mechanical portion of the lateral turbulence is bounded by its value at the 1surface and an assumed residual value at the top of the mechanical mixed layer. The variation between these two limits is assumed to be linear. Based on observations from numerous field studies, Panofsky and Dutton (1984) report that, in purely mechanical turbulence, the lateral variance near the surface has the form

$$\sigma_{v0}{}^2 = Cu_*{}^2 \qquad \textbf{(39)}$$

where the constant, C, ranges between 3 and 5. Based on an analysis of the Kansas data, Izumi (1971) and Hicks (1985) support the form of eq. **(39)** with a value of 3.6 for C.

Between the surface and the top of the mechanically mixed layer, $\sigma^2{}_{vm}$ is assumed to vary linearly as

$$\begin{aligned} \sigma_{vm}^2 &= \left[\frac{\sigma_{vm}^2\{z_{im}\} - \sigma_{vo}^2}{z_{im}} \right] z + \sigma_{vo}^2 \qquad for \;\; z \le z_{im} \\ \sigma_{vm}^2 &= \sigma_{vm}^2\{z_{im}\} \qquad\qquad\qquad for \;\; z > z_{im}, \end{aligned} \qquad \textbf{(40)}$$

where $\sigma_{vm}^2\{z_m\} = \min[\sigma_{vo}^2; 0.25\ m^2 s^{-2}]$ and $\sigma_{vo}{}^2$, the surface value of the lateral turbulence, is equal to 3.6 $u_*{}^2$. This linear variation of $\sigma^2{}_{vm}$ with z is consistent with field observations (e.g., Brost et al. (1982)). In the SBL the total lateral turbulence contains only a mechanical portion and it is given by eq. **(40)**.

Above the mixed layer, lateral turbulence is expected to maintain a modest residual level. Hanna (1983) analyzed ambient measurements of lateral turbulence in stable conditions. He found that even in the lightest wind conditions, the measurements of σ_{vc} were typically 0.5 m s^{-1}, but were observed to be as low as 0.2 m s^{-1}. AERMOD adopts the lower limit of 0.2 m s^{-1} for σ_{vc} in near-surface conditions, as discussed below, but uses the more typical value of 0.5 m s^{-1} for the residual lateral turbulence above the mixed layer. Above the height of the CBL, the model linearly decreases σ_{vc}^2 from $\sigma_{vc}^2\{ z_{ic} \}$ to 0.25 at 1.2 z_{ic} and holds σ_{vc}^2 constant above 1.2 z_{ic}. However, if $\sigma_{vc}^2\{z_{ic} \} < 0.25$ m^2 s^{-2}, then $\sigma_{vc}^2\{z_{ic} \}$ is persisted upward from z_{ic}. Furthermore, it was found that a value of the order $\sigma_{vc}^2 = 0.25$ m^2 s^{-2} provided consistently good model performance (for plumes commonly above z_{im}) during the developmental evaluation (Perry et al. 2005) supporting the presence of residual lateral turbulence in this layer.

Figure 8 shows how the vertical profile of lateral mechanical turbulence changes over a range of mechanical mixing heights, and related friction velocities. The values of u_* used to produce these curves are consistent with the relationship between z_{im} and u_* which is found in eq. **(24)**. For the SBL Figure 8 represents profiles of the total lateral turbulence. In the CBL these curves depict only the mechanical portion of the total lateral variance. Note that for z_{im} = 300 m and 100 m the values σ_{vo}^2 are less than 0.25 m^2 s^{-2}. Therefore, the profiles are constant with height.

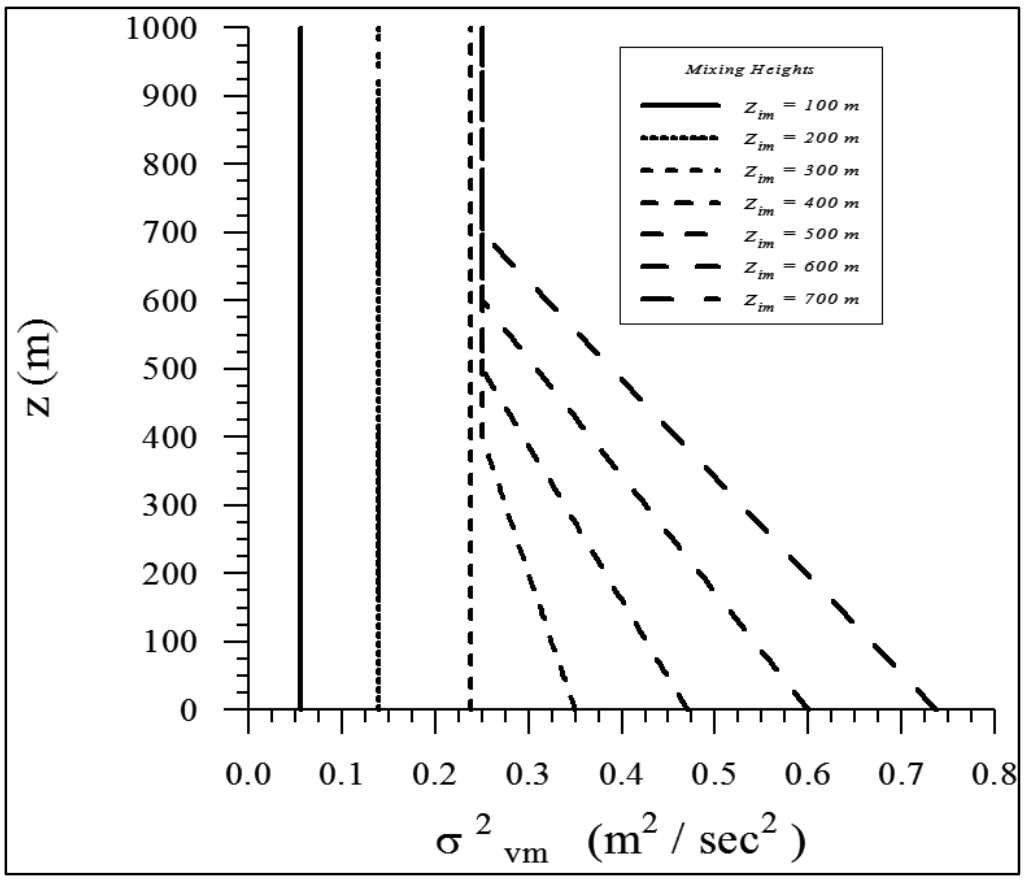

Figure 8. Family of lateral mechanical turbulence profiles over a range of mechanical mixing heights

4.1.6.2 Convective portion of the lateral turbulence

The convective portion of the lateral turbulence within the mixed is constant and calculated as:

$$\sigma_{vc}^2 = 0.35 w_*^2 \quad \textbf{(41)}$$

This constant value of $\sigma_w^2/w_*^2 = 0.35$ is supported by the Minnesota data (Readings et al. 1974; Kaimal et al. 1976) and by data collected at Ashchurch England (Caughey and Palmer 1979).

For $z > z_{ic}$, the model linearly decreases σ_{vc}^2 from $\sigma_{vc}^2\{ z_{ic} \}$ to 0.25 at 1.2 z_{ic} and holds σ_{vc}^2 constant above 1.2 z_{ic}. However, if $\sigma_{vc}^2\{z_{ic}\} < .25$ m^2 s^{-2}, then $\sigma_{vc}^2\{z_{ic}\}$ is persisted upward from z_{ic}.

4.2 Vertical inhomogeneity in the boundary later as treated by the interface

AERMOD is designed to treat the effects on dispersion from vertical variations in wind and turbulence. Consideration of the vertical variation in meteorology is important for properly modeling releases in layers with strong gradients, for capturing the effects of meteorology in layers into which the plume may be vertically dispersing, and to provide a mechanism (in the CBL) by which sources that are released into or penetrate into an elevated stable layer can eventually re-enter the mixed layer. However, AERMOD is a steady-state plume model and therefore can use only a single value of each meteorological parameter to represent the layer through which these parameters are varying. Thus, the model "converts" the inhomogeneous values into equivalent effective or homogeneous values. This technique is applied to u, σ_{vT}, σ_{wT}, $\partial\theta/\partial z$ and the Lagrangian time scale. The effective parameters are denoted by a tilde throughout the document (e.g., effective wind speed is denoted by $\tilde{u}$).

Fundamental to this approach is the concept that the primary layer of importance, relative to receptor concentration, is the one through which plume material travels directly from source to receptor. Figure 9 presents a schematic illustration of the approach AERMOD uses to determine these effective parameters (α is used to generically represent these parameters). The effective parameters are determined by averaging their values over that portion of the layer that contains plume material between the plume centroid height, $H_p\ \{x\}$, (a simplified surrogate for the height of the plume's center of mass) and the receptor height (z_r). In other words, the averaging layer is determined by the vertical half-depth of the plume (defined as 2.15 $\sigma_z\ \{x_r\}$ where x_r is the distance from source to receptor) but is bounded by $H_p\ \{x_r\}$ and z_r. The values

used in the averaging process are taken from AERMOD's vertical profiles. This technique is best illustrated with examples.

Consider the two receptors depicted in Figure 9. Both receptors are located at the same distance x_r from the source but at different heights above ground, i.e., z_{r1} and z_{r2}. An example profile of some parameter α is shown at the far left of the figure. The value of the effective parameter used by AERMOD to represent transport and diffusion from source to receptor depends on the location of the receptor. For receptor 1 the effective parameter value $\tilde{\alpha}_1$ (shown

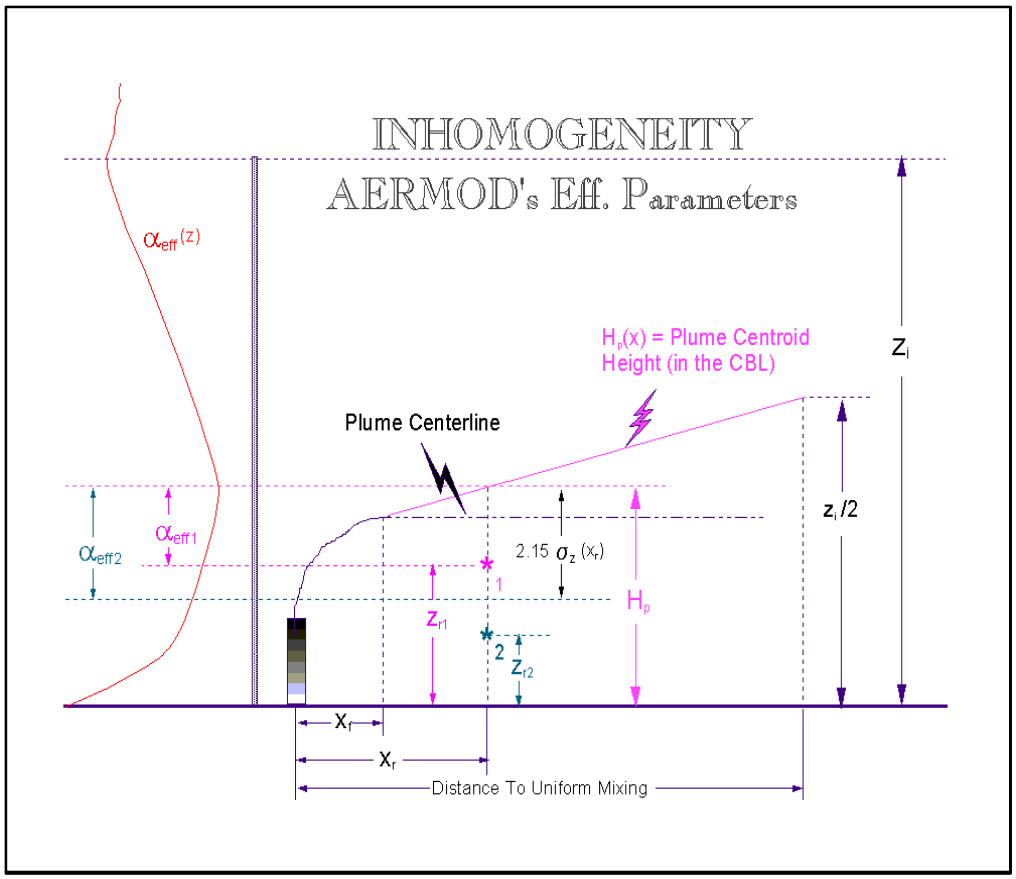

Figure 9. AERMOD's Treatment of the Inhomogeneous Boundary Layer

in the figure as α_{eff1}) is determined by averaging the values of α $\{z\}$ between H_p $\{x_r\}$ and z_{r1}. Therefore, the layer over which this average is taken is smaller than the plume's half-depth. Whereas, $\tilde{\alpha}_2$ (shown in the figure as α_{eff2}) is determined by averaging α $\{z\}$ over the full layer from H_p $\{x_r\}$ down through a depth of $2.15\sigma_z$ $\{x_r\}$ since the receptor is located below the defined lower extent of the plume.

Since σ_z $\{x_r\}$ depends on the effective values of σ_{wT} and u, the plume size is estimated by first using the plume height values of σ_{wT} $\{H_p\}$ and u $\{H_p\}$ to calculate σ_z $\{x_r\}$. As illustrated in Figure 9 $\sigma_z\{x_r\}$ is then used to determine the layer over which $\tilde{\sigma}_{wT}\{x_r\}$ and $\tilde{u}\{x_r\}$ are calculated. Once the averaging layer for a given plume and receptor is established the effective values, $\tilde{\alpha}$, are computed as simple averages:

$$\tilde{\alpha} = \frac{1}{\left(h_t - h_b\right)} \int_{h_b}^{h_t} \alpha\{z\}\, dz \qquad \textbf{(42)}$$

where h_b and h_t are the bottom and top, respectively, of the layer of importance such that:

$$\begin{aligned} h_b &= \left\{ \begin{array}{ll} H_p\{x_r, y_r\}, & if \quad H_p\{x_r, y_r\} \le z_r \\ MAX\left\{\left[H_p\{x_r, y_r\} - 2.15\sigma_z\{x_{sr}\}\right], z_r\right\}, & if \quad H_p\{x_r, y_r\} > z_r \end{array} \right\} \\ h_t &= \left\{ \begin{array}{ll} MIN\left\{\left[H_p\{x_r, y_r\} + 2.15\sigma_z\{x_{sr}\}\right], z_r\right\}, & if \quad H_p\{x_r, y_r\} \le z_r \\ H_p\{x_r, y_r\}, & if \quad H_p\{x_r, y_r\} > z_r \end{array} \right\} \end{aligned} \qquad \textbf{(43)}$$

For all plumes, both limits are bounded by either the z_r or H_p. For both the direct and indirect sources h_t, in eq. **(43)** is not allowed to exceed z_i and if $h_b \ge z_i$ then $\tilde{\alpha} = \alpha\{z_i\}$.

For plumes in stable conditions and for the penetrated source in the CBL, H_p is always set equal to the plume centerline height ($\Delta h_s + h_s$) where h_s is the stack height corrected for stack tip downwash and Δh_s is the stable source plume rise. The stable source plume rise Δh_s is calculated from expressions found in Section 0.

In the CBL, the specification of H_p is somewhat more complicated. Because of limited mixing in the CBL the center of mass of the plume will be the plume height close to the source and the mid-point of the PBL at the distance where it becomes well mixed. Beyond final plume rise, H_p is varied linearly between these limits.

Prior to plume stabilization, i.e., $x < x_f$ (distance to plume stabilization),

$$H_p = h_s + \Delta h_{d,p},$$

where Δh_d is the plume rise for the direct source (estimated from eq. **(91)**), and Δh_p (= h_{ep} - h_s) is the plume rise for the penetrated source, where h_{ep} (penetrated source plume height) is calculated from eq. **(94)**.

The distance to plume stabilization, x_f, is determined following Briggs (Briggs 1975; Briggs 1971) as

$$\begin{aligned} x_f &= 49\, F_b^{5/8} \qquad for \quad F_b < 55 \\ x_f &= 119\, F_b^{2/5} \qquad for \quad F_b \geq 55 \end{aligned} \qquad \textbf{(44)}$$

where the buoyancy flux (F_b) is calculated from eq. **(57)**.

For $F_b = 0$ the distance to final rise is calculated from the ISCST3 ((U.S. Environmental Protection Agency, 1995)) expression

$$x_f = {8 r_s \left(w_s + 3u_p \right)^2} \Big/ {w_s u_p} \qquad \textbf{(45)}$$

where u_p is the wind speed at source height, r_s is the stack radius, and w_s is the stack exit gas velocity.

Beyond plume stabilization ($x > x_f$), H_p varies linearly between the stabilized plume height ($H\{x_f\}$) and the mid-point of the mixed layer ($z_i /2$). This interpolation is performed over the distance range x_f to x_m, where x_m is the distance at which pollutants first become uniformity mixed throughout the boundary layer.

The distance x_m is taken to be the product of the average mixed layer wind speed and the mixing time scale, $z_i/\overline{\sigma}_{wT}$. That is,

$$x_m = \frac{\overline{u}\, z_i}{\overline{\sigma}_{wT}}, \qquad \textbf{(46)}$$

where the averaging of u and σ_{wT} are taken over the depth of the boundary layer.

For distances beyond x_f, H_p is assumed to vary linearly between the plume's stabilized height, $H\{x_f\}$, and $z_i/2$ such that:

$$H_p = H\{x_f\} + \left(\frac{z_i}{2} - H\{x_f\}\right) \cdot \frac{\left(x - x_f\right)}{\left(x_m - x_f\right)} \qquad \textbf{(47)}$$

Note that in the CBL, both the direct and indirect source will have the same α (effective parameter) values. In eq. **(43)** σ_z is the average of the updraft σ_z and the downdraft σ_z, the maximum value of h_t is z_i, and when $h_b \geq z_i$, $\alpha = \alpha\{z_i\}$.

As discussed previously, when multiple vertical measurements of wind direction are available a profile is constructed by linearly interpolating between measurements and persisting the highest and lowest measurements up and down, respectively. The approach taken for selecting a transport wind direction from the profile is different from the above. The transport wind direction is selected as the mid-point of the range between stack height and the stabilized plume height.

5. The AMS/EPA regulatory Model: AERMOD

AERMOD is a steady-state plume model in that it assumes that concentrations at all distances during a modeled hour are governed by the temporally averaged meteorology of the hour. The steady state assumption yields useful results since the statistics of the concentration distribution are of primary concern rather than specific concentrations at particular times and locations. AERMOD has been designed to handle the computation of pollutant impacts in both flat and complex terrain within the same modeling framework. In fact, with the AERMOD structure, there is no need for the specification of terrain type (flat, simple, or complex) relative to stack height since receptors at all elevations are handled with the same general methodology. To define the form of the AERMOD concentration equations, it is necessary to simultaneously discuss the handling of terrain.

In the stable boundary layer (SBL), the concentration distribution is assumed to be Gaussian in both the vertical and horizontal. In the convective boundary layer (CBL), the horizontal distribution is assumed to be Gaussian, but the vertical distribution is described with a bi-Gaussian probability density function (pdf). This behavior of the concentration distributions in the CBL was demonstrated by Willis and Deardorff (1981) and Briggs (1993). Additionally, in the CBL, AERMOD treats "plume lofting," whereby a portion of plume mass, released from a buoyant source, rises to and remains near the top of the boundary layer before becoming vertically mixed throughout the CBL. The model also tracks any plume mass that penetrates into an elevated stable layer, and then allows it to re-enter the boundary layer when and if appropriate.

In urban areas, AERMOD accounts for the dispersive nature of the "convective-like" boundary layer that forms during nighttime conditions by enhancing the turbulence over that which is expected in the adjacent rural, stable boundary layer. The enhanced turbulence is the result of the urban heat flux and associated mixed layer which are estimated from the urban-rural temperature difference as suggested by Oke (1978; 1982).

In complex terrain, AERMOD incorporates the concept of the dividing streamline (Snyder et al., 1985) for stably-stratified conditions. Where appropriate the plume is modeled as

a combination of two limiting cases: a horizontal plume (terrain impacting) and a terrain-following (terrain responding) plume. That is, AERMOD handles the computation of pollutant impacts in both flat and complex terrain within the same modeling framework. Generally, in stable flows, a two-layer structure develops in which the lower layer remains horizontal while the upper layer tends to rise over the terrain. The concept of a two-layer flow, distinguished at the dividing streamline height (H_c), was first suggested by theoretical arguments of Sheppard (1956) and demonstrated through laboratory experiments, particularly those of Snyder et al. (1985). In neutral and unstable conditions $H_c = 0$.

A plume embedded in the flow below H_c tends to remain horizontal; it might go around the hill or impact on it. A plume above H_c will ride over the hill. Associated with this is a tendency for the plume to be depressed toward the terrain surface, for the flow to speed up, and for vertical turbulent intensities to increase. These effects in the vertical structure of the flow are accounted for in models such as the Complex Terrain Dispersion Model (CTDMPLUS) (Perry 1992). However, because of the model complexity, input data demands for CTDMPLUS are considerable. EPA policy (Code of Federal Regulations 1997) requires the collection of wind and turbulence data at plume height when applying CTDMPLUS in a regulatory application. As previously stated, the model development goals for AERMOD include having methods that capture the essential physics, provide plausible concentration estimates, and demand reasonable model inputs while remaining as simple as possible. Therefore, AERMIC arrived at a terrain formulation in AERMOD that considers vertical flow distortion effects in the plume, while avoiding much of the complexity of the CTDMPLUS modeling approach. Lateral flow channeling effects on the plume are not considered by AERMOD.

AERMOD captures the effect of flow above and below the dividing streamline by weighting the plume concentration associated with two possible extreme states of the boundary layer (horizontal plume and terrain-following). As is discussed below, the relative weighting of the two states depends on: 1) the degree of atmospheric stability; 2) the wind speed; and 3) the plume height relative to terrain. In stable conditions, the horizontal plume "dominates" and is given greater weight while in neutral and unstable conditions, the plume traveling over the terrain is more heavily weighted.

5.1 General structure of AERMOD including terrain

In general, AERMOD models a plume as a combination of two limiting cases: a horizontal plume (terrain impacting) and a terrain-following plume. Therefore, for all situations, the total concentration, at a receptor, is bounded by the concentration predictions from these states. In flat terrain the two states are equivalent. By incorporating the concept of the dividing streamline height, in elevated terrain, AERMOD's total concentration is calculated as a weighted sum of the concentrations associated with these two limiting cases or plume states (Venkatram et al. 2001).

The AERMOD terrain pre-processor (AERMAP) uses gridded terrain data to calculate a representative terrain-influence height (h_c) for each receptor with which AERMOD computes receptor specific H_c values. Through this approach, AERMOD handles the computation of pollutant impacts in both flat and elevated terrain within the same modeling framework thereby obviating the need to differentiate between the formulations for simple and complex terrain (as required with previous regulatory models) .

The general concentration equation, which applies in stable or convective conditions is given by

$$C_T\{x_r, y_r, z_r\} = f \cdot C_{c,s}\{x_r, y_r, z_r\} + (1-f)\, C_{c,s}\{x_r, y_r, z_p\} \qquad \textbf{(48)}$$

where $C_T\{x_r,y_r,z_r\}$ is the total concentration $C_{c,s}\{z_r,y_r,z^r\}$ is the contribution from the horizontal plume state (subscripts c and s refer to convective and stable conditions, respectively), $C_{c,s}\{z_r,y_r,z^r\}$ is the contribution from terrain-following state, f is the plume state weighting function, $\{x_r, y_r, z_r\}$ is the coordinate representation of a receptor (with z_r defined relative to stack base elevation) $z_p = z_r - z_t$ is the height of a receptor above local ground, and z_t is the terrain height at a receptor. Note that in flat terrain, $z_t = 0$, $z_p = z_r$ and the concentration (eq. **(48)**) reduces to the form for a single horizontal plume. It is important to note that for any concentration calculation all heights (z) are referenced to stack base elevation. Figure 10 illustrates the relationship between the actual plume and AERMOD's characterization of it.

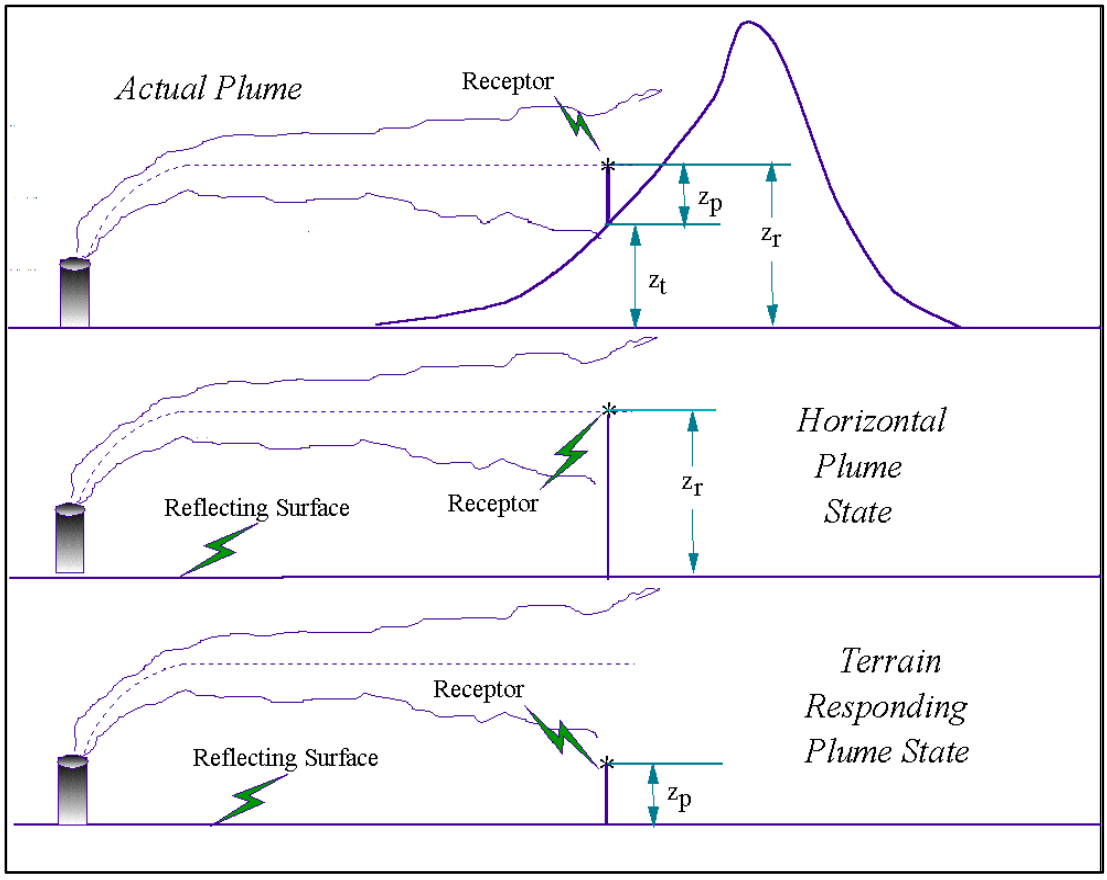

Figure 10. AERMOD two state approach. The total concentration predicted by AERMOD is the weighted sum of the two extreme possible plume states

The formulation of the weighting factor requires the computation of H_c. Using the receptor specific terrain height scale (h_c) from AERMAP, H_c is calculated from the same algorithms found in CTDMPLUS as:

$$1/2 \cdot u^2\{H_c\} = \int_{H_c}^{h_c} N^2\left(h_c - z\right)dz. \qquad \textbf{(49)}$$

where $u\ \{H_c\}$ is the wind speed at height H_c, and $N = \left[\frac{g}{\theta}\frac{\partial\theta}{\partial z}\right]^{1/2}$ is the Brunt-Vaisala frequency. The height scale, h_c, characterizes the height of the surrounding terrain that most dominates the flow in the vicinity of the receptor.

The weighting between the two states of the plume depends on the relationship between H_c and the vertical concentration distribution at the receptor location. Assuming that the wind speed increases with height, H_c can be thought of as the level in the stable atmosphere where the flow has sufficient kinetic energy to overcome the stratification and rise to the height of the terrain. However, in determining the amount of plume material in the terrain-following state at a receptor, it is only important to know the lowest height in the flow where the kinetic energy is sufficient for a streamline to just maintain its height above the surface, i.e. terrain-following. Whether it will be deflected further and reach the top of some specified hill is not important for determining the amount of plume material in the terrain-following state for this receptor. Venkatram et al. (2001) first proposed the idea that for real terrain, often characterized by a number of irregularly-shaped hills, H_c should be defined in relation to a terrain-following height at each receptor location. This is in contrast to the more classical definition where H_c is defined in relation to the top of a single representative hill upon which may reside many receptor locations.

In the AERMOD approach, plume height, receptor elevation, and H_c will determine how much plume material resides in each plume state. For a receptor at elevation z_t and an effective plume at height h_e the height that the streamlines must reach to be in the terrain-following state is z_t+h_e. Therefore the terrain height of importance, h_c, in determining H_c is simply equal to this local terrain-following height. Any actual terrain above $h_c = z_t + h_e$ is of no consequence to the concentration at the receptor. This receptor and plume dependent approach to computing H_c assumes that there is sufficient terrain affecting the flow near the receptor to vertically force the streamlines to the terrain-following level. If the actual surrounding terrain does not reach the height of the terrain-following state, h_c is calculated from the highest actual terrain height in the vicinity of the receptor. Therefore, for any receptor, h_c is defined as the minimum of the highest actual terrain and the local terrain-following height. Given h_c, the dividing streamline height is computed with the same integral formula found in the CTDMPLUS model.

The fraction of the plume mass below H_c (i.e., ϕ_p) is computed as:

$$\varphi_p = \frac{\int_0^{H_c} C_s\{x_r, y_r, z_r\}\, dz}{\int_0^{\infty} C_s\{x_r, y_r, z_r\}\, dz} \qquad \textbf{(50)}$$

where $C_s\{x_r.y_r,z_r\}$ is the concentration in the absence of the hill for stable conditions. In convective conditions $H_c = 0$ and $\varphi_p = 0$. As described by Venkatram et al. (2001), the plume state weighting factor f is given by $f = 0.5(1 + \varphi_p)$. When the plume is entirely below H_c ($\varphi_p = 1.0$ and $f = 1.0$) the concentration is determined only by the horizontal plume. When the plume is entirely above the critical dividing streamline height or when the atmosphere is either neutral or convective, ($\varphi_p = 0$ and $f = 0.5$). Therefore, during convective conditions the concentration at an elevated receptor is simply the average of the contributions from the two states. As plumes above H_c encounter terrain and are deflected vertically, there is also a tendency for plume material to approach the terrain surface and to spread out around the sides of the terrain. To simulate this the estimated concentration is constrained to always contain a component from the horizontal state. Therefore, under no conditions is the plume allowed to completely approach the terrain-following state. For flat terrain, the contributions from the two states are equal, and are equally weighted.

Figure 11 illustrates how the weighting factor is constructed and its relationship to the estimate of concentration as a weighted sum of two limiting plume states.

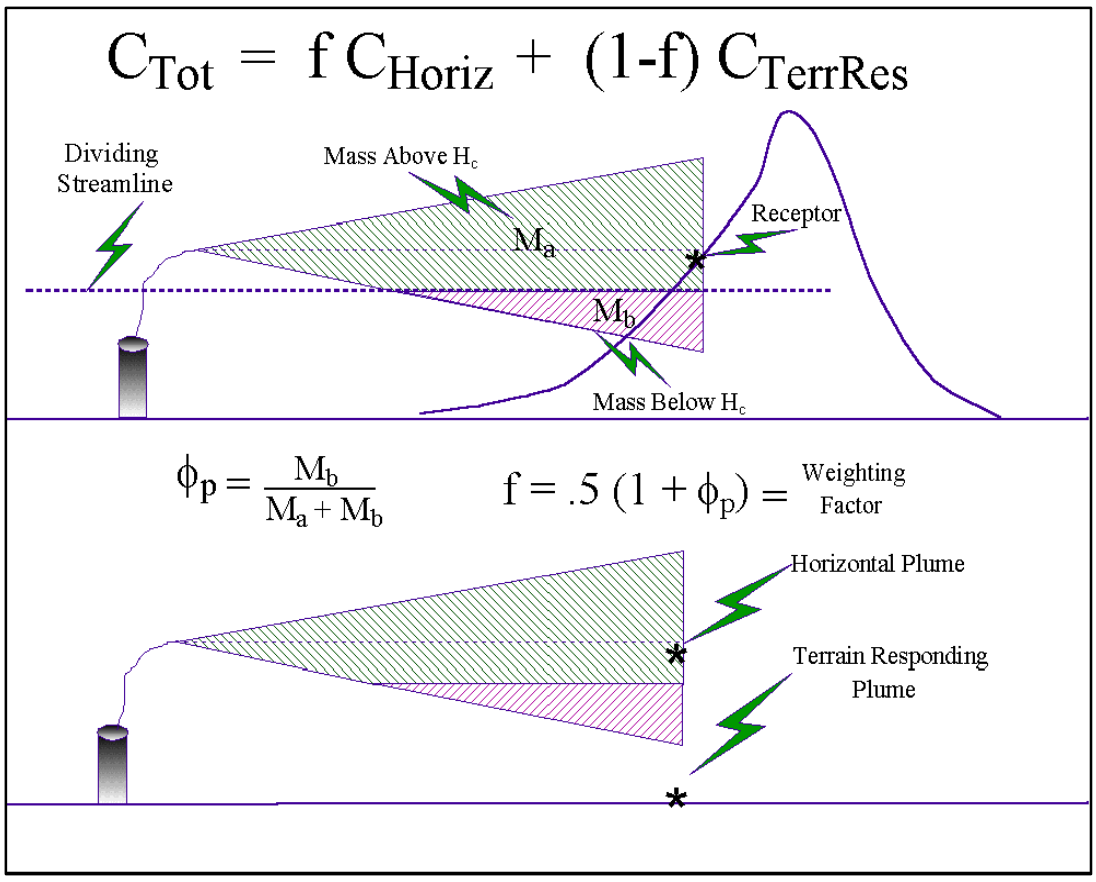

Figure 11. Treatment of Terrain in AERMOD. Construction of the weighting factor used in calculating total concentration

The general form of the expressions for concentration in each term of eq. **(48)** for both the CBL and the SBL can be written as follows:

$$C\{x,y,z\} = \left(Q/\tilde{u}\right) P_y\{y;x\}\, P_z\{z;x\}, \qquad \textbf{(51)}$$

where Q is the source emission rate, $\tilde{u}$ is the effective wind speed, and p_y and p_z are probability density functions (pdf) which describe the lateral and vertical concentration distributions, respectively. AERMOD assumes a traditional Gaussian pdf for both the lateral and vertical distributions in the SBL and for the lateral distribution in the CBL. The CBL's vertical distribution of plume material reflects the distinctly non-Gaussian nature of the vertical velocity distribution in convectively mixed layers. The specific form for the concentration distribution in the CBL is found in eq. **(54)** which uses the notation $C_c\ \{x_r, y_r, z_r\}$. Similarly, in the SBL, the

concentration takes the form of eq. **(67)** and used the notation $C_s\{x_r, y_r, z_r\}$.

AERMOD simulates five different plume types depending on the atmospheric stability and on the location in and above the boundary layer: 1) direct, 2) indirect, 3) penetrated, 4) injected and 5) stable. All of these plumes will be discussed, in detail, throughout the remainder of this document. During stable conditions, plumes are modeled with the familiar horizontal and vertical Gaussian formulations. During convective conditions ($L<0$) the horizontal distribution is still Gaussian; the vertical concentration distribution results from a combination of three plume types: 1) the direct plume material within the mixed layer that initially does not interact with the mixed layer lid; 2) the indirect plume material within the mixed layer that rises up and tends to initially loft near the mixed layer top; and 3) the penetrated plume material that is released in the mixed layer but, due to its buoyancy, penetrates into the elevated stable layer.

During convective conditions, AERMOD also handles a special case referred to as an injected source where the stack top (or release height) is greater than the mixing height. Injected sources are modeled as plumes in stable conditions, however the influence of the turbulence and the winds within the mixed layer are considered in the inhomogeneity calculations as the plume material passes through the mixed layer to reach receptors.

As described above, AERMOD accounts for the vertical variation of meteorology through the use of effective values of wind speed, turbulence, and the Lagrangian time scale. Being a steady state plume model, AERMOD uses a single value of each meteorological variable to represent the state of the dispersive layer for each modeling period (typically one hour). Specifically, the effective parameters are determined by averaging values from the meteorological profile within the layer between the plume's center of mass and the receptor. Effective variables or parameters are denoted by an overbar tilde (e.g., $\tilde{u}$).

5.2 Concentration predictions in the CBL

In AERMOD, the dispersion formulation for the convective boundary layer (CBL) represents one of the more significant model advances by comparison with existing regulatory models. One assumes that plume sections are emitted into a traveling train of convective

elements - updrafts and downdrafts - that move with the mean wind. The vertical and lateral velocities in each element are assumed to be random variables and characterized by their probability density functions (pdf). The mean concentration is found from the pdf of the position of source-emitted "particles"; this position pdf in turn is derived from the pdf of the lateral and vertical velocities as described by Weil et al. (1997); also see Misra (1982), Venkatram (1983), and Weil (1988a).

In the CBL, the pdf of the vertical velocity (w) is positively skewed and results in a non-Gaussian vertical concentration distribution, F_z (Lamb 1982). The positive skewness is consistent with the higher frequency of occurrence of downdrafts than updrafts; for an elevated non-buoyant source the skewness also leads to the decent of the plume centerline, as defined by the locus of maximum concentration (Lamb 1982; Weil 1988a). Figure 12 presents a schematic representation of an instantaneous plume in a convective boundary layer and its corresponding ensemble average. The base concentration prediction in AERMOD is representative of a one hour average. Notice that since a larger percentage of the instantaneous plume is effected by downdrafts, the ensemble average has a general downward trend. Since downdrafts are more prevalent the average velocity of the downdrafts is correspondingly weaker than the average updraft velocity to insure that mass is conserved. In AERMOD, a skewed vertical velocity pdf is modeled using a bi-Gaussian distribution, which has been shown to be a good approximation to laboratory convection tank data (Baerentsen and Berkowicz 1984). In contrast to the vertical component, the lateral velocity pdf is approximately Gaussian (Lamb 1982), and this pdf and the resulting concentration distribution, F_y, are assumed to be Gaussian.

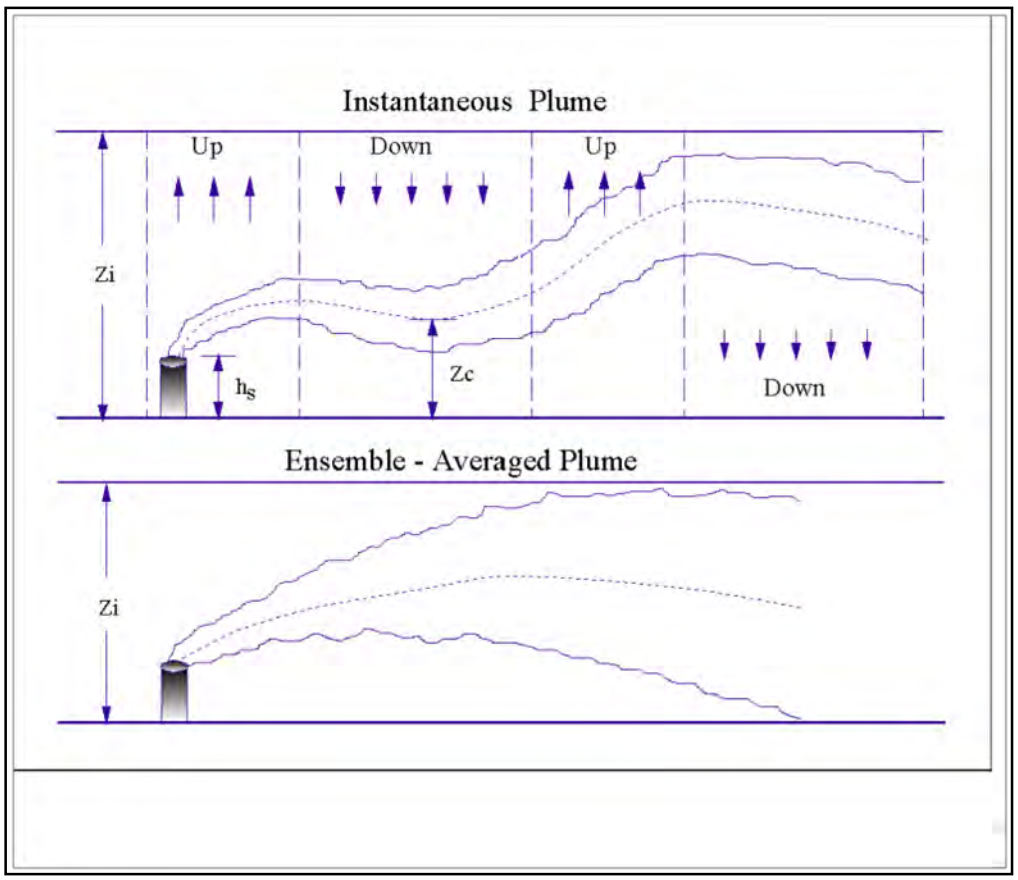

Figure 12. Instantaneous and corresponding ensemble-averaged plume in the CBL

In addition to the non-Gaussian F_z, AERMOD has the following features. For buoyant releases, there is no "final" plume rise assumed. Instead, the plume or particle trajectories are determined by the addition of a distance-dependent plume rise and the random vertical displacement caused by the vertical distribution of w. Ground level concentrations first appear when the negative or downdraft velocities are sufficiently large to overcome the plume rise velocity and carry plume sections to the surface. The direct transport of plume material to the ground is treated by the "direct" source located at the stack. That is, the direct source treats that portion of the plume's mass to first reach the ground, and all subsequent reflections of the mass at $z = z_i$ and 0 (where z_i is the mixed layer height in the CBL (Cimorelli et al., 2004). For plume segments or particles initially rising in updrafts, an "indirect" or modified-image source is included (above the mixed layer) to address the initial quasi-reflection of plume material at $z = z_i$, i.e., for material that does not penetrate the elevated inversion. This source is labeled "indirect" because it is not a true image source (i.e., as is found in models such as ISC) - the plume is not

perfectly reflected about z_i. Thus, the indirect source treats that portion of the plume's mass that first reaches z_i and all subsequent reflections of that particular mass at $z = 0$ and z_i. For the indirect source, a plume rise (Δh_i) is added to delay the downward dispersion of material from the CBL top (see Figure 13); this mimics the plume's lofting behavior, i.e., the tendency of buoyant plumes to remain temporarily near z_i and resist downward mixing. For non-buoyant sources the indirect source reduces to the first image source (as found in ISCST3) resulting from the first reflection at $z = z_i$. Additionally, a "penetrated" source or plume (above the CBL top) is included to account for material that initially penetrates the elevated inversion but is subsequently reentrained by and disperses in the growing CBL.

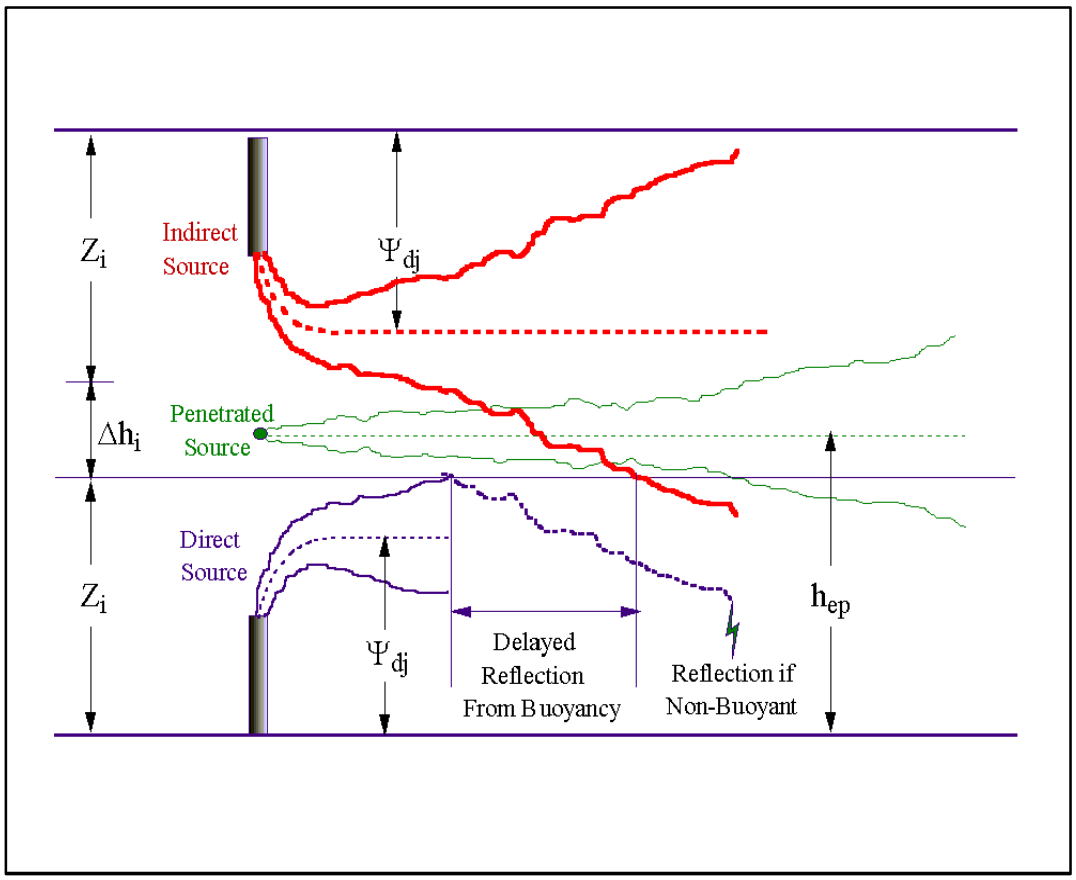

Figure 13. AERMOD's three plume treatment of the CBL

In line with the above concepts there are three main mathematical sources that contribute to the modeled concentration field: 1) the direct source (at the stack), 2) the indirect source, and 3) the penetrated source. The strength of the direct source is $f_p Q$, where Q is the source emission

rate and f_p is the calculated fraction of the plume mass trapped in the CBL ($0 \le f_p \le 1$). Likewise, the indirect source strength is f_pQ since this (modified image) source is included to satisfy the no-flux boundary condition at $z = z_i$ for the trapped material. The strength of the penetrated source is $(1\text{-}f_p)Q$, which is the fraction of the source emission that initially penetrates into the elevated stable layer. In addition to the three main sources, other image sources are included to satisfy the no-flux conditions at $z = 0$ and z_i.

For material dispersing within a convective layer, the conceptual picture (see Figure 12) is a plume embedded within a field of updrafts and downdrafts that are sufficiently large to displace the plume section within it. The relationship between the particle (or air parcel) height, z_c and w is found by superposing the plume rise (Δh) and the vertical displacement due to w (i.e., wx/u), as

$$z_c = h_s + \Delta h + \frac{wx}{u}, \qquad \textbf{(52)}$$

where h_s is the stack height (corrected for stack tip downwash), u is the mean wind speed (a vertical average over the convective boundary layer) and x is the downwind distance. The Δh above includes source momentum and buoyancy effects as given by eq. **(91)** below (see Briggs (1984)). The F_z or pdf of z_c is found from the vertical velocity pdf p_w as described in Weil et al. (1997). In the CBL a good approximation to p_w is the superposition of two Gaussian distributions (Baerentsen and Berkowicz 1984; Weil 1988a) such that

$$p_w = \frac{\lambda_1}{\sqrt{2\pi}\sigma_{w1}} \exp\left(-\frac{\left(w - \overline{w_1}\right)^2}{2\sigma_{w1}^2} \right) + \frac{\lambda_2}{\sqrt{2\pi}\sigma_{w2}} \exp\left(-\frac{\left(w - \overline{w_2}\right)^2}{2\sigma_{w2}^2} \right), \qquad \textbf{(53)}$$

where λ_1 and λ_2 are weighting coefficients for the two distributions with $\lambda_1 + \lambda_2 = 1$(the subscripts 1 and 2 refer to the updraft and downdraft distributions, respectively). The parameters of the pdf (w_1, w_2, σ_{w1}, σ_{w2}, λ_1, λ_2) are functions of σ_w (the "total" or overall root mean square vertical turbulent velocity), the vertical velocity skewness $S = \overline{w}^3/\sigma_w^3$ (where $\overline{w}^3$ is the third moment of

w), and a parameter $R = \sigma_{w1}/\overline{w_1} = -\sigma_{w2}/\overline{w_2} = 2$. An expanded discussion of the pdf parameters is given in Weil et al. (1997).

The instantaneous plume is assumed to have a Gaussian concentration distribution about its randomly varying centerline. The mean or average concentration is found by summing the concentrations due to all of the random centerline displacements. This averaging process results in a skewed distribution which AERMOD represents as a bi-Gaussian pdf (i.e., one for updrafts and the other for downdrafts). Figure 14 illustrates the bi-Gaussian approach to approximate the skewed vertical concentration distribution in the CBL. The figure shows two mean trajectories, each representing the average of many individual trajectories of parcels (or particles) released into downdrafts (the downdraft plume) or updrafts (the updraft plume). The velocities determining these mean trajectories are: 1) the mean horizontal wind speed (u), 2) the vertical velocity due to plume buoyancy (v_{buoy}), and 3) the mean updraft ($\overline{w_1}$) or downdraft ($\overline{w_2}$) velocity. The mean height of each trajectory, $\overline{z}_{c1}$ or $\overline{z}_{c2}$, can be found by averaging eq. **(53)**. These parcel (or particle) height distributions are thus related to concentration and are characterized by σ_{z1} ($= \sigma_{w1}x/u$) and σ_{z2} ($= \sigma_{w2}x/u$), the standard deviations of the two concentration distributions comprising the bi-Gaussian form as derived in Weil et al. (1997).

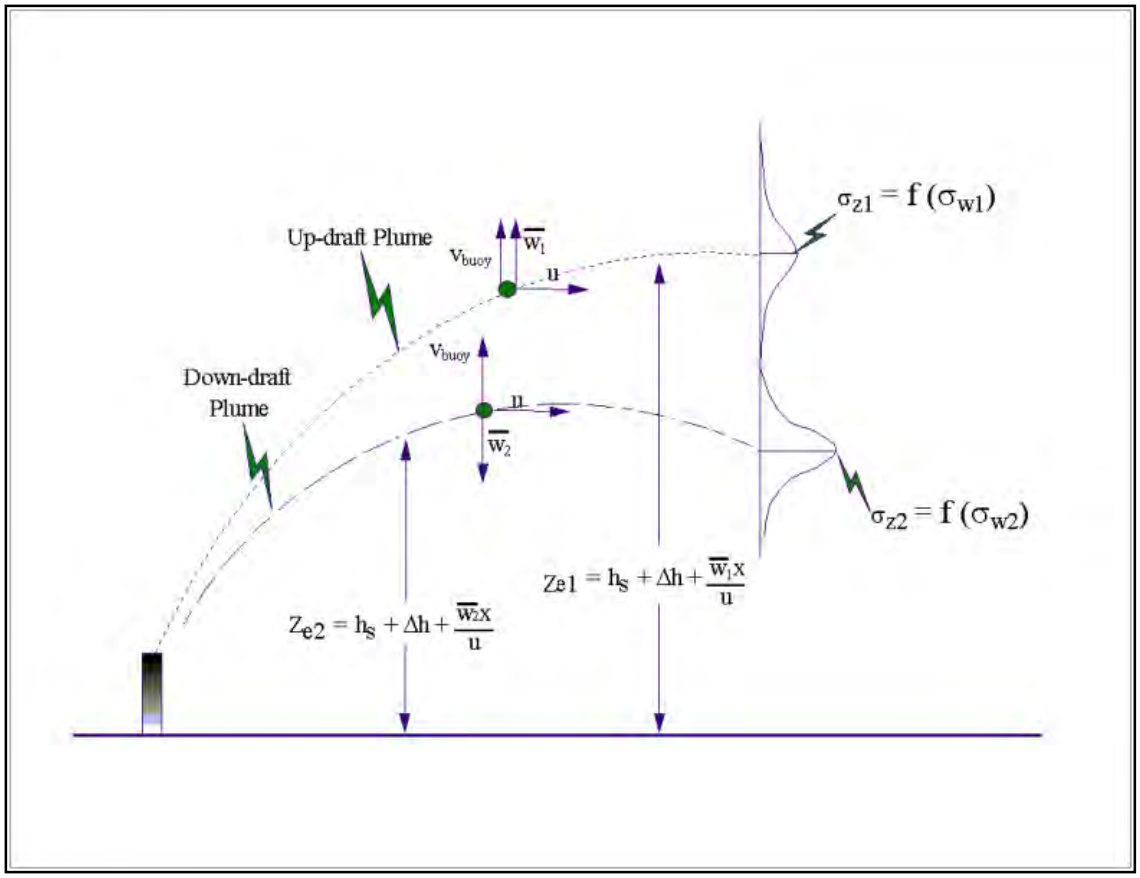

Figure 14. AERMOD's pdf approach for plume dispersion in the CBL. AERMOD approximates the skewed distribution by superimposing two Gaussian distributions, the updraft and downdraft distributions

Figure 15 compares the bi-Gaussian pdf with the Gaussian form, which is symmetric about $w = 0$. As can be seen, for the negative and positive tails of the distributions, the bi-Gaussian pdf is biased towards smaller and larger p_w values, respectively, than the Gaussian. In addition, for the bi-Gaussian forms, approximately 60% of the area under the p_w curve is on the negative side of the w axis and approximately 40% on the positive side. This is consistent with the results of numerical simulations and field observations (Lamb 1982; Weil 1988a).

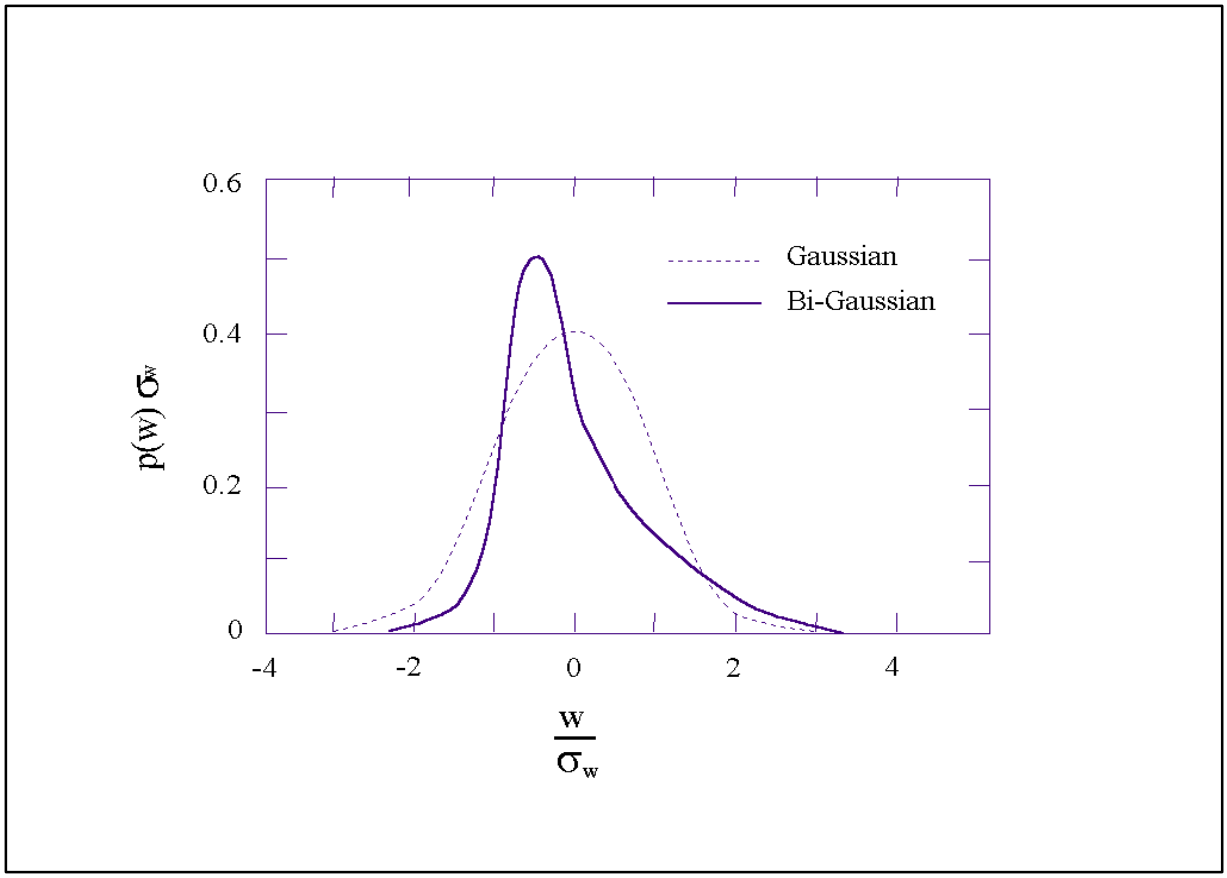

Figure 15. Probability density functon of the vertical velocity. While the Gaussian curve is unskewed, the bi-Gaussian curve has a skewness of S=1

In the pdf approach used here (Weil et al. 1997), there are, as mentioned in the previous section, three primary sources that contribute to the modeled concentration field: 1) the "direct" or real source at the stack, 2) an "indirect" source that the model locates above the CBL top to account for the slow downward dispersion of buoyant plumes that "loft" or remain near, but below, z_i , and 3) a "penetrated source" that contains the portion of plume material that has penetrated into the stable layer above z_i. The direct source describes the dispersion of plume material that reaches the ground directly from the source via downdrafts. The indirect source is included to treat the first interaction of the "updraft" plume with the elevated inversion - that is, for plume sections that initially rise to the CBL top in updrafts and return to the ground via downdrafts. Image sources are added to treat the subsequent plume interactions with the ground and inversion and to satisfy the zero-flux conditions at $z = 0$ and at $z = z_i$. This source plays the same role as the first image source above z_i in the standard Gaussian model, but differs in the treatment of plume buoyancy. For the indirect source, a modified reflection approach is adopted

in which the vertical velocity is reflected at $z = z_i$, but an "indirect" source plume rise Δh_i is added to delay the downward dispersion of plume material from the CBL top. This is intended to mimic the lofting behavior. The penetrated source is included to account for material that initially penetrates the elevated inversion but subsequently can reenter the CBL via turbulent mixing of the plume and eventual reentrainment into the CBL. Figure 13 illustrates this three plume approach; a fundamental feature of AERMOD's convective model. In AERMOD, the total concentration (C_c) in the CBL is found by summing the contribution from the three sources. For the horizontal plume state, the C_c is given by

$$C_c\{x_r, y_r, z_r\} = C_d\{x_r, y_r, z_r\} + C_r\{x_r, y_r, z_r\} + C_p\{x_r, y_r, z_r\}, \qquad \textbf{(54)}$$

where C_d, C_r, and C_p are the contributions from the direct, indirect and penetrated sources, respectively. The total concentration for the terrain-following state has the form of eq. **(54)** but with z_r replaced by z_p.

The fraction f_p of the source material that remains trapped in the CBL is found from

$$\begin{aligned} f_p &= 0 && \text{if} \quad \Delta h_h < 0.5\Delta h_{eq} \\ f_p &= 1 && \text{if} \quad \Delta h_h > 1.5\Delta h_{eq} \\ f_p &= \frac{\Delta h_h}{\Delta h_{eq}} - 0.5 && \text{if} \quad 0.5\Delta h_{eq} < \Delta h_h > 1.5\Delta h_{eq}. \end{aligned} \qquad \textbf{(55)}$$

where $\Delta h_h = z_i - h_s$, and Δh_{eq} is the equilibrium plume rise in a stable environment. The Δh_{eq} has the form Berkowicz et al. (1986)

$$\Delta h_{eq} = \left(2.6^3 P_s + (2/3)^3\right)^{1/3} \Delta h_h \qquad \textbf{(56)}$$

where $P_s = F_b/uN_h^2\Delta h_h^3$ is the penetration parameter, and the stack buoyancy flux (F_b), and Brunt-Vaisala wfrequency (N_h) are given respectively by

$$F_b = g w_s r_s^2 \frac{\Delta T}{T_s} \quad \textbf{(57)}$$

and

$$N_h = \left[\frac{g}{\theta\{z_i\}} \frac{\partial \theta}{\partial z}\bigg|_{z>z_i} \right]^{1/2}. \quad \textbf{(58)}$$

Here, u is the wind speed at stack height; g is the gravitational acceleration; w_s, r_s, and T_s are the stack exit velocity, radius, and temperature, respectively; and θ is the ambient potential temperature. The N_h in eq. **(58)** is based on the potential temperature gradient in the elevated stable layer, provided by AERMET, capping the CBL. In general this layer is within z_i and z_i + 500 m.

5.2.1 Direct Source contribution to concentration calculations in the CBL

Following Weil et al. (1997), the concentration due to the direct plume is given by:

$$C_d\{x_r, y_r, z\} = \frac{Qf_p}{\sqrt{2\pi}\tilde{u}} F_y \cdot \sum_{j=1}^{2} \sum_{m=0}^{\infty} \frac{\lambda_j}{\sigma_{zj}} \left[\exp\left(-\frac{\left(z - \Psi_{dj} - 2mz_i\right)^2}{2\sigma_{zj}^2} \right) + \exp\left(-\frac{\left(z + \Psi_{dj} + 2mz_i\right)^2}{2\sigma_{zj}^2} \right) \right], \quad \textbf{(59)}$$

where

$$\Psi_{dj} = h_s + \Delta h_d + \frac{\overline{w}_j x}{u}, \quad \textbf{(60)}$$

u is the wind speed at stack top, $F_y \left(= \frac{1}{\sqrt{2\pi}\sigma_y} \exp\left(\frac{-y^2}{2\sigma_y^2}\right) \right)$ the lateral distribution function with meander (discussed in Section 0), $\overline{w_j} = a_j w_*$ (a_j is defined below in eq. **(62)**, Δh_d is the direct source plume rise calculated from eq. **(91)**, and $z = z_r$ and z_p in the horizontal and terrain-following states, respectively. Here, Ψ_{dj} and σ_{zj} are the effective source height and vertical

dispersion parameter corresponding to each of the two distributions in eq. **(53)**. The subscript *j* is equal to 1 for updrafts and 2 for downdrafts. The lateral and vertical dispersion parameters (σ_y and σ_{zj}), resulting from the combined effects of ambient, buoyancy-induced, and building-induced turbulence are calculated as discussed in Sections 0 and 0 respectively. Here, σ_{zj} (with *j* = 1 or 2) is the vertical dispersion parameter corresponding to each of the Gaussian distributions used in the bi-Gaussian pdf, (see Section 0) and λ_j, the weighting coefficient for each distribution in eq.**(53)**, is calculated from Weil et al. (1997) as

$$\begin{aligned}\lambda_1 &= +\frac{\overline{w}_2}{\overline{w}_2 - \overline{w}_1} = +\frac{a_2}{a_2 - a_1} \\ \lambda_2 &= -\frac{\overline{w}_1}{\overline{w}_2 - \overline{w}_1} = -\frac{a_1}{a_2 - a_1}\end{aligned} \qquad \textbf{(61)}$$

where

$$\begin{aligned}a_1 &= \frac{\widetilde{\sigma}_{wT}}{w_*}\left(\frac{\alpha S}{2} + \frac{1}{2}\left(\alpha^2 S^2 + \frac{4}{\beta}\right)^{1/2}\right) \\ a_2 &= \frac{\widetilde{\sigma}_{wT}}{w_*}\left(\frac{\alpha S}{2} - \frac{1}{2}\left(\alpha^2 S^2 + \frac{4}{\beta}\right)^{1/2}\right)\end{aligned} \qquad \textbf{(62)}$$

Recall that $\widetilde{\sigma}_{wT}$ is the total effective vertical turbulence and is calculated from eq. **(34)**. The parameters appearing in eq. **(62)** are given by

$$\begin{aligned}\frac{\overline{w}^3}{w_*^3} &= 0.125 \qquad for \quad H_p\{x\} \geq 0.1 z_i \\ \frac{\overline{w}^3}{w_*^3} &= 1.25\frac{H_p\{x\}}{z_i} \qquad for \quad H_p\{x\} < 0.1 z_i\end{aligned} \qquad \textbf{(63)}$$

where,

$$\alpha = \frac{1+R^2}{1+3R^2}$$
$$\beta = 1+R^2 \qquad \textbf{(64)}$$
$$S = \frac{\overline{w}^3 / w_*^3}{\left(\widetilde{\sigma}_{wT}/w_*\right)^3} \equiv Skewness\ \ factor,$$

and R is assumed to be 2.0 (Weil et al., 1997). Likewise, the term $\overline{w_j}\ x/u$ in eq. **(60)** follows from the F_z derivation and the w_j appearing in the bi-Gaussian form (see discussion of eq. **(53)**). The lateral dispersion parameter ($\sigma_{y,}$) is calculated from eq. **(75)** (Weil et al., 1997).

In eq. **(59)**, an image plume is used to satisfy the no-flux condition at the ground, i.e., an image plume from a source at $z = -h_s$, which results in the exponential terms containing $z + \Psi_{dj}$ on the right-hand side of eq. **(59)**. This image source results in a positive flux of material at $z = z_i$, and additional image sources are introduced at $z = 2\ z_i + h_s$, $-2\ z_i - h_s$, $4z_i + h_s$, $-4z_i - h_s$, etc. to satisfy all the subsequent no-flux conditions occurring at $z = 0$ and z_i.

5.2.2 Indirect Source contribution to concentration calculations in the CBL

The concentration due to the indirect source is calculated from:

$$C_r\{x_r, y_r, z\} = \frac{Qf_p}{\sqrt{2\pi}\,\widetilde{u}} \cdot F_y \cdot \sum_{j=1}^{2}\sum_{m=1}^{\infty} \frac{\lambda_j}{\sigma_{zj}} \left[\exp\left(-\frac{\left(z + \Psi_{rj} - 2mz_i\right)^2}{2\sigma_{zj}^2} \right) + \exp\left(-\frac{\left(z - \Psi_{rj} + 2mz_i\right)^2}{2\sigma_{zj}^2} \right) \right], \qquad \textbf{(65}$$

where $\Psi_{rj} = \Psi_{dj} - \Delta h_i$, and z is either z_r.(for the horizontal plume state) or z_p (for the terrain-following state). As shown in Figure 13, the indirect plume is modeled as a reflected version of the direct plume with an adjustment (Δh_i - calculated from eq. **(92)**) to the reflected plume height to account for the delay in vertical mixing due to plume lofting at the top of the boundary layer.

5.2.3 Penetrated source contribution to concentration calculations in the CBL

For the penetrated source the concentration expression has a Gaussian form in both the vertical and lateral directions. The concentration due to this source is given by:

$$C_p\{x_r, y_r, z\} = \frac{Q\left(1-f_p\right)}{\sqrt{2\pi}\,\tilde{u}\,\sigma_{zp}} F_y \cdot \sum_{m=-\infty}^{\infty}\left[\exp\left(-\frac{\left(z-h_{ep}+2mz_{ieff}\right)^2}{2\sigma_{zp}^2}\right)+\exp\left(-\frac{\left(z+h_{ep}+2mz_{ieff}\right)^2}{2\sigma_{zp}^2}\right)\right] \quad \textbf{(6}$$

where z_{ieff} is the height of the upper reflecting surface in a stable layer (see Section 0) and z is either z_r for the horizontal plume state or z_p for the terrain-following state. The vertical dispersion parameters (σ_{zp}) are calculated as described in Section 0.

The penetrated plume height, h_{ep}, is taken as the height of the plume centroid above the mixed layer and is calculated from eq. **(94)**.

5.3 Concentrations in the SBL

For stable conditions, the AERMOD concentration expression (C_s in eq. **(48)**) has the Gaussian form, and is similar to that used in many other steady-state plume models (e.g., HPDM (Hanna and Paine 1989)). The C_s is given by

$$C_s\{x_r, y_r, z\} = \frac{Q}{\sqrt{2\pi}\tilde{u}\,\sigma_{zs}} \cdot F_y \cdot \sum_{m=-\infty}^{\infty}\left[\exp\left(-\frac{\left(z-h_{es}-2mz_{ieff}\right)^2}{2\sigma_{zs}^2}\right)+\exp\left(-\frac{\left(z+h_{es}+2mz_{ieff}\right)^2}{2\sigma_{zs}^2}\right)\right], \quad \textbf{(67)}$$

where z_{ieff} is the effective mechanical mixed layer height, σ_{zs} is the total vertical dispersion in the SBL (see discussion in Section 0), and h_{es} is the plume height (i.e., stack height plus the plume rise - see Section 0).

Above the mechanical mixed layer height, z_{im} (eq. **(26)**), the turbulence level is generally expected to be small and thus supports little vertical mixing of the plume. AERMOD is

designed (in the SBL) with an effective mixing lid, z_{ieff}, that retards but does not prevent plume material from spreading into the region above the estimated mechanical mixed layer. When the final plume height is well below z_{im}, the plume does not interact with z_{im}. When the plume is below z_{im} yet the "upper edge" (plume height plus 2.15 σ_{zs}) of the stabilized plume reaches z_{im}, the effective mixing lid is allowed to increase and remain at a level near the upper edge of the plume. In this way, AERMOD allows the plume to disperse downwards, but where the turbulence aloft is low, vertical plume growth is limited by an effective reflecting surface that is folding back only the extreme tail of the vertical plume distribution. There is no strong concentration doubling effect as occurs with reflections from an assumed hard lid. Downward dispersion is primarily a factor of σ_w averaged from the receptor to the plume height. If the plume height is above the mixed layer height, the calculation of the effective σ_w will include regions in which σ_w is likely to be small. This, in effect, retards plume growth by an amount dependent upon how much of the plume is above z_{im}. Therefore, whether the plume is above or below z_{im}, the region of low turbulence above z_{im} will have an appropriate effect on the concentration distribution within the mixing layer.

When the plume buoyancy carries the rising plume into the relatively non-turbulent layer above z_{im}, the reflecting surface is still placed at 2.15 σ_{zs} above the effective plume height because there will be plume spread due to plume buoyancy and downward mixing is still important. Therefore, in the SBL, plume material is assumed to reflect off an elevated surface which is defined as:

$$z_{ieff} = MAX\left[\left(h_{es} + 2.15\sigma_{zs}\{h_{es}\};\ z_{im}\right)\right]. \qquad \textbf{(68)}$$

where σ_{zs} in eq. **(68)** is determined from equations found in Section 0 with σ_{wT} and u evaluated at h_{es}; not as an effective parameter. It is important to note that z_{ieff} depends on downwind distance since σ_{zs} is distance dependent. In fact, as eq. **(68)** suggests, this effective reflecting surface is only folding back the extreme tail of the upward distribution. Also, if the height of the receptor $z_r \geq z_{ieff}$ then the effective reflecting surface is not considered. This approach is also implemented for the penetrated source. For the penetrated and injected sources z_{ieff} is calculated using eq. **(68)** with σ_{zs} and h_{es} replaced by σ_{zp} and h_{ep} respectively.

5.4 Treatment of lateral plume meander

In AERMOD we include the effect that lower-frequency, non-diffusing eddies (i.e., meander) have on plume concentration. Meander (or the slow lateral back and forth shifting of the plume) decreases the likelihood of seeing a coherent plume after long travel times. This effect on plume concentration could best be modeled with a particle trajectory model, since these models estimate the concentration at a receptor by counting the number of times a particle is seen in the receptor volume. However, as a simple steady state model, AERMOD is not capable of producing such information. AERMOD accounts for meander by interpolating between two concentration limits: the coherent plume limit (which assumes that the wind direction is distributed about a well-defined mean direction with variations due solely to lateral turbulence) and the random plume limit, (which assumes an equal probability of any wind direction).

For the coherent plume, the horizontal distribution function (F_{yC}) has the familiar Gaussian form:

$$F_{yC} = \frac{1}{\sqrt{2\pi}\sigma_y} \exp\left(\frac{-y^2}{2\sigma_y^2}\right) \qquad \textbf{(69)}$$

where σ_y is the lateral dispersion parameter (see Section 0). For the random plume limit, the wind direction (and plume material) is uniformly distributed through an angle of 2π. Therefore, the horizontal distribution function F_{yR} takes the simple form:

$$F_{yR} = \frac{1}{2\pi x_r} \qquad \textbf{(70)}$$

where x_r is radial distance to the receptor. Although the form of the vertical distribution function remains unchanged for the two plumes, its magnitude is based on downwind distance for the coherent plume and radial distance for the random plume.

Once the two concentration limits (C_{Ch} - coherent plume; C_R - random plume) have been calculated, the total concentration for stable or convective conditions ($C_{c,s}$) is determined by interpolation. Interpolation between the coherent and random plume concentrations is accomplished by assuming that the total horizontal "energy" is distributed between the wind's mean and turbulent components. That is,

$$C_{c,s} = C_{Ch}\left(1-\sigma_r^2/\sigma_h^2\right)+C_R\left(\sigma_r^2/\sigma_h^2\right) \qquad \textbf{(71)}$$

where σ_h^2 is a measure of the total horizontal wind energy and σ_r^2 is a measure of the random component of the wind energy. Therefore, the ratio σ_r^2/σ_h^2 is an indicator of the importance of the random component and can therefore be used to weight the two concentrations as done in eq. **(71)**.

The horizontal wind is composed of a mean component $\overline{u}$, and random components σ_u and σ_v. Thus, a measure of the total horizontal wind "energy" (given that the alongwind and crosswind fluctuations are assumed equal i.e., $\sigma_u = \sigma_v$), can be represented as

$$\sigma_h^{\,2} = 2\widetilde{\sigma}_v^{\,2} + \overline{u}^2 \qquad \textbf{(72)}$$

where $\overline{u} = (\tilde{u}^2 - 2\tilde{\sigma}_v^2)^{1/2}$. The random energy component is initially $2\tilde{\sigma}_v^2$ and becomes equal to σ_h^2 at large travel times from the source when information on the mean wind at the source becomes irrelevant to the predictions of the plume's position. The evolution of the random component of the horizontal wind energy can be expressed as

$$\sigma_r^2 = 2\tilde{\sigma}_v^2 + \overline{u}^2\left(1-\exp\left({}^{-x_r}/_{\tilde{u}T_r}\right)\right) \qquad \textbf{(73)}$$

where T_r is a time scale (= 24 hrs) at which mean wind information at the source is no longer correlated with the location of plume material at a downwind receptor. Analyses involving autocorrelation of wind statistics (Brett and Tuller 1991) suggest that after a period of approximately one complete diurnal cycle, plume transport is "randomized." Equation **(73)**

shows that at small travel times, $\sigma_r^2 = 2\tilde{\sigma}_v^2$, while at large times (or distances) $\sigma_r^2 = 2\tilde{\sigma}_v^2 + \overline{u}^2$, which is the total horizontal kinetic energy (σ_h^2) of the fluid. Therefore, the relative contributions of the coherent and random horizontal distribution functions (eq. **(71)**) are based on the fraction of random energy contained in the system (i.e., σ_r^2/σ_h^2).

The application of eq. **(71)** is relatively straight forward in the SBL. Since concentrations in the SBL are represented as a single plume, C_s can be calculated directly from eq. **(71)**. By contrast for convective conditions the situation is complicated by the inclusion of plume penetration. Since σ_r^2 depends on the effective parameters (eq. **(73)**), the concentration weighting factors found in eq. **(71)** will be different for the non-penetrated and penetrated plumes of the CBL. This is handled by combining the penetrated and non-penetrated weighting factors ($\sigma_r^2/\sigma_h^2|_P$ and $\sigma_r^2/\sigma_h^2|_{NP}$) into a single effective factor ($\sigma_r^2/\sigma_h^2|_{CBL}$). That is,

$$\left.\sigma_r^2 \middle/ \sigma_h^2\right|_{CBL} = f_p \cdot \left.\sigma_r^2 \middle/ \sigma_h^2\right|_P + \left(1 - f_p\right) \cdot \left.\sigma_r^2 \middle/ \sigma_h^2\right|_{NP} \qquad \textbf{(74)}$$

where f_p (see eq. **(55)**) is the fraction of the source material that remains trapped in the CBL. Using eq. **(74)**, concentrations in the CBL (C_c) are calculated from eq. **(71)** with (σ_r^2/σ_h^2) replaced by ($\sigma_r^2/\sigma_h^2|_{CBL}$).

5.5 Estimation of dispersion coefficients

The overall standard deviations ($\sigma_{y,z}$) of the lateral and vertical concentration distributions are a combination of the dispersion (represented by σ_{ya}, σ_{za}) resulting from ambient turbulence, and dispersion (σ_b) from turbulence induced by plume buoyancy. Building induced dispersion is not included here since a separate approach (see Section 0) is taken for situations in which building wake effects contribute to the total dispersion. Dispersion induced by ambient turbulence is known to vary significantly with height, having its strongest variation near the earth's surface. Unlike present regulatory models, AERMOD has been designed to account for the effect of variations of turbulence with height on dispersion through its use of "effective parameters" (see Section 0), which are denoted by an overscript tilde, e.g., $\tilde{\sigma}_{wT}$.

AERMOD treats vertical dispersion from ambient turbulence (σ_{za}) as a combination of a specific treatment for surface dispersion and the more traditional approach based on Taylor (1921) for elevated dispersion. Using this approach good agreement with observations was achieved in the SBL. However, the results in the CBL indicated that the treatment of lateral dispersion near the surface was problematic. This problem was corrected through the development of an empirical relationship for σ_{ya} near the surface using the full (CBL and SBL) Prairie Grass data set. A description of the resulting formulations for σ_{ya} & σ_{za} is presented in the next section.

The approach used to combine the above contributions to dispersion assumes that the effects are independent of one another. Thus, the total dispersion coefficients, for situations that do not include building downwash effects, are calculated from the following general expression (Pasquill and Smith 1983):

$$\sigma_{y,z}^2 = \sigma_{ya,za}^2 + \sigma_b^2, \qquad \textbf{(75)}$$

where the subscripts y and z are deleted from σ_b because σ_{yb} is assumed equal to σ_{zb}. With the exception of the CBL's penetrated source the form of eq. **(75)** applies to all source dispersion in both the CBL and SBL such that $\sigma_{y,z}$ becomes $\sigma_{ys,zs}$ and $\sigma_{yjs,zj}$ and $\sigma_{ya,za}$ becomes $\sigma_{yas,zas}$ and $\sigma_{yajs,zaj}$ for the SBL and CBL, respectively. For the penetrated source, the total dispersion is assumed to include ambient and buoyancy induced turbulence only; building wakes are assumed to have little influence. For the injected source, the total dispersion is calculated as if the source were in the SBL.

A comment on notation: eq. **(75)** applies for both lateral and vertical dispersion in the SBL and CBL. In references to the SBL, σ_z appears as σ_{zs} in the dispersion equation; σ_{za} appears as σ_{zas}. In reference to the CBL, σ_z appears as σ_{zj} for the dispersion expression applicable to the direct and indirect sources and σ_{za} appears as σ_{aj}; for the penetrated source σ_z appears as σ_{zp} in the dispersion expression.

5.5.1 Dispersion from ambient turbulence

5.5.1.1 Lateral dispersion from ambient turbulence

In general terms, the ambient component of the lateral dispersion is based upon Taylor (1921) such that:

$$\sigma_{ya} = \frac{\tilde{\sigma}_v \, x}{\tilde{u}\left(1 + \frac{x/\tilde{u}}{2T_{Ly}}\right)^p} \qquad \textbf{(76)}$$

where $p = 0.5$, u is the wind speed, σ_v is the root-mean-square lateral turbulence velocity, and T_{Ly} is the Lagrangian integral time for the lateral turbulence. Application of eq. **(76)** in a preliminary version of AERMOD yielded poor concentration estimates in comparison to those found in the Prairie Grass field experiments (Barad 1958). Specifically, the lateral spread was not well matched. Therefore, the lateral dispersion expression was reformulated to allow for an empirical fit to the Prairie Grass data.

Using an approach similar to that of Venkatram et al. (1984) T_{Ly} is found to be l/σ_v where l is an appropriate length scale for lateral turbulence. Equation **(76)** can be written in terms of the non-dimensional downwind distance X and a non-dimensional height scale α as:

$$\sigma_{ya} = \frac{\tilde{\sigma}_v x}{\tilde{u}\left(1 + \alpha X\right)^p} \qquad \textbf{(77)}$$

where $X(= \tilde{\sigma}_v \, x/\tilde{u} \, z)$ is the non-dimensional distance with u and σ_v given by effective parameters, where $\alpha = z_i / l$, and z_i is the mixed layer height.

Based on a preliminary comparison of σ_{ya} (eq. **(77)**) with selected stable and convective cases from the Prairie Grass experiment (Barad 1958) α was found equal to 78 and p equal to

0.3. As such, α is treated as a fitting parameter. In later comparisons against the full Prairie Grass data set (Figure 16), eq. **(77)** tended towards the lower envelope of this widely scattered data (i.e., lateral dispersion estimates are on the lower end of the distribution of measurements). However, the preliminary values of α (= 78) and p (= 0.3) produced good agreement between AERMOD concentration predictions and observations (Brode 2002). Therefore, these preliminary values were retained in AERMOD, and eq. **(77)** applies for the calculation of σ_{ya} for all plumes in both the SBL and CBL.

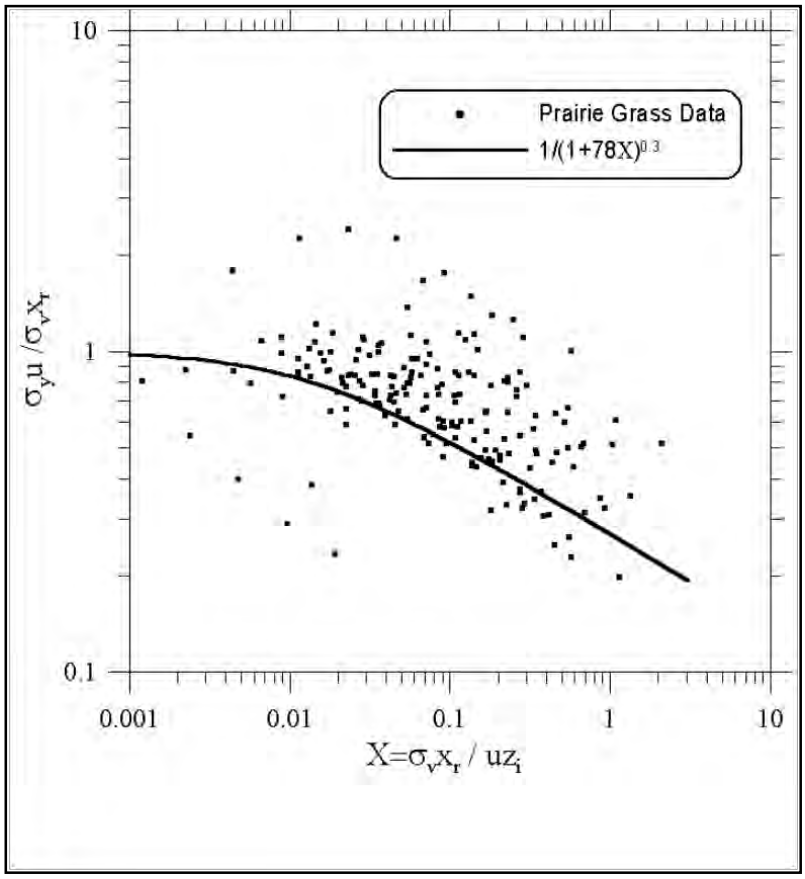

Figure 16. Lateral spread (Fy) as a function of non-dimensional distance (X). The data is taken from the Prairie Grass experiment (Barad, 1958)

The ambient component of the lateral dispersion for the penetrated source, i.e. a source which has been released below z_i, but penetrates above, is calculated using eq. **(77)** with h_{es} set equal to h_{ep} (the height of the penetrated source). However, for the injected source, i.e. source released above z_i, no substitution is needed since these sources are modeled as a stable source.

To account for the increase in the turbulence length scale and hence the Lagrangian time scale with release heights greater than that at Prairie Grass, α is scaled as follows:

$$\alpha = 78\left(z_{PG}/z_{\max}\right) \qquad \textbf{(78)}$$

where z_{PG} = 0.46 m (Prairie Grass release height), and $z_{max} = \max(z; z_{PG})$. To insure that α does not become unrealistically large for surface releases, z is not allowed below z_{PG} (i.e., 0.46 m). In the SBL, $z = h_{es}$; in the CBL $z = h_s$; for penetrated sources, $z = h_{ep}$. . As α becomes small for large release heights, σ_{ya} would tend to grow linearly with downwind distance.

5.5.1.2 Vertical dispersion from ambient turbulence

For sources in the SBL (and for sources in the CBL that are emitted directly into the stable layer above the mixed layer), the ambient portion of the vertical dispersion (σ_{zas}) is composed of an elevated (σ_{zes}) and near-surface (σ_{zgs}) component. For $h_{es} < z_i$ simple interpolation provides a smooth transition between the two components.

$$\sigma_{zas} = \left(1 - \frac{h_{es}}{z_i}\right)\sigma_{zgs} + \left(\frac{h_{es}}{z_i}\right)\sigma_{zes}. \qquad \textbf{(79)}$$

For $h_{es} \geq z_i$ σ_{zas} is set equal to σ_{zes}. The expressions for calculating h_{es} are found in Section 0. It should be noted, for sources in the SBL, that σ_{zas} is the specific form of the ambient portion of the vertical dispersion (i.e., σ_{za} in eq. **(75)**).

In the SBL, the elevated portion of the vertical dispersion follows the form of eq. **(76)**:

$$\sigma_{zes} = \widetilde{\sigma}_{wT}\left(x/\widetilde{u}\right)\Big/\left(1 + \frac{x/\widetilde{u}}{2T_{Lzs}}\right)^{1/2}, \qquad \textbf{(80)}$$

where σ_{wT} is the vertical turbulence due to the mechanical mixing (Cimorelli et al., 2004).

As with the lateral component, the Lagrangian time scale (T_{Lzs}) for the vertical turbulence can be written in the form (Venkatram et al. 1984)

$$T_{Lzs} = \frac{l}{\widetilde{\sigma}_{wT}} \tag{81}$$

The length scale l is an interpolation between the limiting length scales for neutral conditions and stable conditions

$$\frac{1}{l} = \frac{1}{l_n} + \frac{1}{l_s}. \tag{82}$$

where $l_n = 0.36\, h_{es}$ and $l_s = 0.27\ \tilde{\sigma}_{wT}/N$. Under very stable conditions or at large heights, l approaches l_s. When conditions are near neutral, N is very small and l approaches l_n.

By combining eqs. **(80)**, **(81)**, and **(82)** we find the following expression that is used by AERMOD to compute σ_{zes}, the elevated portion of the vertical dispersion for the stable source:

$$\sigma_{zes} = \frac{\widetilde{\sigma}_{wT}\, t}{\left[1 + \frac{\widetilde{\sigma}_{wT}\, t}{2}\left(\frac{1}{0.36 h_{es}} + \frac{N}{0.27\widetilde{\sigma}_{wT}}\right)\right]^{1/2}}. \tag{83}$$

Finally, to complete the description of eq. **(79)**, the surface portion of vertical dispersion (σ_{zgs}) in the SBL, is calculated from Venkatram (1992) as

$$\sigma_{zgs} = \sqrt{\frac{2}{\pi}}\left(\frac{u_* x}{\tilde{u}}\right)\left(1 + 0.7\frac{x}{L}\right)^{-1/3} \tag{84}$$

For the direct and indirect sources in the CBL, the ambient portion of the vertical dispersion (σ_{za} of eq. **(75)**) is denoted as σ_{zaj} (j = 1, 2) to distinguish between updrafts and downdrafts. σ_{zaj} is composed of an elevated (σ_{zej}) and surface (σ_{zg}) portion and is given by

$$\sigma_{zaj}^2 = \sigma_{zej}^2 + \sigma_{zg}^2, \qquad \textbf{(85)}$$

where the elevated portion (σ_{zej}) is obtained from Weil et al. (1997)as

$$\sigma_{zej} = \alpha_b \frac{\sigma_{wj}\, x}{\tilde{u}}, \qquad \textbf{(86)}$$

where σ_{wj} is a parameter in the bi-Gaussian pdf (eq.**(53)**).

The expression $\alpha_b = \min(0.6 + 4H_p/z_i, 10.0)$ designed to be 1.0 above the surface layer ($H_p > 0.1\ z_i$) and to otherwise match Venkatram's (1992) result for vertical dispersion from a surface source in a neutral boundary layer.

For the CBL, the vertical dispersion from a source within the surface layer ($H_p\{x\} < 0.1\ z_i$) is parameterized by

$$\sigma_{zg} = b_c\left(1 - 10\left(H_p / z_i\right)\right)\cdot\left(u_*/\tilde{u}\right)^2 \cdot\left(x^2/|L|\right) \qquad \textbf{(87)}$$

where $b_c = 0.5$, u_* is the friction velocity, and L is the Monin-Obukhov length; above the surface layer ($H_p > 0.1 z_i$), σ_{zg} is assumed to equal zero. In the limit of a surface release ($H_p = 0$), the parameterization of eq. **(87)** follows the form suggested by Venkatram (1992) for vertical dispersion in the unstable surface layer; i.e., $\sigma_z \propto (u_*/\tilde{u})^2 x^2/|L|$. The parameterization is designed to: 1) agree with Venkatram's result in the limit of a surface release, 2) provide good agreement between the modeled and observed concentrations from the Prairie Grass experiment (Perry et al., 2005), and 3) decrease with source height in the surface layer and ultimately vanish

for above the surface layer. The constant b_c was chosen to satisfy the second design requirement. In the limit of a neutral boundary layer σ_{zg} is equal to zero.

The total vertical dispersion for the penetrated source σ_{zp} (= σ_z in eq. **(75)**) is a combination of both ambient and buoyancy effects. The ambient portion of the vertical dispersion for the penetrated source contains only an elevated component σ_{zes} (= σ_{zss}) since it is assumed to be decoupled from the ground surface by its location above z_i and therefore unaffected by the underlying surface. The ambient vertical dispersion for the penetrated source is computed as the elevated portion of a stable source (σ_{zes} of eq. **(83)**) with $N = 0$ and with no contribution from the surface component. The Brunt-Vaisala frequency, N, is set to zero because the penetrated plume passes through the well mixed layer (where $N \approx 0$) prior to dispersing to receptors within the mixed layer.

5.5.2 Buoyancy induced dispersion (BID) component of σ_y and σ_z

For all plumes, the buoyancy induced dispersion (BID) is calculated following Pasquill (Pasquill 1976) and Weil (1988b) as

$$\sigma_b = \frac{0.4\Delta h}{\sqrt{2}}, \qquad \textbf{(88)}$$

where Δh is the plume rise appropriate for each of the plume types (direct, indirect, penetrated, and stable plumes). The direct source plume rise is calculated from eq. **(91)**, stable plume rise (Δh_s) is calculated from eq. **(95)** and the plume rise for the penetrated source $\Delta h_p = h_{ep} - h_s$ where h_{ep} is calculated from eq. **(94)**).

5.5.3 Treatment of building downwash

AERMOD incorporates the Plume Rise Model Enhancements (PRIME) (Schulman et al. 2000) algorithms for estimating enhanced plume growth and restricted plume rise for plumes affected by building wakes (U.S. Environmental Protection Agency, 1995). PRIME partitions plume mass between a cavity recirculation region and a dispersion enhanced wake region based

upon the fraction of plume mass that is calculated to intercept the cavity boundaries. These boundaries are established from estimates of the locations of the lateral and vertical separation streamlines. Dispersion of the recirculated cavity mass is based on building geometry and is assumed to be uniformly mixed in the vertical. At the boundary of the cavity region, cavity mass is emitted into the wake region. Here, it is combined with plume mass that was not captured by the cavity and dispersed at an enhanced rate based on source location, release height and building geometry. The enhancement of turbulence within the wake decays gradually with distance, allowing for a smooth transition to ambient levels of turbulence in the far-field. A probability density function model and an eddy diffusivity model (Weil 1996) are used for dispersion estimates in the near-wake and far-wake regions, respectively. Plume rise, for sources influenced by a building, is estimated using a numerical model that includes effects from streamline deflection near the building, vertical wind speed shear, enhanced dilution from the turbulent wake and velocity deficit. In general, these building induced effects act to restrict the rise that the plume would have in the absence of the building.

PRIME was originally designed (Schulman et al., 2000) to enhance plume growth using Pasquill Gifford (PG) dispersion (Pasquill 1961; Gifford 1961). AERMOD's estimate of plume growth is based on dispersion parameters derived from profiles of turbulence (see Section 0), not from radiation base turbulence surrogates as is done in the PG approach. A basic design tenet for incorporating PRIME into AERMOD was to be as faithful as possible to the PRIME formulation while ensuring that 1) AERMOD's ambient dispersion was used in place of PG dispersion and 2) far beyond the wake region, where building influences should be insignificant, concentrations approach the AERMOD estimate. Therefore, within the wake, PRIME algorithms are use exclusively to calculate concentration with AERMOD-derived ambient turbulent intensities as input. To insure a smooth transition between concentrations estimated by PRIME, within the wake, and AERMOD estimates in the far field, concentrations beyond the wake are estimated as the weighted sum of the two calculations. That is, beyond the wake the total concentration (C_{total}) is calculated as follows:

$$C_{Total} = \gamma\, C_{\mathrm{Pr}\,ime} + (1-\gamma)\, C_{AERMOD} \qquad \textbf{(89)}$$

where C_{prime} is the concentration estimated using the PRIME algorithms with AERMOD-derived meteorological inputs, C_{AERMOD} is the concentration estimated using AERMOD without considering building wake effects, and γ the weighting parameter. The weighting parameter, γ, is designed such that the contribution from the PRIME calculation decreases exponentially with vertical, lateral and downwind distance from the wake. It is calculated as follows:

$$\gamma = \exp\left(\frac{-\left(x-\sigma_{xg}\right)^2}{2\sigma_{xg}^2}\right)\exp\left(\frac{-\left(y-\sigma_{yg}\right)^2}{2\sigma_{yg}^2}\right)\exp\left(\frac{-\left(z-\sigma_{zg}\right)^2}{2\sigma_{zg}^2}\right) \qquad \textbf{(90)}$$

where x is the downwind distance from the upwind edge of the building to the receptor, y is the lateral (crosswind) distance from the building centerline to the receptor, z is the receptor height above ground, σ_{xg} is longitudinal dimension of the wake, σ_{yg} is the distance from the building centerline to lateral edge of the wake, and σ_{zg} is the height of the wake at the receptor location.

5.6 Plume rise calculations in AERMOD

5.6.1 Plume rise in the CBL

The plume rise for the direct source is given by the superposition of source momentum and buoyancy effects following Briggs (1984).

$$\Delta h_d = \left(\frac{3F_m x}{\beta_1^2 u_p^2} + \frac{3}{2\beta_1^2}\cdot\frac{F_b x^2}{u_p^3}\right)^{1/3} \qquad \textbf{(91)}$$

where $F_m = (T/T_s)w_s^2 r_s^2$ the stack momentum flux, $F_b = g w_s r_s^2 (\Delta T/T_s)$ is the stack buoyant flux, r_s is the stack radius corrected for stack tip downwash, and β_1 (= 0.6) is an entrainment parameter. It should be noted that u_p is the wind speed used for calculating plume rise. In the CBL u_p is set equal to $u\{h_s\}$.

As shown in Figure 13, the indirect plume, which is included to treat the no flux condition at $z = z_i$, is modeled as a reflected version of the direct plume with an adjustment (Δh_i) to the reflected plume height to account for the delay in vertical mixing due to plume lofting at the top of the boundary layer. That height adjustment is given by

$$\Delta h_i = \left(\frac{2F_b z_i}{\alpha_r u_p r_y r_z} \right)^{1/2} \frac{x}{u_p}, \qquad \textbf{(92)}$$

where r_y and r_z are the lofting plume half-widths in the lateral and vertical directions, u_p is the wind speed used for plume rise, and $\alpha_r = 1.4$. The produce of cross-wind dimensions of the assumed elliptical plume is calculated from Weil et al. (1997) as

$$r_y r_z = r_h^2 + \frac{a_e \lambda_y^{3/2}}{4} \cdot \frac{w_*^2 x^2}{u_p^2} \qquad \textbf{(93)}$$

where $r_h = \beta_2 (z_i - h_s)$, $\beta_2 = 0.4$, $\lambda_y = 2.3$, and $a_e = 0.1$ (dimensionless entrainment parameter). For a derivation and discussion of Δh_i see Weil et al. (1997).

The height that the penetrated source achieves above z_i is calculated as the equilibrium plume rise in a stratified environment and is determined by the source buoyancy flux, the stable stratification above z_i, and the mean wind speed. In line with Weil et al. (1997), the penetrated source plume height, h_{ep}, is taken as the centroid of plume material above the inversion. For complete penetration ($f_p = 0$) $h_{ep} = h_s + \Delta h_{eq}$. However, for partial penetration ($f_p > 0$), h_{ep} is chosen as the average of the heights of the upper plume edge $h_s + 1.5\ \Delta h_{eq}$ and z_i, or

$$h_{ep} = \frac{h_s + z_i}{2} + 0.75 \Delta h_{eq}. \qquad \textbf{(94)}$$

where Δh_{eq} is defined in eq.**(56)**.

5.6.2 Plume rise in the SBL

Plume rise in the SBL is taken from Weil (1988b), which is modified by using an iterative approach which is similar to that found in Perry et al. (1989). When a plume rises in an atmosphere with a positive potential temperature gradient, plume buoyancy decreases because the ambient potential temperature increases as the plume rises; thus, plume buoyancy with respect to the surroundings decreases. To account for this, the plume rise equations have to be modified. With this modification, AERMOD computes stable plume rise, Δh_s, from Weil et al. (1988b) as

$$\Delta h_s = 2.66\left(\frac{F_b}{N^2 u_p}\right)^{1/3}\cdot\left[\frac{N' F_m}{F_b}\sin\left(\frac{N' x}{u_p}\right)+1-\cos\left(\frac{N' x}{u_p}\right)\right]^{1/3}, \qquad \textbf{(95)}$$

where $N' = 0.7N$ with N given by eq. **(58)**. N and u are evaluated initially at stack height. Once plume rise has been computed, subsequent plume rise estimates are made (iteratively until convergence) by averaging the u and N values at stack top with those at $h_s + \Delta h_s/2$. Equation **(95)** is used for downwind distances that are less than the distance to final rise (x_f). Beyond x_f, Δh_s remains constant. The distance at which the stable plume reaches its maximum rise is given by

$$x_f = \frac{u_p}{N'}\arctan\left(\frac{-F_m N'}{F_b}\right). \qquad \textbf{(96)}$$

Upon substituting eq. **(95)** for x in eq. **(97)** the maximum final rise of the stable plume $\Delta h_s\{x_f\}$ reduces to:

$$\Delta h_s\{x_f\} = 2.66\left(\frac{F_b}{u_p N^2}\right)^{1/3}. \qquad \textbf{(97)}$$

As with eq. **(95)**, the velocity, u_p, and N in eq. **(97)** are evaluated initially at stack height and then iteratively.

When the atmosphere is close to neutral, the Brunt Vaisala frequency, N, is close to zero, and eq. **(95)** can predict an unrealistically large plume rise. Under, these circumstances, plume rise is limited by atmospheric turbulence. This happens when the rate of plume rise under neutral conditions is comparable to σ_w. Under these conditions, stable plume rise (eq. **(97)**) is limited by the neutral rise calculated from Weil (1985) as

$$\Delta h_s = 1.2\, L_n^{3/5} \left(h_s + 1.2\, L_n \right)^{2/5} \qquad \textbf{(98)}$$

where the neutral length scale $L_n = F_b/(u_p u_*^2)$.

As the wind speed approaches zero, eq. **(95)** again predicts unrealistic values. In these near-calm conditions the stable plume rise (eq. **(97)**) is limited by the calm rise expression that is based on the work of Morton et al. (1956) and Briggs (1969) such that,

$$\Delta h_s = \frac{4 F_b^{1/4}}{N^{3/4}}. \qquad \textbf{(99)}$$

Finally, the stable plume rise is limited by a calculation of the unstable rise (see Section 0).

5.7 Source characterization

AERMOD gives the user the ability to characterize a source as either a point, an area, or a volume. AERMOD additionally has the capability of characterizing irregularly shaped area sources.

Point sources are characterized exactly as in the ISC3 model (U.S. Environmental Protection Agency, 1995). The input to the model includes the location, elevation, emission rate,

stack height, stack gas temperature, stack gas exit velocity, and stack inside diameter. The temperature, exit velocity, and diameter are required for plume rise calculations.

Similarly, volume sources require the same input as the ISC3 model. This includes the location, elevation height (optional), height of release, emission rate, the initial lateral plume size (σ_y) and initial vertical plume size (σ_z). AERMOD differs from ISC3 in the treatment of volume sources only in how the initial plume size is implemented. Where ISC3 uses the virtual source technique to account for initial plume size, AERMOD adds the square of the initial plume size to the square of the ambient plume size:

$$\sigma_y^2 = \sigma_{yl}^2 + \sigma_{yo}^2 \qquad \textbf{(100)}$$

where σ_{yo} is the initial horizontal plume size, σ_{yl} is the plume size before accounting for the initial size, and σ_y is the resultant plume size after accounting for the initial size.

The area source treatment is enhanced from that available in ISC3. In addition to being input as squares or rectangles, area sources may be input as circles or polygons. A polygon may be defined by up to 20 vertices. A circle is defined by inputting its center location and radius. The AERMOD code uses this information to create an equivalent nearly-circular polygon of 20 sides, with the same area as the circle.

As with ISC3, AERMOD allows for the calculation of a simple half-life decay.

5.8 Plume volume molar ration method (PVMRM)

PVMRM was first introduced in AERMOD in version 04300 as an option for modeling the conversion of NOx to NO2 in the presence of ozone. The implementation is based on the work of Hanrahan (1999) and adapted for AERMOD. Details regarding the formulation of the PVMRM option in AERMOD, and preliminary model evaluation results are available in U.S. Environmental Protection Agency (2015).

5.8.1 Definition of plume volume

5.8.1.1 Total vs. relative dispersion

The PVMRM determines the conversion rate for NO_x to NO_2 based on a calculation of the NO_x moles emitted into the plume, and the amount of O_3 moles contained within the volume of the plume between the source and receptor. The dispersion algorithms in AERMOD and other steady-state plume models are based on the use of total dispersion coefficients, which are formulated to represent the time-averaged spread of the plume. A more appropriate definition of the volume of the plume for purposes of determining the ozone moles available for conversion of NOx is based on the instantaneous volume of the plume, which is represented by the use of relative dispersion coefficients, (Cole and Summerhays, 1979; Bange, 1991). The implementation of PVMRM in AERMOD is based on the use of relative dispersion coefficients to calculate the plume volume. Weil (1996 and 1998) has defined formulas for relative dispersion that are consistent with the AERMOD treatment of dispersion, and which can be calculated using meteorological parameters available within AERMOD.

5.8.1.2 Calculation of relative dispersion coefficients

The formula for relative dispersion combines the effects of buoyancy-induced turbulence, which should dominate close to the source, and ambient turbulence, which begins to dominate further downwind. Since the travel time from the source to the receptor is important for defining relative dispersion, the relative dispersion coefficients are calculated based on the radial distance from source to receptor. Weil (1996 and 1998) assumes relative dispersion (σ_r) to be isotropic, so that $\sigma_{rx} = \sigma_{ry} = \sigma_{rz} = \sigma_r$. The relative dispersion (σ_r) due to the combined effects of buoyancy- induced turbulence (σ_{rb}) and ambient turbulence (σ_{ra}) is parameterized as follows:

$$\sigma_r = (\sigma_{rb}^3 + \sigma_{ra}^3)^{1/3} \qquad \textbf{(101)}$$

The buoyancy-induced dispersion term, σ_{rb}, is calculated in AERMOD as

$$\sigma \frac{0.4\ \Delta h}{\sqrt{2}} \quad \textbf{(102)}$$

where Δh is the plume rise. Relative dispersion due to ambient turbulence, σ_{ra}, is parameterized by

$$\sigma_{ra} = \frac{a_1 \varepsilon^{1/2} t^{3/2}}{1 + a_2 t / T_{Lr}} \quad \textbf{(103)}$$

where a_1 is a constant (= 0.57), $a_2 = 0.62\ a_1$, t is the plume travel time (= x/U), and T_{Lr} is a Lagrangian time scale for relative dispersion defined as

$$T_{Lr} = a_{r1} \frac{z_i}{\sigma_w} \quad \textbf{(104)}$$

where $a_{r1} = 0.46$, z_i is the mixing height, and σ_w is the vertical turbulence parameter. The turbulence dissipation rate, γ, is calculated as follows, based on Weil (1996):

$$\varepsilon = \frac{b \sigma_w^2}{T_{Lr}} \quad \textbf{(105)}$$

where b is a constant (= 0.78). The values of wind speed (U) and σ_w used in eqs. **(103)** through **(105)** are the effective values, calculated as averages across the layer from the plume centroid height to the receptor height (up to $2.15\Phi_z$), following the procedure used in AERMOD to calculate effective values. Using the effective values of σ_w, AERMOD calculates effective values of the turbulence dissipation rate, γ.

Since the relative dispersion coefficients are source- and meteorology-dependent in AERMOD, the model generates a table of relative dispersion coefficients as a function of distance for the dominant source for each receptor and each hour in order to complete the plume volume calculation.

The original PVMRM utilized the relative dispersion coefficients described above to define the plume volume. These relative dispersion coefficients are applicable to unstable/ convective conditions, but are likely to overpredict the plume volume for stable conditions, resulting in overpredictions of NO_2 concentrations. The PVMRM algorithm was modified for version 15181 to use the "standard" total dispersion coefficients incorporated in AERMOD to define the plume volume during stable conditions.

5.8.1.3 Treatment of volume and area sources

If the dominant source is a volume source, then the initial lateral and vertical dimensions of the volume source are included in the calculation of the relative dispersion coefficients for purposes of calculating the plume volume, as follows:

$$\sigma_r = (\sigma_{rb}^3 + \sigma_{ra}^3 + \sigma_0)^{1/3} \quad \textbf{(106)}$$

where σ_0 is the initial dispersion coefficient of the volume source calculated as $\sqrt{\sigma_{y0}\sigma_{z0}}$ based on the initial lateral (Φ_{y0}) and vertical (Φ_{z0}) dimensions input by the user. If a volume source is included among the major contributing sources it is treated the same as a point source in defining the combined plume volume.

For application of PVMRM to area sources, the plume volume is extended laterally if necessary to include the projected width of the area source or sources that are included among the major contributing sources. The emissions from an area source are included in the calculation of the NO_x moles emitted into the plume if the centroid of the area source is within the box defined by the alongwind and crosswind extent of major contributing sources. In addition, if an area source is the dominant source, then the relative dispersion coefficients are calculated based on the radial distance from the centroid of the area source to the receptor.

5.8.1.4 Defining extent of plume

Since relative dispersion coefficients are used to define the plume volume, the number of standard deviations from the plume centerline, n_z, used in the calculation of plume volume was increased from the value used by Hanrahan (1999) for ISCST3. The ISCST3 postprocessor version used a value of 1.282 for n_z, corresponding to 80 percent of the area under the normal curve. The plume volume calculations for AERMOD are based on a value of $n_z = 4.0$, which corresponds to about 99.99 percent of the area under the normal curve. The minimum value of the dispersion coefficient was also reduced from the 15m minimum used with ISCST3 to a minimum of 5m for AERMOD in order to maintain approximately the same minimum plume volume in AERMOD as used for ISCST3. A minimum value of 4.8m in AERMOD would provide the same minimum plume volume as used by ISCST3 with $n_z = 1.282$ and a minimum dispersion coefficient of 15m.

The original implementation of PVMRM used four (4) times the relative dispersion coefficients to define the plume volume, which accounts for more than 99.99% of the plume. Given the fact that the PVMRM option in AERMOD assumes full and instantaneous mixing of the NO and O3 within the plume, using such a large percentage of the plume volume may introduce a bias to overpredict ambient concentrations of NO_2. Beginning with version 15181, the PVMRM option uses 2.58 times the relative dispersion coefficients to define the plume volume for unstable conditions, which accounts for about 99% of the plume. For stable conditions, the PVMRM option uses 1.282 times the total dispersion coefficients to define the plume volume, consistent with the original approach proposed by Hanrahan (1999), which accounts for about 80 percent of the plume volume. However, since AERMOD incorporates a horizontal meander algorithm that increases lateral plume spread beyond that accounted for based on dispersion coefficients, the number of sigmas used to define the plume volume for stable conditions is adjusted to account for meander, i.e.,

$$NSUBZ = \min(2.15,1{,}282 * (SYEFF/SY)$$

where SYEFF is the effective σ_y value that replicates the plume centerline associated with meander, but based on a standard Gaussian plume calculation.

The original implementation of PVMRM used the radial distance from source to receptor to calculate the plume volume and the moles of NOx contained in the plume. Beginning with version 15181, the downwind distance is used to calculate these values. Use of the downwind distance provides a more realistic estimate of NOx conversion consistent with a straight-line, steady-state plume model, such as AERMOD.

5.8.1.5 Adaption for AERMOD terrain algorithm

The vertical dimension of the plume volume is based on the relative dispersion coefficient for the dominant source and the range in plume heights for the major contributing sources. Since the effective plume heights differ for the terrain following and terrain responding components, the vertical dimension was modified to calculate the range of plume heights separately for both the terrain following and terrain responding components, and then use a weighted value for the vertical dimension based on the terrain (plume state) weighting factor, *f*, defined in Section 0.

5.8.1.6 Treatment of penetrated plumes

For unstable conditions with partial or full plume penetration above the mixing height, z_i, separate relative dispersion coefficients are calculated for the penetrated portion of the dominant plume. For cases with partial penetration for the dominant plume, AERMOD calculates two plume volumes, one based on relative dispersion coefficients for the direct source and another based on the relative dispersion coefficients for the penetrated source. Since AERMOD uses the same dispersion coefficients for the direct and indirect sources, separate values of relative dispersion coefficients for the indirect source are not needed. The effective plume volume used in the application of PVMRM is based on a weighted average of the direct and penetrated plume volumes using the plume penetration factor (PPF) for the dominant source. The model stores the plume centroid heights for both the direct and penetrated plumes for all sources at each receptor, and these are used to incorporate the effect of the major contributing sources on the volumes for the direct and penetrated plumes.

5.8.2 Minimum ozone concentration for stable conditions

Conditions for implementation with ISCST3, due to the fact that surface measurements may be artificially low during nighttime stable conditions due to the formation of a stable vertical temperature gradient. Since the AERMOD model does not use Pasquill-Gifford (P-G) stability categories, this minimum ozone concentration was modified to use Monin-Obukhov length as the stability parameter. The AERMOD model first keeps track of the maximum ozone concentration over the previous 24 hours. If the Monin-Obukhov length is positive (i.e. stable), with a value of less than 50 meters (very stable), then the maximum ozone concentration over the previous 24 hours is used as the minimum value. If the Monin-Obukhov length is positive and the value is over 500 meters (nearly neutral), then no minimum ozone concentration is applied for that hour. If the Monin-Obukhov length is between 50 meter and 500 meters, then the minimum ozone concentration is determined by linear interpolation, i.e., the minimum value is calculated as O3MAX * (500 – L)/450, where O3MAX is the maximum ozone concentration over the previous 24 hours, and L is the Monin-Obukhov length in meters.

5.9 Adjustments for the urban boundary layer

Although urban surface characteristics (roughness, albedo, etc.) influence the boundary layer parameters at all times, the effects of the urban sublayer on the structure of the boundary layer is largest at night and relatively absent during the day (Oke 1998). An urban "convective-like" boundary layer forms during nighttime hours when stable rural air flows onto a warmer urban surface. Following sunset, the urban surface cools at a slower rate than the rural surface because buildings in the urban area trap the outgoing thermal radiation and the urban subsurface has a larger thermal capacity. AERMOD accounts for this by enhancing the turbulence above that found in the rural stable boundary layer (i.e., a convective-like urban contribution to the total turbulence in the urban SBL). The convective contribution is a function of the convective velocity scale, which in turn, depends on the surface heat flux and the urban mixed layer height. The upward heat flux is a function of the urban-rural temperature difference.

The urban-rural temperature difference depends on a large number of factors that cannot easily be included in applied models such as AERMOD. For simplicity, the data presented in

Oke (1973; 1982) is used to construct an empirical model. Oke presents observed urban-rural temperature differences for a number of Canadian cities with populations varying from about 1000 up to 2,000,000. These data represent the maximum urban effect for each city since they were collected during ideal conditions of clear skies, low winds, and low humidities. An empirical fit to the data yields the following relationship

$$\Delta T_{u-r} = \Delta T_{\max}\left[\, 0.1 \ln\left(P/P_o\right) + 1.0 \,\right], \qquad \textbf{(107)}$$

where ΔT_{max} = 12 ℃, P_o = 2,000,000 (the city population associated with the maximum temperature difference in Oke's data), and P is the population of the urban area being modeled.

Since the ambient nighttime temperature of an urban area is higher than its surrounding rural area, an upward surface heat flux must exist in the urban area. It is assumed that this upward surface heat flux is related to the urban-rural temperature difference through the following relationship

$$H_u = \alpha \rho c_p \Delta T_{u-r} u_*, \qquad \textbf{(108)}$$

where α is an empirical constant, ρ is the density of air, and c_p is the specific heat at constant pressure. This expression is analogous to the bulk transfer parameterization of heat flux over a homogeneous surface (e.g., Businger (1973)),with α defined as the "bulk" transfer coefficient. We chose α to ensure that the upward heat flux is consistent with maximum measured values of the order of 0.1 m s^{-1} °C . Because ΔT_{u-r} has a maximum value on the order of 10 °C, and u_* is on the order of 0.1 m s^{-1}, α should have a maximum value on the order of 0.1. Although we assume that α has a maximum (city center) value of about 0.1, AERMOD uses an effective value of α that is averaged over the entire urban area. Assuming a linear variation of α from 0 at the edge of the urban area to about 0.1 at the center of the urban area results in an areal average equal to one-third of that at the center (since the volume of cone is one-third of that of a right circular cylinder of the same height). Therefore, AERMIC tested an area-averaged value of α equal to 0.03 against the Indianapolis data. This choice for α is consistent with measured values

of the upward heat flux in Canadian cities reported by Oke (1973; 1982). The results of the developmental testing indicated that this choice for α resulted in an adequate fit between observations and AERMOD-predicted concentrations.

The mixing height in the nighttime urban boundary layer, z_{iu}, is based on empirical evidence presented in Oke (1973; 1982) that, in turn, suggests the following relationships:

$$z_{iu} \approx R^{1/2} \ \ and \ \ R \approx P^{1/2}, \qquad \textbf{(109)}$$

where R is a measure of the city size and P is the population of the city. The first relationship is based on the observed growth of the internal convective boundary layer next to shorelines (Venkatram 1978). The second relationship implicitly assumes that population densities do not vary substantially from city to city.

Equation **(103)** leads to the following equation for the nocturnal urban boundary layer height due to convective effects alone:

$$z_{iuc} = z_{iuo}\left(P/P_o\right)^{1/4} \qquad \textbf{(110)}$$

where z_{iuo} is the boundary layer height corresponding to P_o. Based on lidar measurements taken in Indianapolis (1991), and estimates of z_{iu} found by Bornstein (1968) in a study conducted in New York city, z_{iuo} is set to 400 m in AERMOD.

In addition, since effects from urban heating should not cause z_{iu} to be less than the mechanical mixing height, z_{iu} is restricted from being less than z_{im}. Therefore, the mixed layer height for the nighttime urban boundary layer is computed as:

$$z_{iu} = Max\left[z_{iuc};\, z_{im}\right]. \qquad \textbf{(111)}$$

Once the urban mixing height has been estimated, a surrogate convective velocity scale (appropriate for the magnitude of convective turbulence present) is computed by substituting z_{iu} and H_u into the definitional equation for w_* (Deardorff 1970). That is,

$$w_{*u} = \left(\frac{g H_u z_{iuc}}{\rho c_p T} \right)^{1/3} \qquad \textbf{(112)}$$

where w_{*u} is the urban nighttime convective velocity scale and T is the near-surface air temperature.

Having estimated w_{*u} the turbulence in the nighttime urban can be enhanced using the expressions found in Section 0. However, since for low level sources σ_{wT} depends primarily on u_* (see eqs. **(34)** and **(35)**) it is not possible to directly enhance σ_{wT} for these sources using w_{*u}. Therefore, an effective friction velocity (u_{*eff}) is developed as a surrogate for w_{*u} in the lower portion of urban PBL. We define u_{*eff} as the friction velocity that is consistent with $\sigma_{wm} = \sigma_{wc}$ at $z = 7z_o$. Assuming that $z = 7z_o$ is always less $0.1z_{iuc}$, u_{*eff} is estimated by equating σ_{wc} (eq. **(35)**) with σ_{wm} (eq. **(37)**) and solving for u_*. Once u_{*eff} is found, the urban friction velocity for nighttime conditions (u_{*u}) is calculated as the maximum of u_{*eff} and u_* (the rural and daytime urban friction velocity).

Then using the enhanced velocity scales u_{*u} and w_{*u}, the nighttime convective portion of the turbulence in the urban boundary layer is computed using the expressions turbulence found in Section 0. That is, σ_{wc} and σ_{wm} are calculated from eqs. **(35)** and **(37)** , respectively, with w_{*u} used in place of the daytime convective velocity scale (w_*) and u_{*u} substituted for the rural u_*. Furthermore, for consistency purposes, a urban nighttime Monin-Obukhov length is calculated using eq. **(8)** with substitutions u_{*u} for u_* and H_u (eq. **(108)**) for H.

Finally, the total nighttime turbulence in the urban boundary layer is calculated as the sum (in quadrature) of the convective and mechanical portions. With these enhanced levels, vertical dispersion due to ambient turbulence (σ_{za}) in the urban boundary layer is calculated from eq. **(83)** (the SBL formulation for σ_{za}) with the urban PBL assumed to be neutral (i.e., $N =$

0). For the lateral dispersion in the urban boundary layer, σ_{ya} is calculated using the SBL formulation given by eq.**(76)**.

The potential temperature gradient in the night-time urban boundary layer is set equal to the upwind rural profile (Section 0) for all heights above z_{iu}, and is assumed to be equal to a small positive value below z_{iu}; i.e.,

$$\begin{aligned} \partial\theta/\partial z &= 10^{-5} && for \quad z \le z_{iu} \\ \partial\theta/\partial z &= rural\ \ value && for \quad z > z_{iu}. \end{aligned} \qquad \textbf{(113)}$$

For plumes below z_{iu} , the effective reflection surface is set equal to the height of the urban boundary layer (i.e., $z_{ieff} = z_{iu}$). Plumes that rise above z_{iu} ($h_{es} > z_{iu}$) are modeled with a z_{ieff} that is calculated from eq. **(68)** with z_{im} replaced by z_{iu}. Plume rise in the urban stable boundary layer is calculated from eqs. **(95)-(99)** with $\partial\theta/\partial z$ taken from eq.**(113)**.

Use of this value for $\partial\theta/\partial z$ provides an appropriate near-neutral plume rise formulation that is expected within the nocturnal urban boundary layer. However, plume height in these conditions is not allowed to exceed 1.25 z_{iu}.

For daytime conditions ($L < 0$) in urban areas, AERMOD uses the same formulations as in rural areas (i.e., no urban-related adjustments to boundary layer characteristics).

6. List of symbols

B_o	Bowen ratio - ratio of the sensible to latent heat fluxes (dimensionless)
C_{AERMOD}	concentration estimated using AERMOD without considering building wake effects (g m^{-3})
$C_{c,s}\{x_r,y_r,z_r\}$	concentration contribution from the horizontal plume state - convective and stable (g m^{-3})
$C_{c,s}\{x_r,y_r,z_p\}$	concentration contribution from the terrain-following plume state - convective and stable (g m^{-3})
$C_c\{x_r,y_r,z_r\}$	total concentration (CBL) (g m^{-3})
$C_d\{x_r,y_r,z_r\}$	concentration contribution from the direct source (CBL) (g m^{-3})
$C_p\{x_r,y_r,z_r\}$	concentration contribution from the penetrated source (CBL) (g m^{-3})
$C_r\{x_r,y_r,z_r\}$	concentration contribution from the indirect source (CBL) (g m^{-3})
$C_s\{x_r,y_r,z_r\}$	total concentration (SBL) (g m^{-3})
$C_T\{x_r,y_r,z_r\}$	total concentration (CBL) (g m^{-3})
C_{ch}	concentration from the coherent plume used in meander calculations (gm^{-3})
C_R	concentration from the random plume used in meander calculations (g m^{-3})
C_D	neutral drag coefficient (cal g^{-1} $^{\circ}C^{-1}$)
C_{prime}	concentration estimated using the PRIME algorithms with AERMOD-derived meteorological inputs (g m^{-3})
c_p	specific heat at constant pressure (= 1004 J g^{-1} K^{-1})
F_b	plume buoyancy flux (m^4 s^3)
F_y	total horizontal distribution function - with meander (m^{-1})
F_{yC}	horizontal distribution function for a coherent plume (m^{-1})
F_{yR}	horizontal distribution function for a random plume (m^{-1})
F_G	flux of heat into the ground (W m^{-2})
F_m	plume momentum flux (m^4s^2)
F_z	total vertical distribution function (m^{-1})
f	plume state weighting function (dimensionless)
f_p	fraction of plume mass contained in CBL = (1 - penetration factor) dimensionless)
g	acceleration due to gravity (9.8 m s^{-2})
H	sensible heat flux (W m^{-2})
H_c	critical dividing streamline (m)
H_p	plume centroid height (m)
H_u	heat flux in the nighttime boundary layer (W m^{-2})
h_c	receptor specific terrain height scale (m)
h_{ep}	penetrated source plume height above stack base (m)
h_s	stack height corrected for stack tip downwash (m)
Δh	general symbol for distance dependent plume rise (m)

Δh_d	plume rise for the direct source (m)
Δh_{eq}	equilibrium plume rise in a stable environment (m)
Δh_h	depth of the layer between z_i and the stack top (m)
Δh_p	plume rise for the penetrated source (m)
Δh_i	plume rise for the indirect source (m)
Δh_s	plume rise for the stable source (m)
i_z	vertical turbulence intensity
k	von Karman constant k = 0.4 (dimensionless)
l	length scale used in determining the Lagrangian time scale (m)
l_n	neutral length scale - a component of l (m)
l_s	stable length scale - a component of l (m)
L	Monin-Obukhov length (m)
N	Brunt-Vaisala frequency (s^{-1})
N_h	Brunt-Vaisala frequency above z_i (s^{-1})
n	cloud cover (fractional)
P	population of urban area
p_y	lateral probability density function
p_z	vertical probability density function
p_w	probability density function of the instantaneous vertical velocities
Q	source emission rate (g/s)
R	solar insolation (W m^{-2})
R_n	net radiation (W m^{-2})
R_o	*clear sky solar insolation (W m^{-2})*
$r(\varphi)$	Albedo {solar elevation} (dimensionless)
r'	noontime albedo (dimensionless)
r_s	stack radius - corrected for stack tip downwash (m)
r_y	lateral dimension of an elliptical plume
r_z	vertical dimension of an elliptical plume
S	skewness factor (dimensionless)
T	ambient temperature (K)
T_{Ly}	lateral lagrangian time scale (sec)
T_{Lzc}	vertical lagrangian time scale for the CBL (sec)
T_{Lzs}	vertical lagrangian time scale for the SBL (sec)
T_r	time scale used in the meander algorithm (sec)
T_{ref}	ambient temperature - at reference temperature height (K)
T_s	stack gas temperature (K)
T_u	urban surface temperature (K)
t	time (sec)
ΔT	difference between stack gas and ambient temperature (K)
ΔT_{u-r}	urban-rural temperature difference (K)

u	wind speed (m s^{-1})
u_{cr}	minimum speed for which the expression for u*, in the SBL, has a rea*l* valued solution (m s^{-1})
u_o	defined in eq. **(14)** and used in eq. **(15)**
u_p	wind speed that is used for plume rise (m s^{-1})
u_{ref}	wind speed at reference height (m s^{-1})
u_{th}	wind speed instrument threshold - separate value for each data set (offsite & onsite) (m s^{-1})
u_*	surface friction velocity (m s^{-1})
u_{*eff}	effective surface friction velocity - surrogate for w_{*u} (m s^{-1})
u_{*u}	surface friction velocity for nighttime urban conditions (m s^{-1})
w	random vertical velocity in the CBL (m s^{-1})
$\overline{w}_j$	mean vertical velocity for the updraft (j = 1) and the downdraft (j = 2) distributions (m-s^{-1})
w_s	stack exit gas velocity (m-s^{-1})
w_*	convective velocity scale (m-s^{-1})
w_{*u}	urban nighttime convective velocity scale (m-s^{-1})
X	non-dimensional downwind distance (dimensionless)
x_r	downwind distance to a receptor (m)
x_f	distance to final plume rise (m) - eq. **(44)** for the CBL; eq. **(96)** for the SBL
x_m	downwind distance at which plume material uniformly mixed throughout the boundary layer (m)
(x_r,y_r,z_r)	receptor location
(x_t,y_t,z_t)	terrain point location
z_{base}	user specified elevation for the base of the temperature profile (i.e., meteorological tower)
z_c	total height of the plume in the CBL considering both plume rise and effects from convective turbulence (m)
z_i	mixing height (m): z_i = MAX [z_{ic}; z_{im}] in the CBL and z_i = z_{im} in the SBL
z_{ic}	convective mixing height (m)
z_{ie}	equilibrium height of stable boundary layer
z_{ieff}	height of the reflecting surface in the SBL or in the stable layer above the above the CBL (m)
z_{im}	mechanical mixing height (m)
z_{iu}	urban nighttime boundary layer mixing height (m)
z_{iuc}	urban nighttime boundary layer mixing height due to convective effects alone (m)
z_{msl}	height of stack base above mean sea level (m)
z_o	surface roughness length (m)

z_{PG}	release height used in the Prairie Grass experiment (m)
z_p	receptor "flagpole" height - height of a receptor above local terrain (m)
z_r	height of the receptor above local source base (m)
z_{ref}	reference height for wind (m)
z_{Tref}	reference height for temperature (m)
z_t	height of the terrain above mean sea level (m)
$\tilde{\alpha}$	general symbol used to represent the effective parameters in the treatment of the inhomogeneous boundary layer. In the text the effective values of the parameters u, σ_w, σ_v and TL are denoted by underscoring the character
γ	parameter used to weight C_{AERMOD} and C_{Prime} in estimating concentrations that are influenced by building downwash (dimensionless)
θ	potential temperature (K)
θ_*	temperature scale (K)
λ_j	weighting coefficient for the updraft (j = 1) and downdraft (j = 2) distributions of eqs. **(53)**,**(59)** and **(65)**
ρ	density of air (kg m^{-3})
σ_b	buoyancy induced dispersion for the direct & indirect sources (m)
σ_h^2	total horizontal wind "energy" used in the meander algorithm (m^2)
σ_r^2	random "energy" component of the total horizontal wind "energy" used in the meander algorithm (m^2)
σ_{SB}	Stephen Boltzman constant (5.67×10^{-8} $Wm^{-2}K^{-4}$)
σ_u	along-wind turbulence (m s^{-1})
σ_v	lateral turbulence (m s^{-1})
σ_{vc}	convective portion of the lateral turbulence (m s^{-1})
σ_{vo}	surface value of the lateral turbulence (m s^{-1})
σ_{vm}	mechanical portion of the lateral turbulence (m s^{-1})
σ_{vT}	total lateral turbulence (m s^{-1})
σ_w	vertical turbulence (m s^{-1})
σ_{wc}	convective portion of the vertical turbulence (m s^{-1})
σ_{wm}	mechanical portion of the vertical turbulence (m s^{-1})
σ_{wml}	mechanical portion of the vertical turbulence generated in the PBL (m s^{-1})
σ_{wmr}	mechanical portion of the vertical turbulence above the PBL (residual) (m s^{-1})
σ_{wT}	total vertical turbulence (m s^{-1})
σ_{xg}	longitudinal dimension of the building wake (m)
σ_y	total lateral dispersion for the direct & indirect sources (m)
$\sigma_{ya,zaj}$	ambient turbulence induced dispersion for the direct & indirect sources (m)
σ_{zas}	ambient dispersion for the stable source (m)
σ_{yg}	distance from the building centerline to lateral edge of the building wake (m)
σ_{yl}	lateral spread from combined effects of ambient turbulence and building downwash (m)

σ_{zp}	total dispersion for the penetrated source (m)
σ_{zs}	total dispersion for the stable source (m)
σ_{zaj}	ambient vertical dispersion for the updraft & downdrafts plumes (j = 1,2), respectively, for both the direct & indirect sources (m)
σ_{zej}	elevated portion of σ_{zaj} (m)
σ_{zes}	elevated portion of σ_{zas} (m)
σ_{zg}	height of the building wake at the receptor location (m)
σ_{zj}	total vertical dispersion for the updrafts and downdrafts (j = 1,2 respectively), for both the direct and indirect sources
σ_{zg}	surface portion of σ_{zaj} (m)
σ_{zgs}	surface portion of σ_{zas} (m)
τ	time constant controlling the temporal interpolation of z_{im} (sec)
φ	solar elevation angle
φ_p	fraction of plume mass below H_c (dimensionless)
Ψ_{dj}	total height of the direct source plume (i.e. release height + buoyancy + convection) (m)
Ψ_{rj}	total height of the indirect source plume (m)
ψ_m	similarity function for momentum (stability correction) - eq. **(7)** for the CBL and eq. **(29)** for the SBL (dimensionless)

Appendix A: Input / output needs and data usage

A.1 AERMET input data needs

Besides defining surface characteristics, the user provides several files of hourly meteorological data for processing by AERMET. At the present time AERMET is designed to accept data from any for the following sources: 1) standard hourly National Weather Service (NWS) data from the most representative site; 2) morning soundings of winds, temperature, and dew point from the nearest NWS upper air station; and 3) site-specific wind, temperature, turbulence, pressure, and radiation measurements (if available).

The minimum measured and/or derived data needed to run the AERMOD modeling system are as follows:

A.1.1 Meteorology

- wind speed (u);
- wind direction;
- cloud cover - opaque first then total (n);
- ambient temperature (t);
- morning sounding.

Cloud cover is also used in dry deposition calculations in the AERMOD model. Therefore, if cloud cover is missing and the Bulk Richardson Number Scheme is being used (see 3.3.1) then an equivalent could cover is calculated as follows, based on van Ulden and Holtslag (van Ulden and Holtslag 1985):

$$n_{eq} = \left(\frac{1 - \theta_* / 0.09}{0.5} \right)^{0.5} \qquad \textbf{(114)}$$

where θ_* is the temperature scale as calculated from eq. **(18)**.

A.1.2 Directionally and/or Monthly Varying Surface Characteristics

- noon time albedo (r');
- Bowen ratio (B_o);
- roughness length (z_o) -

For AERMET, the user can specify monthly variations of three surface characteristics for up to 12 upwind direction sectors. These include: the albedo (r), which is the fraction of radiation reflected by the surface; the Bowen ratio (B_o), which is the ratio of the sensible heat flux to the evaporation heat flux; and the surface roughness length (z_o) , which is the height above the ground at which the horizontal wind velocity is typically zero. The user will be guided by look-up tables (in the AERMET user's guide) of typical values for these three variables for a variety of seasons and land use types. The information presented in the user's guide is not be considered regulatory guidance. The user is encouraged to research the literature to determine the most appropriate values for surface characteristics, for a specific application.

A.1.3 Other

- Latitude;
- longitude;
- time zone;
- wind speed instrument threshold for each data set (u_{th}).

A.1.4 Optional

- solar radiation;
- net radiation (R_n);
- profile of vertical turbulence (σ_w);
- profile of lateral turbulence (σ_v)

A.2 Selection and use of measured winds, temperature, and turbulence in AERMET

A.2.1 Threshold Wind Speed

The user is required to define a threshold wind speed (u_{th}) for site-specific data sets. Although the current version of AERMOD cannot accept a separate u_{th} for NWS data, a separate u_{th} should be selected for each on-site data set being used.

A.2.2 Reference Temperature and Height

The reference height for temperature (z_{Tref}), and thus the reference temperature, is selected as the lowest level of data which is available between z_o & 100 m.

A.2.3 Reference Wind Speed and Height

The reference height for winds (z_{ref}), and thus the reference wind speed (u_{ref}), is selected as the lowest level of data which is available between 7 z_o & 100m. Although the current version of AERMOD cannot accept a separate z_{ref} for offsite data, we believe that a separate z_{ref} should be selected for each data set being used.

If no valid observation of the reference wind speed or direction exists between these limits the hour is considered missing and a message is written to the AERMET message file. For the wind speed to be valid its value must be greater than or equal to the threshold wind speed. AERMOD processes hours of invalid wind speed, e.g. calms, in the same manner as ISC (EPA calms policy).

All observed wind speeds in a measured profile that are less than u_{th} are set to missing and are therefore not used in the construction of the wind speed profile (profiling of winds is accomplished in AERMOD).

A.2.4 Calculating the Potential Temperature Gradient above the Mixing Height from Sounding Data

AERMET calculates $d\theta/dz$ for the layer above z_i as follows:

- If the sounding extends at least 500 m above z_i the first 500 m above z_i is used to determine $d\theta/dz$ above z_i.
- If the sounding extends at least 250 m above z_i (but not 500 m) then the available sounding above z_i is used to determine $d\theta/dz$ above z_i.
- AERMET limits $d\theta/dz$ above z_i to a minimum of 0.005 K m^{-1}.
- If the sounding extends less than 250 m above z_i then set $d\theta/dz$ = 0.005 K m^{-1} (a default value).

A.2.5 Measured Turbulence

All measured turbulence values are passed to AERMOD if the hour is non-missing. This is true even for those levels where the wind speed is below u_{th}. Based on measurements with research grade instruments, reasonable minimum turbulence levels in non-calm conditions for vertical turbulence (σ_w) and lateral turbulence (σ_v) values are set by AERMOD to 0.02 m s^{-1} and 0.2 m s^{-1}, respectively. Although these lower limits are applied to the measured values of the turbulence the calculated profile values of σ_w and σ_v are not subjected to any lower limits. We do not restrict these estimated profiles because it would bias the calculation of the effective values of turbulence, which are averages through the layer between the receptor and the plume height, in determining the dispersion of the plume. However, as discussed in Section 0, these limits are applied to the effective values of turbulence and wind speed.

A.2.6 Data Substitution for Missing On-Site Data

If on-site data are missing for an hour, the hour is considered missing unless the user specifies a substitute data set. AERMET does not default to NWS (or any other offsite) data.

A.3 Information passed by AERMET to AERMOD

The following information is passed from AERMET to AERMOD for each hour of the meteorological data record.

- All observations of wind speed (u)*;* wind direction*;* ambient temperature (T)*;* lateral turbulence (σ_v); & vertical turbulence (σ_w) with their associated measurement heights.
- Sensible heat flux (H), friction velocity (u_*), Monin Obukhov length L, z_{im} (for all hours), z_{ic} & w_* (for convective hours only), z_o , $r\{\varphi\}$, & B_o, $d\theta/dz$ (above z_i), u_{ref} , wind direction at the reference height, z_{ref}, ambient temperature at the reference height (T_{ref}) (not used in AERMOD), & the reference height for temperature (z_{Tref})

A.4 Restrictions on the growth of the PBL height

AERMET restricts the growth of z_i to a reasonable maximum of 4000 m. This restriction applies to both calculated and measured mixing heights. Although mixing heights in excess of 4000 m may occur on rare occasions, in desert climates, the additional effect on surface concentration is most likely insignificant.

A.5 Initializing the mechanical mixing height smoothing procedure

If $\{t + \Delta t\}$, in eq. **(26)**, is the first hour of the data set then no smoothing takes place. Furthermore, if a missing value occurs at time step t then smoothing is not performed at time step $\{t + \Delta t\}$ but is restarted for subsequent hours.

A.6 Determining the mixing height when the sounding is too shallow

The left hand side of eq. **(22)** is determined from the morning temperature sounding and the right hand side from the daytime history of surface heat flux. When the temperature sounding, obtained from the NWS, does not reach a height which is greater than the convective mixing height, we must assume a profile for the potential temperature gradient in order to estimate z_{ic}. This is accomplished as follows:

- Determine $d\theta/dz$ in the top 500 m layer of the sounding. However, if part of the 500 m layer is within the first 100 m of the PBL, the layer should be reduced (to a minimum thickness of 250 m) to avoid using the portion of the sounding that is below 100 m. If the above conditions cannot be satisfied then z_{ic} is defined as missing.
- Extend the sounding by persisting $d\theta/dz$ up and recomputing z_{ic}.
- Provide warning messages which tell users
  - the height of the actual sounding top,
  - that $d\theta/dz$ has been extrapolated above the sounding z_{ic}, and
  - that z_{ic} has been recomputed.
- Allow the user to reject the "fixed-up" value for z_{ic} by defining it as missing.

A.7 Input data needs for AERMAP

The following data is required input for AERMAP

- DEM formatted terrain data (x_t, y_t, z_t),
- Design of receptor grid; AERMAP accepts either polar, Cartesian or discrete receptors.

A.8 Information passed by AERMAP to AERMOD

AERMAP passes the following parameters to AERMOD: x_r, y_r, z_r, z_t, & the height scale (h_c) for each receptor.

A.9 Wind speed and turbulence limits used in model calculations

When calculating the effective parameters, limits are placed on the such that:

$$\begin{aligned} \sigma_w\{z\} &= Max\left[\sigma_w\{z\};\ 0.02\ ms^{-1}\right] \\ \sigma_v\{z\} &= Max\left[\sigma_v\{z\};\ 0.05u\{h_s\};\ 0.2\ ms^{-1}\right]. \end{aligned} \qquad \textbf{(115)}$$

These limits are also applied when selecting the turbulence for plume rise calculations.

Dilution of the plume is determined by the wind that corresponds to the average over the magnitudes of the wind vectors during a given time interval. But measurements only give the vector averaged wind, which can be zero, even though the dilution wind is not zero. We can estimate the dilution wind by assuming that the vector wind, u_v, can be expressed as

$$u_v = (\overline{u} + u',\, v') \qquad \textbf{(116)}$$

where $\overline{u}$ is the mean measured wind, and the primed quantities refer to the turbulent fluctuations. The assumption being made is $\overline{u_v} = \overline{u}$. If we assume that the measured velocity fluctuations correspond only to the angular variations of a constant vector, u_v, we can write from eq. **(116)** that

$$u_v^2 = \overline{u}^2 + \sigma_v^2 + \sigma_u^2 . \qquad \textbf{(117)}$$

In this simple model, u_v , is the dilution wind. If we take $\sigma_u = \sigma_v$, the dilution wind can be written as

$$u\{h_s\} = \sqrt{u\{h_s\}^2 + 2\,\sigma_v^2} . \qquad \textbf{(118)}$$

This formulation assures that the dilution wind is not zero as long as either $\overline{u}$ or σ_v is not zero. Similarly, at the time of plume rise calculations, the effective turbulence and effective wind speed will be recalculated using eqs. **(115)** and **(118)**, where the turbulence and winds will be evaluated at stack top.

A.10 Using profiles for interpolating between observations

When observations are available AERMOD uses the similarity profile functions to interpolate adjacent measurements. Figure 17 illustrates how AERMOD's INTERFACE uses the expected shape of a meteorological profile to interpolate between observations.

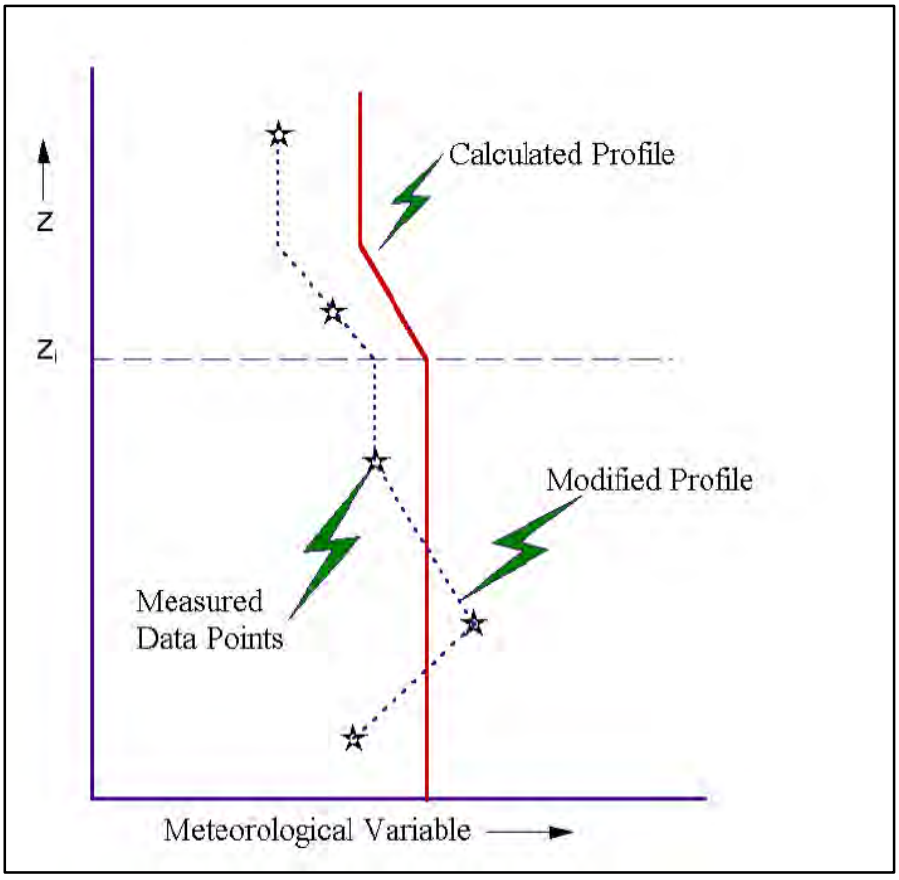

Figure 17. AERMOD's construction of a continuous meteorological profile by interpolating between observations.

For a gridded profile height between two observed profile heights, the observations are interpolated to the gridded height while maintaining the shape of the similarity profile. This is accomplished as follows:

1. the observations are linearly interpolated to the gridded profile height;

2. the similarity function is evaluated at the gridded profile height;

3. the similarity function is evaluated at the observed profile heights immediately above and below the grid height and linearly interpolated to the grid height;

4. the ratio of the value obtained in 2 to the value obtained in 3 is applied to the value obtained in 1.

For a gridded profile height above the highest observation, the procedure is modified slightly:

1. the observation at the highest observed profile height is extrapolated by persisting the value upward;

2. the similarity function is evaluated at the grid height;

3. the similarity function is evaluated at the highest height in the observed profile;

4. the ratio of the value obtained in 2 to the value obtained in 3 is applied to the value obtained in 1.

A similar procedure for extrapolating to heights above the observed profile is applied to heights below the lowest observed profile height.

A.11 Using measured mixing heights

If measured mixing heights are available, then they are treated in the following manner: If $L>0$ (SBL) the measured mixing height is defined as z_{ie} and it is treated the same as a calculated mechanical mixing height (smoothed as explained in Section 0). If $L<0$ (CBL) the measured mixing height is defined as z_{ic}, and z_{ie} is calculated from eq. **(24)**, smoothed, then proceed as if both z_{ic} and the smoothed z_{im} had been calculated values.

If a user has "measured" mixing heights available (and chooses to use them), AERMET defaults to substituting calculated mixing heights for missing measurements and a message is written that a substitution has occurred. If the user elects to substitute calculations for missing measurements, AERMET will print out a message to the message file for each hour that a substitution has occurred.

Appendix B: Model evaluation results

B.1 Introduction

This evaluation presents a benchmark of model performance based on the original field studies presented in Cimorelli, et al, 2005 and Perry, et al, 2005. The evaluation focused on the benchmarking the performance proposed (15181) and final (16216) versions of the AERMOD modeling system associated with the 2016 update to the *Guideline on Air Quality Models*. The statistical analysis determines the best performing version of the model for 14 of the original 17 databases, including the adjust u* option formally adopted as a regulatory option in the final version of AERMOD (16216).

B.2 Database descriptions

The 14 databases used in this evaluation are briefly described in this section and summarized in Table 1. The stack heights, terrain complexity, urban/rural status, importance of downwash, inclusion of turbulence parameters and meteorological data included for the database are listed for each area. A more complete description of these databases can be found in U.S. EPA, 2003. The databases are arranged by the following hierarchy: Two categories of turbulence inclusion (inclusion of turbulence or no turbulence). Within each of those categories, databases were ordered by complexity of terrain (complex or flat), and within those two categories, databases were ordered by increasing height.

Table 1. AERMOD evaluation databases used for comparisons of AERMOD 15181 and AERMOD 16216. Databases in gray are also subject to the EPA's protocol for determining best performing model.

Location	Stack heights	Urban /rural	Terrain	Downwash	Turbulence parameters	Site specific AERMET inputs
Martins Creek	59, 76, 183 m	Rural	Complex	Yes	10 m σ_v, σ_w	10m wind, temperature; 90-420 m wind (every 30 m).
Tracy	91 m	Rural	Complex	No	σ_v, σ_w	10 and 50-400 m (every 25 m) wind, temperature
Lovett	145 m	Rural	Complex	No	σ_v, σ_w	10, 50, and 100 m wind, temperature
Westvaco	190 m	Rural	Complex	No	σ_v, σ_w	30, 210, 326, 366, and 416 m wind, temperature[1]
DAEC	1 m, 24 m, 46 m	Rural	Flat	Yes	σ_v	Insolation, 10, 23.5 and 50 m wind, temperature
EOCR	1, 25, 30 m	Rural	Flat	Yes	σ_v	4, 10, and 30 m wind, temperature
Alaska	39.2 m	Rural	Flat	Yes	σ_v, σ_w	33 m wind, temperature
Indianapolis	84 m	Urban	Flat	No	σ_v, σ_w	Station pressure, net radiation, 10 m wind, temperature
Kincaid	187 m	Rural	Flat	No	σ_v, σ_w	Net radiation, insolation, 10 , 30, and 50 m wind, temperature
AGA	9.8, 14.5, 24.4 m	Rural	Flat	Yes	None	10 m wind and temperature
Millston	3 stacks 29 m (freon) 48 m (SF6)	Rural	Flat	Yes	None	10 m wind speed ; 43.3 m wind and temperature
Bowline	2 stacks 86.87 m	Rural	Flat	Yes	None	100 m winds and temperature
Baldwin	3 stacks 184.4 m	Rural	Flat	Yes	None[2]	10 and 100 m wind, temperature
Clifty Creek	3 stacks 207.9 m	Rural	Flat/Elev	No	None	10 m temperature; 60 m wind

- 1. 30 m observations removed from AERMOD profile before running AERMOD.

B.2.1 Martin's Creek

The Martins Creek Steam Electric Station is located in a rural area along the Delaware River on the Pennsylvania/New Jersey border, approximately 30 km northeast of Allentown, PA and 95 km north of Philadelphia, PA (Figure B-1). The area is characterized by complex terrain rising above the stacks. Sources included multiple tall stacks ranging from 59 to 183 m in height, including Martins Creek and three background sources located between 5 and 10 km from Martins Creek. The seven SO_2 monitors were located on Scotts Mountain, which is about 2.5 - 8 km southeast of the Martins Creek facility. On-site meteorological data covered the period from 1 May 1992 through 19 May 1993. Hourly temperature, wind speed, wind direction, and sigma-theta (standard deviation of the horizontal wind direction) at 10 m were recorded from an instrumented tower located in a flat area approximately 2.5 km west of the plant. In addition, hourly multi-level wind measurements were taken by a sodar located approximately three km southwest of the Martins Creek station.

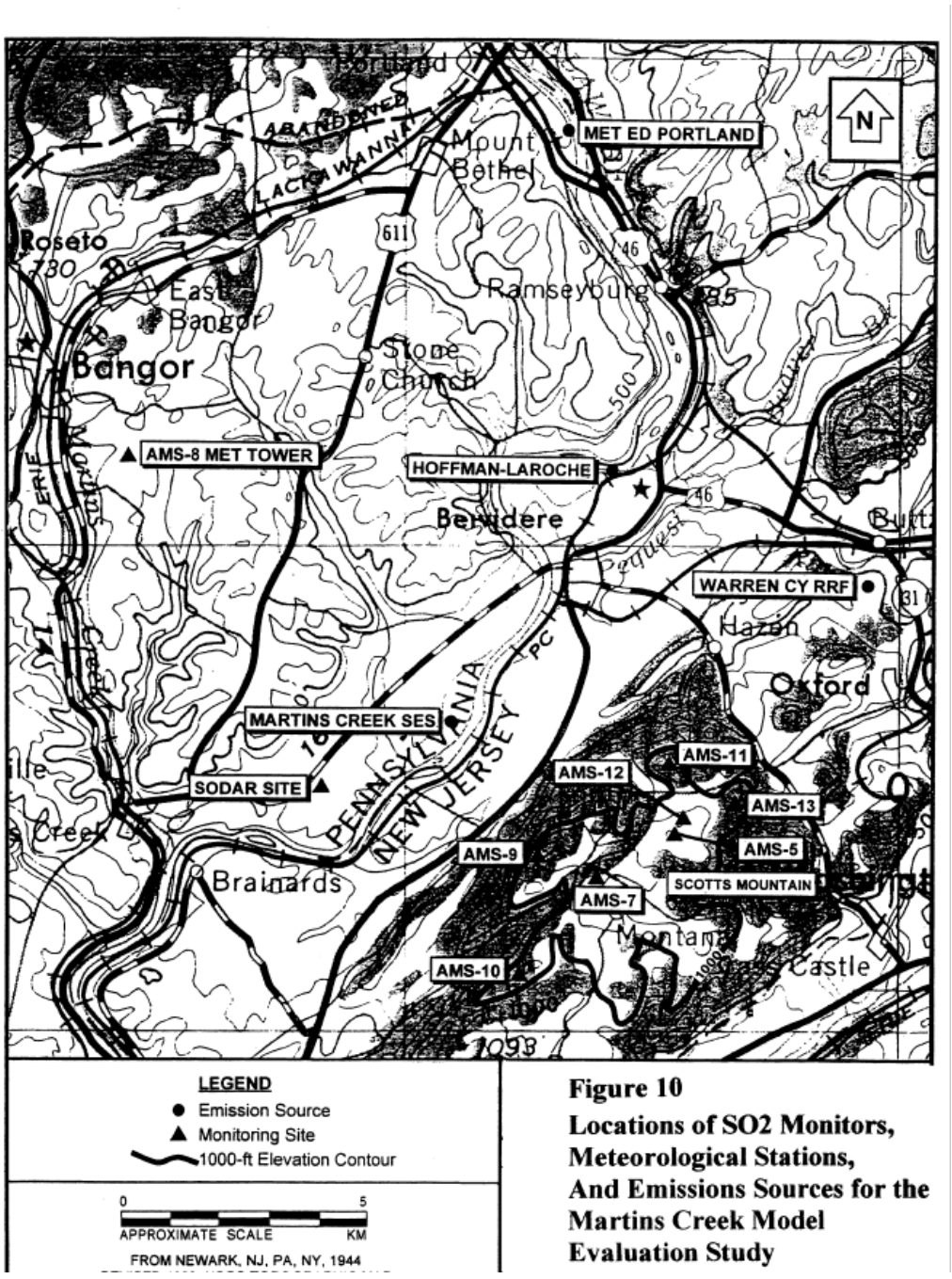

Figure 10
Locations of SO2 Monitors, Meteorological Stations, And Emissions Sources for the Martins Creek Model Evaluation Study

Figure B-1. Martin's Creek study area.

B.2.2 Tracy

The Tracy Power Plant is located 27 km east of Reno, Nevada in the rural Truckee River valley completely surrounded by mountainous terrain (Figure B-2). A field tracer study was conducted at the power plant in August 1984 with SF_6 being released with the moderately buoyant plume from a 91-m stack. A total of 128 hours of data were collected over 14 experimental periods. Stable atmospheric conditions were dominant for this study. Site-specific meteorological data (wind, temperature, and turbulence) for Tracy were collected from an instrumented 150-m tower located 1.2 km east of the power plant. The wind measurements from the tower were extended above 150 meters using a Doppler acoustic sounder and temperature measurements were extended with a tethersonde.

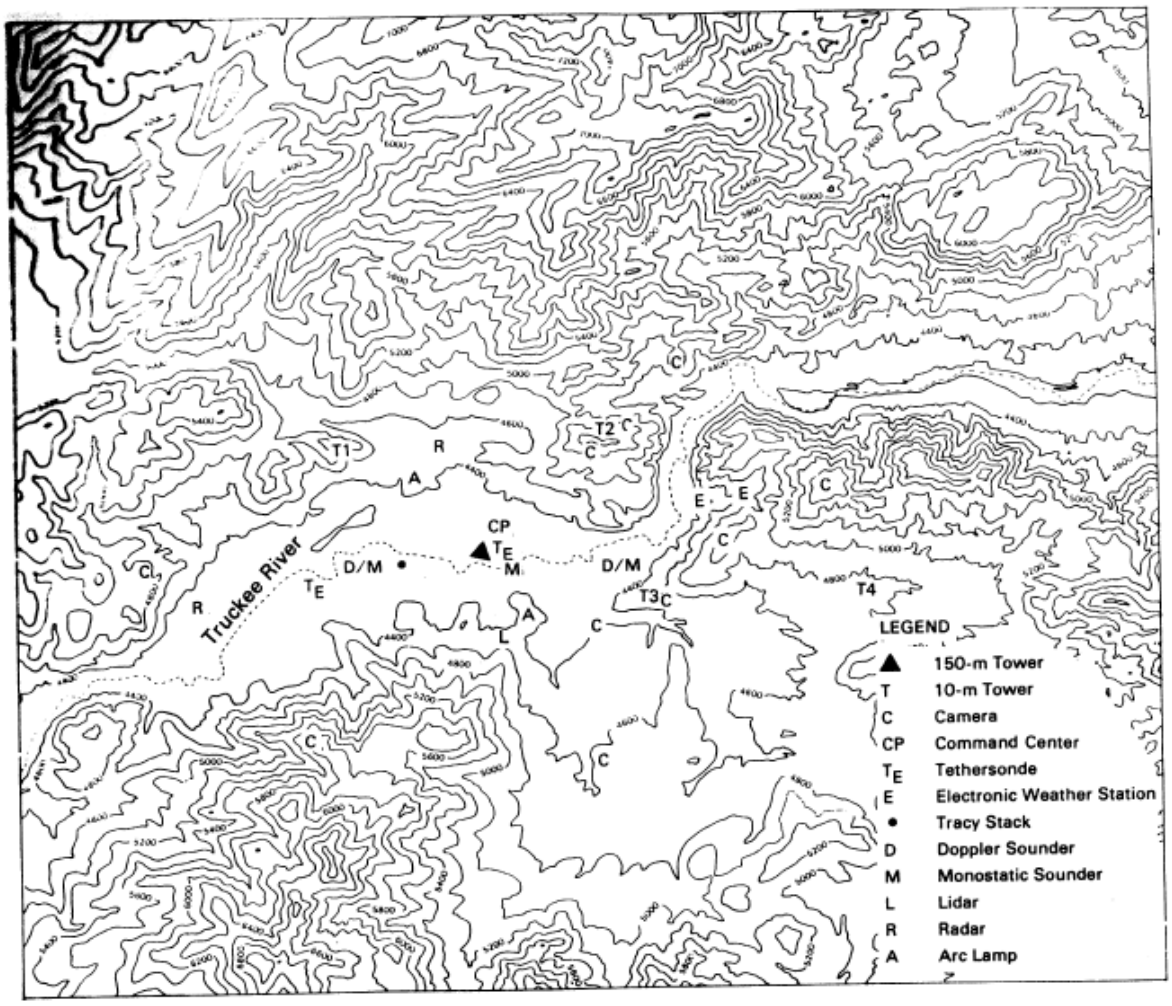

Figure B-2. Tracy power plant study area.

B.2.3 Lovett

The Lovett Power Plant study consisted of a buoyant, continuous release of SO2 from a 145-m tall stack located in a complex terrain, rural area in New York State (Figure B-3). The data spanned one year from December 1987 through December 1988. Data were collected from 12 monitoring sites (ten on elevated terrain and two near stack-base elevation) that were located about 2 to 3 km from the plant. The monitors provided hourly-averaged concentrations. The important terrain features rise approximately 250 m to 330 m above stack base at about 2 to 3 km downwind from the stack. Meteorological data include winds, turbulence, and ΔT from a towe instrumented at 10 m, 50 m, and 100 m. National Weather Service surface data were available from a station 45 km away.

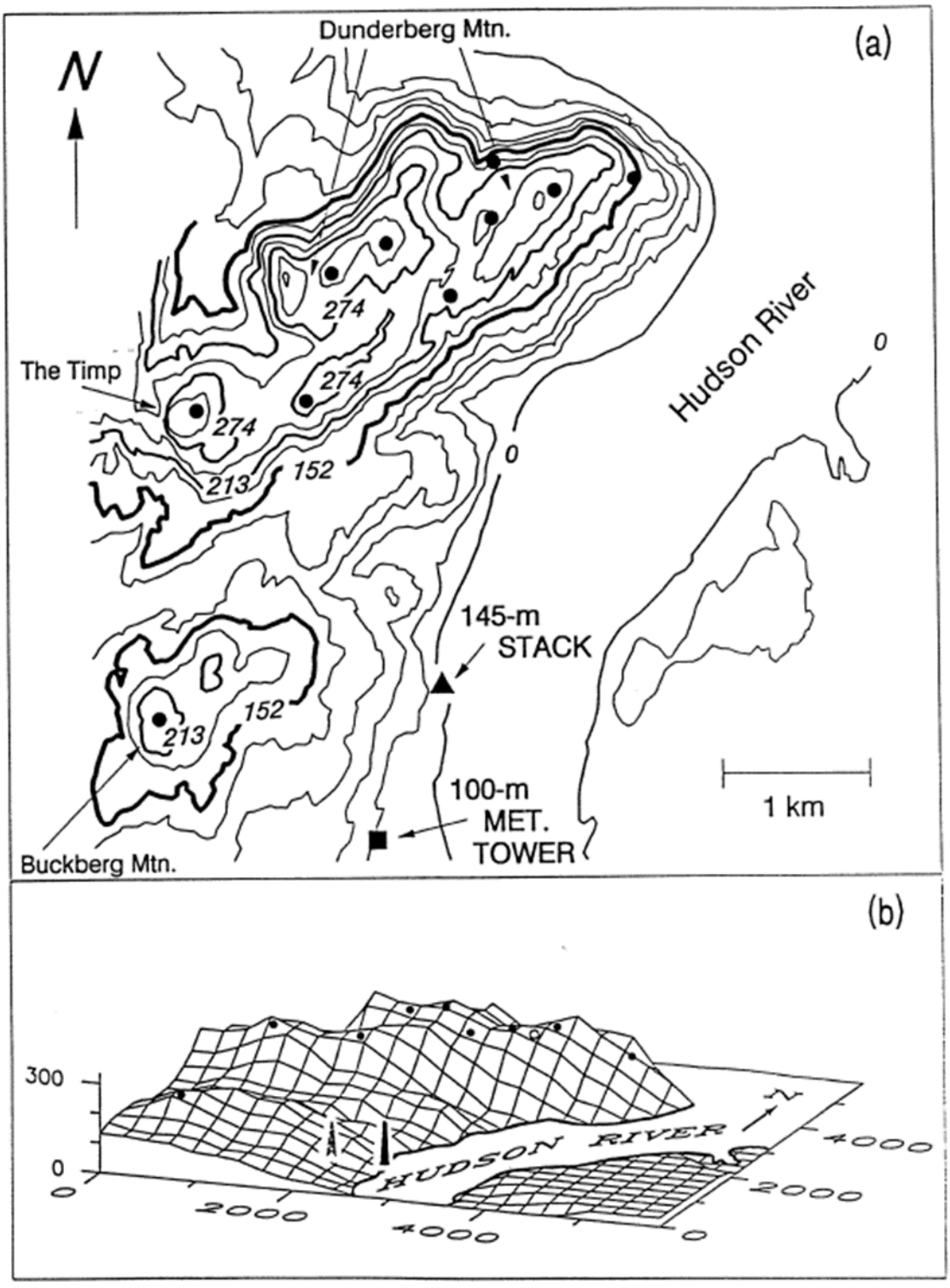

Figure B-3. Lovett study area.

B.2.4 Westvaco

The Westvaco Corporation's pulp and paper mill in rural Luke, Maryland is located in a complex terrain setting in the Potomac River valley (Figure B-4). A single 183-m buoyant source was modeled for this evaluation. There were 11 SO_2 monitors surrounding the facility, with eight monitors well above stack top on the high terrain east and south of the mill at a distance of 800 - 1500 m. Hourly meteorological data (wind, temperature, and turbulence) were collected between December 1980 and November 1991 at three instrumented towers: the 100-m Beryl tower in the river valley about 400 m southwest of the facility; the 30-m Luke Hill tower on a ridge 900 meters north-northwest of the facility; and the 100-m Met tower located 900 m eastsoutheast of the facility on a ridge across the river.

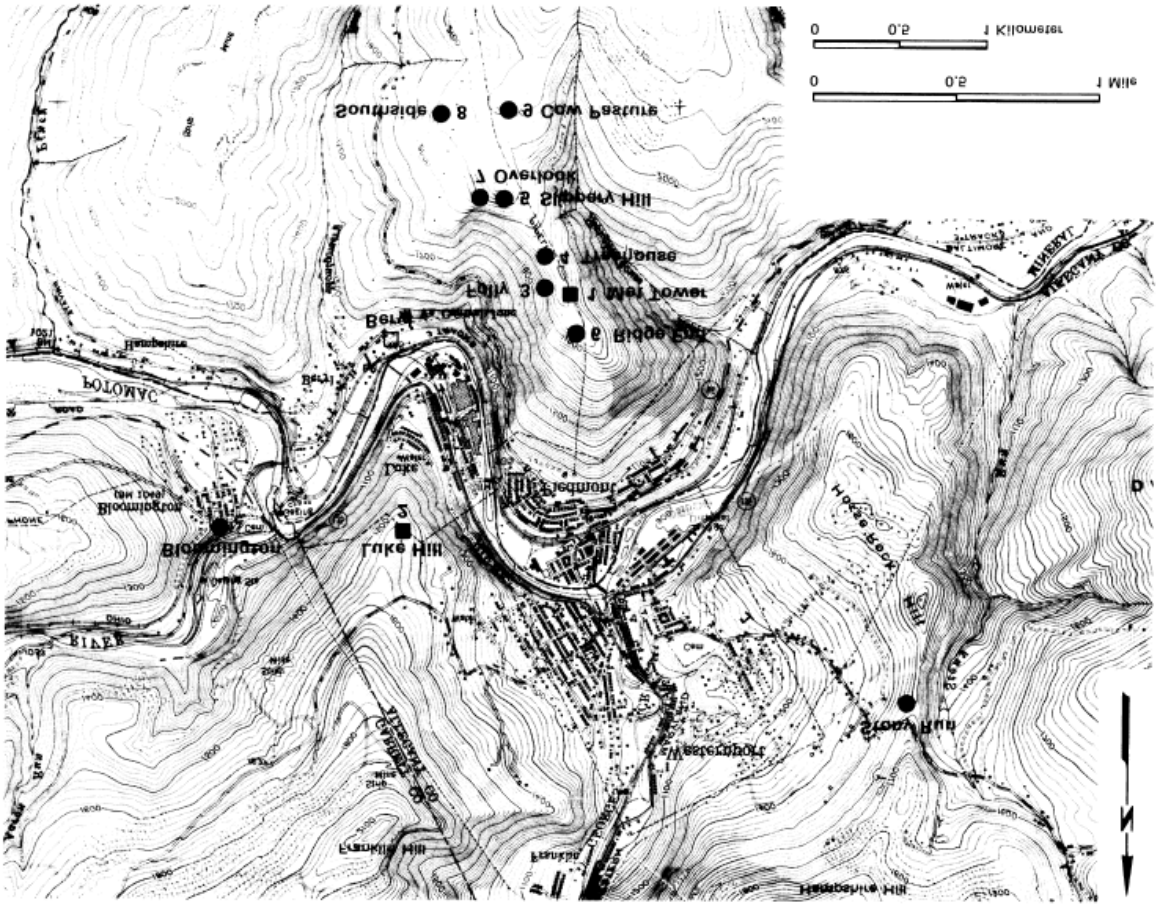

Figure B-4. Westvaco study area.

B.2.5 DAEC

The Duane Arnold Energy Center (DAEC) is located in rural Iowa, located about 16 km northwest of Cedar Rapids. It is located in a river valley with some bluffs on the east side. Terrain varies by about 30 m across the receptor network with the eastern half of the semicircular receptor arcs being flat and the western half elevated. The tracer study[35] involved SF_6 releases from two rooftops (46-m and 24-m levels) and the ground (1-m level). Building tiers for the rooftop releases were 43 and 24 m high, respectively. The 1-m and 24-m releases were non-buoyant, non-momentum, while the 46-m release was close to ambient, but had about a 10 m/s exit velocity. The number of tracer release hours was 12, 16 and 11 from the release heights of 46 m, 24 m, and 1 m, respectively. There were two arcs of monitors at downwind distances of 300 and 1000 m (see Figure B-5). Meteorological data consisted of winds at 10, 24, and 50 m. The meteorological conditions were mostly convective (30 out of 39 hours), with fairly light wind speeds. Only one hour had a wind speed above 4 m/s (4.6) , and almost half of the hours were less than 2 m/s.

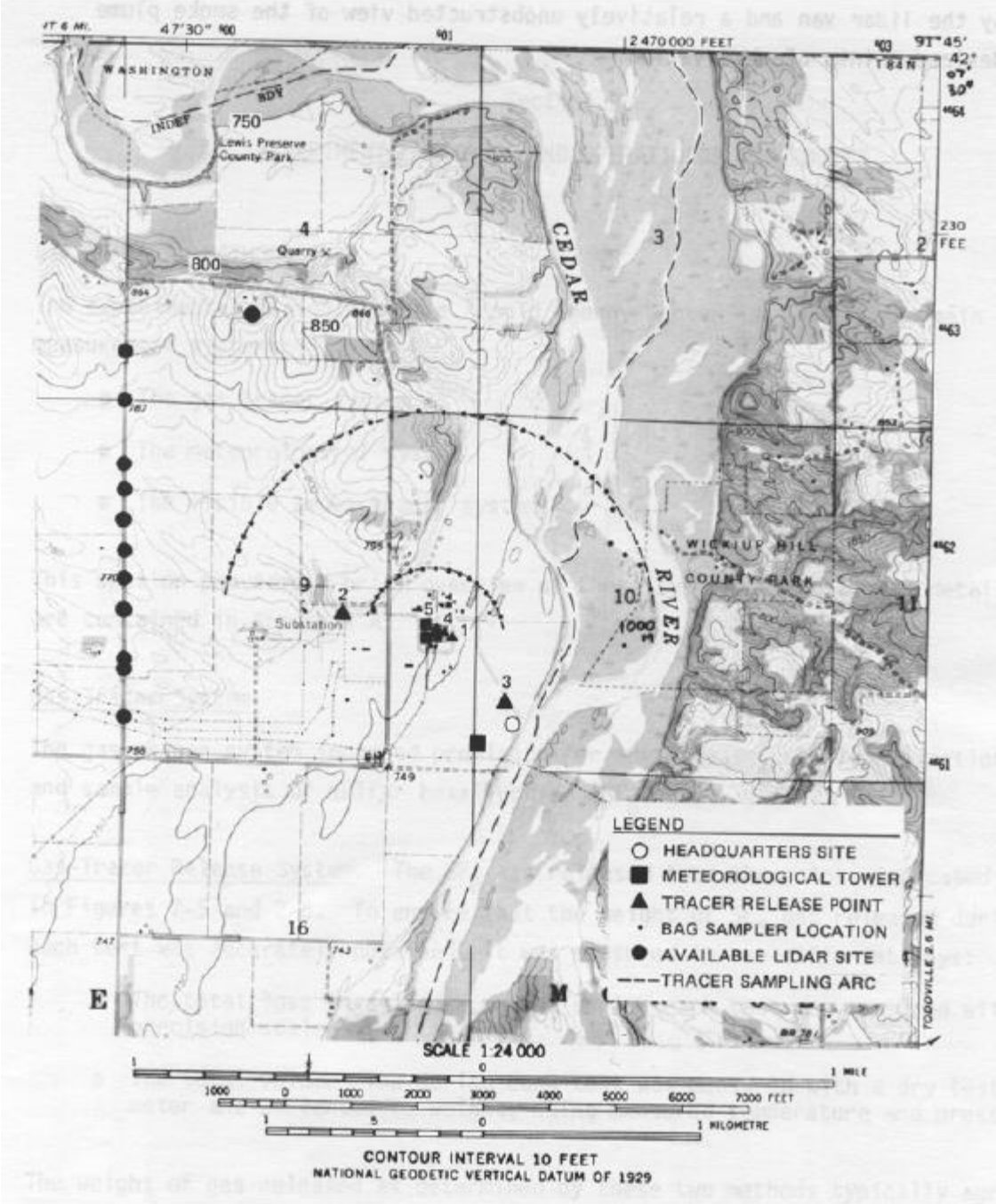

Figure B-5. DAEC study area (SF_6 releases).

B.2.6 EOCR

The EOCR study involved the simultaneous release of three tracer gases (SF_6, F_{12}, and Freon-$12B_2$) at three levels around the Experimental Organically Cooled Reactor (EOCR) test

reactor building at the Idaho National Engineering Laboratory in Southeast Idaho. The terrain was flat with low-lying shrubs. The main building was 25 m high with an effective width of 25 m. The tracer releases typically occurred simultaneously, and were conducted during 22 separate time periods. Tracer sampler coverage was provided at eight concentric rings at distances of about 50, 100, 200, 400, 800, 1200, and 1600 m from the release points (see Figure B-6). The stability classes ranged from stable to unstable. The 10-m wind speeds for the cases selected ranged from 3 to 8 m/s.

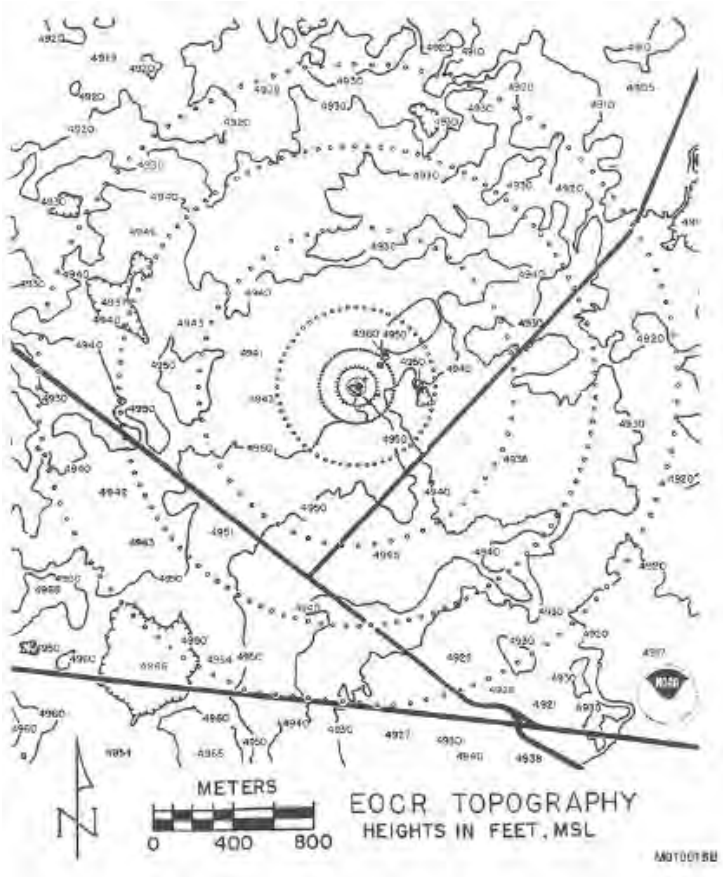

Figure B-6. Terrain map featuring the entire EOCR grid with the source at the grid center (SF_6 releases). Arcs are at distances of about 40, 80, 200, 400, 800, 1200, and 1600 m.

B.2.7 Alaska

The Alaska North Slope tracer study (see Figure B-7) involved 44 hours of buoyant SF_6 releases from a 39-m high turbine stack. Tracer sampler coverage ranged over seven arcs from 50 to 3,000 m downwind. Meteorological data, including wind speed, wind direction,

temperature, sigma-theta, and sigma-w, were available from an on-site tower at the 33-m level. Atmospheric stability and wind speed profiles were influenced by the smooth snow-covered tundra surface with negligible levels of solar radiation in the autumn months. All experiments (44 usable hours) were conducted during the abbreviated day light hours (0900 – 1600). Wind speeds taken at the 33-m level during the tests were less than 6 m/s during one and part of another test, between 6 and 15 m/s during four tests, and in excess of 15 m/s during three tests. Stability conditions were generally neutral or slightly stable.

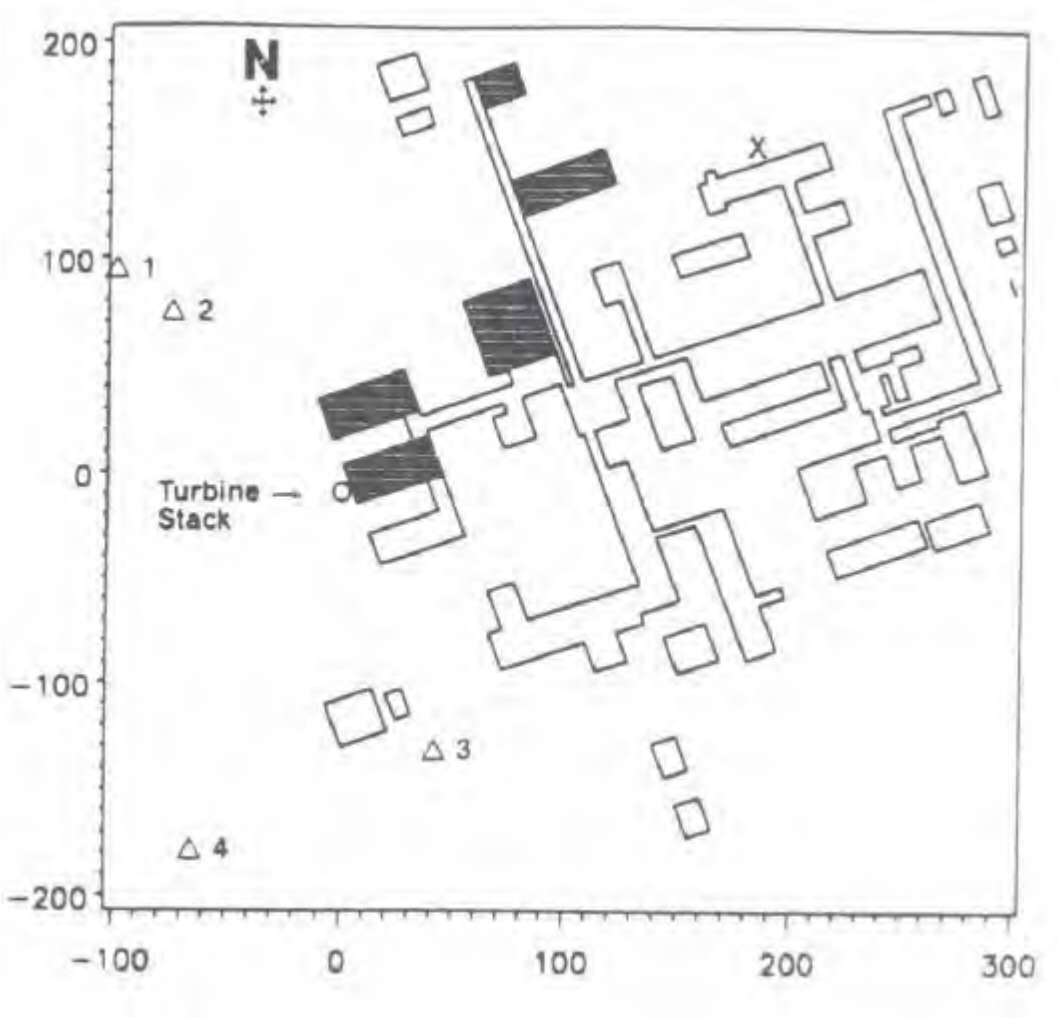

Figure B-7. Depiction of Alaska North Slope Oil Gathering Center turbine stack, meteorological tower (X), and camera locations used to visualize plume rise.

B.2.8 Indianapolis

The Indianapolis study consisted of an elevated, buoyant tracer (SF6) released in a flat-terrain urban to suburban area from a single 84-m stack (Figure B-8). Data are available for approximately a four- to five-week period with 177 monitors providing 1-hour averaged samples along arcs from 250 m to 12 km downwind for a total of 1,297 arc-hours. Meteorological data included wind speed and direction, sigma-theta on a 94-meter tower; and wind speed, ΔT (2m - 10m) and other supporting surface data at three other 10-m towers (Figure B-9). Observed plume rise and estimates of plume sigma-y are also available from the database.

Figure B-8. Map showing the location of the Perry-K Station (A), the Hoosier Dome (B), and the central Indianapolis business district (C). The downtown surface meteorological site is located at (D) and the "bank tower" site was on top of the building at (E).

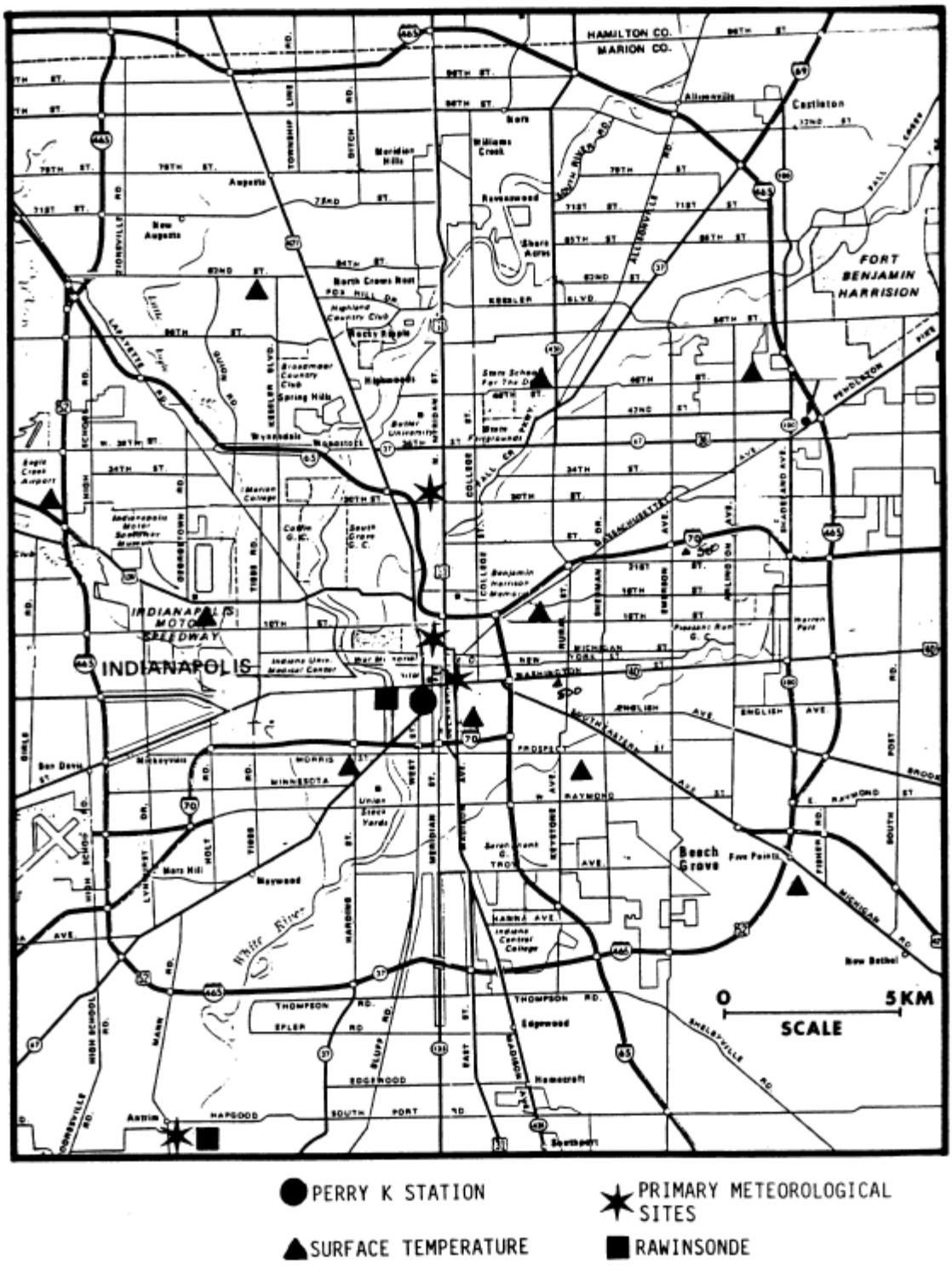

Figure B-9. Indianapolis meteorological sites and emissions site (Perry K Station).

B.2.9 Kincaid

The Kincaid SO2 study was conducted in a flat rural area of Illinois. It involved a buoyant, continuous release of SO2 from a 187-m stack in rural flat terrain. The study included about six months of data between April 1980 and June 1981 (a total of 4,614 hours of samples). There were 30 SO2 monitoring stations providing 1-hour averaged samples from about 2 km to 20 km downwind of the stack. Meteorological data included wind speed, direction, and temperature from a tower instrumented at 2, 10, 50, and 100 m levels, and nearby National Weather Service (NWS) data.

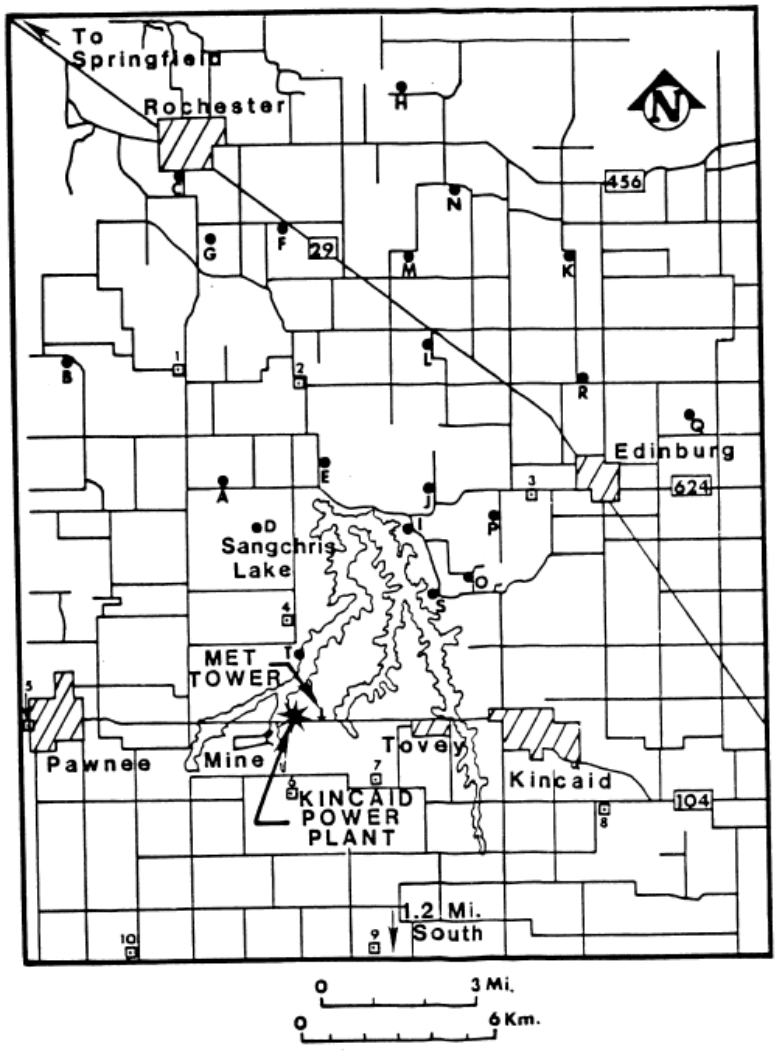

Figure B-10. Kincaid study area.

B.2.10 AGA

The AGA experiments[39] occurred during spring and summer 1980 at gas compressor stations in Texas and Kansas. At each test facility, one of the gas compressor stacks was retrofitted to accommodate SF_6 tracer gas emissions. In addition, stack height extensions were provided for some of the experiments (with the normal stack height close to 10 m). The stack height to building height ratios for the tests ranged from 0.95 to 2.52. There were a total of 63 tracer releases over the course of the tests, and the tracer samplers were located between 50 and 200 m away from the release point (see Figure B-11). An instrumented 10-m tower was operated at both experimental sites. The tracer releases were generally restricted to daytime hours. Stability classes range from neutral to extremely unstable, except for three hours that were slightly stable. Wind speeds range from 2 to 11 m/s over the 63 hours.

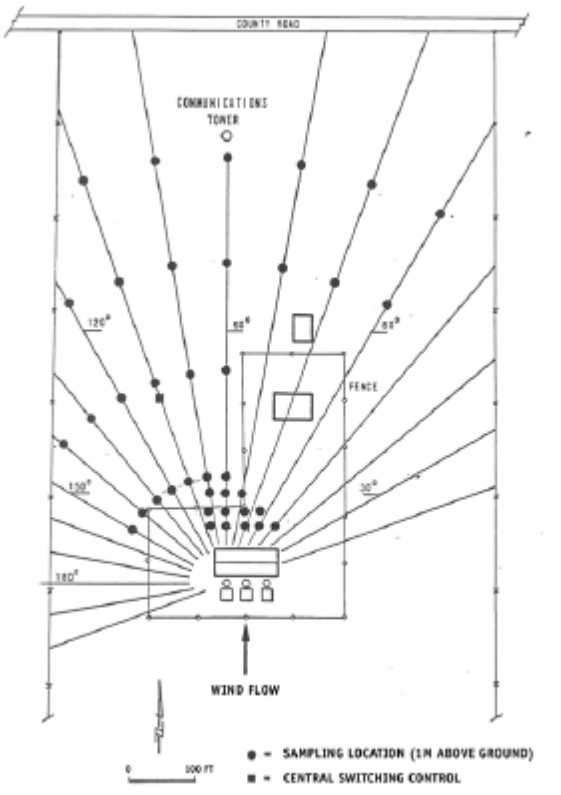

Figure B-11. Plan view of the locations of tracer samplers at Site 1, AGA field study (SF_6 releases)

B.2.11 Millstone

The Millstone nuclear power plant is located on the Connecticut coast, near Niantic. The model evaluation database features 36 hours of SF_6 emissions from a 48-m reactor stack and 26 hours of Freon emissions from a 29-m turbine stack. Exit temperatures were close to ambient (about 295K) with exit velocities of about 10 m/s for both the reactor stack (48.3 m) and the three turbine stacks (29.1 m). These stacks were associated with 45-m and 28-m building tiers, respectively. The monitoring data consisted of three arcs at 350, 800 and 1,500 m. Meteorological data were available from an on-site tower at the 10-m and 43-m levels. There was about an even split between stable and unstable hours, with mostly on-shore winds and fairly high wind speeds. There were only 3 stable hours with wind speed less than 4 m/s, and the majority was above about 7 m/s and several above 10 m/s. Figure B-12 shows the layout of the study area.

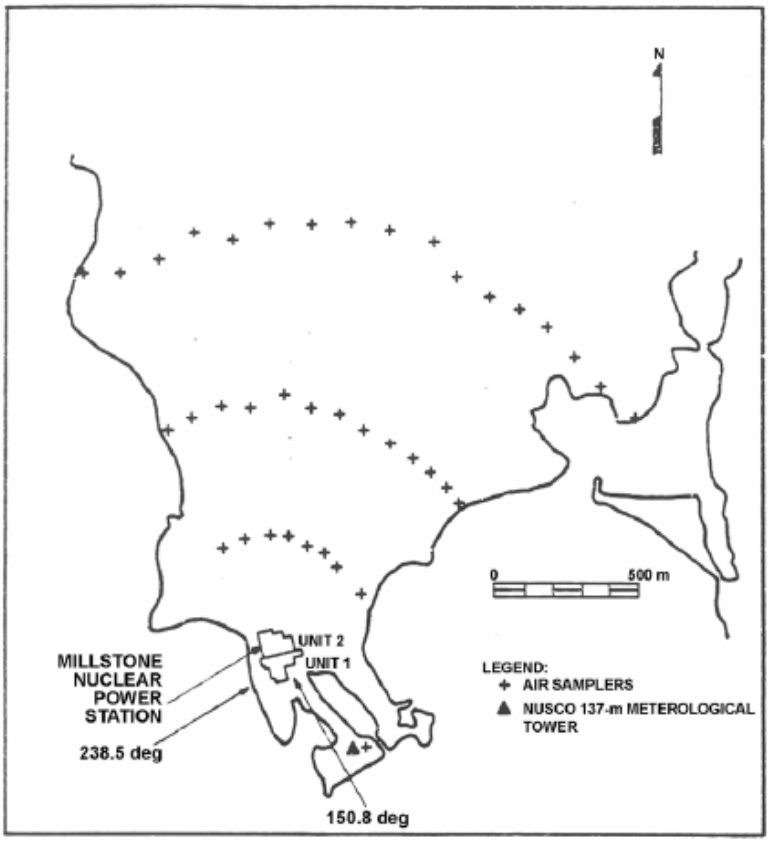

Figure B-12. Millstone study area (SF_6 and freon releases)

B.2.12 Bowline

The Bowline Point site[33], located in the Hudson River valley in New York State, is shown in Figure B-13 (topographic map). The electric utility site included two 600-MW units, each with an 86.9-m stack and a dominant roof tier with a height of 65.2 m high in a rural area. There were four monitoring sites as shown in Figure B-13 that ranged from about 250 to 850 m from the stacks. Hourly emissions data was determined from load data, coal analyses, and site-specific relationships between loads and fuel consumption. Meteorological data was obtained from a 100-m tower at the site. This site was also used as an independent evaluation database with the entire year included.

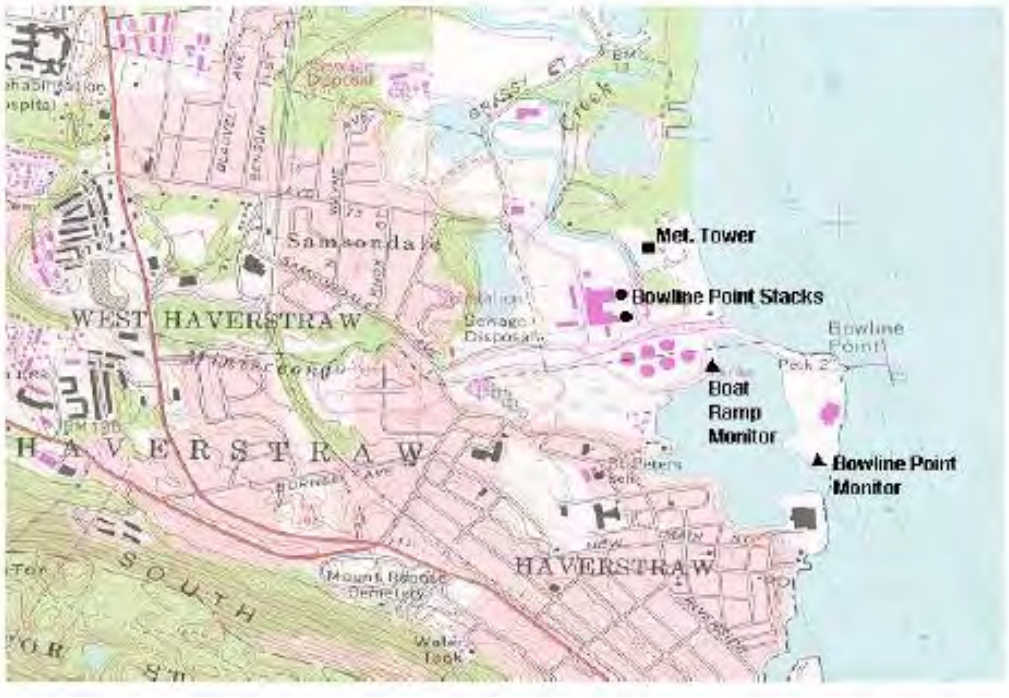

Figure B-13. Bowline Point study area (SO_2 releases)

B.2.13 Baldwin

The Baldwin Power Plant is located in a rural, flat terrain setting of southwestern Illinois and has three identical 184-m stacks aligned approximately north-south with a horizontal spacing of about 100 m. There were 10 SO2 monitors that surrounded the facility, ranging in

distance from two to ten km. On-site meteorological data was available during the study period of 1 April 1982 through 31 March 1983 and consisted of hourly averaged wind speed, wind direction, and temperature measurements taken at 10 m and wind speed and wind direction at 100 m.

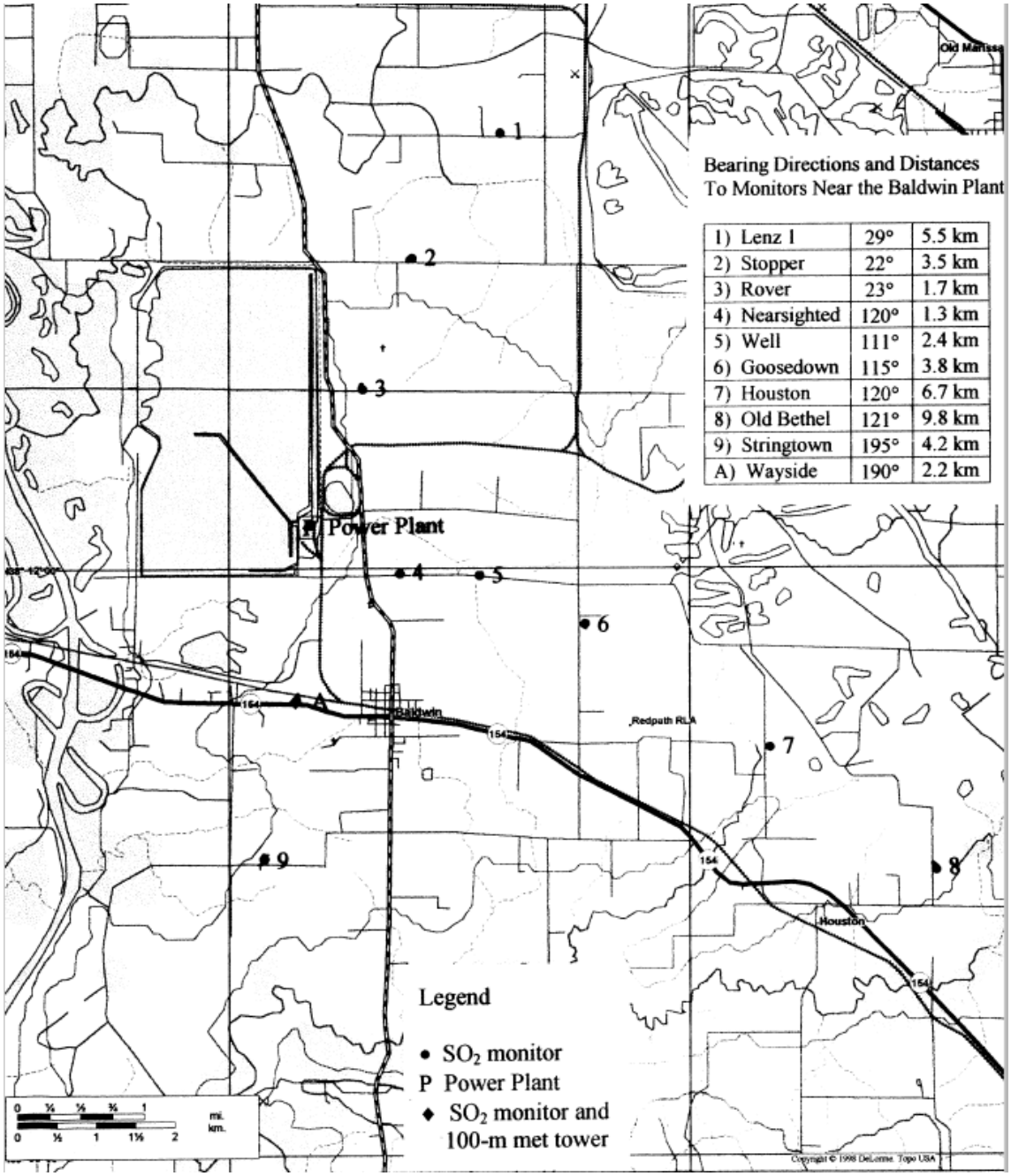

Figure B-14. Baldwin study area.

B.2.14 Clifty Creek

The Clifty Creek Power Plant is located in rural southern Indiana along the Ohio River with emissions from three 208-m stacks during this study (Figure B-15). The area immediately north of the facility is characterized by cliffs rising about 115 m above the river and intersected by creek valleys. Six nearby SO2 monitors (out to 16 km from the stacks) provided hourly averaged concentration data. Meteorological data from a nearby 60-m tower covered the two-year period from 1 January 1975 through 31 December 1976, although only the data from 1975 were used in this evaluation. This database was also used in a major EPA-funded evaluation of rural air quality dispersion models in the early 1980s.

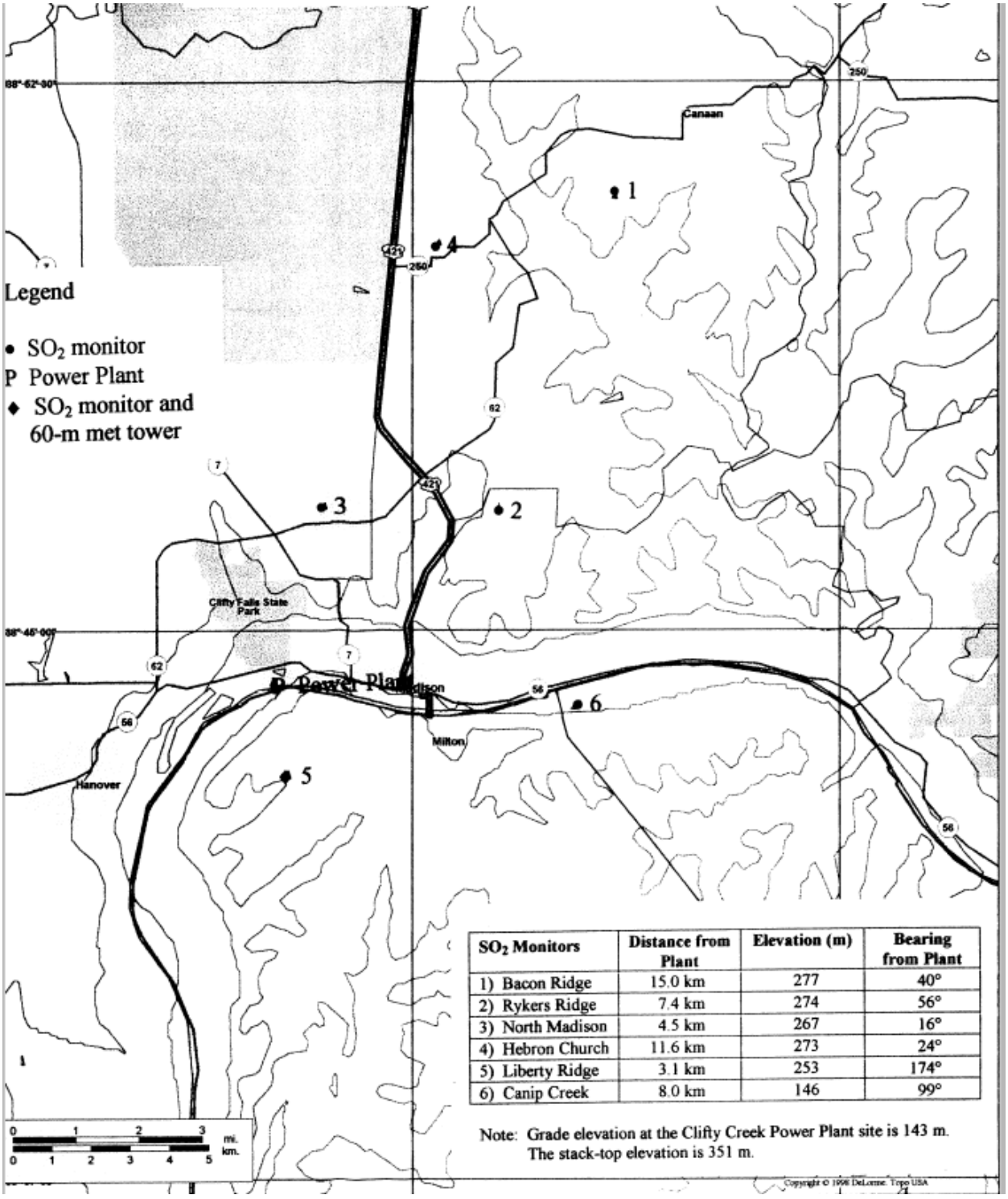

SO_2 Monitors	Distance from Plant	Elevation (m)	Bearing from Plant
1) Bacon Ridge	15.0 km	277	40°
2) Rykers Ridge	7.4 km	274	56°
3) North Madison	4.5 km	267	16°
4) Hebron Church	11.6 km	273	24°
5) Liberty Ridge	3.1 km	253	174°
6) Canip Creek	8.0 km	146	99°

Figure B-15. Clifty Creek study area.

B.3 Evaluation methodology

B.3.1 AERMET/AERMOD comparisons

Two versions of AERMET/AERMOD will be compared using Robust highest concentrations and the EPA Protocol for determining best performing model. AERMET 15181/AERMOD 15181 will be compared against AERMET 16216/AERMOD 16216 with various combinations of adjusted or non-adjusted surface friction velocity (u*) and inclusion/exclusion of turbulence parameters (s_v and s_w). The modeled scenarios are:

- 15181_no_u*_with_turb: AERMET/AERMOD 15181 with no u* adjustment and turbulence included in the meteorological data
- 15181_no_u*_no_turb: AERMET/AERMOD 15181 with no u* adjustment and no turbuluence included in the meteorological data
- 16216_no_u*_witih turb: AERMET/AERMOD 16216 with no u* adjustment and turbulence included in the meteorological data
- 16216_with_u*_no_turb: AERMET/AERMOD 16216 with u* adjustment and no turbulence included in the meteorological data.
- 16216_no_u*_no_turb:AERMET/AERMOD 16216 with no u* adjustment and no turbulence included in the meteorological data.

B.3.2 Evaluation procedures

B.3.2.1 Robust highest concentrations

Robust highest concentrations (RHC) were calculated for each averaging period of each database. The RHC statistic is calculated as:

$$HC = \mathrm{X}(N) + [\bar{\mathrm{X}} - \mathrm{X}(N)] \times \ln\left[\frac{3N-1}{2}\right] \quad \textbf{(119)}$$

where X(N) is the Nth largest value, X is the average of N-1 values, and N is the number of

values exceeding the threshold value, usually 26.

For the 1-hour RHC, the RHC is calculated based on N=26 across all modeled and monitored values, i.e. not paired in time or space. For the 3-hour and 24-hour the RHC is calculated separately for each monitor within the network for observations and modeled values. The highest observed RHC is then compared to the highest modeled RHC.

B.3.2.2 EPA Protocol for determining best performing model

AERMOD output among the different meteorological datasets was evaluated using the EPA Protocol for determining the best performing model, or Cox-Tikvart method (U.S. EPA, 1992; Cox and Tikvart, 1990). The protocol uses a two-step process for determining the better performing model when comparing models. The first step is a screening test that fails to perform at a minimal operational level. The second test applies to those models that pass the screening test that uses bootstrapping to generate a probability distribution of feasible outcomes (U.S. EPA, 1992). This section will discuss the methodology using the evaluation cases as examples.

The first step is to perform a screening test based on fractional bias:

$$FB = 2\left[\frac{OB - PR}{OB + PR}\right] \quad \textbf{(120)}$$

where FB is the fractional bias, OB is the average of the highest 25 observed concentrations and PR is the average of the highest 25 predicted averages. The fractional bias is also calculated for the standard deviation where OB and PR refer to the standard deviation of the highest 25 observed and predicted concentrations respectively. This is done across all monitors and modeled receptors, unpaired in time and space for the 3-hour and 24-hour averaging periods. The fractional bias of the means is plotted against the fractional bias of the standard deviation. Biases that exceed a factor-of-two under-prediction or over-prediction are considered grounds for excluding a model for further evaluation (U.S. EPA, 1992).

Models that pass the screening test are subjected to a more comprehensive statistical comparison that involves both an operational and scientific component using the RHC (Eq. 1).

For the evaluations presented here, the screening step was skipped. The operational component is to measure the model's ability to estimate concentration statistics most directly used for regulatory purposes and the scientific component evaluates the model's ability to perform accurately throughout the range of meteorological conditions and the geographic area of concern (U.S. EPA, 1992).

The operational component of the evaluation compares performance in terms of the largest network-wide RHC test statistic. The RHC is calculated separately for each monitor within the network for observations and modeled values. The highest observed RHC is then compared to the highest modeled RHC using equation 2, where RHC now replaces the means of the top 25 values of observed or modeled concentrations. Absolute fractional bias (the absolute value of fractional bias), AFB is calculated for 3 and 24-hour averages.

The scientific component of the evaluation is also based on absolute fractional bias but the bias is calculated using the RHC for each meteorological condition and monitor. The meteorological conditions are a function of atmospheric stability and wind speed. For the purposes of these studies, six unique conditions were defined based on two wind speed categories (below and above 2.0 m/s) and three stability categories: unstable, neutral, and stable. [1] In this evaluation, only 1-hour concentrations are used and the AFB is based on RHC values paired in space and stability/wind speed combination.

A composite performance measure (CPM) is calculated from the 1-hour, 3-hour, and 24-hour AFB's:

$$CPM = \frac{1}{3} \times \left(\overline{AFB_{i,j}}\right) + \frac{2}{3} \times \left[\frac{AFB_3 - AFB_{24}}{2}\right] \quad \textbf{(121)}$$

where $AFB_{i,j}$ is the absolute fractional bias for monitor i and meteorological condition j, $\overline{AFB_{i,j}}$ is the average absolute fractional bias across all monitors and meteorological conditions, AFB_3 is

[1] In U.S. EPA (1992), the three stability categories are related to the Pasquill-Gifford categories, unstable being A, B, and C, neutral being D, and stable being E and F. Since AERMOD does not use the stability categories, the stability class was determined using Monin-Obukhov length and surface roughness using methodology from AERMOD subroutine LTOPG.

the absolute fractional bias for the 3-hour average, and AFB_{24} is the absolute fractional bias for the 24-hour average. Once CPM values have been calculated for each model, a model comparison measure is calculated to compare the models:

$$MCM_{A,B} = CPM_A - CPM_B \quad \textbf{(122)}$$

where CPM_A is the CPM for model A and CPM_B is the CPM for model B. When more than two models are being compared simultaneously, the number of MCM values is equal to the total of the number of unique combinations of two models. For Martins Creek, Lovett, Westvaco, and Kincaid, there are four scenarios each, so there were six MCM comparisons for each location. For Bowline, Baldwin, and Clifty Creek, there are three scenarios each, resulting in three MCM comparisons for each location.

In order to determine if the difference between models was statistically significant, the standard error was calculated. A bootstrapping technique was used to create 1000 sample years based on methodology outlined in U.S. EPA (1992). The original data is divided into 3-day blocks. Within each season, the 3-day blocks are sampled with replacement until a total season is created. The process is repeated until a 1000 boot-strap years are created[2]. The standard error is calculated as the standard deviation of the bootstrap generated outcomes for the MCM.

The magnitude and sign of the MCM are indicative of relative performance of each pair of models. The smaller the CPM the better the overall performance of the model. This means that for two models, A and B, a negative difference between the CPM for A and CPM for B implies that model A is performing better (Model A has a smaller CPM) while a positive difference indicates that Model B is performing better.

Since more than two scenarios are being evaluated in these studies, simultaneous confidence intervals of 90 and 95 percent were calculated. These were calculated by finding the

[2] The bootstrapping was completed using the SAS© SURVEYSELECT procedure with resampling for 1000 replicates.

90th and 95th percentiles of the distribution across all MCM values from the bootstrapping procedure for all model comparisons. The confidence intervals were then found by:

$$CI_{X,A,B} = MCM_{A,B} \pm c_X s_{A,B} \quad \textbf{(123)}$$

where $CI_{X,A,B}$ is the confidence interval for X percent (90 or 95th) for models A and B, $MCM_{A,B}$ is as defined in Equation 4, c_X is the X percentile of the MCM values from the bootstrap results and $s_{A,B}$ is the standard deviation of the bootstrap MCM results for models A and B. Note that in Equation 5, $MCM_{A,B}$ is the MCM value from the original data, not the bootstrap results.

For each pair of model comparisons, the significance of the model comparison measure depended on whether the confidence interval overlapped zero. If the confidence interval overlapped zero, then the two models were not performing at a level which was considered statistically different. Otherwise, if they did not overlap zero, then there was a statistically significant difference between the two models.

B.4. Results

B.4.1 Turbulence cases

Table 2 lists the hourly observed and modeled RHC, as well as 3-hour and 24-hour RHC for applicable database, for the databases that initially included turbulence. Table 3 lists the RHC values for those databases initially without turbulence. The modeled scenario(s) closest to the observed RHC are highlighted in gray for each database.

Results in Table 2 indicate that for the most part for the databases with turbulence data, the 15181 results or 16216 cases without the u* adjustment and with turbulence data were the better performers against observations. For a few instances, depending on the averaging period, the 16216 cases with the u* adjustment and no turbulence, or the 16216 cases with no u* adjustment and no turbulence were the better performers.

Table 3 indicates that for the non-turbulence databases, the use of adjusted u* increased modeled performance in some cases depending on the averaging period or stack height. while decreasing or not changing model performance in other cases, depending on averaging period or stack height. For the databases that had multiple averaging periods (Martins Creek, Lovett,

Westvaco, and Kincaid), there was not a consistent better performing model across the averaging periods. For example, for Martins Creek, 16216_with_u*_no_turb performed better for the 1 and 24-hour averaging period, while 16216_no_u*_with_turb performed better for the 3-hour period. For DAEC, which had observed concentrations for emissions from different stack heights, the better performing modeling appeared to be dependent on stack height. Overall, it appears that the use of adjusted u* did not increase model performance for most of the cases and that the inclusion of turbulence is more important to model performance than the u* adjustment.

Table 2. Hourly, 3-hour, and 24-hour RHC for turbulence cases. Best performing model compared to observed RHC are highlighted in gray.

Database	Avg. period (hr)	RHC				
		Observed	AERMOD version			
			15181	16216		
			No_u*_with turb	No_u*_with turb	With_u*_no_turb	No_u*_no_turb
Martins Creek	1	1216	1133	1133	1034	1427
	3	461	497	497	505	655
	24	79	141	141	129	156
Tracy	1	15	13	13	18	25
Lovett	1	426	374	374	538	622
	3	187	169	169	239	254
	24	52	48	48	63	68
Westvaco	1	2757	2460	2460	1252	2091
	3	1575	1731	1731	783	1654
	24	480	524	524	457	615
DAEC (h=1m)	1	346	241	240	188	222
DAEC (h=24m)	1	253	84	88	70	74
DAEC (h=46m)	1	140	91	91	59	99
EOCR	1	3763	5820	5797	5712	8225
Alaska	1	6	5	5	8	8
Indianapolis	1	6	4	4	4	5
Kincaid	1	1611	1313	1312	717	717
	3	618	615	635	470	470
	24	113	101	103	167	167

B.4.2 Non-turbulence cases

Table 3 lists the RHC values for the non-turbulence databases. In these databases, because of the lack of turbulence in the meteorological data, the effect of the u* adjustment has more impact in improving model performance.

Table 3. Hourly, 3-hour, and 24-hour RHC for non-turbulence cases. Best performing model compared to observed RHC are highlighted in gray.

Database	Avg. period (hr)	RHC			
		Observed	AERMOD version		
			15181	16216	
			No_u*_no_turb	With_u*_no_turb	No_u*_no_turb
AGA	1	296	281	262	281
Millston (Freon)	1	76	101	96	101
Millston (SF6)	1	79	35	33	36
Bowline	1	763	547	552	547
	3	469	523	514	522
	24	204	290	307	290
Baldwin	1	2348	3531	3531	3531
	3	920	1184	1183	1184
	24	209	230	231	230
Clifty Creek	1	1451	1360	1360	1360
	3	796	870	871	870
	24	243	165	170	165

B.4.3 Statistical evaluations

While the review of RHC can indicate general model performance, the use of the EPA Protocol for Determining Best Model provides a statistical basis of determing the best performing model. Tables 4 and 5 show the composite performance measure (CPM) for the turbulence databases and non-turbulence databases respectively. For the databases with turbulence (Table 4), the best performing model was either 15181_no_u*_with_turb or 16216_no_u*_with_turb, meaning the use of adjusted u* did not increase model performance and the use of turbulence was important to model performance. For the non-turbulence

databases (Table 5), the use of adjusted u* increased model performance for Baldwin and Clifty Creek, while for Bowline, the use of adjusted u* slightly decreased model performance.

Table 4. Composite Performance Measure (CPM) for turbulence cases. Scenarios with lowest CPM's for each study location are highlighted in gray.

	Database			
Scenario	Martins Creek	Lovett	Westvaco	Kincaid
15181_no_u*_with_turb	0.35	0.40	0.41	0.37
16216_no_u*_with_turb	0.35	0.40	0.41	0.37
16216_with_u*_no_turb	0.31	0.52	0.60	0.56
16216_no_u*_no_turb	0.49	0.58	0.44	0.56

Table 5. Composite Performance Measure (CPM) for non-turbulence databases. Scenarios with lowest CPM's for each study location are highlighted in gray.

	Database		
Scenario	Bowline	Baldwin	Clifty Creek
15181_no_u*_no_turb	0.47	0.46	0.51
16216_no_u*_no_turb	0.47	0.46	0.51
16216_with_u*_no_turb	0.50	0.45	0.49

Tables 6 through 9 show the model comparison measure (MCM) for the turbulence databases while Tables 10 through 12 show the MCM for the non-turbulence databases. Also shown are the 90 and 95% confidence intervals of the MCM based on the bootstrapping results. Confidence intervals highlighted in gray indicated statistical significance in the specific MCM cases.

Martins Creek (Table 6): The better performing models was 16216_with_u*_no_turb Also, the MCM results indicate that the use of adjusted u* with no turbulence is not statistically significant when compared to 15181_no_u*_with_turb or 16216_no_u_with_turb. There were three statistically significant MCM pairings that were statistically significant at the 90% confidence interval and these were the difference between 16216_no_u*_no_turb and the other three cases, indicating that not using adjusted u* and not using turbulence noticeably decreases model performance. At the 95% confidence interval, the only statistically significant difference was between 16216_no_u*_no_turb and 16216_with_u*_no_turb.

Lovett (Table 7): All cases of AERMET/AERMOD 16216 are statistically insignificant when compared AERMET/AERMOD 15181 at both the 90% and 95% CI, all all 16216 cases are statistically insignificant compared to each other.

Westvaco (Table 8): The use of adjusted u* decreases model performance significantly at both the 90% and 95% CI. The use of no adjusted u* and no turbulence also decreases model performance at a statistically significant level.

Kincaid (Table 9): None of the MCM differences were statistically significant at 90% or 95% CI. The better performers were 15181 or 16216 with no u* adjustment and inclusion of turbulence, but as previously stated, were not statistically different from the adjusted u* case or the case with no adjusted u* and no turbulence.

For the non-turbulence databases (Tables 10-12), the use of adjusted u* was statistically insignificant compared to not using adjusted u*.

Table 6. Martins Creek Model Comparison Measure (MCM) results. Confidence intervals highlighted in gray are significant at that percent.

MCM Comparison	MCM	Confidence Intervals			
		90%		95%	
		Lower bound	Upper bound	Lower bound	Upper bound
16216_with_u*_no_turb - 15181_no_u*_with_turb	-0.04	-0.15	0.07	-0.18	0.10
16216_no_u*_with_turb - 15181_no_u*_with_turb	$3.8x10^{-9}$	-0.10	0.10	-0.13	0.13
16216_no_u*_no_turb - 15181_no_u*_with_turb	0.14	0.02	0.26	-0.01	0.30
16216_with_u*_no_turb - 16216_no_u*_with_turb	-0.04	-0.14	0.07	-0.18	0.10
16216_no_u*_no_turb - 16216_no_u*_with_turb	0.14	0.02	0.27	-0.01	0.30
16216_no_u*_no_turb - 16216_with_u*_no_turb	0.18	0.05	0.32	0.01	0.35

Table 7. Lovett Model Comparison Measure (MCM) results. Confidence intervals highlighted in gray are significant at that percent.

MCM Comparison	MCM	Confidence Intervals			
		90%		95%	
		Lower bound	Upper bound	Upper bound	Lower bound
16216_with_u*_no_turb - 15181_no_u*_with_turb	0.13	-0.05	0.31	-0.10	0.36
16216_no_u*_with_turb - 15181_no_u*_with_turb	$1.2x10^{-4}$	-0.11	0.11	-0.14	0.14
16216_no_u*_no_turb - 15181_no_u*_with_turb	0.18	-0.02	0.38	-0.07	0.43
16216_with_u*_no_turb - 16216_no_u*_with_turb	0.13	-0.06	0.31	-0.11	0.36
16216_no_u*_no_turb - 16216_no_u*_with_turb	0.18	-0.02	0.38	-0.07	0.43
16216_no_u*_no_turb - 16216_with_u*_no_turb	0.05	-0.10	0.20	-0.13	0.24

Table 8. Westvaco Model Comparison Measure (MCM) results. Confidence intervals highlighted in gray are significant at that percent.

MCM Comparison	MCM	Confidence Intervals			
		90%		95%	
		Lower bound	Upper bound	Lower bound	Upper bound
16216_with_u*_no_turb - 15181_no_u*_with_turb	0.19	0.09	0.29	0.05	0.32
16216_no_u*_with_turb - 15181_no_u*_with_turb	$1x10^{-4}$	-0.05	0.06	-0.07	0.07
16216_no_u*_no_turb - 15181_no_u*_with_turb	0.03	-0.03	0.08	-0.05	0.10
16216_with_u*_no_turb - 16216_no_u*_with_turb	0.19	0.09	0.29	0.05	0.32
16216_no_u*_no_turb - 16216_no_u*_with_turb	0.03	-0.03	0.08	-0.05	0.10
16216_no_u*_no_turb - 16216_with_u*_no_turb	-0.16	-0.26	-0.06	-0.29	-0.03

Table 9. Kincaid Model Comparison Measure (MCM) results. Confidence intervals highlighted in gray are significant at that percent.

MCM Comparison	MCM	Confidence Intervals			
		90%		95%	
		Lower bound	Upper bound	Lower bound	Upper bound
16216_with_u*_no_turb - 15181_no_u*_with_turb	0.19	-0.14	0.52	-0.19	0.57
16216_no_u*_with_turb - 15181_no_u*_with_turb	$-1.3x10^{-4}$	-0.41	0.41	-0.48	0.48
16216_no_u*_no_turb - 15181_no_u*_with_turb	0.19	-0.14	0.52	-0.20	0.58
16216_with_u*_no_turb - 16216_no_u*_with_turb	0.19	-0.14	0.52	-0.20	0.57
16216_no_u*_no_turb - 16216_no_u*_with_turb	0.19	-0.15	0.52	-0.20	0.58
16216_no_u*_no_turb - 16216_with_u*_no_turb	$-5.1x10^{-4}$	-0.15	0.15	-0.18	0.18

Table 10. Bowline Model Comparison Measure (MCM) results. Confidence intervals highlighted in gray are significant at that percent.

MCM Comparison	MCM	Confidence Intervals			
		90%		95%	
		Lower bound	Upper bound	Lower bound	Upper bound
16216_no_u*_no_turb -15181_no_u*_no_turb	$2.7x10^{-5}$	-0.08	0.08	-0.10	0.10
16216_with_u*_no_turb -15181_no_u*_no_turb	0.03	-0.05	0.11	-0.07	0.13
16216_no_u*_no_turb -16216_with_u*_no_turb	-0.03	-0.11	0.05	-0.13	0.07

Table 11. Baldwin Model Comparison Measure (MCM) results. Confidence intervals highlighted in gray are significant at that percent.

MCM Comparison	MCM	Confidence Intervals			
		90%		95%	
		Lower bound	Upper bound	Lower bound	Upper bound
16216_no_u*_no_turb - 15181_no_u*_no_turb	$-2.4x10^{-10}$	-0.14	0.14	-0.19	0.19
16216_with_u*_no_turb - 15181_no_u*_no_turb	-0.002	-0.14	0.13	-0. 19	0. 19
16216_no_u*_no_turb - 16216_with_u*_no_turb	0.002	-0.14	0.14	-0. 19	0.20

Table 12. Clifty Creek Model Comparison Measure (MCM) results. Confidence intervals highlighted in gray are significant at that percent.

MCM Comparison	MCM	Confidence Intervals

		90%		95%	
		Lower bound	Upper bound	Lower bound	Upper bound
16216_no_u*_no_turb - 15181_no_u*_no_turb	-1.8×10^{-10}	-0.07	0.07	-0.09	0.09
16216_with_u*_no_turb - 15181_no_u*_no_turb	-0.02	-0.09	0.06	-0.11	0.08
16216_no_u*_no_turb - 16216_with_u*_no_turb	0.02	-0.06	0.09	-0.08	0.11

B.5 Summary/Conclusions

Based on the results the RHC comparisons and the EPA protocol for determining best performing model, in situations involving turbulence, the use of turbulence without adjusting u* usually led to better performance than using adjusted u* without turbulence, especially in areas of complex terrain. In some instances, the differences between the adjusted u* cases were statistically worse than nonadjusted u* cases. For situations where turbulence is not in the meteorological data, the use of adjusted u* often resulted in little change or some increase in model performance. However, the databases without turbulence were in flat terrain and had talk stacks, so model performance for non-turbulence cases with complex terrain cannot be determined from these results

Appendix C: Evaluation of ADJ_U* and LOWWIND3

C.1 Background

As part of the ongoing process of improving the model formulation of the AERMOD Modeling System, an evaluation of two options that address overprediction in low wind conditions was performed. This appendix presents the results of that evaluation. Common scenarios where AERMOD is known to over predict are low-level fugitive emissions and tall stacks located near complex terrain during light winds when the atmosphere is stable. The evaluation was performed using AERMOD version 16216r and the meteorological preprocessor AERMET version 16216. The options assessed include:

1. ADJ_U*, a regulatory option in AERMET that adjusts the surface friction velocity (u*) during low wind conditions for hours that the atmosphere is stable and
2. LOWWIND3, a beta option in AERMOD that increases the minimum value of the lateral turbulence intensity (sigma-v), adjusts the dispersion coefficient, and eliminates upwind dispersion.

The influence of the ADJ_U* and LOWWIND3 options on AERMOD model performance was assessed using a wide array of field study databases, including many of the data sets used to support the initial promulgation of the AERMOD model in 2005. Additional field studies included in the assessment were two conducted by the National Oceanic and Atmospheric Administration (NOAA), the 1974 Idaho Falls study (NOAA, 1974) and the 1974 Oak Ridge, Tennessee (NOAA, 1976), and a study conducted by the U.S. Environmental Protection Agency (EPA) at the Cordero Rojo Mine in Wyoming (U.S. EPA, 1995b).

Where possible, the Cox-Tikvart *Protocol for Determining Best Performing Model* (U.S. EPA, 1992) was applied to the AERMOD results, which compares:

- Mean Fractional Biasses (FBs),
- Robust High Concentrations (RHCs),
- Composite Performance Measures (CPMs), and

- Model Comparison Measures (MCMs).

The Cox-Tikvart protocol also generates confidence intervals on the CPMs and MCMs. For those databases for which the observation data and period of the study was not sufficient to apply the full Cox-Tikvart protocol, the mean FBs and RHCs were computed and compared for each model scenario. When comparing these statistical parameters, the FB ranges from -2.0 to 2.0, with the better performing model having an FB closest to zero. A negative FB indicates model overprediction while a positive FB indicates underprediction. A FB greater than 0.67 (or less than -0.67) means the model underpredicted (or overpredicted) by more than a factor of 2. For the RHC, a ratio greater than 1.0 of the predicted to observed (Pred/Obs) indicates overprediction. A ratio less than 1.0 indicates underprediction. The CPM is computed from the individual FBs for the 1-hr, 3-hr, and 24-hr averaging periods. Similar to the FB, the model scenario with a CPM closest to zero of those scenarios compared, is generally considered the best performer. The MCM is a comparison of the CPMs for different modeling scenarios. Based on the MCM, the differences between two scenarios are insignficant if the confidence interval for the MCM crosses zero.

C.2 Descriptions of Field Studies

C.2.1 Tracy Power Plant, Reno, NV (1984)

The Tracy Power Plant (Tracy) (DiCristofaro *et al.*, 1985), located 27 kilometers east of Reno, Nevada in the rural Truckee River valley is completely surrounded by mountainous terrain. A buoyant plume of SF_6 was released from a 91-meter stack in August of 1984 during predominantly stable atmospheric conditions. The Tracy dataset has an extensive set of meteorological data extending from 10m above ground up to 400m above ground for some parameters. Wind, temperature, and turbulence measurements (*i.e.*, sigma-theta, the standard deviation of horizontal wind direction fluctuations, and sigma-w, the standard deviation of the vertical wind speed fluctuations) were collected from an instrumented 150-m tower. The wind measurements were also taken above 150 meters using a Doppler acoustic sounder, and temperature measurements were extended beyond the tower height with a tethersonde.

The Tracy field study also included the largest number of ambient monitors of any complex terrain study used in evaluating AERMOD performance, including 106 monitors extending across a domain of about 75 square kilometers, and used sulfur hexafluoride (SF6) as a tracer which reduces uncertainty in evaluating model performance by minimizing the influence of background concentrations on the model-to-monitor comparisons.

C.2.2 Lovett Power Plant, New York (1987-1988)

The Lovett Power Plant field study (Lovett) (Paumier et al., 1992) consisted of a buoyant, continuous release of SO_2 from a 145-m tall stack located in a rural area in New York State with complex terrain for a year from December 1987 through December 1988. The terrain rises approximately 250m to 330m above the stack, 2km to 3km from the stack. Ground level concentrations of SO_2 were collected from 12 monitoring sites (ten on elevated terrain and two near stack-base elevation) at a distance of 2 to 3 km from the plant. The monitors provided hourly-averaged concentrations.

The meteorological data includes a 100m meteorological tower with wind speed, wind direction, sigma-theta (turbulence) and temperature collected at the 10m, 50m, and 100m levels. In addition, sigma-w (turbulence) was also collected at the 10m and 100m levels.

It should also be noted that the surface characteristics for the Lovett database were evaluated and were updated from the original values in the database as previously provided on the EPA's Support Center for Regulatory Atmospheric Modeling (SCRAM) website. [3]

C.2.3 Oak Ridge, Tennessee (1974)

The 1974 Oak Ridge, Tennessee (NOAA, 1976) study (Oak Ridge) occurred in complex terrain and was focused on characterizing dispersion of low-level releases during low-wind conditions. It consisted of eleven 1-hour tracer releases during July and August of 1974 with

[3] https://www.epa.gov/scram

three arcs of samplers located at 100m, 200m, and 400m from the release point. The top of the ridge nearest to the source location is about 26m above the ground-level release point. All releases occurred during neutral to stable, low wind conditions with wind speeds less than 1 m/s. Wind speeds at the site were often below the threshold of standard anemometers and were determined by laser anemometry using two lasers and two receivers positioned approximately orthogonal to each other located on the nearby ridges. The evaluation results are based on an "effective" measurement height of 10 meters and used the VECTORWS option in AERMOD to treat the wind speeds as vector, rather than scalar, averages. Turbulence data were not included.

C.2.4 Baldwin Power Plant, Illinois (1982-1983)

Located in rural, flat terrain of southwestern Illinois, the Baldwin Power Plant (Baldwin), Illinois study (Hanna and Chang, 1993) occurred from April 1, 1982 through March 31, 1983. The plant consisted of three identical stacks with a release height of 184 meters, about 100 meters apart along a line oriented north and south. Ground level SO_2 concentrations were collected at 10 monitor locations at distances between two and ten kilometers from the plant. Site-specific hourly averaged wind speed, wind direction, and temperature were collected at a 10-meter height and wind speed and wind direction were collected at 100 meters. Turbulence measurements were not collected.

C.2.5 Kincaid SO_2, Illinois (1980-1981)

The Kincaid SO_2 field study (Kincaid) (Liu and Moore, 1984; Bowne et al., 1983) occurred in rural, flat terrain in Illinois from a continuous, buoyant release of SO_2 from a 187-meter stack. SO_2 was monitored at 30 monitors ranging from 2 kilometers to 20 kilometers downwind of the stack. About six months of data were collected between April 1980 and June 1981. Meteorological data included wind speed and direction, sigma-theta and sigma-w (turbulence) collected on a 94-meter tower; and wind speed, temperature difference between 2-meter and 10-meter heights.

C.2.6 Cordero Rojo Mine, Wyoming (1983)

The 1993 Cordero Rojo Mine field study (Cordero) (U.S. EPA, 1995b) was a two month study conducted by the EPA in 1993 at the Cordero Rojo Mine in eastern Wyoming to compile a comprehensive, quality database for dispersion model evaluation. The study was conducted from May 19 – July 18 during which time-integrated measurements of 24-hour PM10 and TSP were collected along with and coincident meteorological measurements, including sigma-theta (turbulence). The majority of the emissions, approximately 75%, were from roadways.

C.2.7 Idaho Falls, Idaho (1974)

The Idaho Falls study (NOAA, 1974) was conducted at the Idaho National Engineering Laboratory (INEL) in southeastern Idaho. The study was performed with tracer releases in flat terrain with 3 rings of ambient monitors located at 6-degree intervals along concentric arcs located at 100m, 200m, and 400m from the release point. The Idaho Falls study also included a robust set of meteorological data, including vertical profiles of wind speed, wind direction, ambient temperature, and sigma-theta (turbulence) at heights of 2m, 4m, 8m, 16m, 32m, and 64m above ground.

C.2.8 Prairie Grass, Nebraska (1956)

Prairie Grass (Barad22; Haugen23) used a near-surface (0.46m), non-buoyant tracer release of SO_2 in a flat rural area in Nebraska during July and August of 1956. Surface sampling arrays (arcs) were positioned at 50m, 100m, 200m, 400m and 800m downwind. Meteorological data include 2-m level sigma-theta and sigma-w measurements (turbulence) and temperature difference between 2 m and 16 m. Wind speed and wind direction measurements are at heights of 1m, 2m, 4m, 8m, and 16m. Other surface parameters, including friction velocity, Monin-Obukhov length, and lateral plume spread, were estimated.

C.2.9 Other Evaluation Datasets

In addition to Baldwin, Kincaid, Lovett, and Prairie Grass, which were used for the evaluation of the ADJ_U* option, these and other evaluation databases used in the original evaluation of AERMOD (Perry *et al.*, 2005) were modeled with and without the LOWWIND3 option and in combination with ADJ_U* and turbulence measurements (where available). The results are presented collectively as "Other Studies" under the "LOWWIND3" section below. Those that include turbulence data are noted. Refer to the evaluation report (Perry *et al.*, 2005) for descriptions of these field studies:

- American Gas Association (AGA)
- Alaska North Slope (Alaska), *includes turbulence*
- Baldwin
- Bowline Power Plant (Bowline)
- Clifty Creek Power Plant (Clifty Creek)
- Duane Arnold Energy Center (DAEC), *includes turbulence*
- Experimental Organic Cooled Reactor (EOCR), *includes turbulence*
- Indianapolis, *includes turbulence*
- Kincaid, *includes turbulence*
- Lovett
- Martins Creek Steam Electric Station (Martins Creek), *includes turbulence*
- Millston Nuclear Power Plant (Millston)
- Tracy, *includes turbulence*
- Westvaco Corporation (Westvaco), *includes turbulence.*

C.3 ADJ_U*

This section presents results on the evaluation of the ADJ_U* option available in AERMET. The version of the AERMOD Modeling System used in the evaluations considers ADJ_U* as a regulatory option in the absence of turbulence measurements (*i.e.*, sigma-theta and/or sigma-w). There are two primary objectives of the ADJ_U* evaluation. The first, is to evaluate the use of the ADJ_U* option in conjunction with all available site-specific data, particularly those data sets that include turbulence measurements. Since the ADJ_U* option

addresses estimates of turbulence, it is important to understand how this adjustment affects model performance when there are already turbulence measurements available. The second is to evaluate model performance when ADJ_U* is used with data that mimics National Weather Service (NWS) data, *i.e.*, degraded meteorology from the field studies that includes only wind direction and speed. This level of degraded meteorology is very similar to the meteorological data collected at airports nationwide, typically used for regulatory analyses in lieu of site-specific meteorological data, and does not include any measurements of turbulence. Thus, this analysis provides insight into the impact on performance of ADJ_U* in settings similar to the majority of regulatory analyses.

C.3.1 Summary of Results from Each Study

C.3.1.1 Tracy Power Plant, Reno, Nevado (1984)

Given the robust set of meteorological data available from the Tracy study, a meteorological degradation analysis was performed to compare AERMOD results with and without applying ADJ_U* with various degradations of the meteorological data that include:

- Wind and temperature profile with turbulence (Full Met)
- Wind and temperature profile without turbulence;
- Temperature profile without wind profile and without turbulence;
- 10-m temperature, wind profile and turbulence;
- 10-m temperature, wind profile, without turbulence;
- 10-m temperature, 10-m winds, without turbulence (similar to NWS).

The full Cox-Tikvart protocol could not be applied for this analysis, therefore FBs and RHCs were computed and are provided in Table 13. Q-Q plots are presented in Figure 18 through Figure 21. Tracy results show good performance with full meteorology, including turbulence, without ADJ_U* applied. When ADJ_U* is applied to the full meteorology with turbulence measurements, AERMOD underpredicts. When turbulence data are omitted from the full meteorological dataset, AERMOD substantially overpredicts. AERMOD's performance

improves when ADJ_U* is applied. In the cases with meteorology similar to that collected at NWS airport sites, in which there is only a single level of wind and temperature measurements without turbulence data, the results show substantial overprediction when ADJ_U* is not applied. However, there is substantial improvement in model performance when ADJ_U* is applied.

These results for the Tracy field study support the position that the use of site-specific meteorology that includes turbulence data is preferred, though ADJ_U* should not be applied with site-specific turbulence data. However, the ADJ_U* option can substantially improve performance under low-wind, stable conditions when using standard NWS data.

Table 13. Comparison of 1-Hr Fractional Biases and Robust High Concentrations for Tracy

		Observed RHC = 14.98 µg/m³
Scenario†	**FB**	**RHC (Pred/Obs)**
FullMet_NoAdjU* *(incl. Turb)*	-0.02	13.24 (0.88)
FullMet_AdjU* *(incl. Turb)*	0.26	9.46 (0.63)
FullTemp_FullWind_NoTurb_NoAdjU*	-0.61	24.77 (1.65)
FullTemp_FullWind_NoTurb_AdjU*	-0.39	17.54 (1.17)
NoTemp_FullWind_NoTurb_NoAdj U*	-0.80	33.84 (2.26)
NoTemp_FullWind_NoTurb_Adj U*	-0.30	19.24 (1.28)
NoTemp_NoWind_NoTurb_NoAdj U* *(similar to NWS)*	-0.88	42.57 (2.84)
NoTemp_NoWind_NoTurb_Adj U* *(similar to NWS)*	-0.40	25.75 (1.72)

† *Default scenario is bolded. Positive (negative) FB indicates under (over) prediction. Green shading indicates best performer. Yellow shading is outside factor of ± 2 (FB±0.67).*

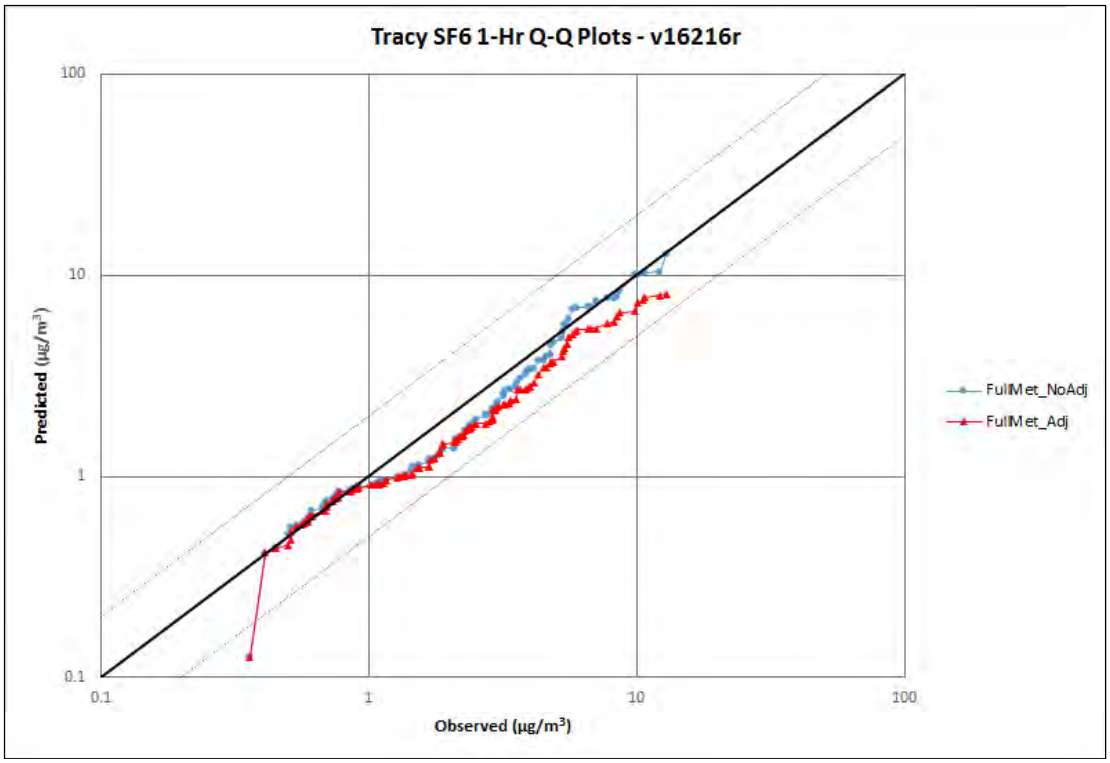

*Figure 18. Tracy - Full Meteorology (Includes Turbulence) - With and Without ADJ_U**

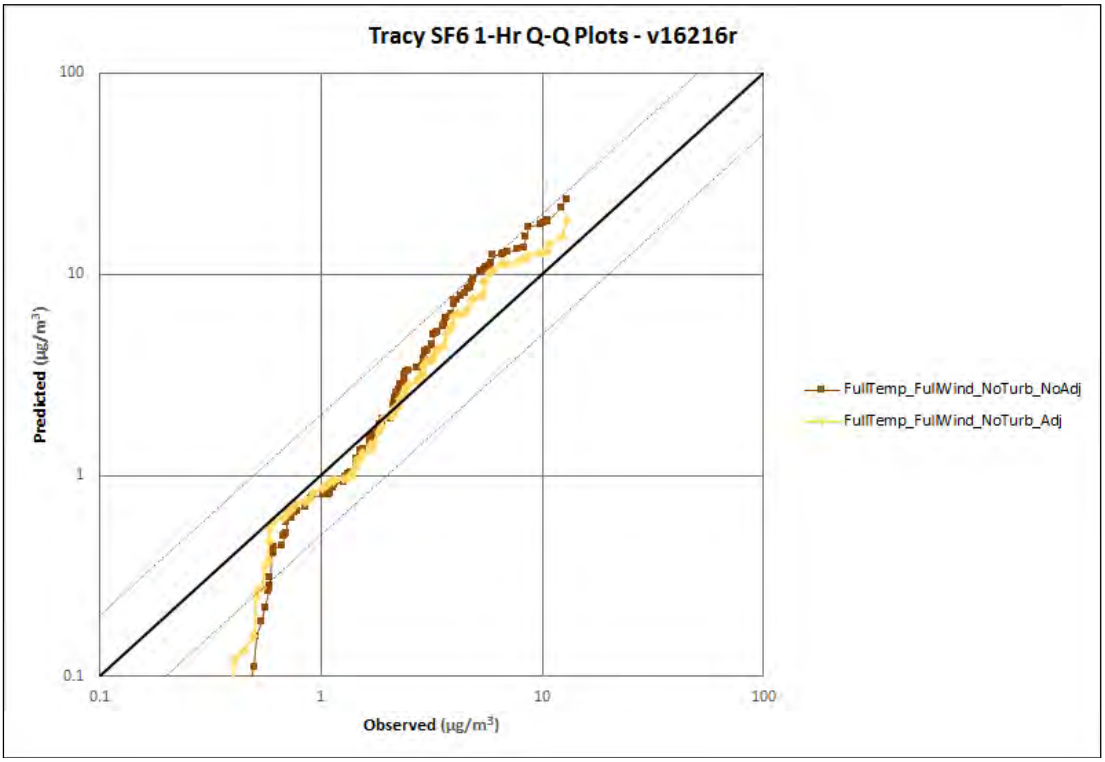

*Figure 19. Tracy – Full Temp and Wind Profiles – No Turbulence - With and Without ADJ_U**

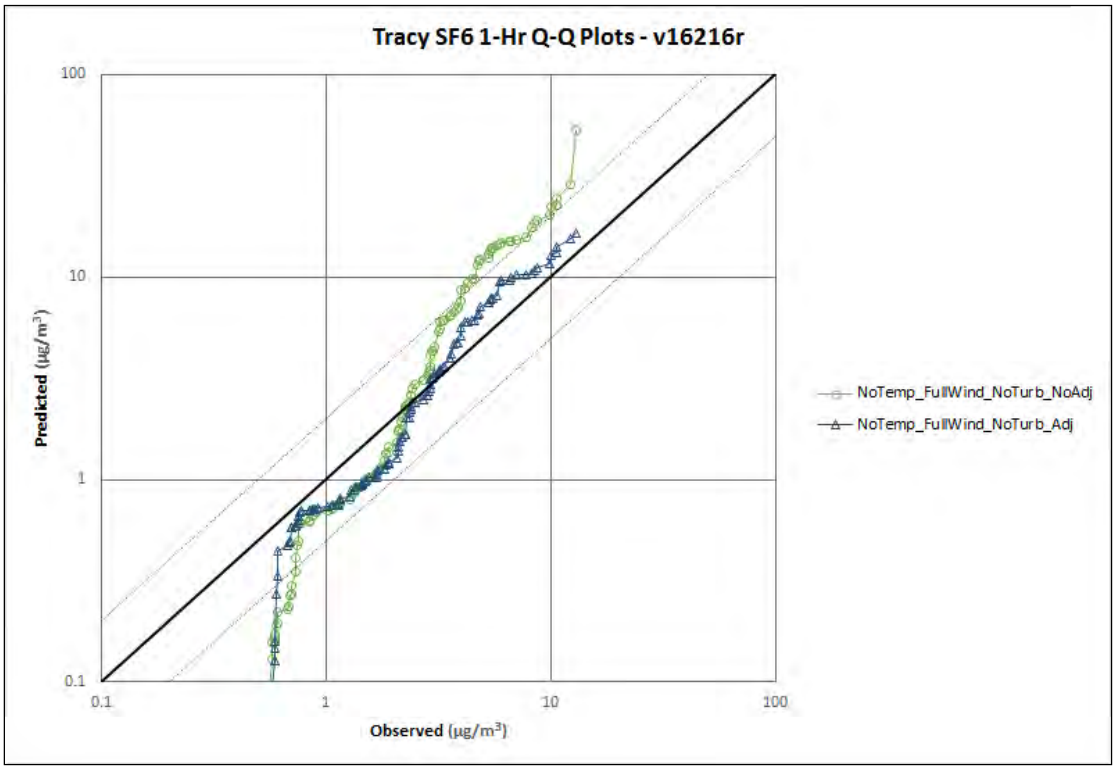

*Figure 20. Tracy – 10-m Temp - Wind Profile – No Turbulence - With and Without ADJ_U**

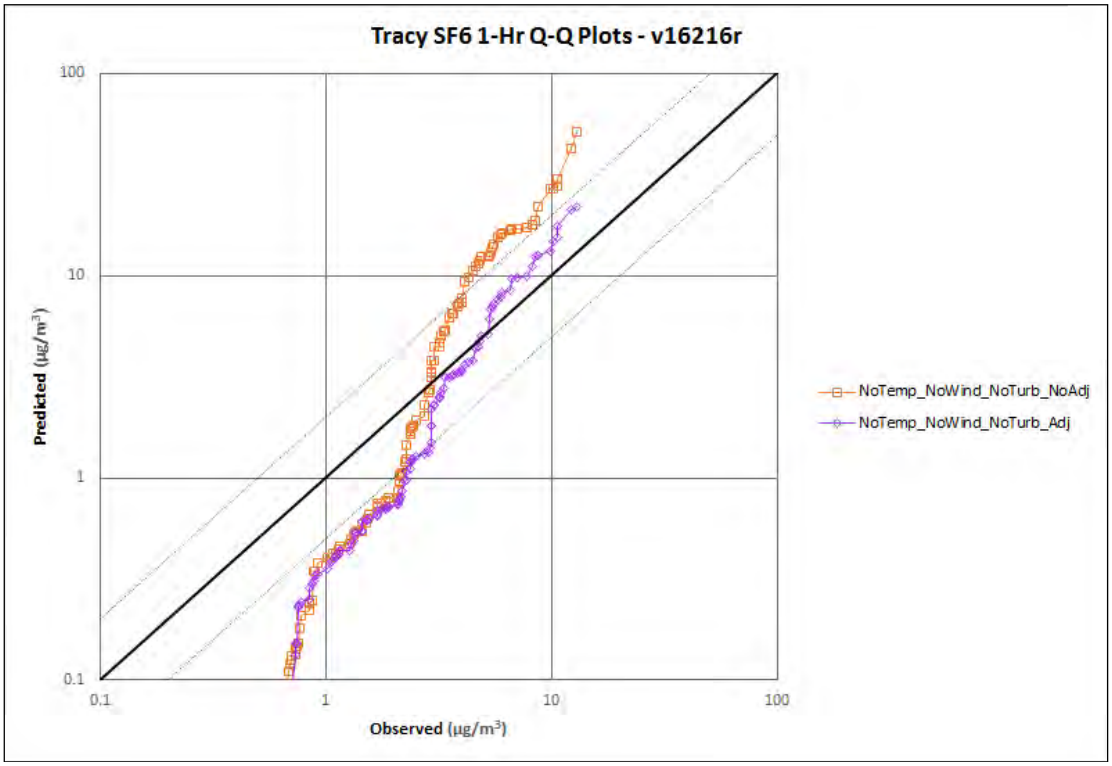

*Figure 21. Tracy – 10-m Temp – 10-m Winds – No Turbulence - With and Without ADJ_U**

C.3.1.2 Lovett Power Plant, New York (1987-1988)

Similar to Tracy, a meteorological degradation analysis was performed for the Lovett evaluation database to compare concentrations modeled with and without the ADJ_U* option, to observed concentrations using site-specific meteorological data that represent varying degrees of degradation, including:

- Wind and temperature profile with turbulence
- Wind and temperature profile without turbulence;
- Temperature profile without wind profile and without turbulence;
- 10-m temperature, wind profile and turbulence;
- 10-m temperature, wind profile, without turbulence;
- 10-m temperature without wind profile and without turbulence.

Table 14 shows the 1-hour, 3-hour, and 24-hour RHC and CPM for each meteorological scenario modeled with and without the ADJ_U* option. The best performing scenario was the full meteorological data without ADJ_U* (shaded green in Table 14), which fits EPA's recommendation that when turbulence data are present, ADJ_U* should not be used. When turbulence data are not included, the results are mixed. For every level of degraded meteorology, the use of the ADJ_U* option appears to improve model performance when comparing the ratios of the predicted to observed 1-hour RHC values. However, the 3-hour and 24-hour RHCs and the CPMs are not consistent with the 1-hour results in every case.

Figure 22 through Figure 24 are Q-Q plots of observed-to-modeled 1-, 3-, and 24-hour concentrations for the meteorological scenarios that include the full meteorological data and degraded meteorology most similar to NWS data. These results support EPA's recommendation on the use of ADJ_U*. For each of the two meteorological scenarios compared in the figures (*i.e.,* full meteorology with turbulence data and degraded NWS-like meteorology), the lower end of the distribution is similar, regardless of the use of ADJ_U* option. At the uppermost end of the distribution, the figures illustrate the best performing scenario is the full meteorological dataset without the ADJ_U* option applied (olive-green points). When ADJ_U* is applied to the full meteorological dataset (orange points), there is a greater bias toward underprediction. For the meteorological scenario most similar to NWS data, there was improved performance at the high

end of the distribution when the ADJ_U* option was applied (blue points), compared to when ADJ_U* was not applied (purple points).

Table 14. Robust High Concentrations and Composite Performance Measures for Lovett Meteorological Degradation Analysis

Scenario†	Robust Highest Concentration (µg/m³) (Pred/Obs)			CPM
	1-hour *(obs = 426)*	**3-hour** *(obs = 187)*	**24-hour** *(obs = 52)*	
Non-adjusted u*; with temperature profile; with wind profile; with turbulence	374 (0.88)	169 (0.90)	48 (0.92)	0.40
Adjusted u*; with temperature profile; with wind profile; with turbulence	361 (0.85)	168 (0.90)	46 (0.88)	0.42
Non-adjusted u*; with 10 m temperature only; with wind profile; with turbulence	654 (1.54)	293 (1.57)	90 (1.73)	0.68
Adjusted u*; with 10 m temperature only; with wind profile; with turbulence	563 (1.32)	295 (1.58)	83 (1.60)	0.65
Non-adjusted u*; with 10 m temperature only; with wind profile; no turbulence	1055 (2.48)	596 (3.19)	120 (2.31)	1.01
Adjusted u*; with 10 m temperature only; with wind profile; no turbulence	1010 (2.37)	547 (2.93)	105 (2.02)	0.94
Non-adjusted u*; with temperature profile; with wind profile; no turbulence	622 (1.46)	254 (1.36)	68 (1.31)	0.57
Adjusted u*; with temperature profile; with wind profile; no turbulence	544 (1.28)	236 1.26()	63 (1.21)	0.52
Non-adjusted u*; with temperature profile; no wind profile; no turbulence	549 (1.29)	165 (0.88)	36 (0.69)	0.47
Adjusted u*; with temperature profile; no wind profile; no turbulence	494 (1.16)	162 (0.87)	34 (0.65)	0.50
Non-adjusted u*; with 10 m temperature only; no wind profile; no turbulence *(similar to NWS)*	1132 (2.66)	523 (2.80)	109 (2.10)	0.91
Adjusted u*; with 10 m temperature only; no wind profile; no turbulence *(similar to NWS)*	1034 (2.43)	601 (3.21)	115 (2.21)	0.95

† *The default scenario is bolded. Green shading indicates best performing scenario.*

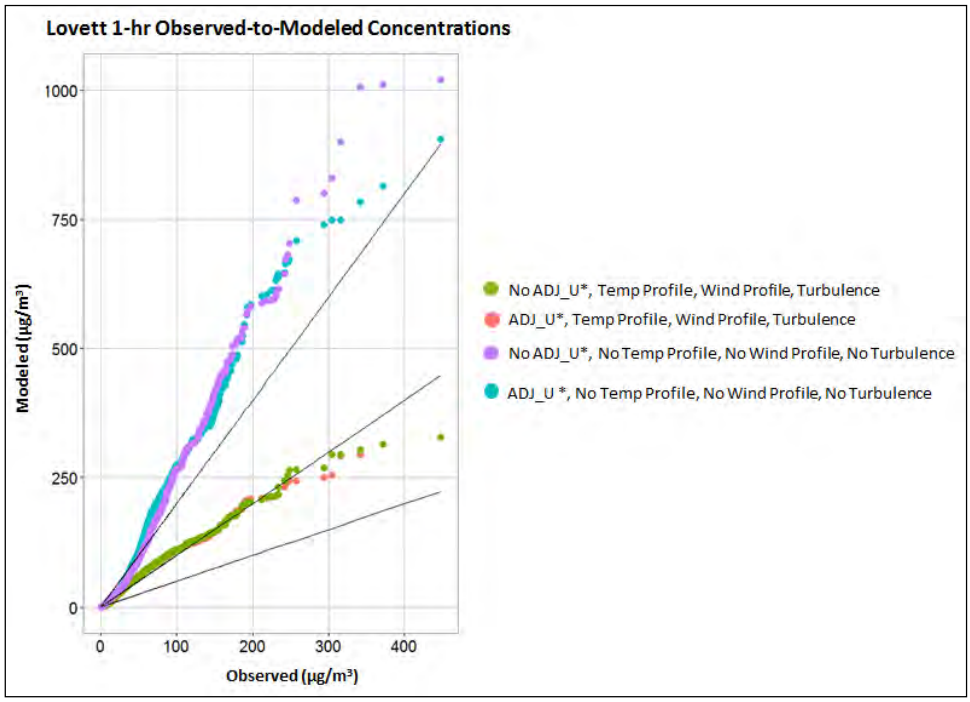

Figure 22. Lovett 1-hr Q-Q Plot for Meteorological Degradation Analysis

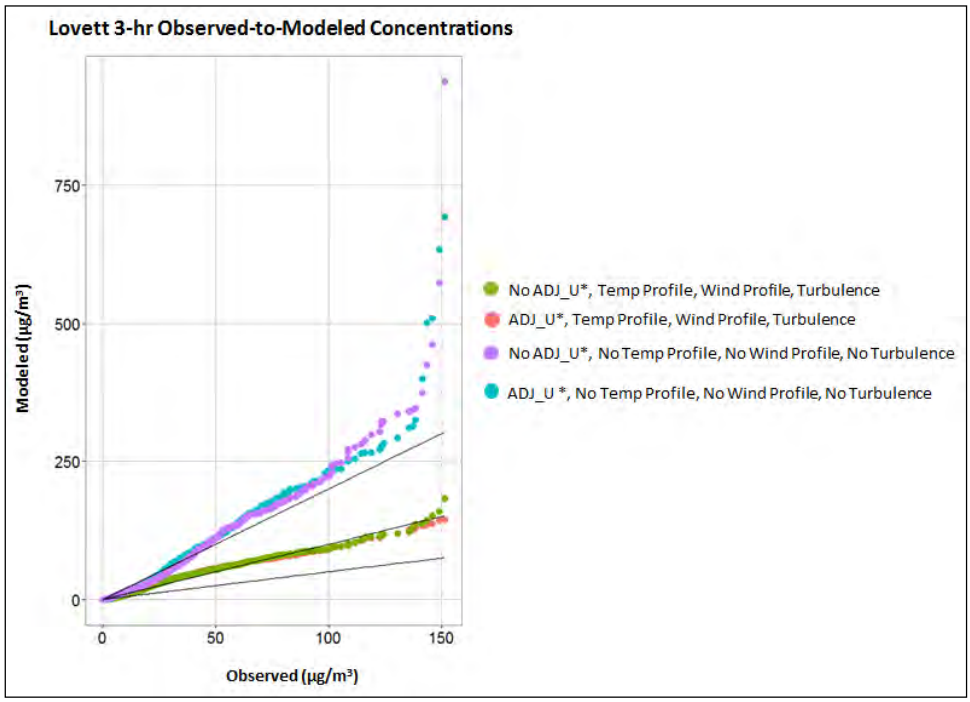

Figure 23. Lovett 3-hr Q-Q Plot for Meteorological Degradation Analysis

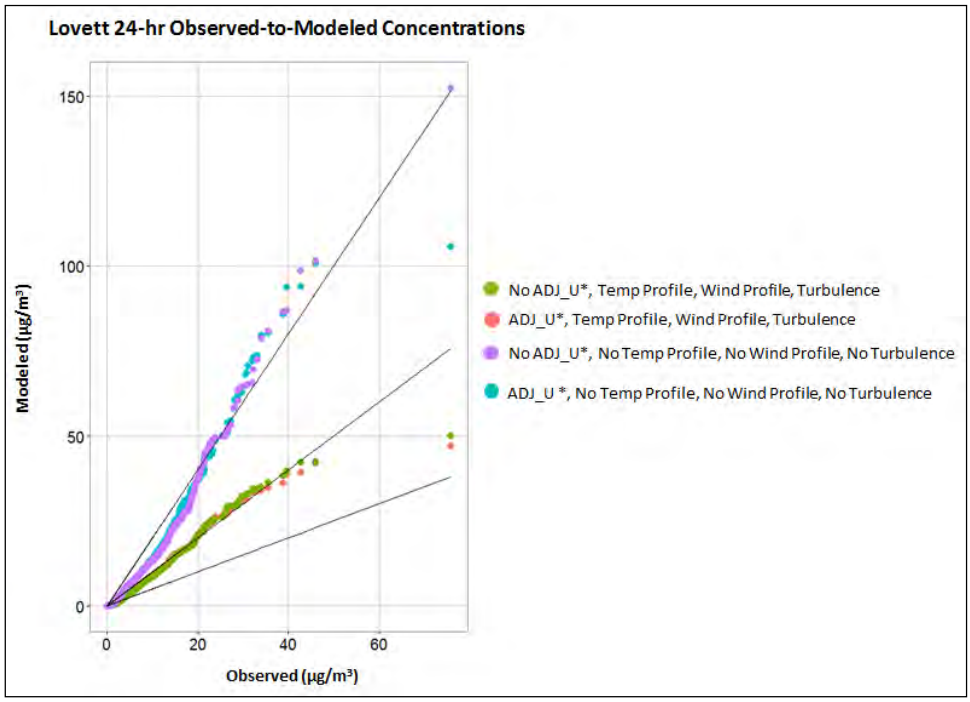

Figure 24. Lovett 24-hr Q-Q Plot for Meteorological Degradation Analysis

C.4.1.3 Oak Ridge, Tennessee (1974)

The Oak Ridge analysis was performed with and without the ADJ_U* option applied. FBs and RHCs were computed and compared for predicted concentrations from each scenario and the observed concentrations. These model performance statistics are based on the arc maximum 1-hour concentration from each receptor arc.

Table 15 compares the FB and RHC for the two modeling configurations and the RHC for the observed concentrations. Figure 25 and Figure 26 are plots of the predicted versus observed receptor arc maximum concentrations by distance and the ratio of predicted-to-observed concentrations by distance, without the use of the ADJ _U* option. Figure 27 and Figure 28 are comparable plots showing results with the ADJ_U* option. Each of the plots display results by receptor arc distance. The tables and figures illustrate the substantial effect the ADJ_U* option can have on the predicted concentrations during low wind conditions, and they demonstrate considerable improvement for the Oak Ridge evaluation when the ADJ_U* is applied.

While the Oak Ridge evaluation results are less robust for evaluating model performance than the evaluation results Tracy and Lovett, there is significant improvement in model-to-monitor comparisons for Oak Ridge based on use of the ADJ_U* option.

Table 15. Oak Ridge Comparison of FBs and RHCs (based on receptor arc maximum concentrations)

		Observed RHC = 82.67 µg/m³
Scenario† *Does not include turbulence*	**FB**	**RHC** (*µg/m³*) **(Pred/Obs)**
Without ADJ_U*	-1.62	798.20 (9.66)
With ADJ_U*	-0.36	116.23 (1.41)

† *Positive (negative) FB indicates under (over) prediction. Green shading indicates best performer. Yellow shading is outside factor of ± 2 (FB±0.67).*

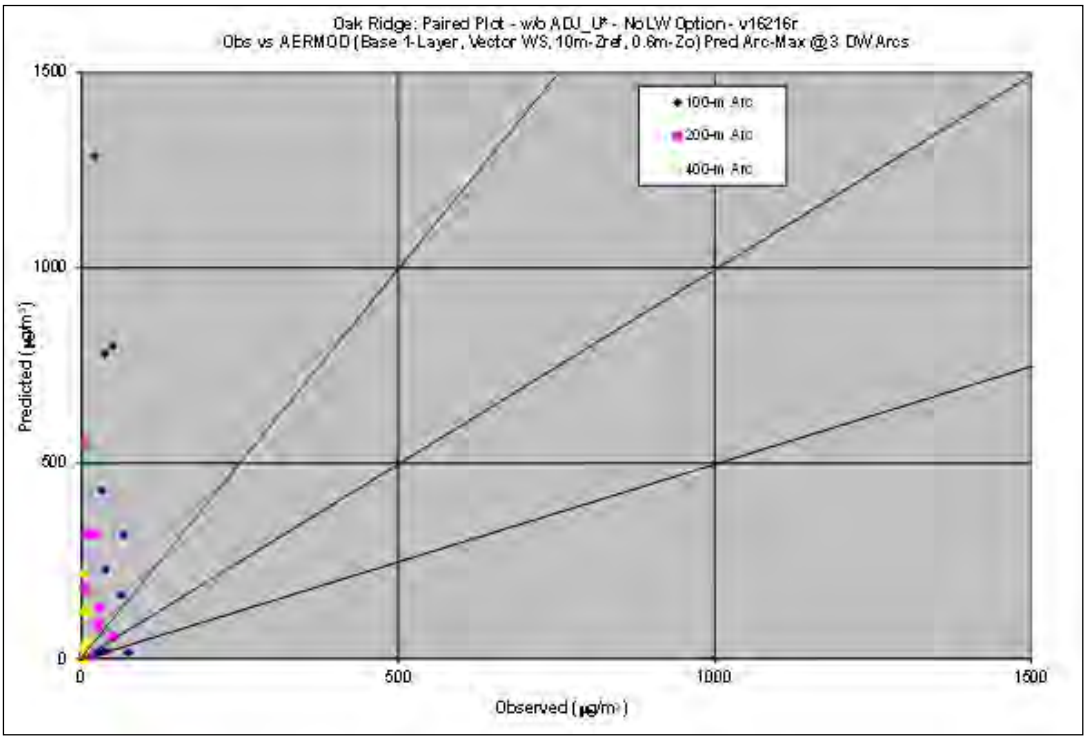

*Figure 25. Oak Ridge Observed-to-Predicted Arc-Max Concentrations Paired in Time, without ADJ_U**

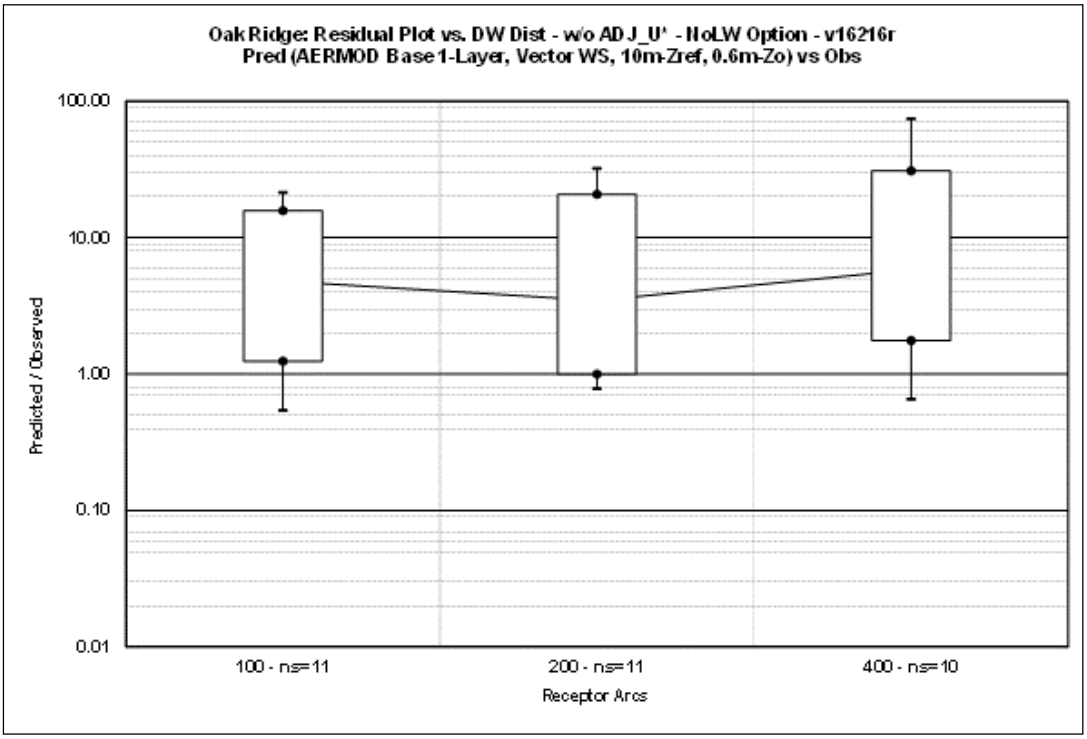

*Figure 26. Oak Ridge, Ratio of Predicted-to-Observed Concentrations, without ADJ_U**

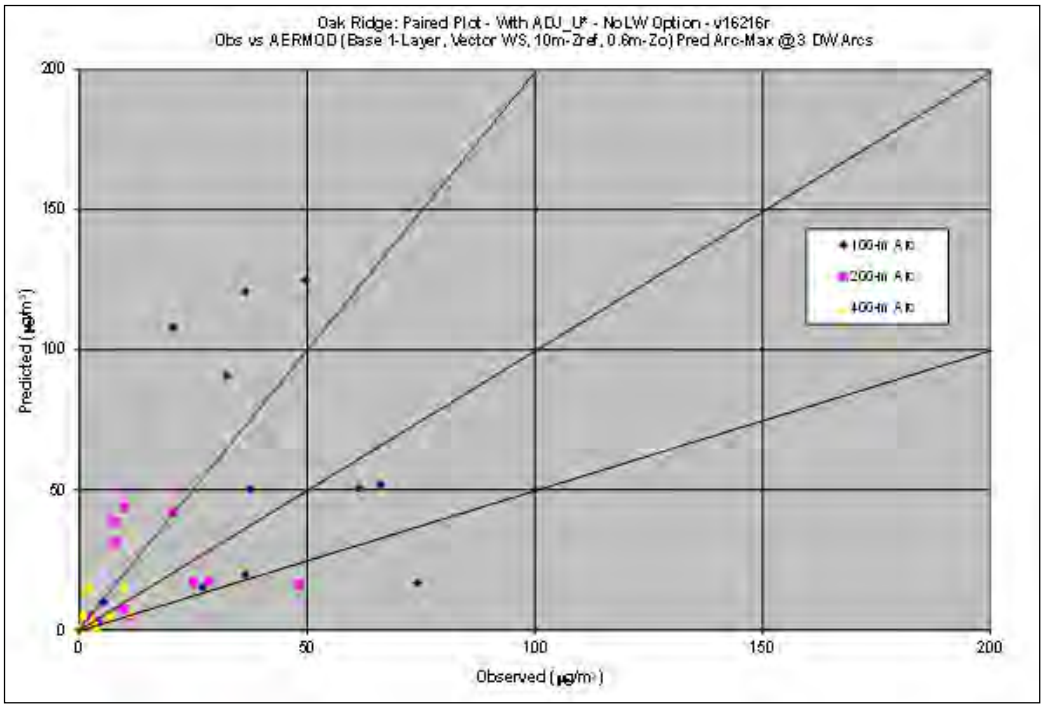

*Figure 27. Oak Ridge Observed-to-Predicted Arc-Max Concentrations Paired in Time, with ADJ_U**

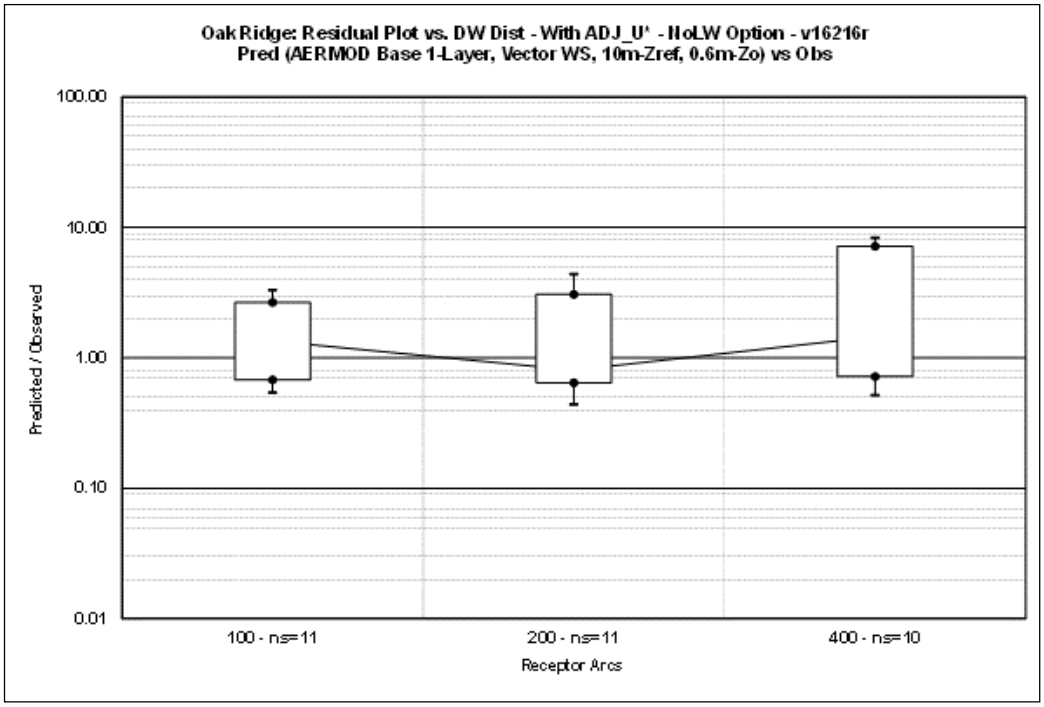

*Figure 28. Oak Ridge, Ratio of Predicted-to-Observed Concentrations, with ADJ_U**

C.3.1.4. Baldwin Power Plant, Illinois (1982-1983)

The Baldwin study was modeled with and without the ADJ_U* option applied to obtain predicted values for 1-hour, 3-hour, and 24-hour averaging periods. RHCs and the MCM comparing the two modeled scenarios are presented in Table 16 and Table 17. Q-Q plots for 1-, 3-, and 24-hour averaged concentrations are provided in Figure 29 through Figure 31, respectively.

The results for the two scenarios (*i.e.*, with and without ADJ_U*) are nearly identical for each averaging period. This is seen in the RHCs, the MCM, and the Q-Q plots. The MCM results show that concentration differences with and without ADJ_U* were statistically insignificant at the 95% confidence interval (intervals cross zero). The plotted curves match so closely in each figure that only one curve is visible. This was expected since the Baldwin study is based on tall stacks in flat terrain, an environment in which the ADJ_U* option should have little to no influence.

Table 16. Comparison of Baldwin Observed and Modeled Robust High Concentrations

Location	Avg. Time (hr)	Robust Highest Concentration ($\mu g/m^3$) (Pred/Obs)		
		Observed	No ADJ_U* No Turbulence	ADJ_U* No Turbulence
Baldwin	1	2348	3531 (1.50)	3531 (1.50)
	3	920	1184 (1.29)	1182 (1.28)
	24	209	230 (1.10)	230 (1.10)

Table 17. Baldwin Model Comparison Measure

Model Scenarios Compared	MCM	90% CI	95% CI
No ADJ_U* - ADJ_U*	0.002	±0.14	±0.19

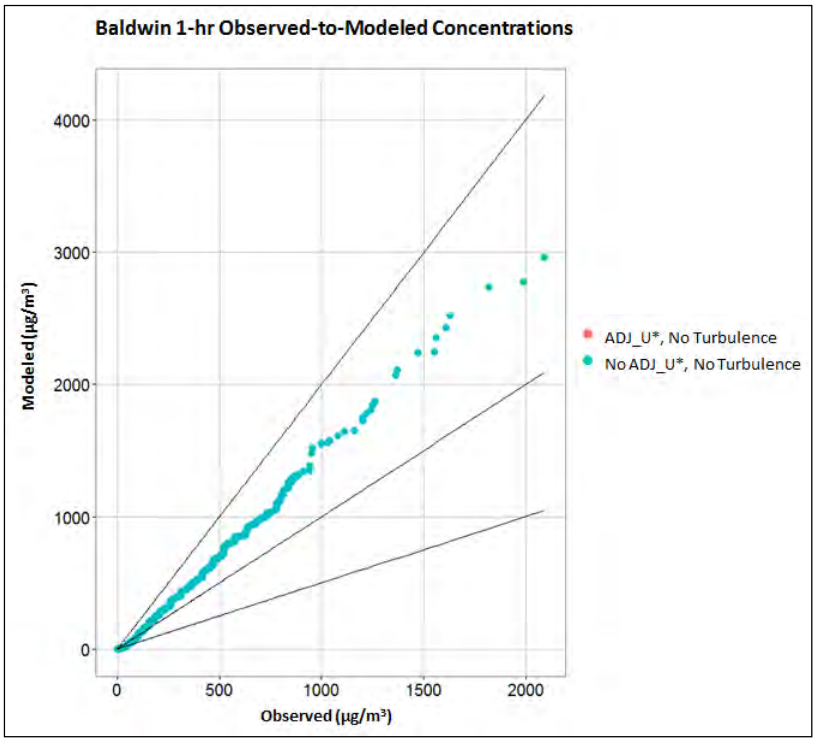

*Figure 29. Baldwin 1-hour Q-Q Plots, With and Without ADJ_U**

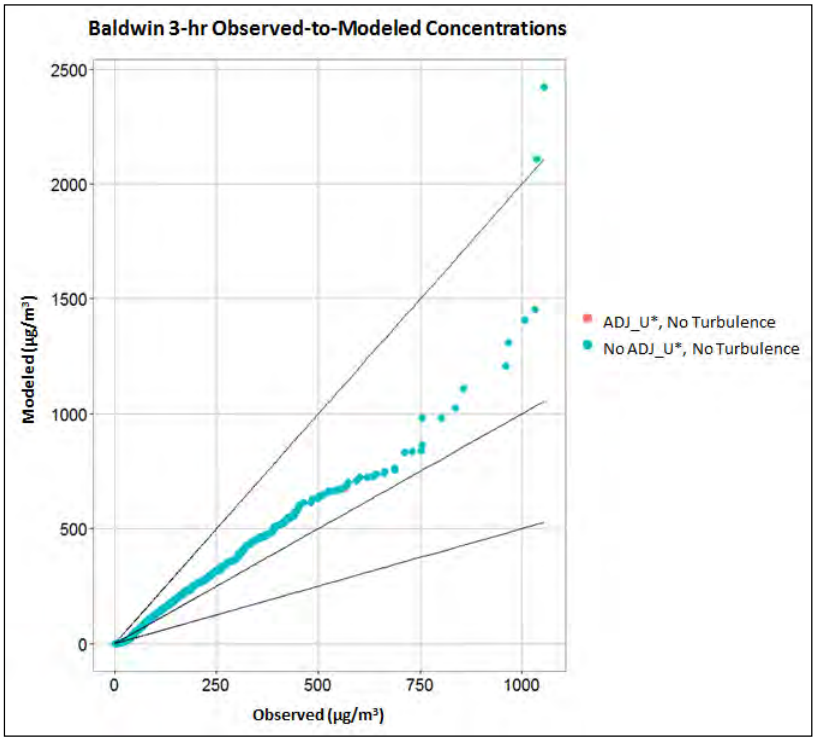

*Figure 30. Baldwin 3-hour Q-Q Plots, With and Without ADJ_U**

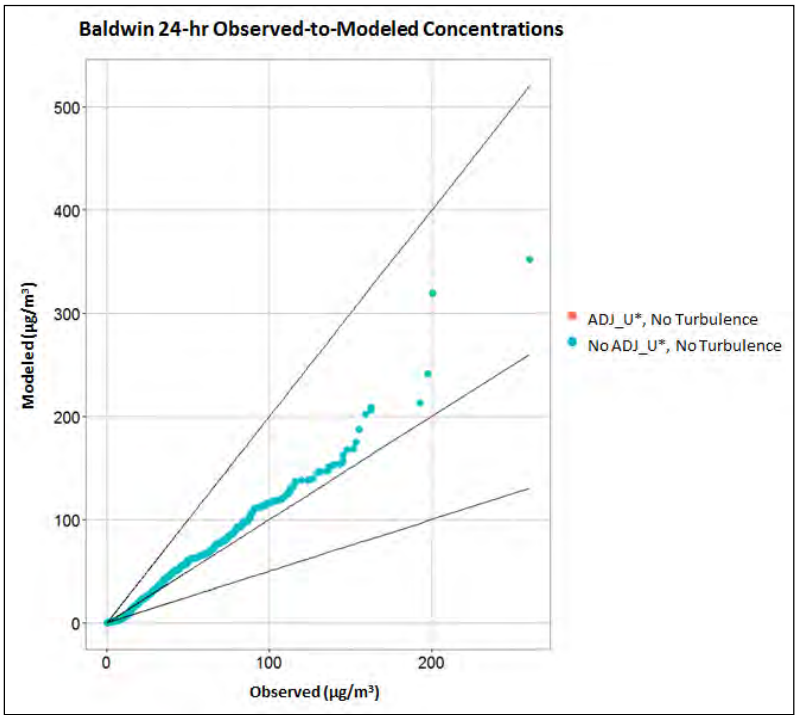

*Figure 31. Baldwin 24-hour Q-Q Plots, With and Without ADJ_U**

C.3.1.5. Kincaid SO_2, Illinois (1980-1981)

Unlike Baldwin, the Kincaid SO2 study does include turbulence measurements. Modeling was performed with and without the ADJ_U* option applied and with and without turbulence measurements included. Predicted 1-hour, 3-hour, and 24-hour average concentrations were generated. RHCs and the MCMs from the different meteorological and model configurations are compared in Table 18 and Figure 19. Q-Q plots for the 1-, 3-, and 24-hour averaged concentrations are presented in Figure 32 through Figure 34.

The use of ADJ_U* had little effect on concentrations, regardless of the inclusion of the turbulence measurements. Like Baldwin, this was expected since the Kincaid study is based on tall stacks in flat terrain. As shown in a comparison of the RHCs and MCM's in Table 18 and Table 19 and the figures that follow, the influencing factor is the turbulence measurements. When turbulence measurements are included, the results are near identical regardless of the use of the ADJ_U* option. For this reason, only one set of points is visible for each the two meteorological scenarios presented in the figures. However, these results do support the position that when the data are available, the preferred option is to use site-specific meteorology with turbulence measurements, without the ADJ_U* option.

Table 18. Comparison of Kincaid Observed and Modeled Robust High Concentrations

Avg. Time (hr)	Robust Highest Concentration *(µg/m³)* (Pred/Obs)				
		No ADJ_U*		ADJ_U*	
	Observed	No Turbulence	With Turbulence†	No Turbulence	With Turbulence
1	1611	717 (0.45)	1311 (0.81)	717 (0.45)	1313 (0.82)
3	618	470 (0.76)	635 (1.03)	470 (0.76)	599 (0.97)
24	113	167 (1.48)	103 (0.91)	167 (1.48)	101 (0.89)

† *Default scenario.*

Table 19. Kincaid Model Comparison Measures

Model Scenarios Compared†	MCM	90% CI	95% CI
ADJ_U*/No Turbulence - No ADJ_U*/No Turbulence	0.00	±0.14	±0.18
No ADJ_U*/With Turbulence - ADJ_U*/With Turbulence	-0.01	±0.39	±0.45
No ADJ_U*/ With Turbulence - No ADJ_U*/No Turbulence	-0.19	±0.31	±0.36
ADJ_U*/ No Turbulence - **No ADJ_U*/With Turbulence**	0.19	±0.31	±0.36
No ADJ_U*/ No Turbulence - ADJ_U*/With Turbulence	0.18	±0.32	±0.37
ADJ_U*/ No Turbulence - ADJ_U*/With Turbulence	0.18	±0.32	±0.36

† *Default scenario is bolded*

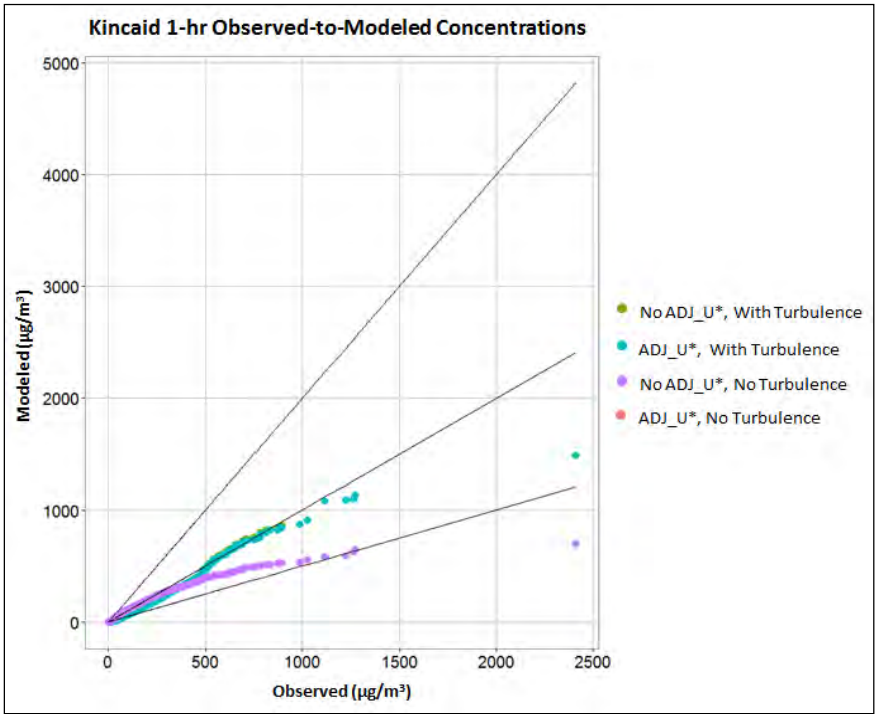

*Figure 32. Kincaid 1-hour Q-Q Plots, w/ and w/o Turbulence, w/ and w/o ADJ_U**

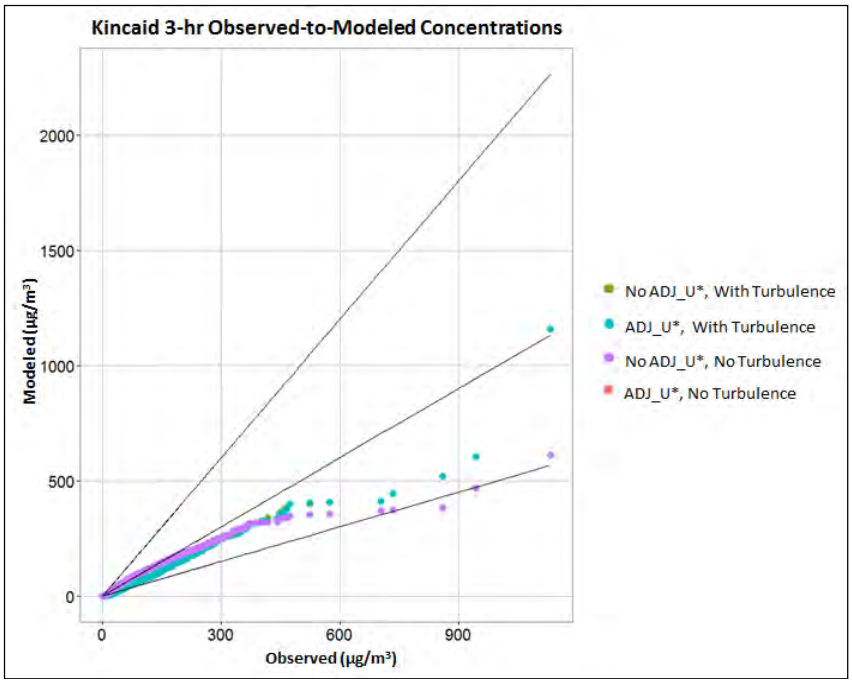

*Figure 33. Kincaid 3-hour Q-Q Plots, w/ and w/o Turbulence, w/ and w/o ADJ_U**

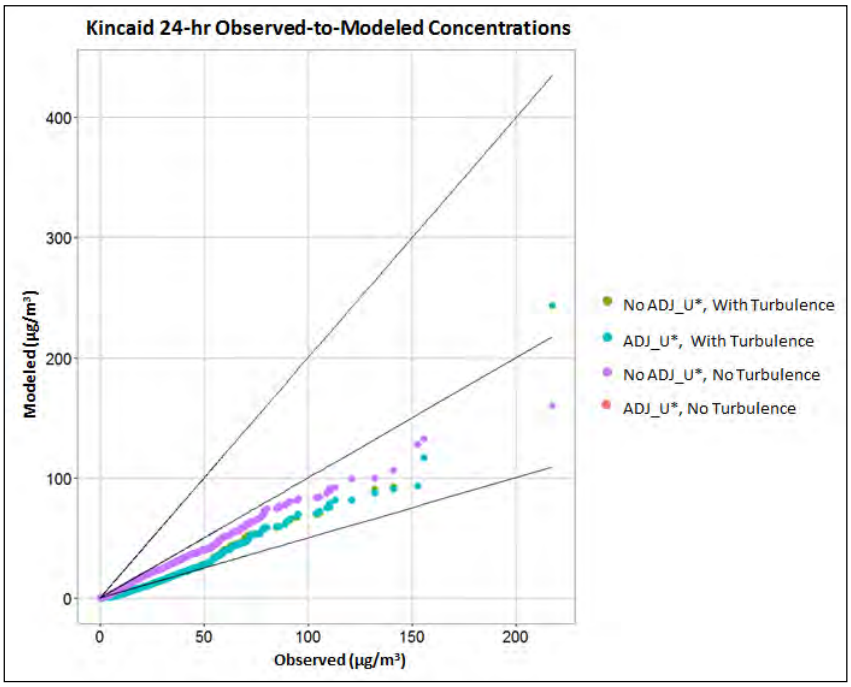

*Figure 34. Kincaid 24-hour Q-Q Plots, w/ and w/o Turbulence, w/ and w/o ADJ_U**

C.3.1.6. Cordero Rojo Mine, Wyoming (1993)

The Cordero mine was modeled with and without the ADJ_U* option applied and with and without turbulence measurements included. The Cox-Tikvart protocol for determining the best performing model was applied to the AERMOD results. The tabular results of the protocol are provided in Table 20 and Table 21. The CPM and MCM values for each modeled scenario are displayed graphically in Figure 43 and Figure 44.

EPA acknowledges there are challenges with the Cordero field study such as determining appropriate source characteristics for the various mining activities that were accounted for in the evaluation, including wind erosion, and determining appropriate emission rates for the various sources included in the study. While AERMOD over predicts in each modeling scenario, the results clearly demonstrate the effect ADJ_U* has on the predicted concentrations. As the sources were characterized in this modeling study, the better performing model scenario is shown to be the use of ADJ_U* in combination with the turbulence data, which is counter to the preferred method of using site-specific meteorology that includes turbulence measurements without the use of the ADJ_U* option. However, in the case of the Cordero study, this result is due the overprediction in all cases and the effect of the ADJ_U* option to further reduce concentrations when applied in combination with turbulence measurements. This method can lead to underprediction for many applications using site-specific data that include turbulence.

Table 20. Cordero Comparison of FBs, RHCs, and CPMs for Multiple Scenarios

Observed RHC = 21.34 µg/m³					
Model†	**FB**	**RHC (Pred/Obs)**	**CPM**	**90% CI**	**95% CI**
16DefTurb	-0.92	57.69 (2.70)	0.71	±0.18	±0.22
16DefNoTurb	-1.06	69.56 (3.26)	0.75	±0.18	±0.22
16AdjTurb	-0.45	33.69 (1.58)	0.43	±0.17	±0.21
16AdjNoTurb	-0.53	36.77 (1.72)	0.46	±0.16	±0.20

† *Default scenario is bolded. Positive (negative) FB indicates under (over) prediction. Green shading indicates best performer. Yellow shading is outside factor of ± 2 (FB±0.67).*

Table 21. Cordero MCMs for Multiple Scenarios

Model Scenarios Compared†	**MCM**	**90% CI**
16DefTurb -16AdjTurb	0.28	±0.28
16DefTurb -16DefNoTurb	-0.04	±0.10
16DefTurb -16AdjNoTurb	0.25	±0.25
16AdjTurb -16DefNoTurb	-0.32	±0.30
16AdjTurb-16AdjNoTurb	-0.03	±0.08
16DefNoTurb-16AdjNoTurb	0.29	±0.27

† *Default scenario is bolded. Yellow shading indicates there is a significant difference between the two scenarios.*

C.3.1.7. Idaho Falls, Idaho (1974)

The evaluation results for Idaho Falls were based in part on information provided by AECOM from a 2009 low wind evaluation study (AECOM, 2010). However, some adjustments to inputs were made based on an independent assessment of surface roughness, and an adjustment was made to the effective tracer release height at Idaho Falls from 1.5 to 3m based on information provided in the NOAA technical memorandum (NOAA, 1974).

The ADJ_U* option was evaluated using:

- Full set of meteorology, which includes multiple levels of wind, temperature, and sigma-theta, and
- Degraded meteorology, which includes the multiple levels of wind and temperature but does not include sigma-theta.

A comparison of the FBs and RHCs based on the 1-hr maximum concentration from each receptor arc for each hour is provided in Table 22. Though each of the modeling scenarios overpredicts the RHC, the effect of applying the ADJ_U* option is evident in its reduction of the RHC.

Table 22. Idaho Falls Comparison of FBs and RHCs (based on all receptor arc-max concentrations)

		Observed RHC = 132.60 µg/m³
Scenario†	**FB**	**RHC** (*µg/m³*) **(Pred/Obs)**
FullMet_NoAdjU* (incl. turbulence)	-0.30	198.05 (1.49)
FullMet_AdjU* (incl. turbulence)	-0.18	176.43 (1.33)
DegMet_NoAdjU* (no turbulence)	-0.80	328.76 (2.48)
DegMet_AdjU* (no turbulence)	-0.64	275.80 (2.08)

† *Default scenario is bolded. Positive (negative) FB indicates under (over) prediction. Green shading indicates best performer. Yellow shading is outside factor of ± 2 (FB±0.67).*

Figure 35 through Figure 38 are plots of observed versus predicted 1-hour concentrations based on the receptor arc-maximum values paired in time and box plots of the ratio of predicted to observed concentrations by distance, with and without the ADJ _U* option, using full meteorology. Figure 39 through Figure 42 are comparable plots for which the turbulence measurements were omitted. Each of the plots display results by receptor arc distance. Using the full set of site-specific meteorology, including turbulence, without the ADJ_U* option (Figure 35 and Figure 36) shows generally good agreement with observed concentration. Applying ADJ_U* to the full set of meteorology shows a tendency to underpredict for most hours when turbulence data are present (Figure 37 and Figure 38). The underprediction is more substantial at the farthest distance.

When turbulence measurements were omitted from the meteorological processing and ADJ_U* was not applied, there is substantial overprediction as shown in Figure 39 and Figure 40. Applying ADJ_U* in this case, as illustrated in Figure 41 and Figure 42, shows a slight improvement in model performance, but there is still substantial overprediction. The best performing scenario is the use of full site-specific meteorology, with turbulence measurements, and without the ADJ_U* option applied (Figure 35 and Figure 36). This is consistent with EPA's position that modeling with a full meteorological dataset that includes turbulence measurements is preferred and results in the best performance. This evaluation also demonstrates a tendency to underpredict when ADJ_U* is applied when turbulence data are present.

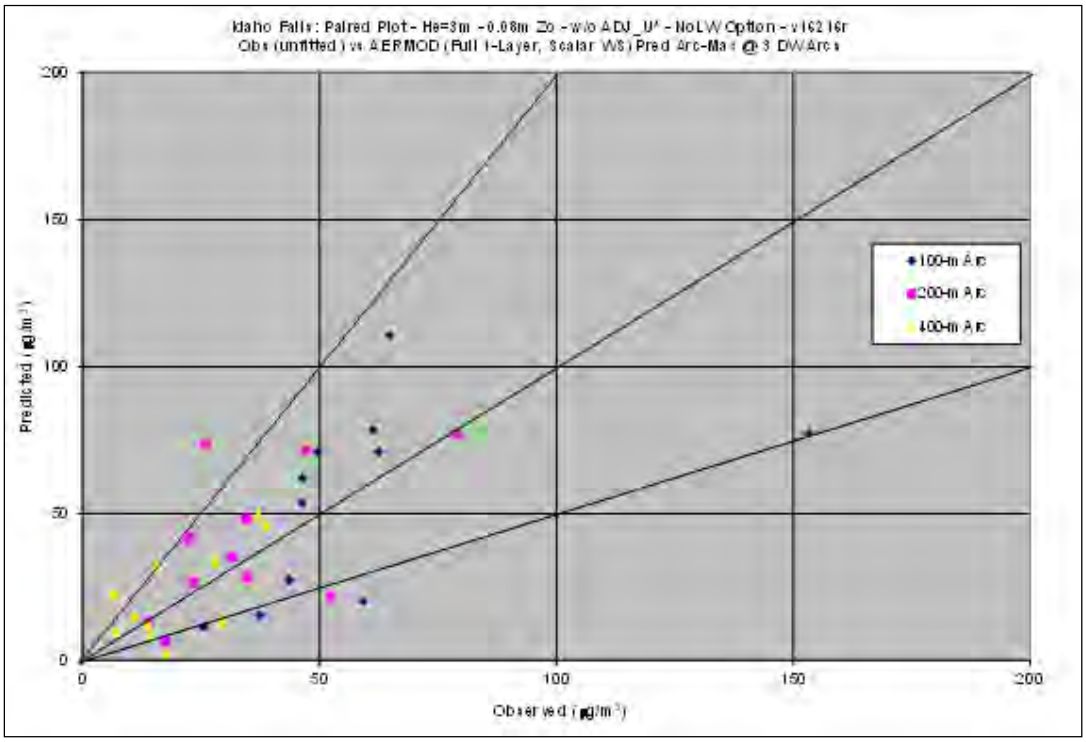

*Figure 35. Idaho Falls Observed-to-Predicted Arc-Max Concentrations Paired in Time, Full Met, No ADJ_U**

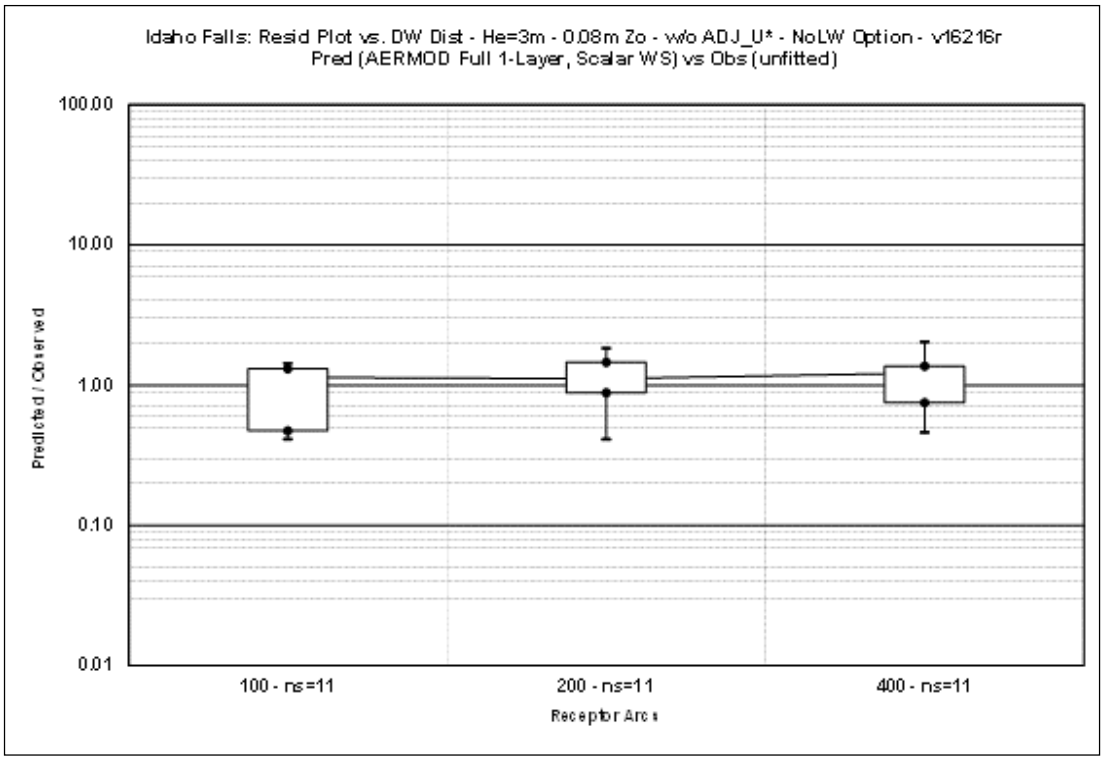

*Figure 36. Idaho Falls Predicted-to-Observed Ratios, Full Met, No ADJ_U**

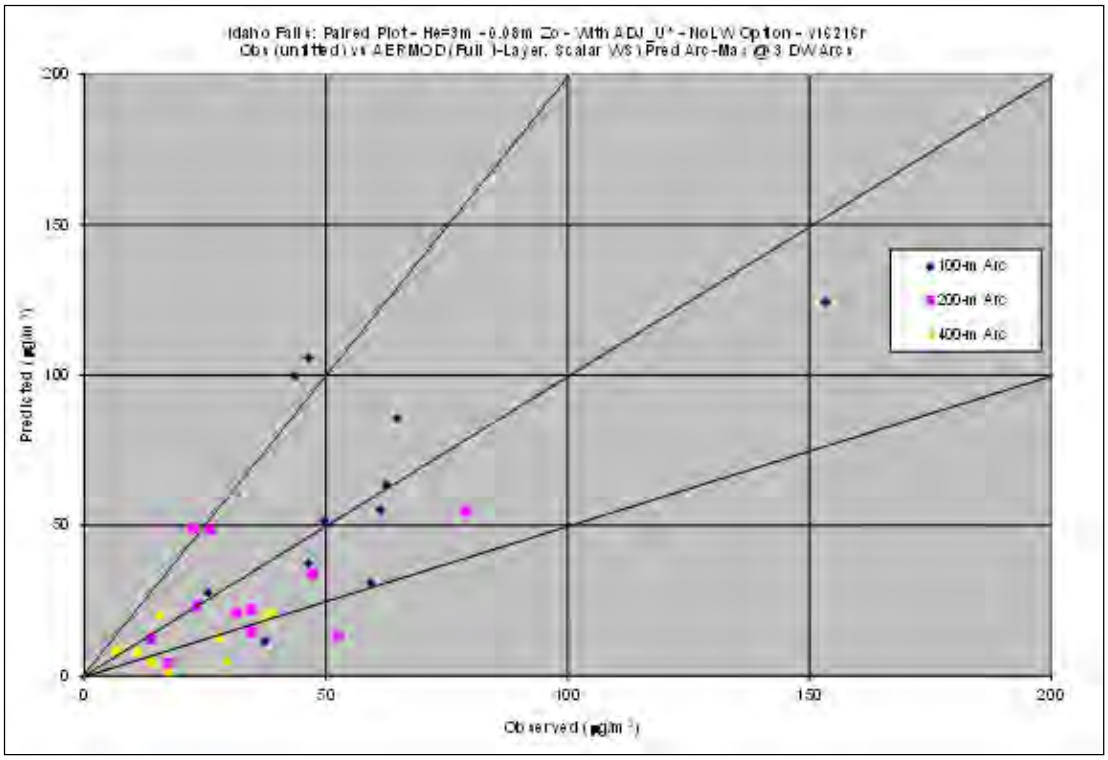

*Figure 37. Idaho Falls 1-hr Observed-to-Predicted Arc-Max Concentrations Paired in Time, Full Met, ADJ_U**

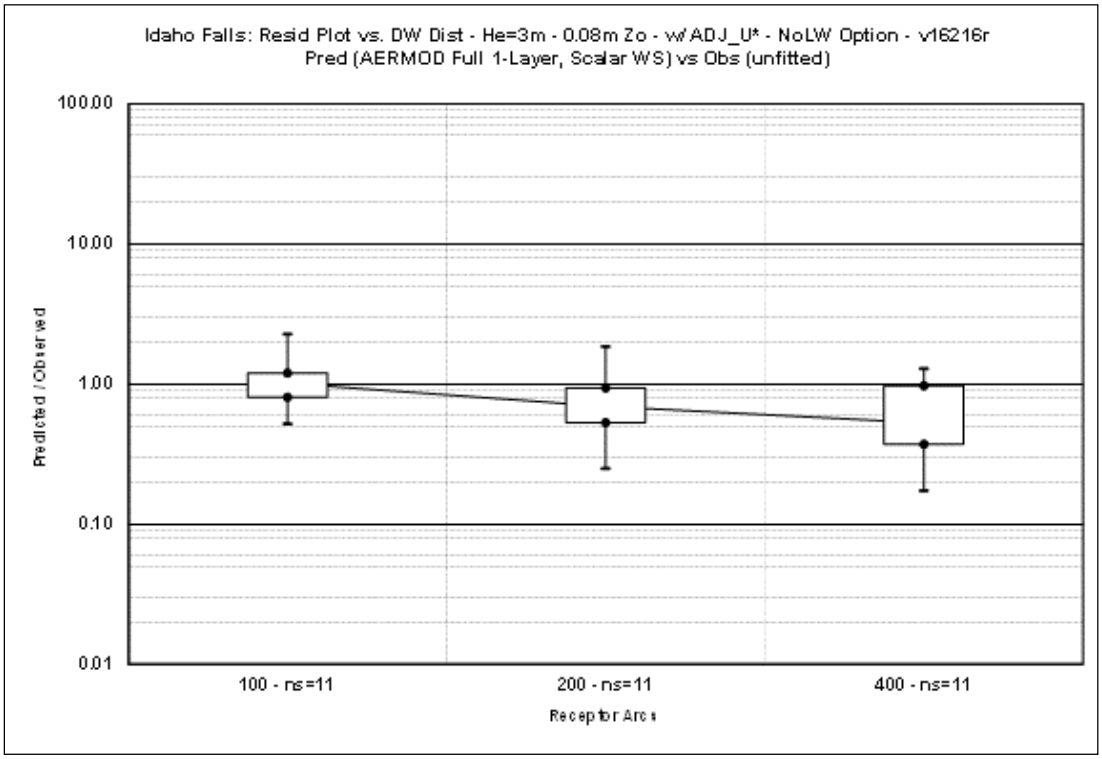

*Figure 38. Idaho Falls 1-hr Predicted-to-Observed Ratios, Full Met, ADJ_U**

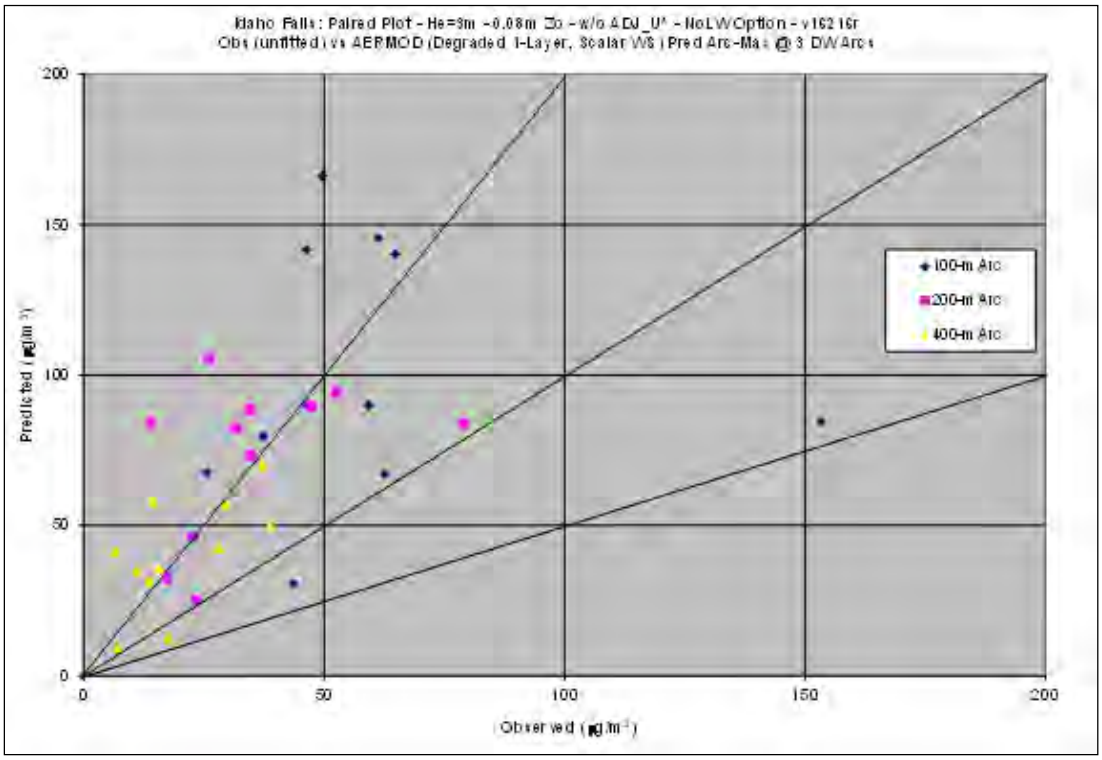

*Figure 39. Idaho Falls 1-hr Observed-to-Predicted Arc-Max Concentrations Paired in Time, No Turbulence, No ADJ_U**

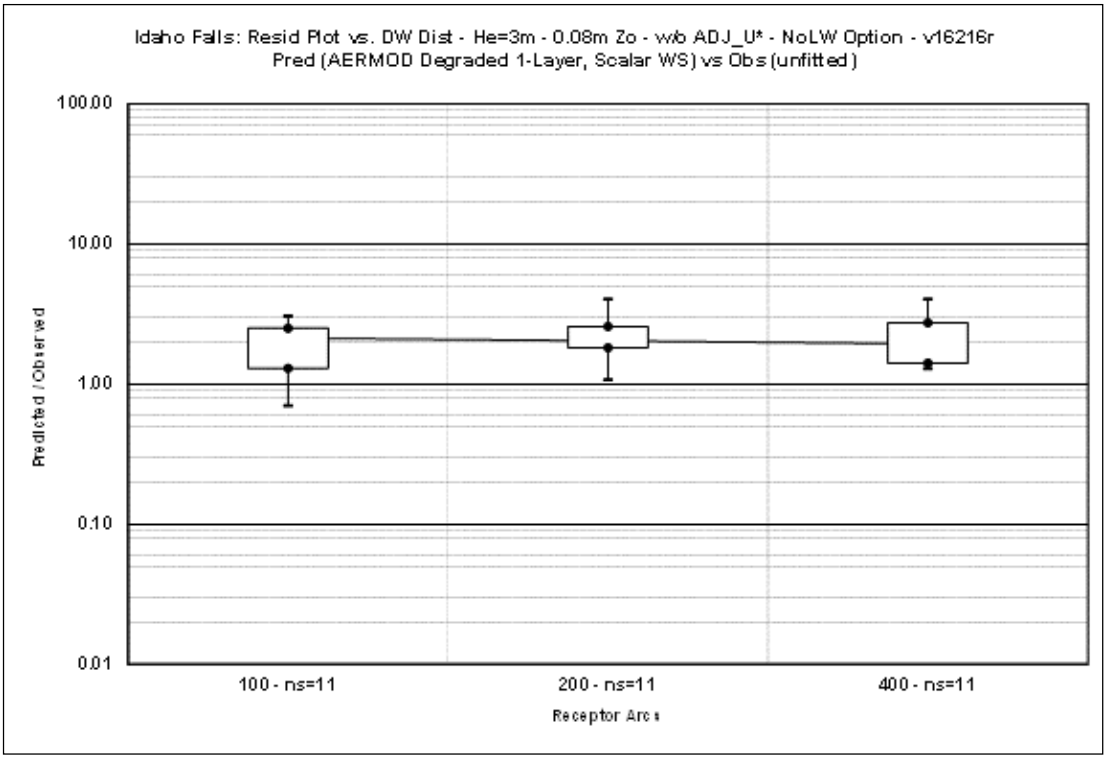

*Figure 40. Idaho Falls 1-hr Predicted-to-Observed Ratios, No Turbulence, No ADJ_U**

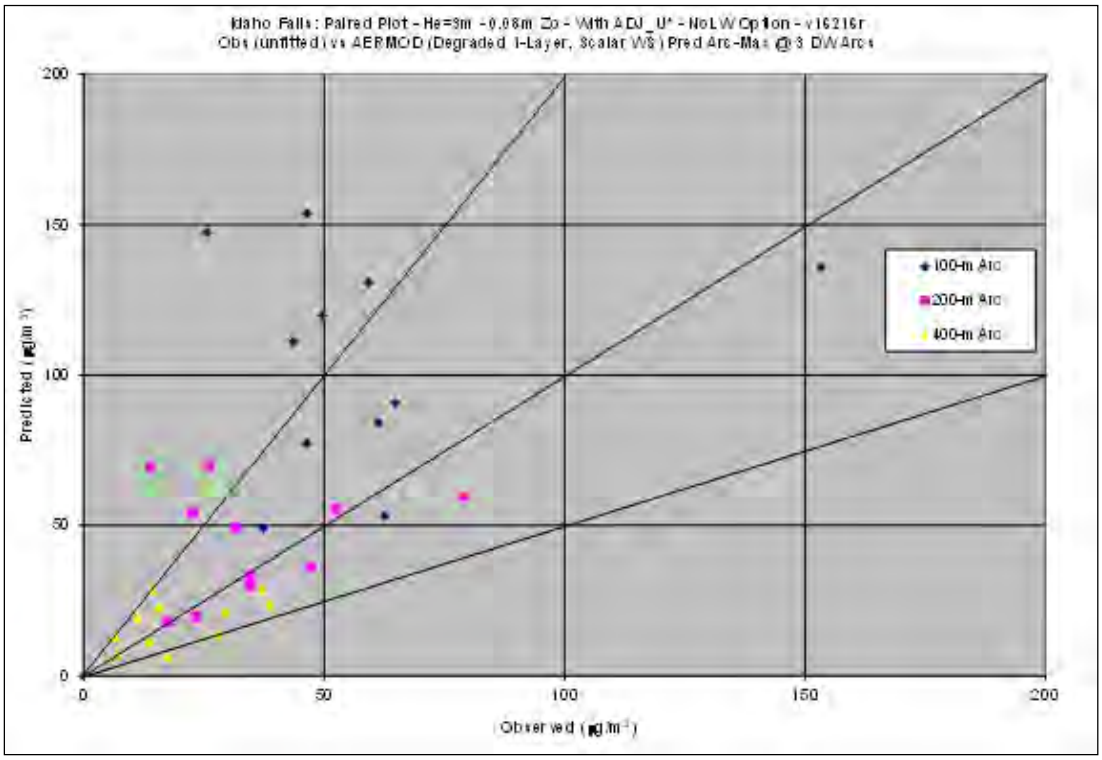

*Figure 41. Idaho Falls 1-hr Observed-to-Predicted Arc-Max Concentrations Paired in Time, No Turbulence, ADJ_U**

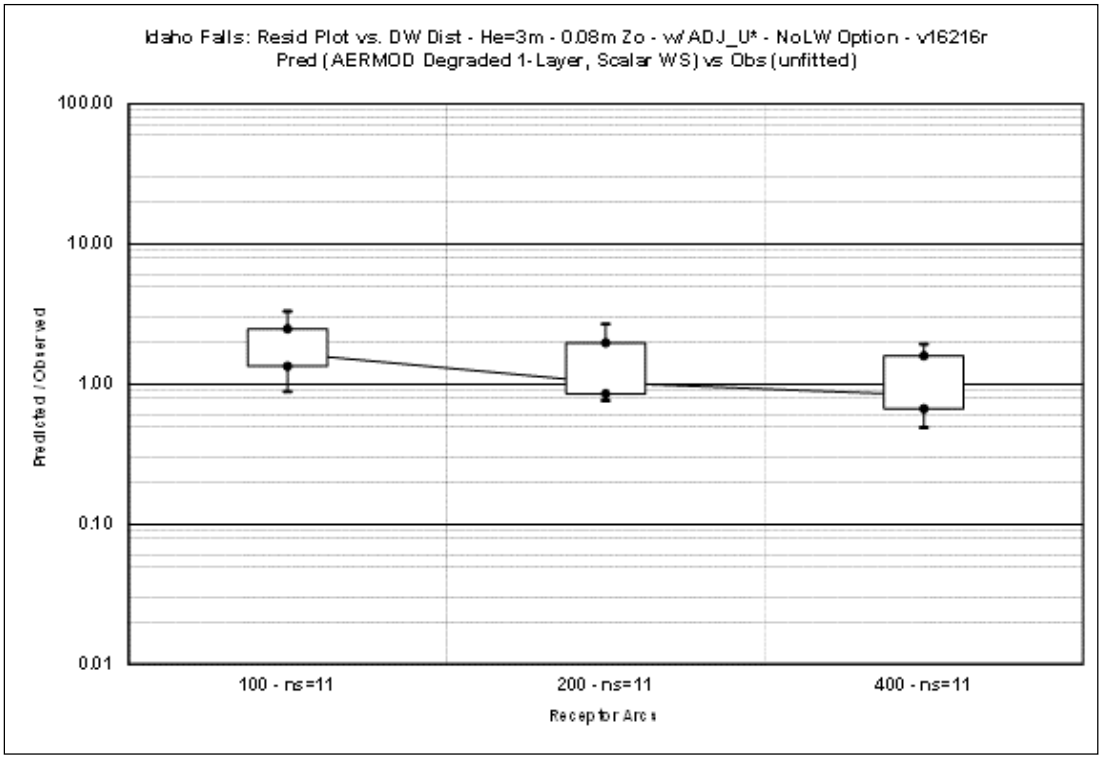

*Figure 42. Idaho Falls 1-hr Predicted-to-Observed Ratios, No Turbulence, ADJ_U**

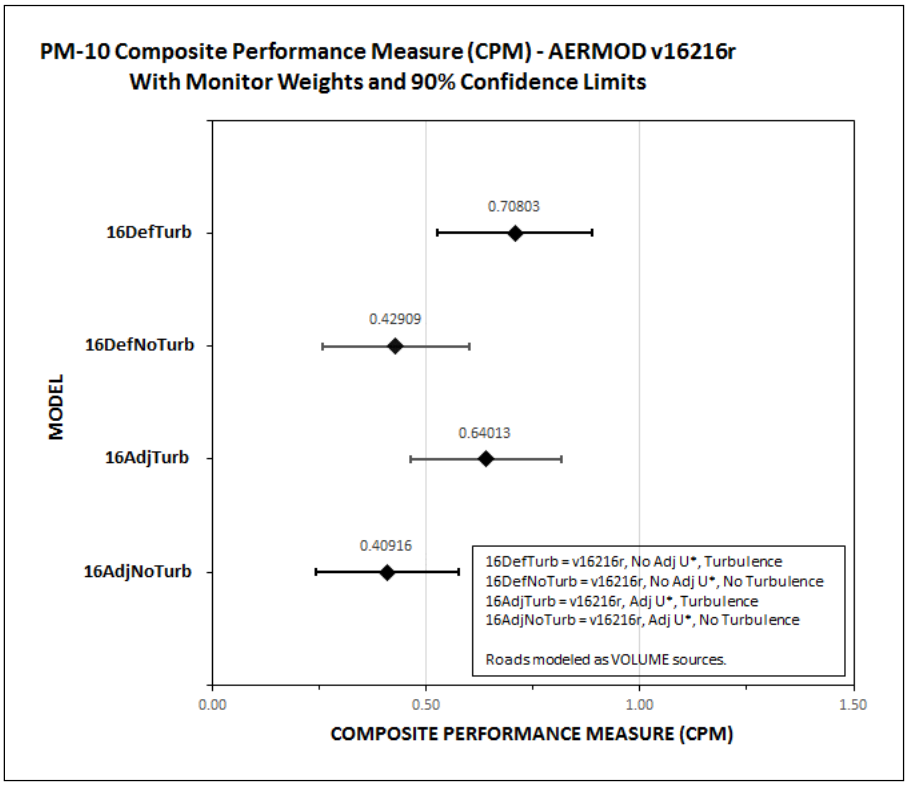

Figure 43. Cordero Composite Performance Measure Comparison (AERMOD v.16216r)

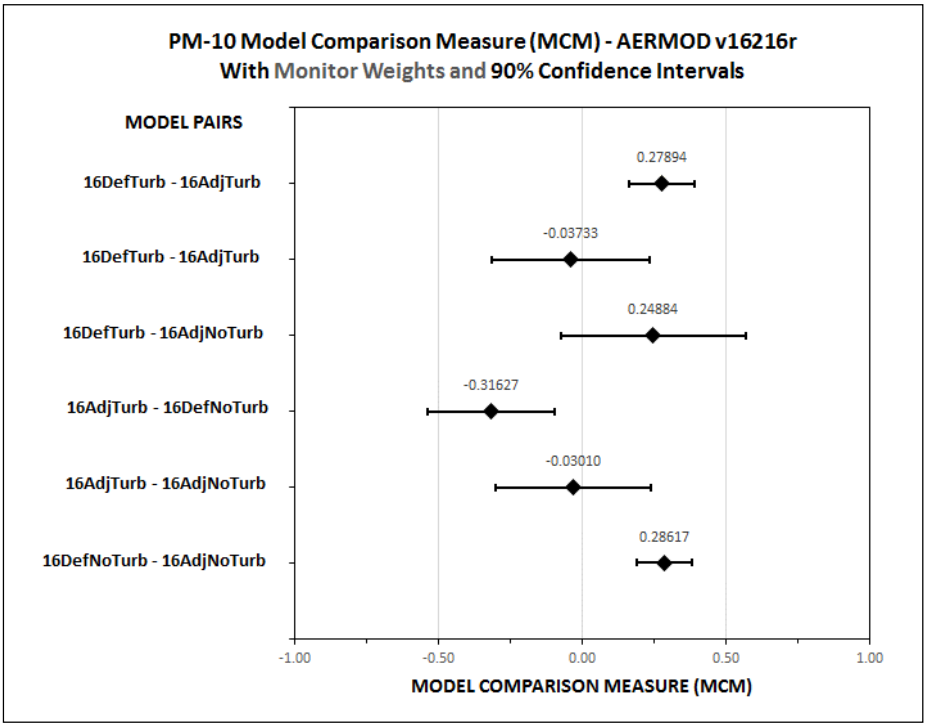

Figure 44. Cordero Model Comparison Measure Comparison (AERMOD v.16216r)

C.3.2. Conclusions from the ADJ_U* Evaluation

The datasets evaluated here represent a wide variety of emissions, terrain, and meteorological scenarios that provide for a broad assessment of the impact of the ADJ_U* option on model performance. As discussed above, the primary interest in the evaluation is the interplay between the ADJ_U* option and site-specific turbulence measurements and an evaluation of the ADJ_U* option without any site-specific turbulence, which mimics the use of NWS data that is typically used in regulatory analyses.

Of the seven studies presented, only the Tracy, Lovett, Kincaid, Cordero, and Idaho Falls studies have turbulence measurements, while the Oak Ridge and Baldwin studies do not. While several of the studies evaluated multiple levels of degraded meteorology, the base analyses are the effects applying the ADJ_U* option to full meteorology, including turbulence when available, and fully degraded meteorology that represents NWS data.

For the evaluation of ADJ_U* with full meteorological data that includes turbulence measurements, the best performing case for several of the field studies (Tracy, Lovett) is when turbulence measurements are included, without the use of the ADJ_U* option. This is shown in Table 23 and Table 24. The ADJ_U* option, when used in conjunction with site-specific turbulence measurements, can lead to underprediction by the model. For the Tracy database, including the ADJ_U* option in AERMET in conjunction with full meteorological data, results in an underprediction of about 40 percent in a comparison of the peak observed and predicted concentrations. ADJ_U* had very little effect on the Kincaid study, regardless whether turbulence measurements were included (Table 25). Applying the ADJ_U* option to the full set of site-specific meteorology with turbulence measurements to the Lovett database also shows a bias toward underprediction. For Cordero and Idaho Falls (Table 26 and Table 27), the model overpredicted concentrations in the base full meteorology scenario. However, when the ADJ_U* option is applied to the full meteorology, the concentrations are reduced (as expected). While this results in better model performance, it only does so in cases where the base meteorology was performing excessively poorly and severely over predicting. If the model originally underpredicted concentrations for a study, the ADJ_U* option would make that

underprediction worse. Based on these findings, it is clear that the proposed ADJ_U* option, when used with site-specific meteorological inputs including turbulence data (*i.e.*, sigma-theta and/or sigma-w), could bias model predictions towards underestimation. This finding forms the bases of the EPA determination that the ADJ_U* option should not be used in AERMET in combination with use of measured turbulence data. The preferred scenario is to model using site-specific meteorological data with turbulence measurements, without ADJ_U* or other LOWWIND option. When turbulence is included, the ADJ_U* option is considered a beta option and requires approval from the EPA Regional Office and concurrence from the EPA Model Clearinghouse (MCH).[4]

[4] See Model Clearinghouse request and concurrence memoranda for the "Use of the ADJ_U* Beta Option in the AERMET Meteorological Processor as an Alternative Model." *Model Clearinghouse Information Storage and Retrieval System (MCHISRS)*, Record No. 16-X-01, February 10, 2016. (https://cfpub.epa.gov/oarweb/MCHISRS)

Table 23. Tracy: Comparison of Full Meteorology with and without the ADJ_U* Option

		Observed RHC = 14.98 µg/m³
Scenario†	**FB**	**RHC (Pred/Obs)**
FullMet_NoAdjU* *(incl. Turb)*	-0.02	13.24 (0.88)
FullMet_AdjU* *(incl. Turb)*	0.26	9.46 (0.63)

† *Default scenario is bolded. Positive (negative) FB indicates under (over) prediction. Green shading indicates best performer.*

Table 24. Lovett: Comparison of Full Meteorology with and without the ADJ_U* Option

	Robust Highest Concentration (µg/m³) (Pred/Obs)			
Scenario†	**1-hour** *(obs = 426)*	**3-hour** *(obs = 187)*	**24-hour** *(obs = 52)*	**CPM**
Non-adjusted u*; with temperature profile; with wind profile; with turbulence	374 (0.88)	169 (0.90)	48 (0.92)	0.40
Adjusted u*; with temperature profile; with wind profile; with turbulence	361 (0.85)	168 (0.90)	46 (0.88)	0.42

† *The default scenario is bolded. Green shading indicates best performing scenario.*

Table 25. Kincaid: Comparison of Full Meteorology with and without the ADJ_U* Option

	Robust Highest Concentration *(µg/m³)* (Pred/Obs)		
		No ADJ_U*	**ADJ_U***
Avg. Time (hr)	**Observed**	**With Turbulence**†	**With Turbulence**
1	1611	1311 (0.81)	1313 (0.82)
3	618	635 (1.03)	599 (0.97)
24	113	103 (0.91)	101 (0.89)

† *Default scenario.*

Table 26. Cordero: Comparison of Full Meteorology with and without the ADJ_U* Option

Observed RHC = 21.34 µg/m³					
Model†	**FB**	**RHC (Pred/Obs)**	**CPM**	**90% CI**	**95% CI**
16DefTurb	-0.92	57.69 (2.70)	0.71	±0.18	±0.22
16AdjTurb	-0.45	33.69 (1.58)	0.43	±0.17	±0.21

† *Default scenario is bolded. Positive (negative) FB indicates under (over) prediction. Green shading indicates best performer. Yellow shading is outside factor of ± 2 (FB±0.67).*

Table 27. Idaho Falls: Comparison of Full Meteorology with and without the ADJ_U Option*

		Observed RHC = 132.60 µg/m³
Scenario†	**FB**	**RHC (*µg/m³*) (Pred/Obs)**
FullMet_NoAdjU* *(incl. turbulence)*	-0.30	198.05 (1.49)
FullMet_AdjU* *(incl. turbulence)*	-0.18	176.43 (1.33)

† *Default scenario is bolded. Positive (negative) FB indicates under (over) prediction. Green shading indicates best performer.*

The evaluation of ADJ_U* using basic or degraded meteorological data that includes only wind direction and wind speed, similar to NWS data, offers a clear picture of when ADJ_U* is useful for model improvement and when it does not have a major impact on model performance. The FB and RHC comparisons for the Tracy, Oak Ridge, Cordero, and Idaho Falls study show clear improvement in model performance when the ADJ_U* option is applied (Table 28 through Table 31). There is effectively no difference in the degraded meteorology cases with and without the ADJ_U* option for the remaining cases (Lovett, Baldwin, and Kincaid). The difference between these two sets of results is a function of the characteristics of the studies themselves and the general scenarios when ADJ_U* is expected to have an impact. Particularly, ADJ_U* is expected to affect low-level sources and elevated sources (tall stacks) in areas with complex terrain. ADJ_U* is not expected to have much effect on elevated sources in flat terrain as is clearly seen in the results for Baldwin and Kincaid.

Table 28. Tracy: Comparison of Degraded Meteorology with and without the ADJ_U* Option

		Observed RHC = 14.98 µg/m³
Scenario†	**FB**	**RHC (Pred/Obs)**
NoTemp_NoWind_NoTurb_NoAdj U* *(similar to NWS)*	-0.88	42.57 (2.84)
NoTemp_NoWind_NoTurb_Adj U* *(similar to NWS)*	-0.40	25.75 (1.72)

† *Positive (negative) FB indicates under (over) prediction. Green shading indicates best performer. Yellow shading is outside factor of ± 2 (FB±0.67).*

Table 29. Oak Ridge: Comparison of Degraded Meteorology with and without the ADJ_U* Option

		Observed RHC = 82.67 µg/m³
Scenario† *Does not include turbulence*	**FB**	**RHC** (*µg/m³*) **(Pred/Obs)**
Without ADJ_U*	-1.62	798.20 (9.66)
With ADJ_U*	-0.36	116.23 (1.41)

† *Positive (negative) FB indicates under (over) prediction. Green shading indicates best performer. Yellow shading is outside factor of ± 2 (FB±0.67).*

Table 30. Cordero: Comparison of Degraded Meteorology with and without the ADJ_U* Option

Observed RHC = 21.34 µg/m³					
Model†	**FB**	**RHC (Pred/Obs)**	**CPM**	**90% CI**	**95% CI**
16DefNoTurb	-1.06	69.56 (3.26)	0.75	±0.18	±0.22
16AdjNoTurb	-0.53	36.77 (1.72)	0.46	±0.16	±0.20

† *Positive (negative) FB indicates under (over) prediction. Green shading indicates best performer. Yellow shading is outside factor of ± 2 (FB±0.67).*

Table 31. Idaho Falls: Comparison of Degraded Meteorology with and without the ADJ_U* Option

		Observed RHC = 132.60 µg/m³
Scenario†	**FB**	**RHC** (*µg/m³*) **(Pred/Obs)**
DegMet_NoAdjU* (no turbulence)	-0.80	328.76 (2.48)
DegMet_AdjU* (no turbulence)	-0.64	275.80 (2.08)

† *Positive (negative) FB indicates under (over) prediction. Green shading indicates best performer. Yellow shading is outside factor of ± 2 (FB±0.67).*

C.4. LOWWIND3

LOWWIND3 is a variation on the existing LOWWIND1 and LOWWIND2 "beta" options introduced in early versions AERMOD. It modifies the minimum value of sigma-v, the lateral turbulence intensity, which is used to determine the lateral plume dispersion coefficient, sigma-y. The LOWWIND3 option also addresses the horizontal meander component in AERMOD that contributes to lateral plume spread, especially during low wind, stable conditions. Furthermore, since the horizontal meander component in AERMOD is a function of the "effective" sigma-v value, lateral plume dispersion may be further enhanced under the LOWWIND3 option by increased meander, beyond the influence of the minimum sigma-v value alone. The default option in AERMOD uses a minimum sigma-v of 0.2 m/s, while the LOWWIND3 option increases the minimum sigma-v to 0.3 m/s and eliminates upwind dispersion. Setting a higher minimum value of sigma-v would tend to increase lateral dispersion during low wind conditions and, therefore, could reduce predicted ambient concentrations. Unlike the ADJ_U* option in AERMET that adjusts u* under stable conditions, the LOWWIND options in AERMOD are applied for both stable and unstable/convective conditions. However, since atmospheric turbulence will generally be higher during unstable/convective conditions than for stable conditions, the potential influence of the minimum sigma-v value on plume dispersion is likely to be much less important during unstable/convective conditions.

The results of the EPA's reassessment of the LOWWIND3 option based on the 1974 Idaho Falls, 1956 Prairie Grass, and a collection of field studies used in the original evaluation of AERMOD (Perry *et al.*, 2005)) are discussed in the sections that follow.

C.4.1. Summary of Results from Each Study

C.4.1.1. Project Prairie Grass, Nebraska (1956)

The Prairie Grass assessment compares modeling scenarios using full meteorology (with turbulence measurements) and degraded meteorology (without turbulence) with and without the ADJ_U* and LOWWIND3 options applied.

Table 32 presents a comparison of the FBs and RHCs based on the 1-hr maximum modeled concentrations for each receptor arc for each hour. Based on the FB values, the default scenario of full meteorology (with turbulence), without the use of the ADJ_U* and LOWWIND3 options is identified as the best performer. However, it is evident in a comparison of the FBs and RHCs that the ADJ_U* option has only a small effect on those scenarios that differ only in the use of ADJ_U*. While each of the modeling scenarios underpredicts the RHC, there are substantial decreases in the RHCs when comparing the scenarios that do not include the LOWWIND3 option to those where LOWWIND3 is applied.

Figure 45 and Figure 46 compare Q-Q plots generated from the 1-hr arc-maximum concentrations for each of the modeled scenarios. Figure 45 demonstrates a general decrease in concentrations and underprediction when ADJ_U* is applied to the base case (full meteorology with turbulence, without ADJ_U*) and further underprediction when both ADJ_U* and LOWWIND3 are applied. Figure 46 shows similar results with degraded meteorology. Concentrations further decrease compared to the both ADJ_U* and LOWWIND3 are applied and the turbulence data are not included. These plots illustrate potential for a decrease in concentrations resulting in underprediction when using the LOWWIND3 option in combination with the ADJ_U* option.

Table 32. Prairie Grass Comparison of FBs and RHCs (based on receptor arc maximum concentrations)

		Observed RHC = 925,087.27 µg/m³
Scenario†	**FB**	**RHC (*µg/m³*) (Pred/Obs)**
FullMet_NoAdjU*_ NoLW *(includes turbulence)*	0.07	908,183.22 (0.98)
FullMet_AdjU*_ NoLW *(includes turbulence)*	0.09	915,189.65 (0.99)
DegMet_NoAdjU*_ NoLW *(no turbulence)*	0.22	819,095.13 (0.89)
DegMet_AdjU*_ NoLW *(no turbulence)*	0.20	846,669.21 (0.92)
FullMet_NoAdjU*_ LW3 *(includes turbulence)*	0.22	738,975.47 (0.80)
FullMet_AdjU*_ LW3 *(includes turbulence)*	0.26	733,058.78 (0.79)
DegMet_NoAdjU*_ LW3 *(no turbulence)*	0.35	669,035.68 (0.72)
DegMet_AdjU*_ LW3 *(no turbulence)*	0.34	698,161.43 (0.75)

† *Default scenario is bolded. Positive (negative) FB indicates under (over) prediction. Green shading indicates best performer.*

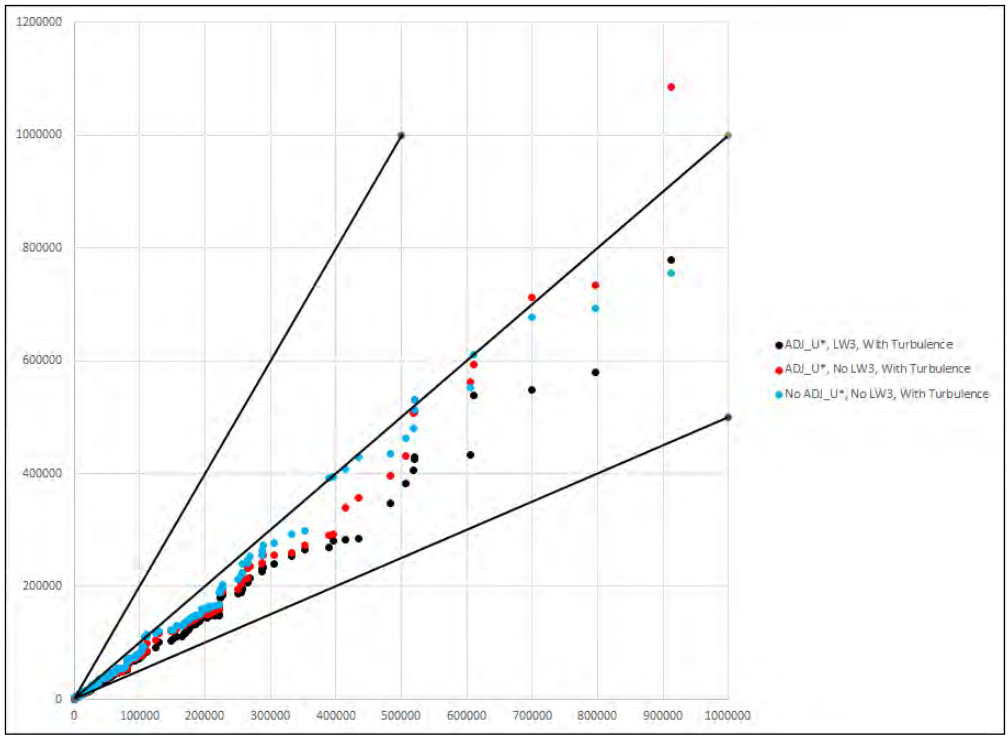

Figure 45. Prairie Grass 1-hr Q-Q Plots, Comparing Base Case to ADJ_U, with Turbulence, with and w/o LW3*

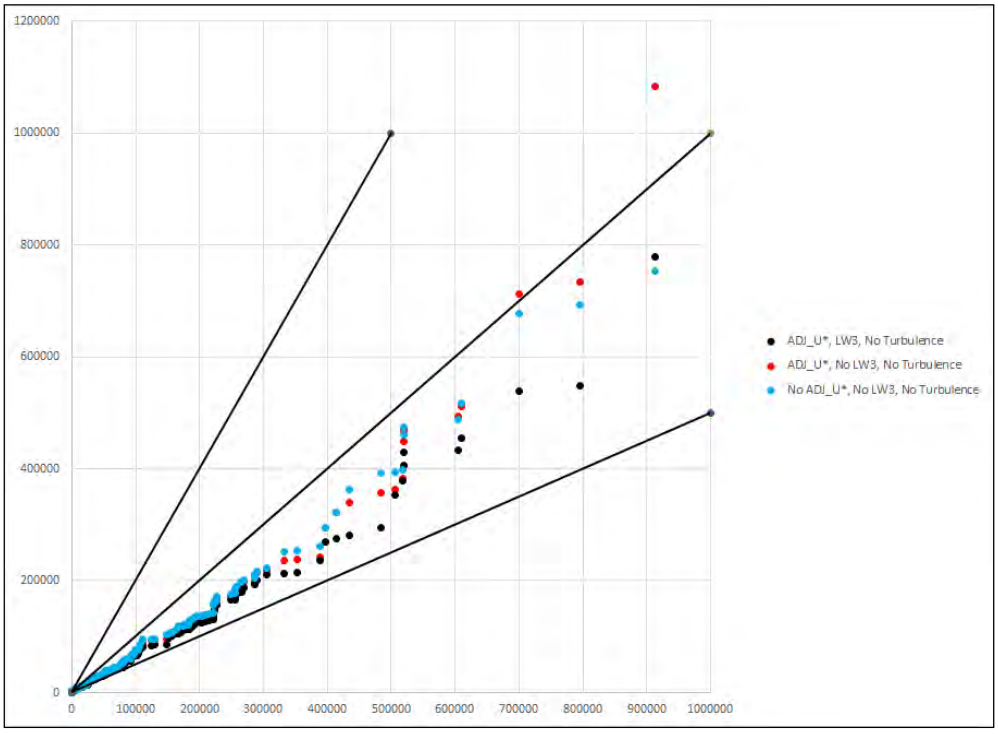

Figure 46. Prairie Grass 1-hr Q-Q Plots Comparing Base Case to ADJ_U, w/o Turbulence, with and w/o LW3*

C.4.1.2. Idaho Falls, Idaho (1974)

The evaluation of ADJ_U* with the 1974 Idaho Falls field study discussed above was extended by adding the LOWWIND3 option in AERMOD. Each scenario that was modeled with and without the ADJ_U* option was subsequently modeled with the LOWWIND3 option to evaluate the potential for underprediction when LOWWIND3 is applied. Table 33 compares the FBs and RHCs for the additional modeling scenarios while Figure 47 through Figure 54 are plots of observed versus predicted 1-hour concentrations based on the receptor arc-maximum values, paired in time, and of the ratio of predicted-to-observed concentrations versus distance, with and without the ADJ _U* option, using full meteorology.

Table 33 demonstrates the potential for the LOWWIND3 option to underpredict, particularly when using site-specific data with turbulence measurements included and when used in conjunction with the ADJ_U* option. Substantial reductions in the RHCs are demonstrated when comparing the modeling scenarios in Table 33 with the comparable scenarios in Table 22 without the LOWWIND3 option applied.

Table 33. Idaho Falls Comparison of FBs and RHCs Using the LW3 Option (based on receptor arc-max concentrations)

		Observed RHC = 132.60 µg/m³
Scenario†	**FB**	**RHC (*µg/m³*) (Pred/Obs)**
FullMet_NoAdjU*_LW3 (incl. turbulence)	0.17	124.10 (0.94)
FullMet_AdjU*_LW3 (incl. turbulence)	0.36	102.84 (0.78)
DegMet_NoAdjU*_LW3 (no turbulence)	-0.22	168.34 (1.27)
DegMet_AdjU*_LW3 (no turbulence)	0.29	133.56 (1.01)

† *Positive (negative) FB indicates under (over) prediction. Green shading indicates best performer.*

Recall Figure 35 and Figure 36 above which represents the full meteorological dataset and includes multiple levels of wind speed and direction, temperature, and sigma-theta, without the ADJ_U* option applied. That scenario demonstrated the best performance of those evaluated, although there was a bias toward overprediction for the majority of the hours

modeled. When the LOWWIND3 option was applied, the results in the paired plot in Figure 47 and Figure 48 show a bias towards underprediction for nearly all hours at each receptor distance. The bias toward underprediction is increased when the LOWWIND3 option is used in conjunction with the ADJ_U* option, illustrated in Figure 49 and Figure 50.

Results are mixed when comparing the application of the LOWWIND3 option, with and without ADJ_U*, when the turbulence measurements were omitted. Figure 39 and Figure 40, above, show a substantial overpredicion without ADJ_U* applied. Results look more favorable in Figure 51 and Figure 52 when LOWWIND3 is applied without the use of ADJ_U*. However, Figure 53 and Figure 54 show substantial underprediction across the two arcs of receptors farthest from the release point when both ADJ_U* and LOWWIND3 were applied.

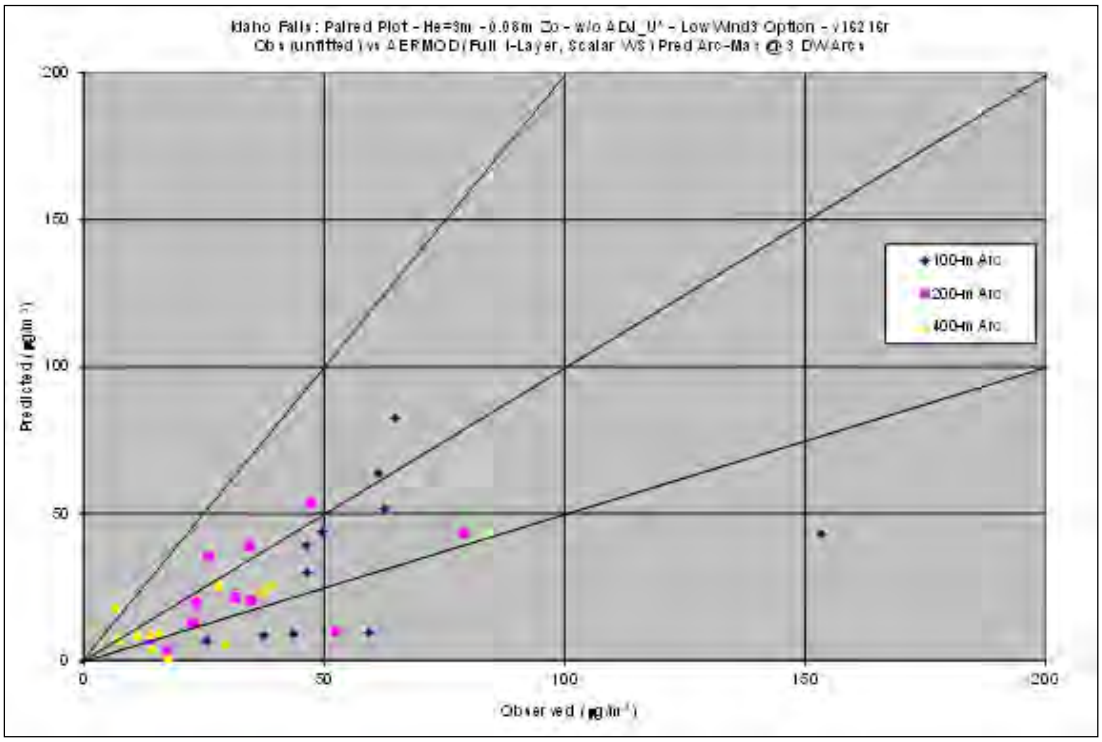

Figure 47. Idaho Falls 1-hr Observed-to-Predicted Arc-Max Concentrations Paired in Time, Full Met, No ADJ_U, with LW3*

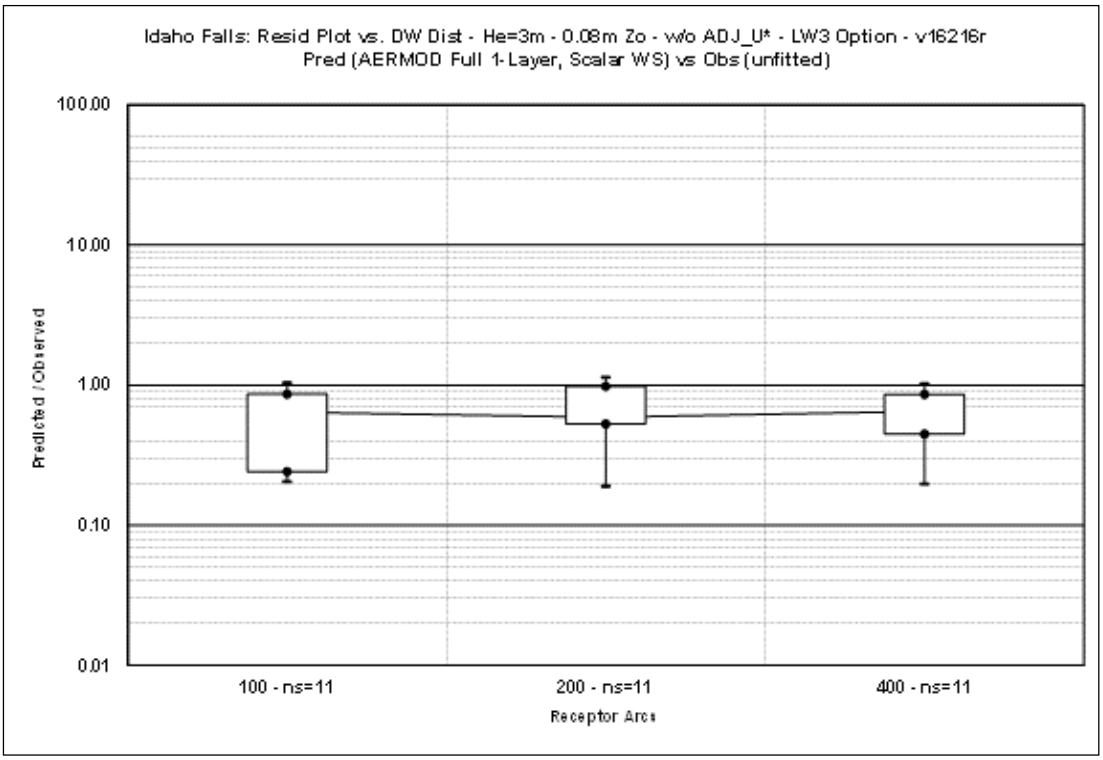

Figure 48. Idaho Falls 1-hr Predicted-to-Observed Ratios, Full Met, No ADJ_U, with LW3*

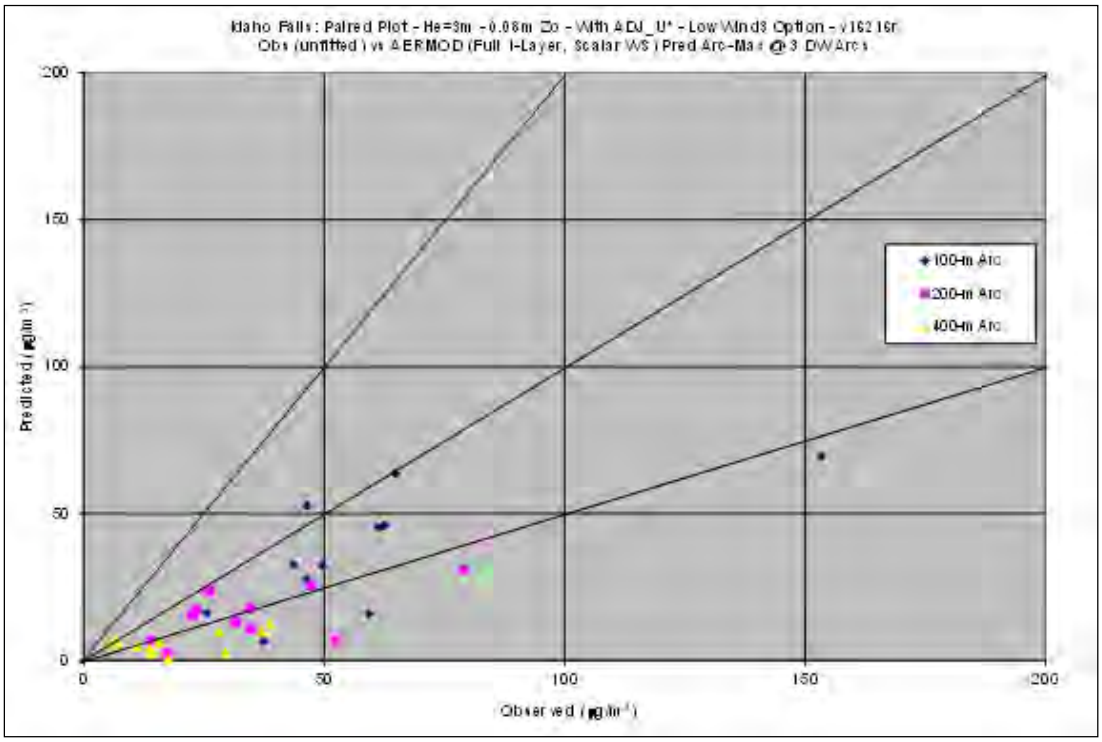

Figure 49. Idaho Falls 1-hr Observed-to-Predicted Arc-Max Concentrations Paired in Time, Full Met, ADJ_U, with LW3*

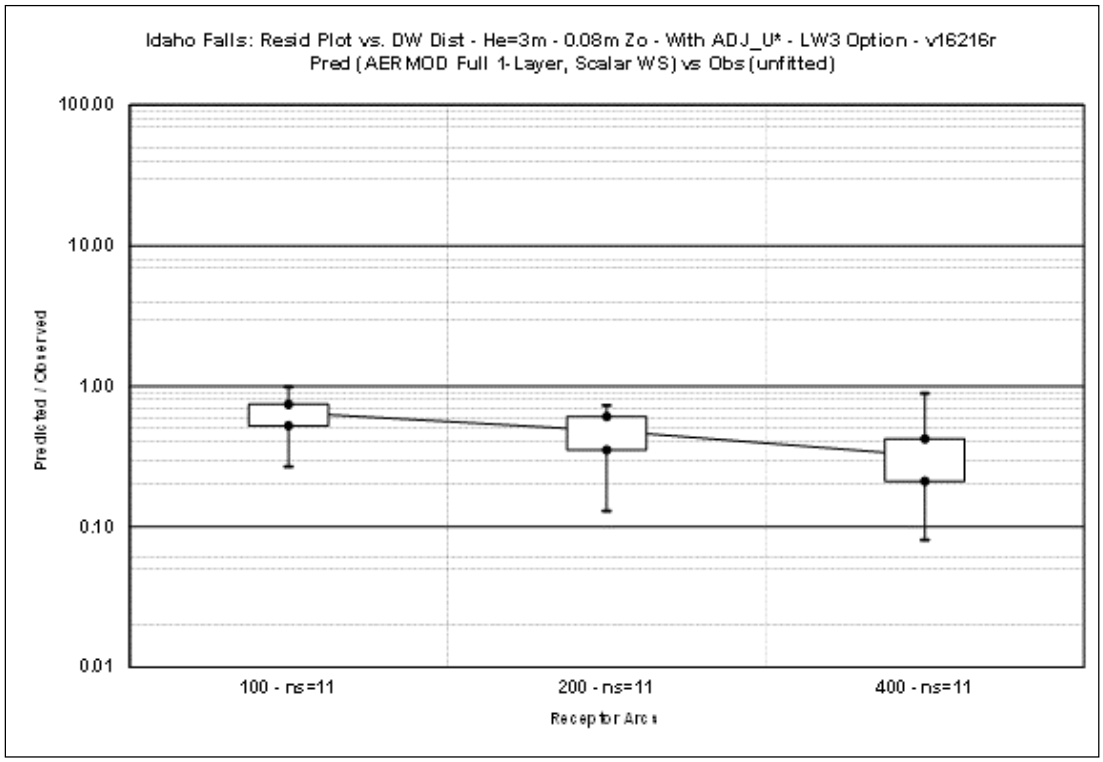

Figure 50. Idaho Falls 1-hr Predicted-to-Observed Ratios, Full Met, ADJ_U, with LW3*

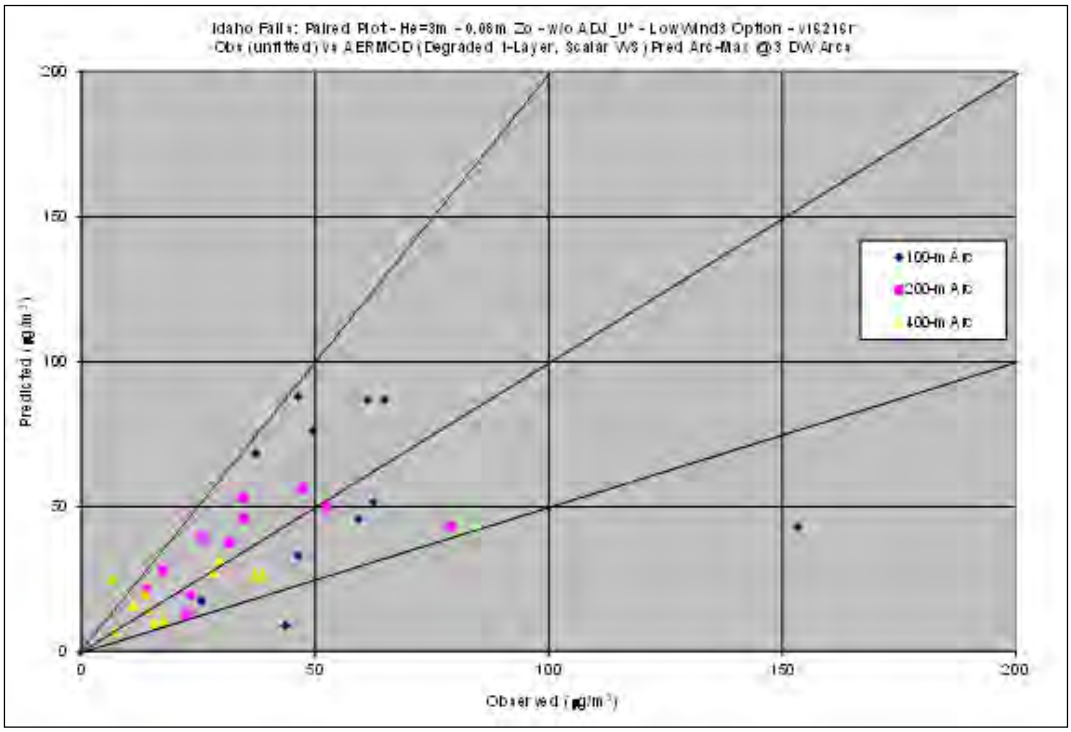

Figure 51. Idaho Falls 1-hr Observed-to-Predicted Arc-Max Concentrations Paired in Time, No Turbulence, No ADJ_U, with LW3*

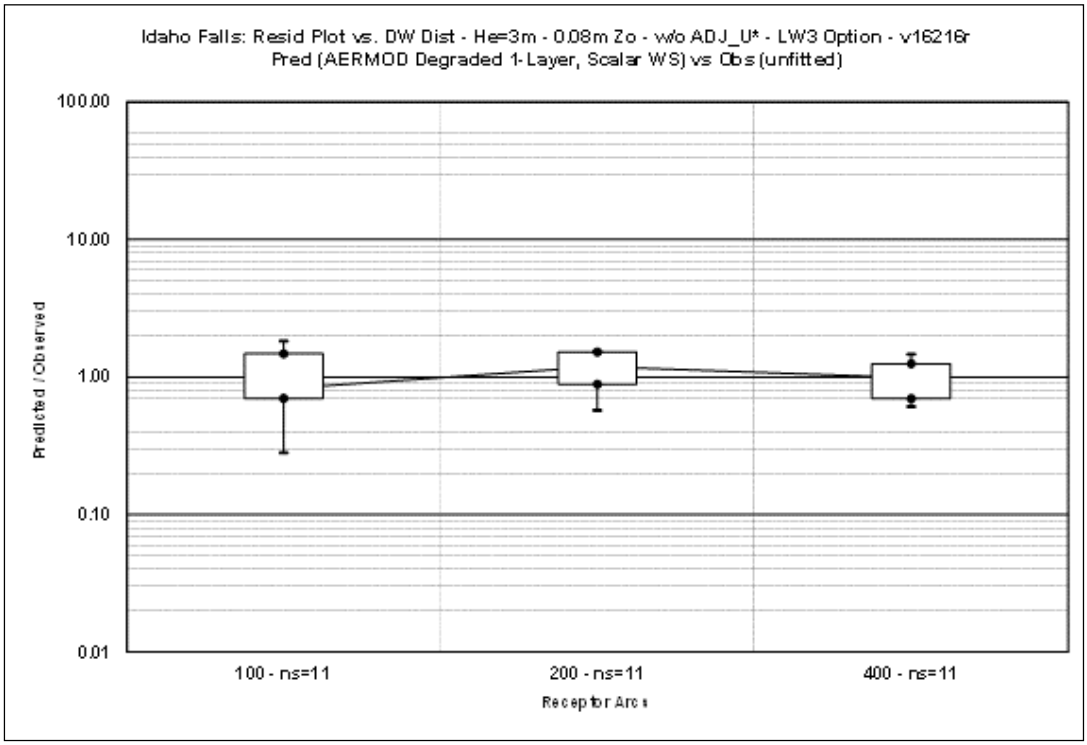

Figure 52. Idaho Falls 1-hr Predicted-to-Observed Ratios, No Turbulence, No ADJ_U, with LW3*

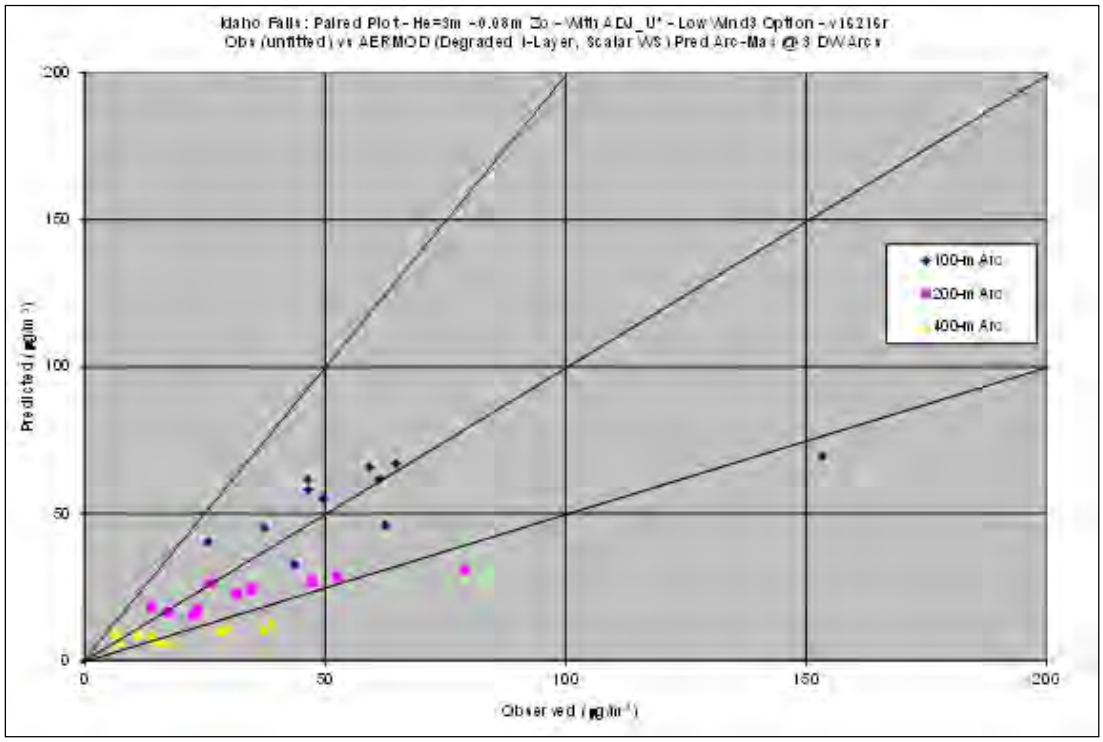

Figure 53. Idaho Falls 1-hr Observed-to-Predicted Arc-Max Concentrations Paired in Time, No Turbulence, ADJ_U, LW3*

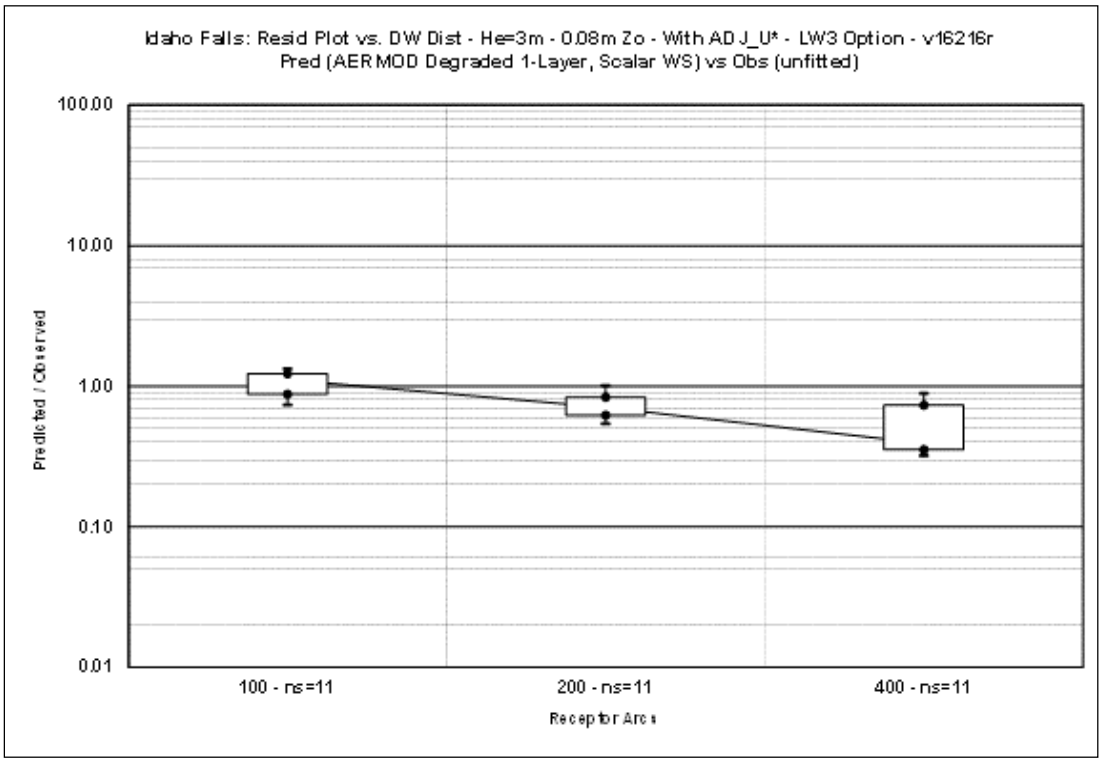

Figure 54. Idaho Falls 1-hr Predicted-to-Observed Ratios, No Turbulence, ADJ_U, with LW3*

C.4.1.3. Other Evaluation Datasets

Listed earlier are many additional datasets that were used in the original evaluation of AREMOD and were also included in this evaluation of the ADJ_U* and LOWWIND3 options. Cox-Tikvart protocol statistics are presented in Table 34 through Table 46. Q-Q plots of 1-hour observed-to-modeled concentrations for each of the sites are provided in Figure 56 through Figure 62. Note that about a third of these field studies do not include turbulence measurements.

An analysis of the Cox-Tikvart statistics and 1-hour Q-Q plots show mixed results. LOWWIND3 has little to no effect on AGA, Alaska, Bowline, DAEC (1 and 24m stack), Indiana, and Millston. Differences tend to be related more to ADJ_U* and/or whether or not turbulence measurements are included. However, LOWWIND3 results show reduced concentrations for the 46 m stack at DAEC, with and without ADJ_U*. LOWWIND3 also has a substantial effect on lowering concentrations for Baldwin, Clifty Creek, EOCR, Kincaid, Lovett, Martins Creek, Tracy, and Westvaco. Reductions using LOWWIND3 result in substantial underprediction when used in combination with ADJ_U* for Clifty Creek, Kincaid, Lovett, Martins Creek, and Tracy. For those field studies that include turbulence measurements (Alaska, DAEC, EOCR, Indiana, Kincaid, Lovett, Martins Creek, Tracy, and Westvaco), the default modeling scenario of using the full meteorology without ADJ_U* and without LOWWIND3 generally shows better performance.

Table 34. Fractional Bias Values for Databases that Do Not Include Turbulence Data

Database	Avg. Period (hr)	Fractional Bias†			
		No ADJ_U* No LW3 No Turbulence‡	ADJ_U* LW3 No Turbulence	No ADJ_U* LW3 No Turbulence	ADJ_U* No LW3 No Turbulence
AGA	1	-0.069	-0.034	-0.061	-0.034
Baldwin	1	-0.394	-0.313	-0.313	-0.394
	3	-0.276	-0.199	-0.199	-0.276
	24	-0.162	-0.076	-0.076	-0.162
Bowline	1	0.043	0.052	0.043	0.052
	3	-0.205	-0.191	-0.205	-0.191
	24	-0.394	-0.431	-0.394	-0.431
Clifty Creek	1	-0.088	0.076	0.076	-0.088
	3	-0.001	0.116	0.116	-0.002
	24	0.410	0.468	0.469	0.409
Millston (Freon)	1	-0.445	-0.363	-0.404	-0.366
Millston (SF6)	1	0.749	0.835	0.794	0.831

† *Positive (negative) indicates under (over) prediction. Green shading indicates best performer. Yellow shading is outside ± factor of 2 (±0.67). Orange shading is best performer and outside a factor of 2.*

‡ *Default scenario is bolded.*

Table 35. Fractional Bias Values for Databases that Include Turbulence Data

Database	Avg. Period (hr)	Fractional Bias†			
		No ADJ_U* No LW3 Turbulence‡	**ADJ_U* LW3 No Turbulence**	**No ADJ_U* LW3 Turbulence**	**ADJ_U* No LW3 No Turbulence**
Alaska	1	-0.181	-0.416	-0.181	-0.416
DAEC (h=1 m)	1	0.228	0.413	0.229	0.412
DAEC (h=24 m)	1	0.985	1.175	0.992	1.146
DAEC (h=46 m)	1	0.480	0.941	0.600	0.782
EOCR	1	-0.415	-0.304	-0.312	-0.374
Indiana	1	0.212	0.414	0.300	0.338
Kincaid	1	0.065	0.648	0.161	0.544
	3	0.253	0.462	0.315	0.386
	24	0.316	0.249	0.363	0.187
Lovett	1	0.042	-0.182	0.200	-0.355
	3	0.036	-0.207	0.122	-0.337
	24	-0.007	-0.165	0.087	-0.256
Martins Creek	1	-0.030	0.128	-0.013	0.018
	3	-0.074	0.103	-0.063	0.073
	24	-0.148	-0.011	-0.136	-0.037
Tracy	1	-0.020	0.025	0.255	-0.387
Westvaco	1	0.117	0.792	0.204	0.780
	3	-0.027	0.735	0.037	0.720
	24	-0.077	0.200	-0.037	0.187

† *Positive (negative) indicates under (over) prediction. Green shading indicates best performer. Yellow shading is outside ± factor of 2 (±0.67). Orange shading is best performer and outside a factor of 2.*

‡ *Default scenario is bolded.*

Table 36. Robust High Concentrations for Databases that Do Not Include Turbulence

Database	Avg. Period (hr)	RHC (µg/m³)† (Pred/Obs)				
		Obs	No ADJ_U* No LW3 No Turbulence‡	ADJ_U* LW3 No Turbulence	No ADJ_U* LW3 No Turbulence	ADJ_U* No LW3 No Turbulence
AGA	1	295.5	281.2 (0.95)	261.9 (0.9)	276.8 (0.9)	262.2 (0.9)
Baldwin	1	2348.1	3531.3 (1.5)	3247.8 (1.4)	3247.8 (1.4)	3531.3 (1.5)
	3	920.2	1183.4 (1.3)	1076.4 (1.2)	1077.6 (1.2)	1182.7 (1.3)
	24	209.0	230.3 (1.1)	203.2 (0.97)	203.1 (0.97)	230.4 (1.1)
Bowline	1	763.4	547.5 (0.7)	552.4 (0.7)	547.5 (0.7)	552.4 (0.7)
	3	469.3	522.4 (1.1)	513.6 (1.1)	522.4 (1.1)	513.7 (1.1)
	24	203.6	208.4 (1.02)	307.6 (1.5)	289.9 (1.4)	307.4 (1.5)
Clifty Creek	1	1451.3	1360.3 (0.9)	1209.3 (0.8)	1209.3 (0.8)	1360.3 (0.9)
	3	795.6	870.2 (1.1)	763.3 (0.96)	762.3 (0.96)	871.2 (1.1)
	24	243.0	164.7 (0.7)	155.2 (0.6)	152.3 (0.6)	170.3 (0.7)
Millston (Freon)	1	75.9	100.7 (1.3)	95.9 (1.3)	92.2 (1.2)	96.5 (1.3)
Millston (SF6)	1	79.2	35.3 (0.4)	33.1 (0.4)	33.6 (0.4)	33.5 (0.4)

† *Green shading indicates best performer.*

‡ *Default scenario is bolded.*

Table 37. Robust High Concentrations for Databases that Include Turbulence

Database	Avg. Period (hr)	RHC (µg/m³)† (Pred/Obs)				
		Obs	No ADJ_U* No LW3 Turbulence‡	ADJ_U* LW3 No Turbulence	No ADJ_U* LW3 Turbulence	ADJ_U* No LW3 No Turbulence
Alaska	1	6.0	5.4 (0.9)	7.7 (1.3)	5.4 (0.9)	7.7 (1.3)
DAEC (h=1 m)	1	345.6	285.6 (0.8)	219.1 (0.6)	285.0 (0.8)	219.4 (0.6)
DAEC (h=24 m)	1	140.4	87.5 (0.6)	67.4 (0.5)	86.9 (0.6)	70.5 (0.5)
DAEC (h=46 m)	1	253.1	114.8 (0.5)	54.2 (0.2)	96.3 (0.4)	73.5 (0.3)
EOCR	1	3762.8	5797.1 (1.5)	5237.8 (1.4)	5077.9 (1.4)	5712.1 (1.5)
Indianapolis	1	5.8	4.3 (0.7)	3.6 (0.6)	4.4 (0.8)	3.8 (0.7)
Kincaid	1	1611.2	1311.5 (0.8)	624.7 (0.4)	1218.6 (0.8)	716.7 (0.4)
	3	618.3	634.9 (1.03)	468.6 (0.8)	593.1 (0.96)	470.2 (0.8)
	24	112.7	102.7 (0.9)	151.2 (1.3)	99.5 (0.9)	166.5 (1.5)
Lovett	1	425.9	374.2 (0.9)	462.7 (1.1)	309.0 (0.7)	537.9 (1.3)
	3	186.6	169.1 (0.9)	218.3 (1.2)	156.1 (0.8)	239.3 (1.3)
	24	51.8	47.7 (0.9)	56.1 (1.1)	43.6 (0.8)	62.8 (1.2)
Martins Creek	1	1215.9	1132.8 (0.9)	878.3 (0.7)	1116.1 (0.9)	1034.1 (0.9)
	3	461.2	497.2 (1.1)	498.2 (1.1)	502.8 (1.1)	505.2 (1.1)
	24	79.3	141.3 (1.8)	120.9 (1.5)	138.8 (1.8)	128.8 (1.6)
Tracy	1	15.0	13.2 (0.9)	11.5 (0.8)	10.4 (0.7)	17.5 (1.2)
Westvaco	1	2756.7	2460.3 (0.9)	1238.0 (0.4)	2143.6 (0.8)	1252.1 (0.5)
	3	1575.0	1730.7 (1.1)	780.8 (0.5)	1579.3 (1.0)	783.2 (0.5)
	24	479.8	523.9 (1.1)	457.8 (0.95)	507.7 (1.1)	457.3 (0.95)

† *Green shading indicates best performer.*

‡ *Default scenario is bolded.*

Table 38. Composite Performance Measures for Databases that Do Not Include Turbulence

Scenario†	CPM		
	Baldwin	Bowline	Clifty Creek
No ADJ_U*, No LW3, No Turbulence	0.46	0.47	0.51
ADJ_U*, LW3, No Turbulence	0.39	0.51	0.50
No ADJ_U*, LW3, No Turbulence	0.39	0.48	0.51
ADJ_U*, no LW3, No Turbulence	0.45	0.50	0.49

† *Default scenario is in bolded. Green shading indicates best performer.*

Table 39. Composite Performance Measures for Databases that Include Turbulence

Scenario†	CPM			
	Kincaid	Lovett	Martins Creek	Westvaco
No ADJ_U*, No LW3, Turbulence	0.37	0.40	0.35	0.41
ADJ_U*, LW3, No Turbulence	0.54	0.45	0.29	0.62
No ADJ_U*, LW3, Turbulence	0.39	0.46	0.35	0.40
ADJ_U*, no LW3, No Turbulence	0.56	0.52	0.31	0.60

† *Default scenario is in bolded. Green shading indicates best performer.*

Table 40. Baldwin Model Comparison Measures

Model Scenarios Compared†	MCM	Confidence Intervals			
		90%		95%	
		Lower bound	Upper bound	Lower bound	Upper bound
No ADJ_U*, LW3, No Turbulence – **No ADJ_U*, No LW3, No Turbulence**	-0.066	-0.193	0.061	-0.238	0.105
ADJ_U*, No LW3, No Turbulence – **No ADJ_U*, No LW3, No Turbulence**	-0.002	-0.135	0.130	-0.181	0.177
ADJ_U*, LW3, No Turbulence – **No ADJ_U*, No LW3, No Turbulence**	-0.069	-0.198	0.060	-0.242	0.105
ADJ_U*, No LW3, No Turbulence – No ADJ_U*, LW3, No Turbulence	0.064	-0.063	0.191	-0.108	0.236
ADJ_U*, LW3, No Turbulence – No ADJ_U*, LW3, No Turbulence	-0.002	-0.121	0.117	-0.163	0.158
ADJ_U*, LW3, No Turbulence – ADJ_U*, No LW3, No Turbulence	-0.066	-0.194	0.061	-0.238	0.106

† *Default scenario is in bolded. The difference in model results for any of the pairs of scenarios compared is not significant.*

Table 41. Bowline Model Comparison Measures

Model Scenarios Compared†	MCM	Confidence Intervals			
		90%		95%	
		Lower bound	Upper bound	Lower bound	Upper bound
No ADJ_U*, LW3, No Turbulence – **No ADJ_U*, No LW3, No Turbulence**	0.030	-0.052	0.113	-0.073	0.133
ADJ_U*, No LW3, No Turbulence – **No ADJ_U*, No LW3, No Turbulence**	0.008	-0.077	0.094	-0.098	0.115
ADJ_U*, LW3, No Turbulence – **No ADJ_U*, No LW3, No Turbulence**	0.039	-0.048	0.126	-0.070	0.147
ADJ_U*, No LW3, No Turbulence – No ADJ_U*, LW3, No Turbulence	0.022	-0.062	0.106	-0.082	0.126
ADJ_U*, LW3, No Turbulence – No ADJ_U*, LW3, No Turbulence	0.030	-0.056	0.116	-0.077	0.138
ADJ_U*, LW3, No Turbulence – ADJ_U*, No LW3, No Turbulence	0.008	-0.073	0.090	-0.093	0.110

† *Default scenario is in bolded. The difference in model results for any of the pairs of scenarios compared is not significant.*

Table 42. Clifty Creek Model Comparison Measures

Model Scenarios Compared†	MCM	Confidence Intervals			
		90%		95%	
		Lower bound	Upper bound	Lower bound	Upper bound
No ADJ_U*, LW3, No Turbulence – **No ADJ_U*, No LW3, No Turbulence**	-0.001	-0.066	0.065	-0.088	0.086
ADJ_U*, No LW3, No Turbulence – **No ADJ_U*, No LW3, No Turbulence**	-0.015	-0.075	0.045	-0.094	0.064
ADJ_U*, LW3, No Turbulence – **No ADJ_U*, No LW3, No Turbulence**	-0.012	-0.079	0.054	-0.100	0.075
ADJ_U*, No LW3, No Turbulence – No ADJ_U*, LW3, No Turbulence	-0.015	-0.080	0.051	-0.101	0.072
ADJ_U*, LW3, No Turbulence – No ADJ_U*, LW3, No Turbulence	-0.012	-0.070	0.046	-0.088	0.065
ADJ_U*, LW3, No Turbulence – ADJ_U*, No LW3, No Turbulence	0.003	-0.065	0.071	-0.087	0.093

† *Default scenario is in bolded. The difference in model results for any of the pairs of scenarios compared is not significant.*

Table 43. Kincaid Model Comparison Measures

Model Scenarios Compared†	MCM	Confidence Intervals			
		90%		95%	
		Lower bound	Upper bound	Lower bound	Upper bound
ADJ_U*, No LW3, No Turbulence – **No ADJ_U*, No LW3, Turbulence**	0.190	-0.126	0.505	-0.176	0.556
No ADJ_U*, LW3, Turbulence – **No ADJ_U*, No LW3, Turbulence**	0.019	-0.389	0.427	-0.454	0.492
ADJ_U*, LW3, No Turbulence – **No ADJ_U*, No LW3, Turbulence**	0.170	-0.138	0.476	-0.187	0.525
ADJ_U*, No LW3, No Turbulence – No ADJ_U*, LW3, Turbulence	0.170	-0.176	0.517	-0.232	0.573
ADJ_U*, LW3, No Turbulence – No ADJ_U*, LW3, Turbulence	0.150	-0.194	0.494	-0.249	0.549
ADJ_U*, LW3, No Turbulence – ADJ_U*, No LW3, No Turbulence	-0.021	-0.175	0.134	-0.200	0.158

† *Default scenario is in bolded. The difference in model results for any of the pairs of scenarios compared is not significant.*

Table 44.Lovett Model Comparison Measures

Model Scenarios Compared†	MCM	Confidence Intervals			
		90%		95%	
		Lower bound	Upper bound	Lower bound	Lower bound
ADJ_U*, No LW3, No Turbulence – **No ADJ_U*, No LW3, Turbulence**	0.128	-0.032	0.287	-0.080	0.336
No ADJ_U*, LW3, Turbulence – **No ADJ_U*, No LW3, Turbulence**	0.063	-0.050	0.177	-0.084	0.211
ADJ_U*, LW3, No Turbulence – **No ADJ_U*, No LW3, Turbulence**	0.054	-0.087	0.196	-0.130	0.234
ADJ_U*, No LW3, No Turbulence – No ADJ_U*, LW3, Turbulence	0.065	-0.118	0.247	-0.174	0.303
ADJ_U*, LW3, No Turbulence – No ADJ_U*, LW3, Turbulence	-0.009	-0.178	0.160	-0.229	0.211
ADJ_U*, LW3, No Turbulence – ADJ_U*, No LW3, No Turbulence	-0.073	-0.188	0.042	-0.223	0.076

† *Default scenario is in bolded. The differences in model results for any of the pairs of scenarios compared is not significant.*

Table 45. Martins Creek Model Comparison Measures

Model Scenarios Compared†	MCM	Confidence Intervals			
		90%		95%	
		Lower bound	Upper bound	Lower bound	Upper bound
ADJ_U*, No LW3, No Turbulence – **No ADJ_U*, No LW3, Turbulence**	-0.039	-0.136	0.059	-0.166	-0.089
No ADJ_U*, LW3, Turbulence – **No ADJ_U*, No LW3, Turbulence**	0.007	-0.086	0.100	-0.115	0.129
ADJ_U*, LW3, No Turbulence – **No ADJ_U*, No LW3, Turbulence**	-0.053	-0.154	0.047	-0.185	0.078
ADJ_U*, No LW3, No Turbulence – No ADJ_U*, LW3, Turbulence	-0.045	-0.142	0.052	-0.172	0.081
ADJ_U*, LW3, No Turbulence – No ADJ_U*, LW3, Turbulence	-0.060	-0.161	0.040	-0.192	0.-071
ADJ_U*, LW3, No Turbulence – ADJ_U*, No LW3, No Turbulence	-0.015	-0.113	0.083	-0.143	0.113

† *Default scenario is in bolded. The differences in model results for any of the pairs of scenarios compared is not significant.*

Table 46. Westvaco Model Comparison Measures

Model Scenarios Compared†	MCM	Confidence Intervals			
		90%		95%	
		Lower bound	Upper bound	Lower bound	Upper bound
ADJ_U*, No LW3, No Turbulence – **No ADJ_U*, No LW3, Turbulence**	0.187	0.088	0.287	0.044	0.330
No ADJ_U*, LW3, Turbulence – **No ADJ_U*, No LW3, Turbulence**	-0.017	-0.076	0.041	-0.101	0.066
ADJ_U*, LW3, No Turbulence – **No ADJ_U*, No LW3, Turbulence**	0.210	0.111	0.309	0.068	0.352
ADJ_U*, No LW3, No Turbulence – No ADJ_U*, LW3, Turbulence	0.205	0.124	0.286	0.089	0.320
ADJ_U*, LW3, No Turbulence – No ADJ_U*, LW3, Turbulence	0.227	0.147	0.308	0.112	0.343
ADJ_U*, LW3, No Turbulence – ADJ_U*, No LW3, No Turbulence	0.022	-0.027	0.072	-0.049	0.094

† *Default scenario is in bolded. Yellow shading indicates there is a significant difference between the two scenarios.*

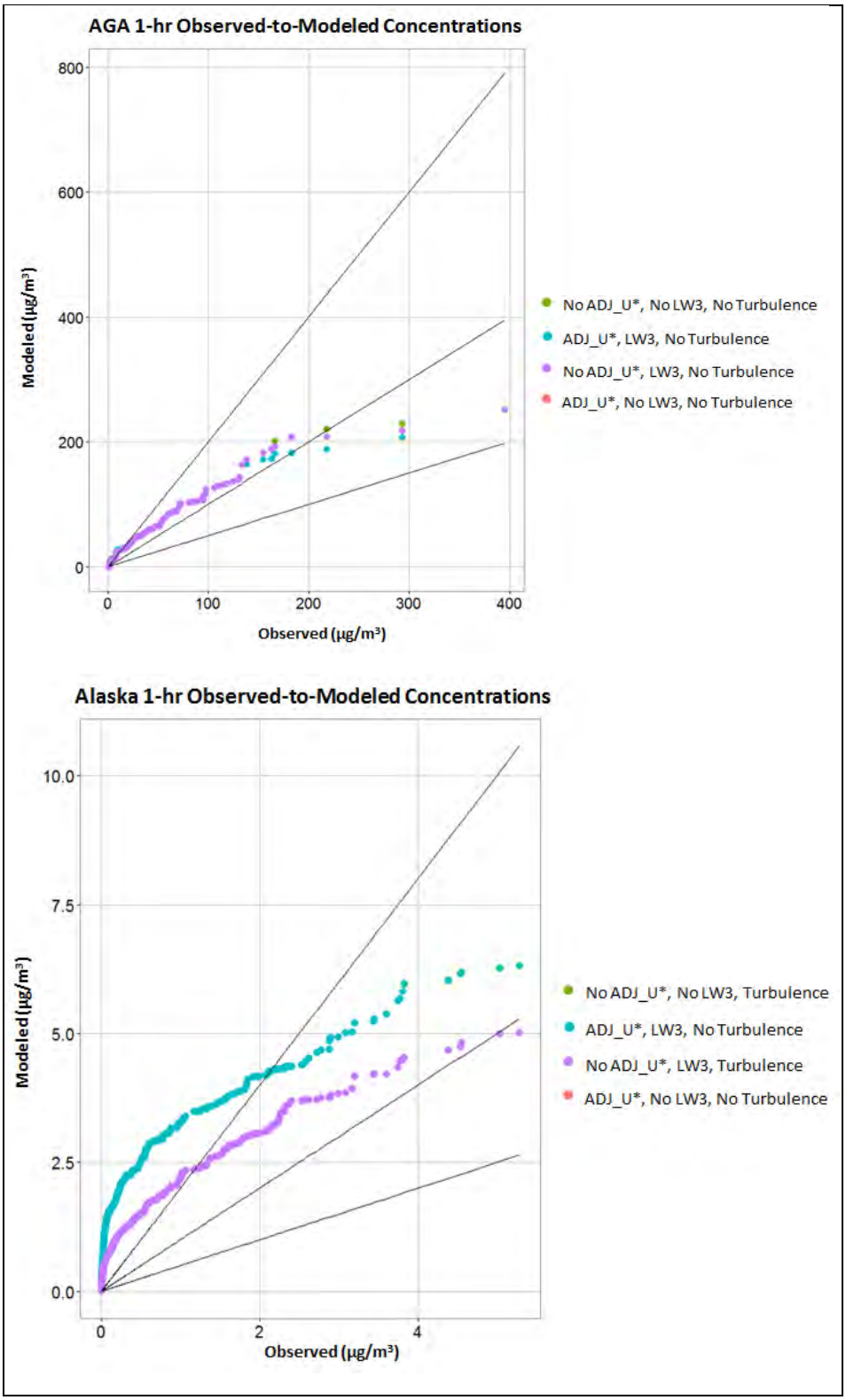

Figure 55. Q-Q Plots for 1-hr Observed-to-Modeled Concentrations for AGA and Alaska

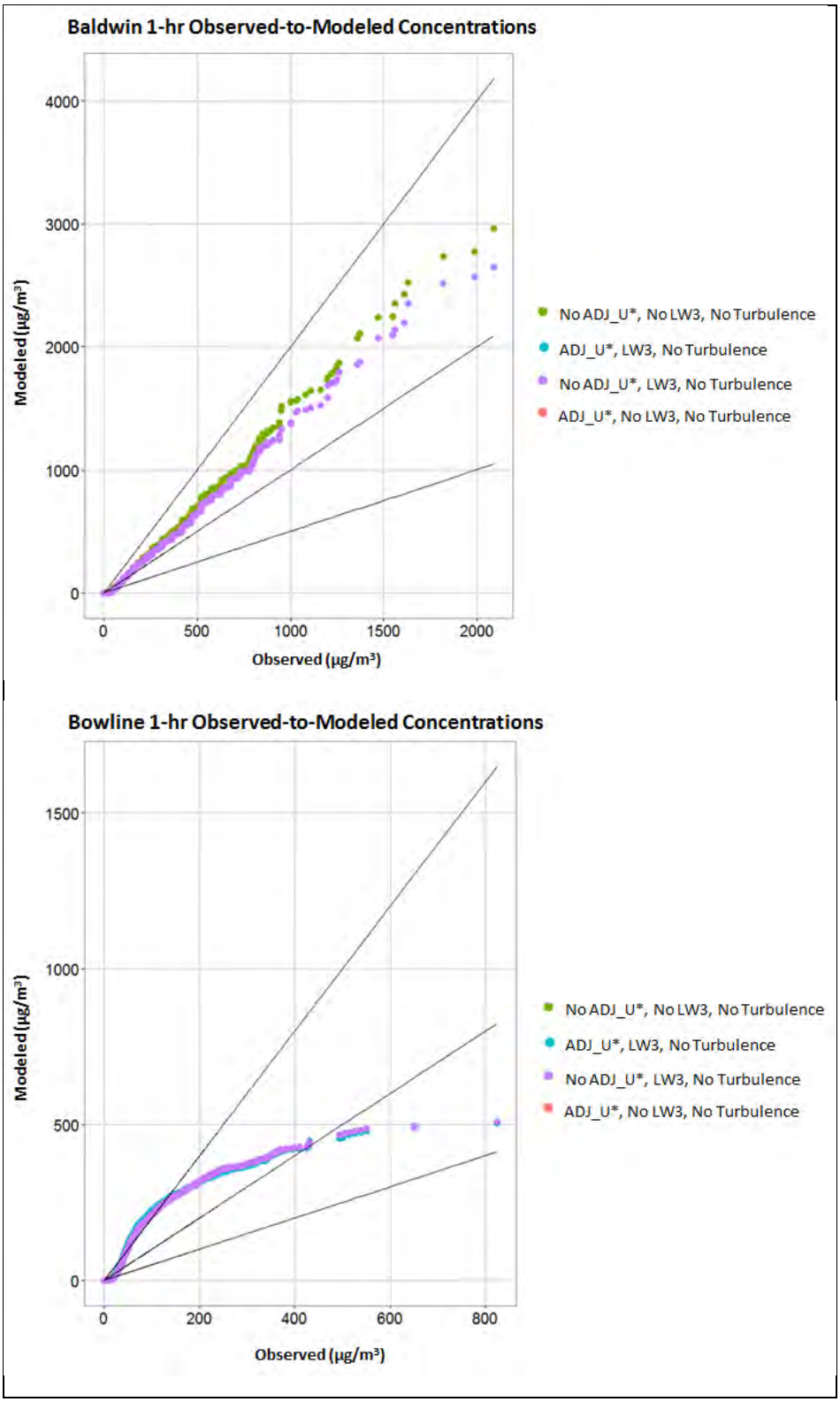

Figure 56. Q-Q Plots for 1-hr Observed-to-Modeled Concentrations for Baldwin, Bowline

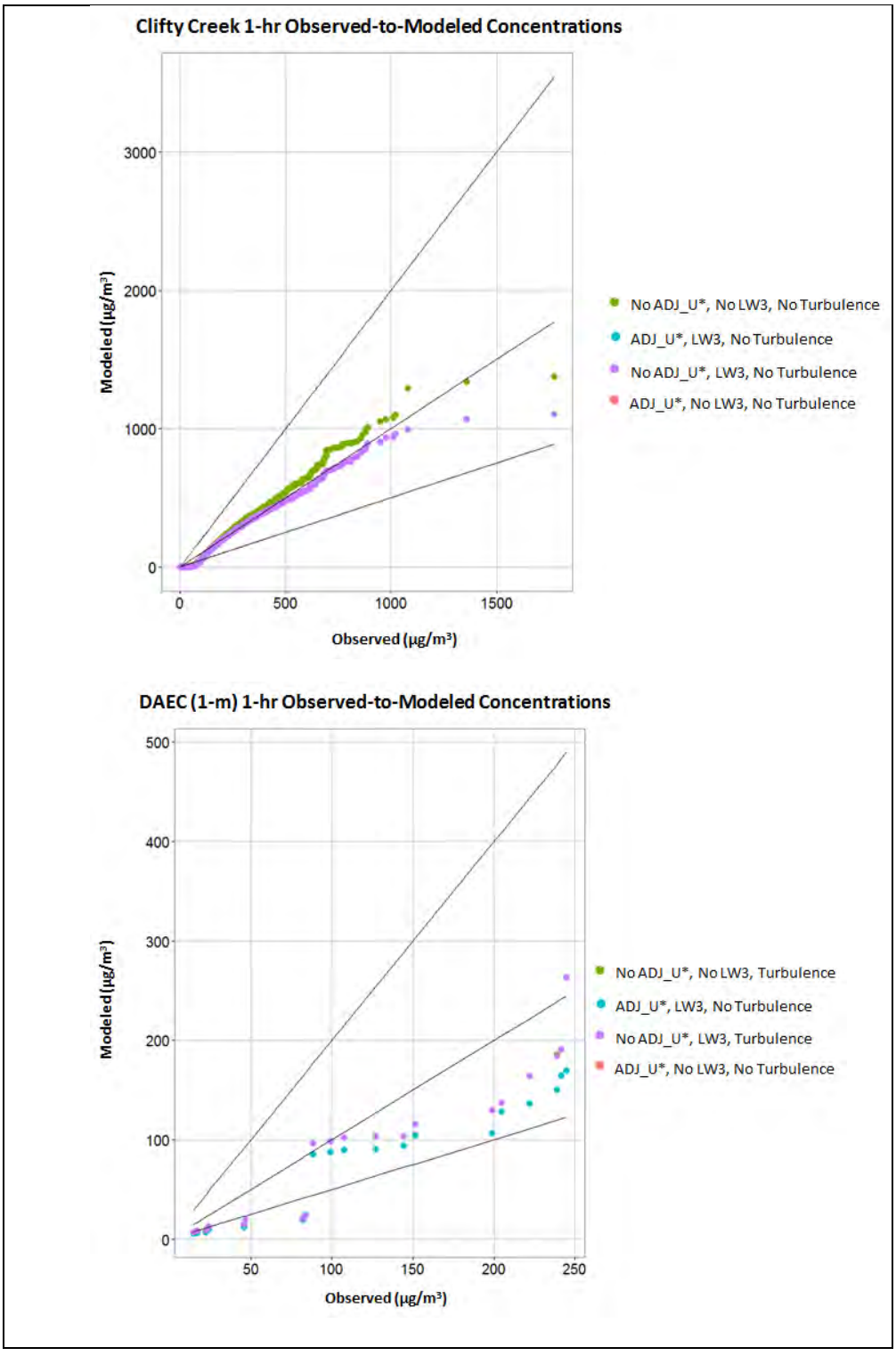

Figure 57. Q-Q Plots for 1-hr Observed-to-Modeled Concentrations for Clifty Creek and DAEC (1-m)

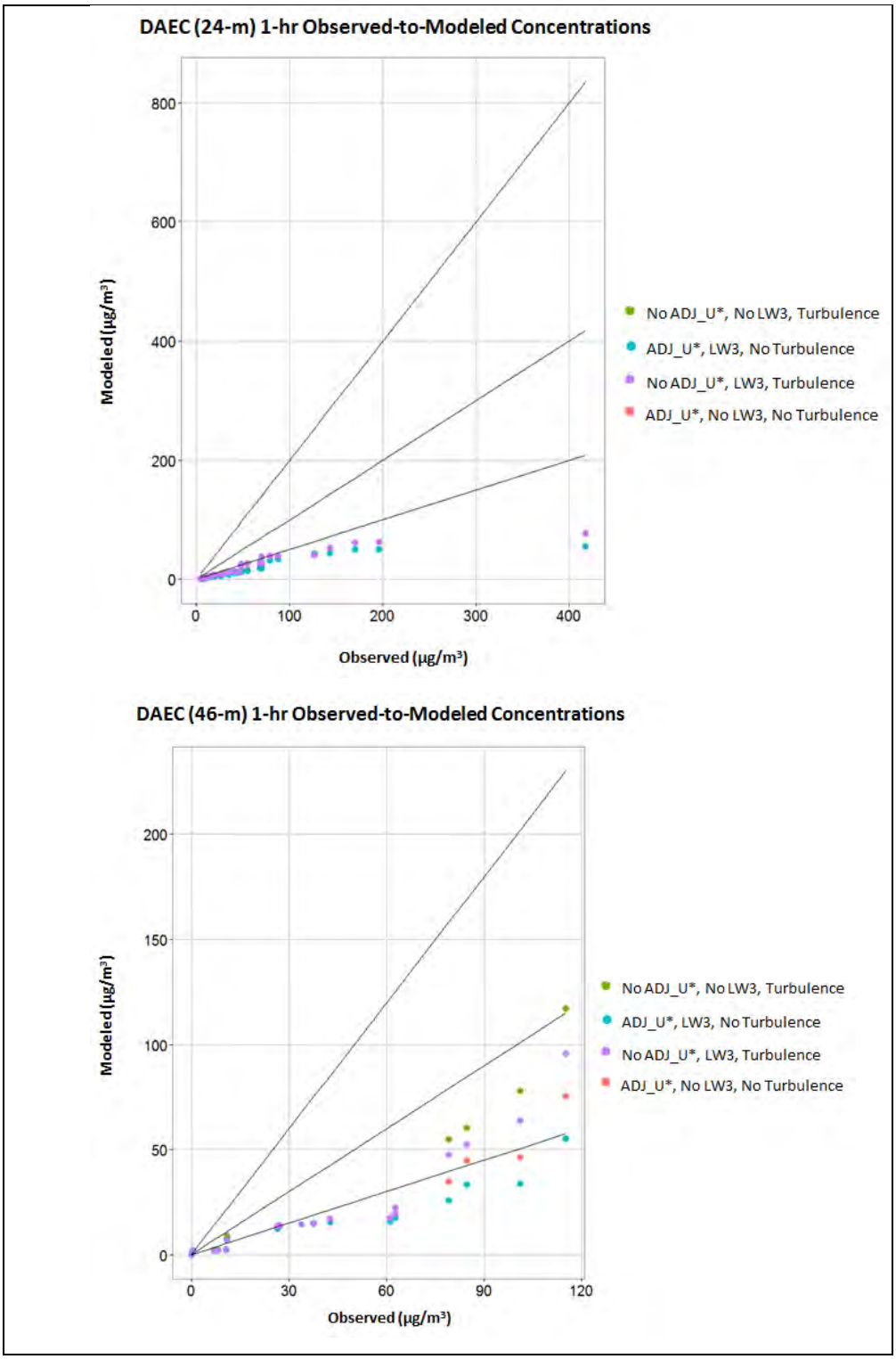

Figure 58. Q-Q Plots for 1-hr Observed-to-Modeled Concentrations for DAEC (24-m and 46-m)

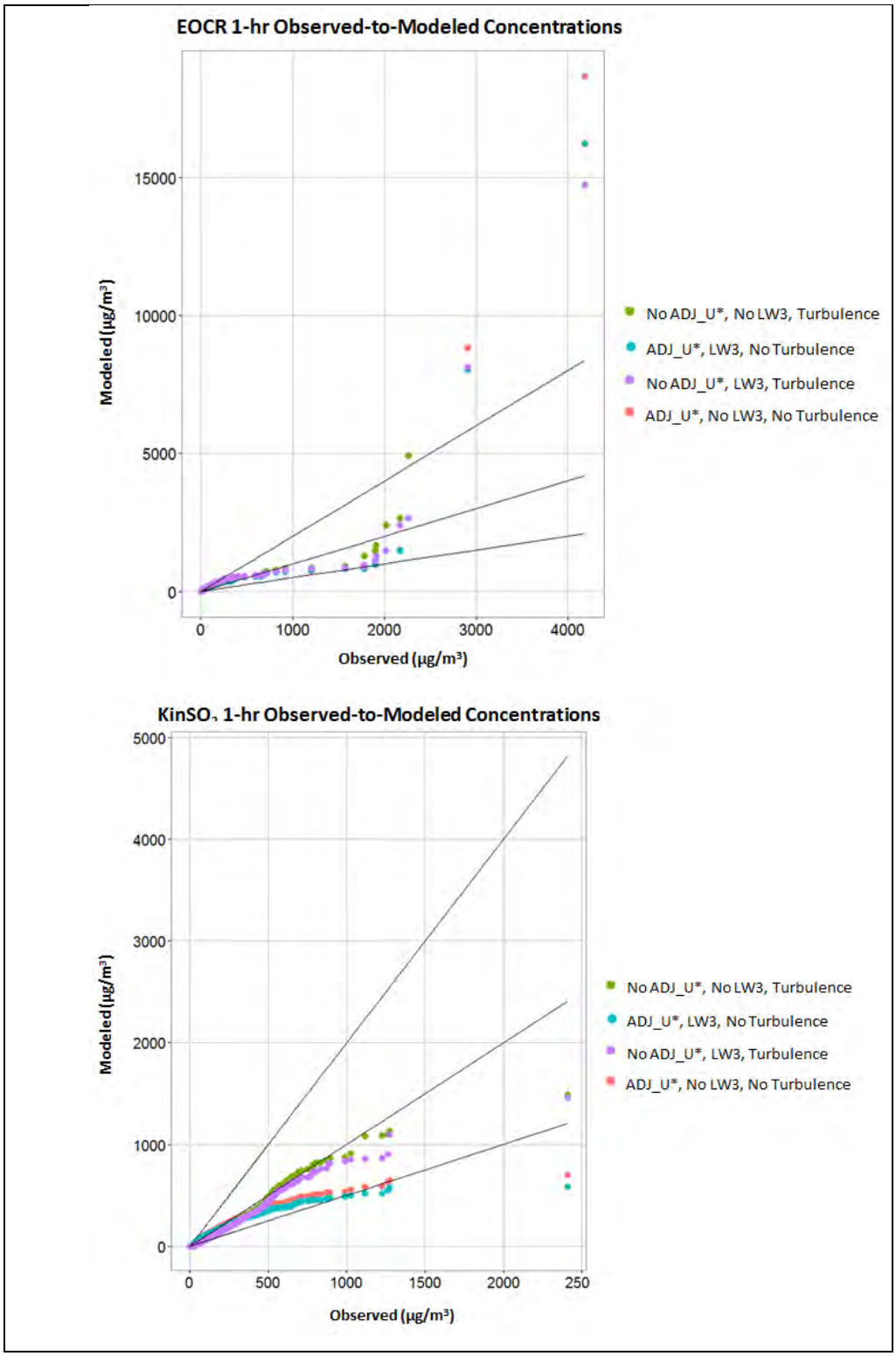

Figure 59. Q-Q Plots for 1-hr Observed-to-Modeled Concentrations for EOCR and Kincaid

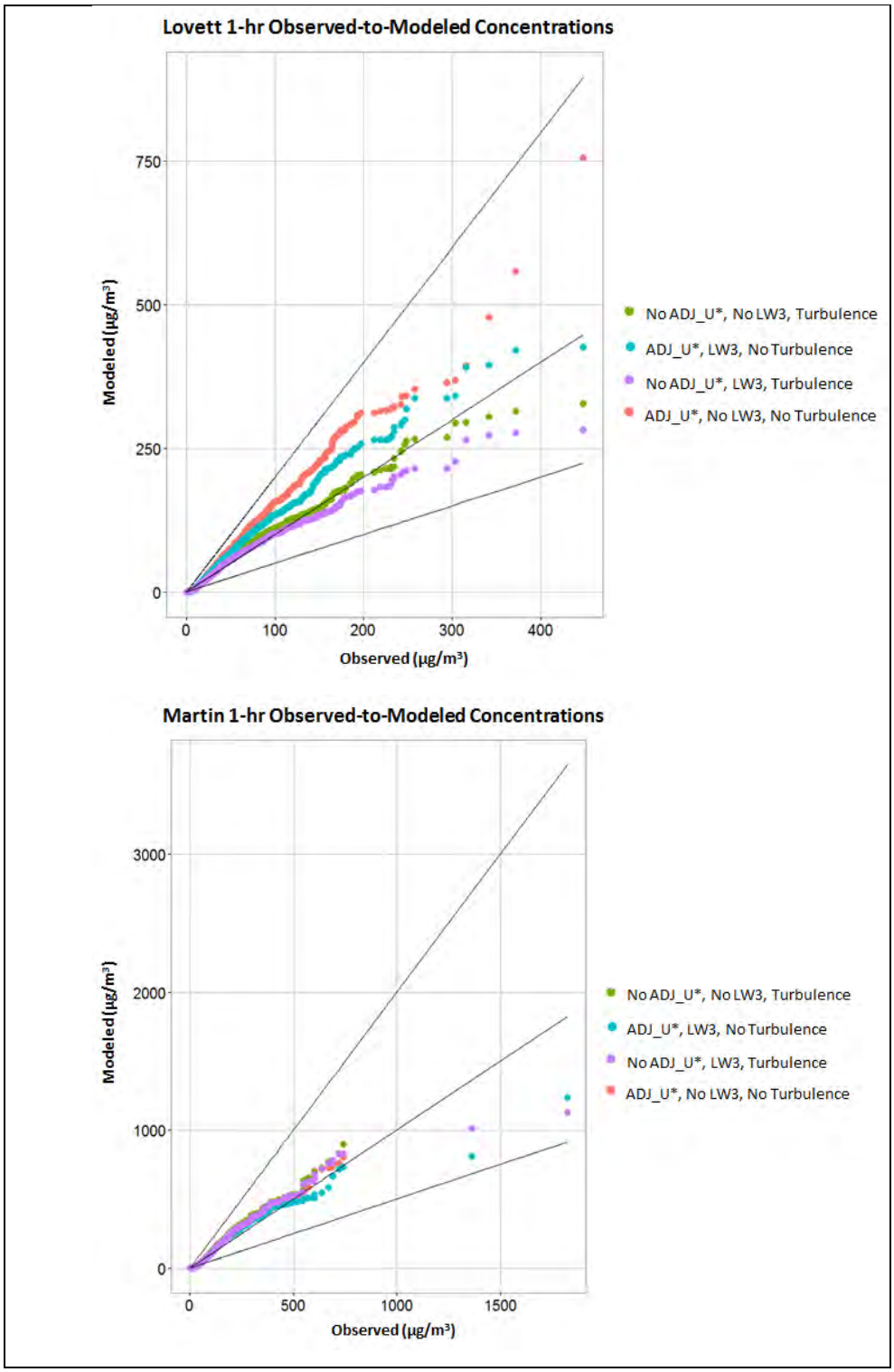

Figure 60. Q-Q Plots for 1-hr Observed-to-Modeled Concentrations for Lovett and Martins Creek

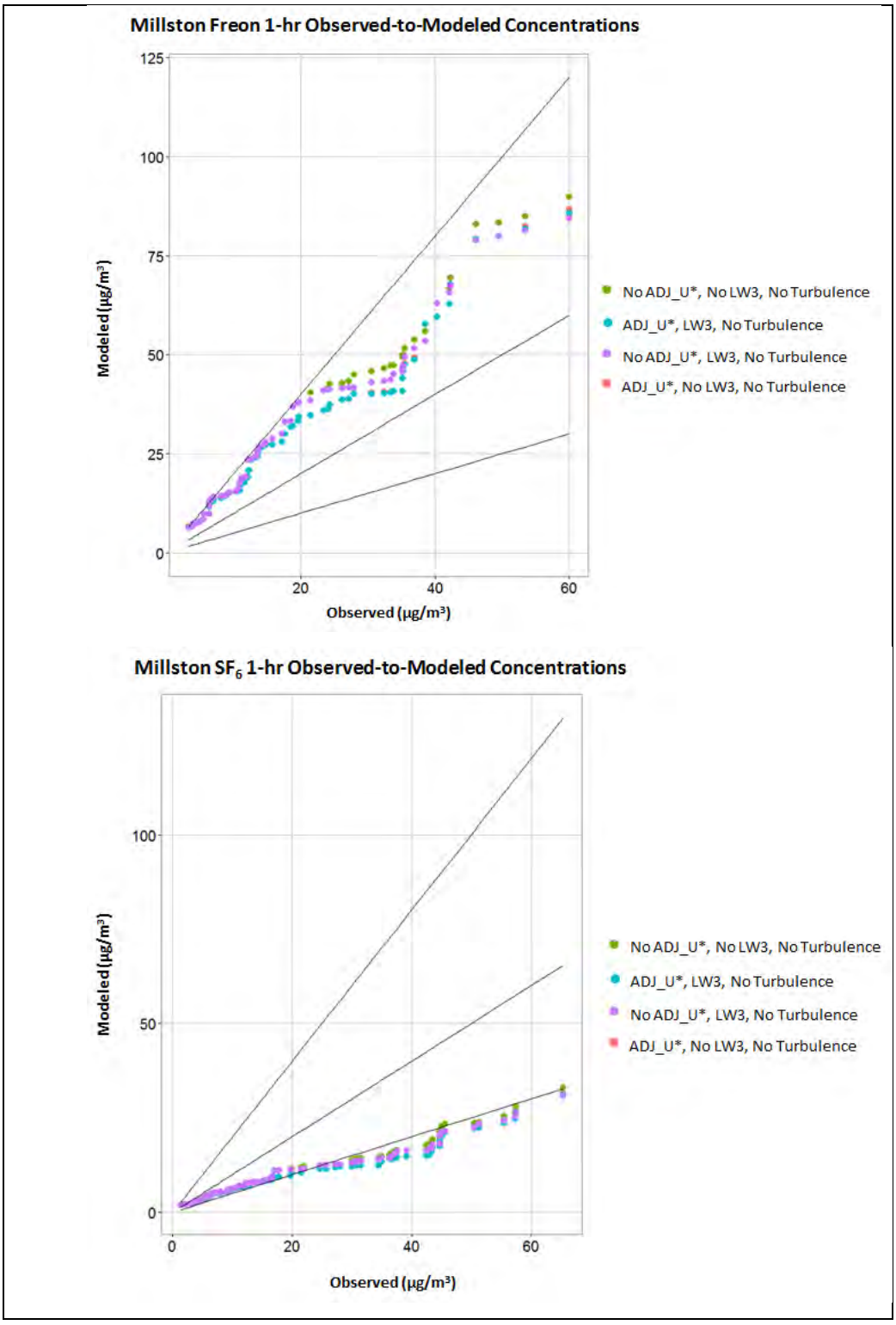

Figure 61. Q-Q Plots for 1-hr Observed-to-Modeled Concentrations for Millston

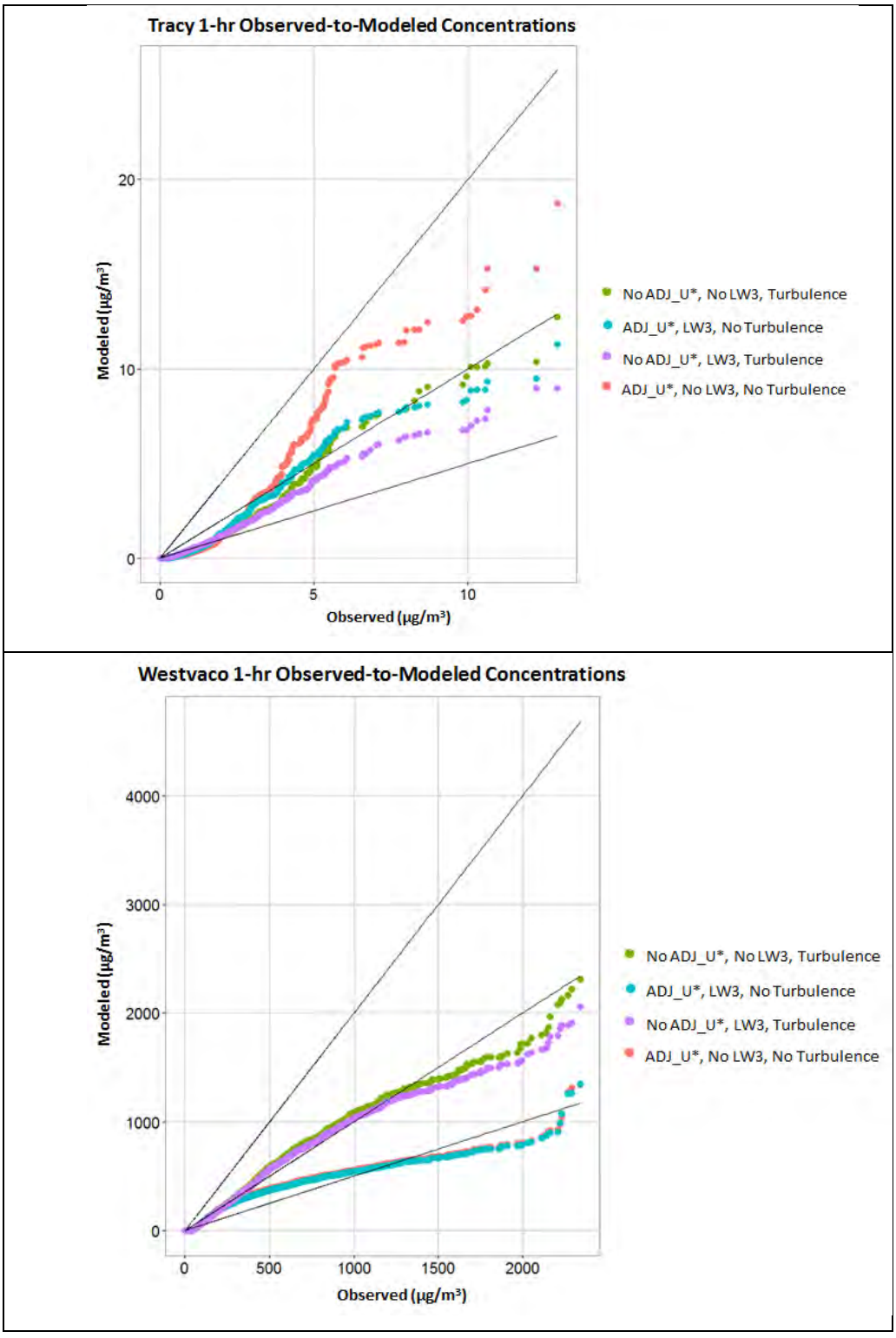

Figure 62. Q-Q Plots for 1-hr Observed-to-Modeled Concentrations for Tracy and Westvaco

C.4.2. Conclusions from the LOWWIND3 Evaluation

The influence of the LOWWIND3 option on model performance is mixed, and has shown a tendency toward underprediction with increasing distance in some cases, especially when LOWWIND3 is applied in conjunction with the ADJ_U* option in AERMET, as demonstrated in the 1974 Idaho Falls field study database (discussed previously) and the Prairie Grass, Kansas field study, which involved a near-surface tracer release in flat terrain. As noted above, there is an interaction between the ADJ_U* option and LOWWIND options because the values of sigma-v derived in AERMOD are based on the surface friction velocity (u*) parameter generated in AERMET. As a result, the ADJ_U* option in conjunction with the LOWWIND3 option influences the AERMOD derived sigma-v parameter and, in some cases, may exacerbate the tendency for AERMOD with LOWWIND3 to underpredict at higher concentrations.

Another aspect of the AERMOD model formulation that may contribute to an increasing bias toward underprediction with distance is the treatment of the "inhomogeneous boundary layer" (IBL) that accounts for changes in key parameters such as wind speed and temperature with height above ground. The IBL approach determines "effective" values of wind speed, temperature, and turbulence that are averaged across a layer of the plume between the plume centerline height and the height of the receptor. The extent of this layer depends on the vertical dispersion coefficient (*i.e.*, sigma-z). Therefore, as the plume grows downwind of the source, the extent of the layer used to calculate the effective parameters will increase (up to specified limits). The potential influence of this aspect of AERMOD formulation on modeled concentrations will depend on several factors, including source characteristics, meteorological conditions, and the topographic characteristics of the modeling domain.

References

AECOM, 2010: AERMOD Low Wind Speed Evaluation Study Results. Prepared for the American Petroleum Institute and Utility Air Regulatory Group. Prepared by AECOM, Westford, MA. March 22, 2010.

Andre, J. C. and L. Mahrt, 1982: The nocturnal surface inversion and influence of clean-air radiative cooling. *J.Atmos.Sci.,* **39,** 864-878.

Baerentsen, J. H. and R. Berkowicz, 1984: Monte Carlo simulation of plume dispersion in the convective boundary layer. *Atmos.Environ.,* **18,** 701-712.

Bange, P., L. Jannsen, F. Nieuwstadt, H. Visser, and J. Erbrink, 1991. "Improvement of the modeling of daytime nitrogen oxidation in plumes by using instantaneous plume dispersion parameters," *Atmos. Environ.*, **25A** (10), 2321-2328.

Barad, M. L., 1958: Project Prairie Grass, A Field Program in Diffusion. Geophysical Research Papers, No. 59, Vols. I and II, AFCRC-TR-58-235, Air Force Cambridge Research Center, 439pp.

Berkowicz, R., Olesen, J. R., and Torp, U., 1986: The Danish Gaussian air pollution model (OLM): Description, test and sensitivity analysis, in view of regulatory applications. *Air Pollution Modeling and Its Application.* De Wispelaire, V. C., Schiermeier, F. A., and Grillani, N. V, Plemum, 453-481pp.

Bornstein, R. D., 1968: Observations of urban heat island effects in New York City. *J.Appl.Meteor.,* **7,** 575-582.

Bowne, N. E., R. J. Londergan, D. R. Murray, and H. S. Borenstein, 1983: Overview, Results, and Conclusions for the EPRI Plume Model Validation and Development Project: Plains Site. EPRI Report EA-3074, Project 1616-1, Electric Power Research Institute, Palo Alto, CA, 234 pp. 1983.

Brett, A. C. and S. E. Tuller, 1991: Autocorrelation of hourly wind speed observations. *J.Appl.Meteor.,* **30,** 823-833.

Briggs, G. A., 1969: Plume rise. USAEC Critical Review Series, TID-25075, NTIS, 81pp.

Briggs, G. A., 1971: Some recent analyses of plume rise observations. *Proceedings of the Second International Clean Air Congress.* Englund, H. M. and Berry, W. T., Academic Press, 1029-1032.

Briggs, G. A., 1973: Diffusion Estimation for Small Emissions. 1973 Annual Report, ATDL-106, Air Resources Atmospheric Turbulence and Diffusion Laboratory, Environmental Res. Lab., NOAA, Oak Ridge, TN.

Briggs, G. A., 1975: Plume rise predictions. *Lectures on Air Pollution and Environmental Impact Analysis.* Haugen, D. A., American Meteorological Society, 59-111pp.

Briggs, G. A., 1984: Plume rise and buoyancy effects. *Atmospheric Science and Power Production.* Randerson, D., U.S. Dept. of Energy, 327-366pp.

Briggs, G. A., 1988: Analysis of diffusion field experiments. *Lectures on Air Pollution Modeling.* Venkatram, A. and Wyngaard, J. C., American Meteorological Society, 63-117.

Briggs, G. A., 1993: Plume dispersion in the convective boundary layer. Part II: Analysis of CONDORS field experiment data. *J.Appl.Meteor.,* **32,** 1388-1425.

Brode, R. W., 2002: Evaluation of the AERMOD Dispersion Model.

Brost, R. A., J. C. Wyngaard, and D. H. Lenschow, 1982: Marine stratocumulus layers: Part II: Turbulence budgets. *J.Atmos.Sci.,* **39,** 818-836.

Businger, J. A., 1973: Turbulent transfer in the atmospheric surface layer. *Workshop on Micrometeorology.* Haugen, D. A., American Meteorological Society.

Businger, J. A., J. C. Wyngaard, Y. Izumi, and E. F. Bradley, 1971: Flux-profile relationships in the atmospheric surface layer. *J.Atmos.Sci.,* **28,** 181-189.

Carruthers, D. J., and Coauthors, 1992: UK atmospheric dispersion modelling system. Air Pollution Modeling and Its Application. Plenum Press, New York.

Carson, D. J., 1973: The development of a dry inversion-capped convectively unstable boundary layer. *Quart.J.Roy.Meteor.Soc.,* **99,** 450-467.

Caughey, S. J. and S. G. Palmer, 1979: Some aspects of turbulence structure through the depth of the convective boundary layer. *Quart.J.Roy.Meteor.Soc.,* **105,** 811-827.

Cimorelli, A. J., S. G. Perry, R. F. Lee, R. J. Paine, A. Venkatram, J. C. Weil, and R. B. Wilson, 1996: Current Progress in the AERMIC Model Development Program. Preprints, *89th Annual Meeting Air and Waste Management Association,* Air and Waste Management Association, Pittsburgh, PA.

Cimorelli, A. J., S. G. Perry, A. Venkatram, J. C. Weil, R. J. Paine, R. B. Wilson, R. F. Lee, W. D. Peters, R. W. Brode, and J. O. Paumier, 2002: AERMOD: Description of Model Formulation (Version 02222). EPA 454/R-02-002d. U. S. Environmental Protection Agency, Research Triangle Park, NC.

Cimorelli, A. J., S. G. Perry, A. Venkatram, J. C. Weil, R. J. Paine, R. B. Wilson, R. F. Lee, W. D. Peters, and R. W. Brode, 2005: AERMOD: A dispersion model for industrial source applications Part I: General model formulation and boundary layer characterization. *J.Appl.Meteor.* **44**, 682-693

Clarke, R. H., A. J. Dyer, R. R. Brook, D. G. Reid, and A. J. Troop, 1971: The Wangara experiment: boundary layer data. Technical Report No. 19, Division of Meteorological Physics CSIRO, Australia.

Cole, H.S. and J.E. Summerhays, 1979. "A review of techniques available for estimating short-term NO_2 concentrations," *J. Air Pollut. Control Assoc.*, **29**(8), 812-817.

Collier, L. R. and J. G. Lockwood, 1975: Reply to comment. *Quart.J.Roy.Meteor.Soc.,* **101,** 390-392.

Cox, W.M. and J.A. Tikvart, 1990: A statistical Procedure for Determining the Best Performing Air Quality Simulation Model. Atmos. Environ., 24A (9): 2387-2395.

Deardorff, J. W., 1970: Convective velocity and temperature scales for the unstable boundary layer for Rayleigh convection. *J.Atmos.Sci.,* **27,** 1211-1213.

Deardorff, J. W., 1972: Numerical investigation of neutral and unstable planetary boundary layers. *J.Atmos.Sci.,* **29,** 91-115.

Deardorff, J. W., 1979: Prediction of convective mixed-layer entrainment for realistic capping inversion structure. *J.Atmos.Sci.,* **36,** 424-436.

Deardorff, J. W., 1980: Progress in Understanding Entrainment at the Top of a Mixed Layer. Preprints, *Workshop on the Planetary Boundary Layer,* American Meteorological Society, Boston, MA.

DiCristofaro, D. C. *et al.*, 1985: EPA Complex Terrain Model Development: Fifth Milestone Report - 1985. EPA-600/3-85-069, U. S. Environmental Protection Agency, Research Triangle Park, North Carolina.

Dyer, A. J., 1974: A review of flux-profile relationships. *Bound.Layer Meteor.,* **7,** 363-372.

Garratt, F. R., 1992: *The Atmospheric Boundary Layer.* Cambridge University Press, New York, New York, 334pp.

Gifford, F. A., 1961: Uses of routine meteorological observations for estimating atmospheric dispersion. *Nuclear Safety,* **2,** 47-51.

Hanna, S. R., 1983: Lateral turbulence intensity and plume meandering during stable conditions. *J.Appl.Meteor.,* **22,** 1424-1430.

Hanna, S. R. and J. S. Chang, 1991: Modification of the Hybrid Plume Dispersion Model (HPDM) for urban conditions and its evaluation using the Indianapolis data set, Volume III: Analysis of urban boundary layer data. EPRI Project No. RP-02736-1, Electric Power Research Institute, Palo Alto, CA.

Hanna, S. R. and J. S. Chang, 1993: Hybrid Plume Dispersion Model (HPDM), improvements and testing at three field sites. *Atmos.Environ.,* **27A,** 1491-1508.

Hanna, S. R. and R. J. Paine, 1989: Hybrid Plume Dispersion Model (HPDM) development and evaluation. *J.Appl.Meteor.,* **28,** 206-224.

Hanna, S. R., J. C. Weil, and R. J. Paine, 1986: Plume Model Development and Evaluation - Hybrid Approach. EPRI Contract No. RP-1616-27, Electric Power Research Institute, Palo Alto, CA.

Hanrahan, P.L., 1999a. "The plume volume molar ratio method for determining NO_2/NO_x ratios in modeling. Part I: Methodology," *J. Air & Waste Manage. Assoc.*, **49**, 1324-1331.

Haugen, D. A. (Editor), 1959: Project Prairie Grass, A field program in diffusion. Geophysical Research Paper, No. 59, Vol. III. Report AFCRC-TR-58-235, Air Force Cambridge Research Center, 439 pp.

Hayes, S. R. and G. E. Moore, 1986: Air quality model performance: a comparative analysis of 15 model evaluation studies. *Atmos.Environ.,* **20,** 1897-1911.

Hicks, B. B., 1985: Behavior of turbulent statistics in the convective boundary layer. *J.Appl.Meteor.,* **24,** 607-614.

Holtslag, A. A. M., 1984: Estimates of diabatic wind speed profiles from near-surface weather observations. *Bound.Layer Meteor.,* **29,** 225-250.

Holtslag, A. A. M. and A. P. van Ulden, 1983: A simple scheme for daytime estimates for the surface fluxes from routine weather data. *J.Climate Appl.Meteor.,* **22,** 517-529.

Irwin, J. S., J. O. Paumier, and R. W. Brode, 1988: Meteorological Processor for Regulatory Models (MPRM) User's Guide. EPA-600/3-88-043, U.S. Environmental Protection Agency, RTP, NC.

Izumi, Y., 1971: Kansas 1968 Field Program Data Report. No. 379, AFCRL-72-0041, Air Force Cambridge Research Laboratory, Bedford, MA, 79pp.

Kaimal, J. C., J. C. Wyngaard, D. A. Haugen, O. R. Cote', Y. Izumi, S. J. Caughey, and C. J. Readings, 1976: Turbulence structure in the convective boundary layer. *J.Atmos.Sci.,* **33,** 2152-2169.

Kasten, F. and G. Czeplak, 1980: Solar and terrestial radiation dependent on the amount and type of cloud. *Solar Energy,* **24,** 177-189.

Lamb, R. G., 1982: Diffusion in the convective boundary layer. *Atmospheric Turbulence and Air Pollution Modelling.* Nieuwstadt, F. T. M. and van Dop, H., Reidel, 159-229pp.

Lee, R. F., R. J. Paine, S. G. Perry, A. J. Cimorelli, J. C. Weil, A. Venkatram, and R. B. Wilson, 1998: Developmental Evaluation of the AERMOD Dispersion Model. Preprints, *10th Joint AMS/AWMA Conference on Application of Air Pollution Meteorology,* American Meteorological Society, Boston.

Lee, R. F., S. G. Perry, A. J. Cimorelli, R. J. Paine, A. Venkatram, J. C. Weil, and R. B. Wilson, 1995: AERMOD - the developmental evaluation. Preprints, *Tewnty-First NATO/CCMS International Technical Meeting on Air Pollution Modeling and Its Application,* Baltimore, MD, U.S.A.

Liu, M. K., and G. E. Moore: 1984: Diagnostic validation of plume models at a plains site. EPRI Report No. EA-3077, Research Project 1616-9, Electric Power Research Institute, Palo Alto, CA. (1984)

Luhar, A.K., and K. N. Rayner, 2009: "Methods to Estimate Surface Fluxes of Momentum and Heat from Routine Weather Observations for Dispersion Applications under Stable Stratification", *Boundary-Layer Meteorology*, **132**, 437–454.

Misra, P. K., 1982: Dispersion of non-buoyant particles inside a convective boundary layer. *Atmos.Environ.,* **16,** 239-243.

Morton, B. R., G. I. Taylor, and J. S. Turner, 1956: Turbulent gravitational convection from maintained and instantaneous sources. *Proc.Roy.Soc.London,* **A234,** 1-23.

Nieuwstadt, F. T. M. and H. van Dop, 1982: *Atmospheric Turbulence and Air Pollution Modelling.* Reidel, 358pp.

NOAA, 1974: Technical Memorandum ERL ARL-52, 1974. "Diffusion under Low Wind Speed, Inversion Conditions." Sagendorf, J. F., C. Dickson. Air Resources Laboratory, Idaho Falls, Idaho.

NOAA, 1976: Technical Memorandum ERL ARL-61, 1976. "Diffusion under Low Wind Speed Conditions near Oak Ridge, Tennessee." Wilson, R. B., G. Start, C. Dickson, N. Ricks. Air Resources Laboratory, Idaho Falls, Idaho.

Oke, T. R., 1973: City size and the urban heat island. *Atmos.Environ.,* **7,** 769-779.

Oke, T. R., 1978: *Boundary Layer Climates.* John Wiley and Sons, New York, New York, 372pp.

Oke, T. R., 1982: The energetic basis of the urban heat island. *Quart.J.Roy.Meteor.Soc.,* **108,** 1-24.

Oke, T. R., 1998: An algorithmic scheme to estimate hourly heat island magnitude. Preprints, *2nd Urban Environment Symposium,* American Meteorological Society, Boston, MA, 80-83.

Paine, R. J. and B. A. Egan, 1987: User's guide to the Rough Terrain Diffusion Model (RTDM) - Rev. 3.20. ERT Document PD-535-585, ENSR, Acton, MA, 260pp.

Paine, R. J. and S. B. Kendall, 1993: Comparison of observed profiles of winds, temperature, and turbulence with theoretical results. Preprints, *Joint conference of the American Meteorological Society and Air & Waste Management Association Specialty Conference: The Role of Meteorology in Managing the Environment in the 90s, Scottsdale, AZ. Publication VIP-29,* Air & Waste Management Association, Pittsburgh, PA.

Panofsky, H. A. and J. A. Dutton, 1984: *Atmospheric Turbulence: Models and Methods for Engineering Applications.* John Wiley and Sons, New York, 417pp.

Panofsky, H. A., H. Tennekes, D. H. Lenschow, and J. C. Wyngaard, 1977: The characteristics of turbulent velocity components in the surface layer under convective conditions. *Bound.Layer Meteor.,* **11,** 355-361.

Pasquill, F., 1961: The estimation of the dispersion of windborne material. *Meteorol.Mag.,* **90,** 33-49.

Pasquill, F., 1976: Atmospheric dispersion parameters in Gaussian plume modeling - Part III: possible requirements for change in the Turner's Workbook values. EPA-600/4-76-030B, U. S. Environmental Protection Agency, Research Triangle Park, NC.

Pasquill, F. and F. R. Smith, 1983: *Atmospheric Diffusion.* John Wiley and Sons Inc., New York, 440pp.

Paumier, J. O., S. G. Perry, and D. J. Burns, 1992: CTDMPLUS: A dispersion model for sources near complex topography. Part II: Performance characteristics. *J. Appl. Meteor.*, 31, 646–660.

Perry, S. G., 1992: CTDMPLUS: A dispersion model for sources in complex topography. Part I: Technical formulations. *J.Appl.Meteor.,* **31,** 633-645.

Perry, S. G., D. J. Burns, R. J. Adams, R. J. Paine, M. G. Dennis, M. T. Mills, D. G. Strimaitis, R. J. Yamartino, and E. M. Insley, 1989: User's Guide to the Complex Terrain Dispersion Model Plus Algorithms for Unstable Situations (CTDMPLUS) Volume 1: Model Description and User Instructions. EPA/600/8-89/041, U.S. Environmental Protection Agency, RTP, NC, 196pp.

Perry, S. G., A. J. Cimorelli, R. F. Lee, R. J. Paine, A. Venkatram, J. C. Weil, and R. B. Wilson, 1994: AERMOD: A dispersion model for industrial source applications. Preprints, *87th Annual Meeting Air and Waste Management Association,* Air and Waste Management Association, Pittsburgh, PA.

Perry, S. G., A. J. Cimorelli, R. J. Paine, R. W. Brode, J. C. Weil, A. Venkatram, R. B. Wilson, R. F. Lee, and W. D. Peters, 2005: AERMOD: A dispersion model for industrial source applications Part II: Model performance against seventeen field-study databases. *J.Appl.Meteor*. **44**, 694-708.

Qian, W., and A. Venkatram, 2011: "Performance of Steady-State Dispersion Models UnderLow Wind-Speed Conditions", *Boundary Layer Meteorology*, **138**, 475-491.

Readings, C. J., D. A. Haugen, and J. C. Kaimal, 1974: The 1973 Minnesota atmospheric boundary layer experiment. *Weather,* **29,** 309-312.

Schulman, L. L., D. G. Strimaitis, and J. S. Scire, 2000: Development and evaluation of the PRIME plume rise and building downwash model. *Journal of the Air & Waste Management Association,* **50,** 378-390.

Sheppard, P. A., 1956: Airflow over mountains. *Quart.J.Roy.Meteor.Soc.,* **82,** 528-529.

Smith, M. E., 1984: Review of the attributes and performance of 10 rural diffusion models. *Bull.Amer.Meteor.Soc.,* **65,** 554-558.

Snyder, W. H., R. S. Thompson, R. E. Eskridge, R. E. Lawson, I. P. Castro, J. T. Lee, J. C. R. Hunt, and Y. Ogawa, 1985: The structure of the strongly stratified flow over hills: Dividing streamline concept. *J.Fluid Mech.,* **152,** 249-288.

Stull, R. B., 1983: A heat flux history length scale for the nocturnal boundary layer. *Tulles,* **35A,** 219-230.

Sykes, R. I., D. S. Henn, and S. F. Parker, 1996: SCIPUFF - A generalized hazard dispersion model. Preprints, *9th Joint Conference on Applications of Air Pollution Meteorology with AWMA, Amer. Meteor. Soc.,* American Meteorological Society, Boston, 184-188.

Taylor, G. I., 1921: Diffusion by continuous movements. *Proc.London Math.Soc.,* **Ser. 2(20),** 196-211.

Turner, D. B., T. Chico, and J. Catalano, 1986: TUPOS - A Multiple Source Gaussian Dispersion Algorithm Using On-site Turbulence Data. EPA/600/8-86/010, U.S. Environmental Protection Agency, RTP, NC, 39pp.

U.S. Environmental Protection Agency, 1992: Protocol for Determining the Best Performing Model. EPA-454/R-92-025, U.S. Environmental Protection Agency, RTP, NC.

U.S. Environmental Protection Agency, 1995a: User's Guide for the Industrial Source Complex (ISC3) Dispersion Models (revised) Volume I - User Instructions. EPA-454/b-95-003a, U.S. Environmental Protection Agency, Research Triangle Park, NC.

U.S. Environmental Protection Agency, 1995b: *Modeling Fugitive Dust Impacts from Surface Coal Mining Operations – Phase III.* U.S. Environmental Protection Agency, Office of Air Quality Planning and Standards, EPA-454/R-96-002. December 1995.

U.S. Environmental Protection Agency, 2003: AERMOD: Latest Features and Evaluation Results. EPA-454/R-03-003, U.S. Environmental Protection Agency, RTP, NC.

U.S. Enviromental Protection Agency, 2002: Compendium of Reports from the Peer Review Process for AERMOD. U.S. Environmental Protection Agency, RTP, NC. *http://www.epa.gov/scram001/7thconf/aermod/dockrpt.pdf*.

U.S. Environmental Protection Agency, 2015a: Technical Support Document (TSD) for NO2-related AERMOD modifications. EPA document EPA-454/B-15-004. July 2015.

U.S. Environmental Protection Agency, 2015b: Addendum: User's Guide for the AMS/EPA Regulatory Model – AERMOD. EPA-454/B-03-001. June 2015.

USGS, 1994: The 1994 plan for the National Spatial Data Infrastructure - Building the foundation of an information based society. Federal Geographic Data Committee Report. U.S. Geological Survey, Reston, VA. *https://www.fgdc.gov/policyandplanning/NSDI Strategy 1994.pdf*.

van Ulden, A. P. and A. A. M. Holtslag, 1983: The stability of the atmospheric surface layer during nightime. Preprints, *Sixth Symposium on Turbulence and Diffusion,* American Meteorological Society, Boston, 257-260.

van Ulden, A. P. and A. A. M. Holtslag, 1985: Estimation of atmospheric boundary layer parameters for diffusion applications. *J.Climate Appl.Meteor.,* **24,** 1196-1207.

Venkatram, A., 1978: Estimating the convective velocity scale for diffusion applications. *Bound.Layer Meteor.,* **15,** 447-452.

Venkatram, A., 1980: Estimating the Monin-Obukhov length in the stable boundary layer for dispersion calculations. *Bound.Layer Meteor.,* **19,** 481-485.

Venkatram, A., 1982: A semi-empirical method to compute concentration associated with surface releases in the stable boundary layer. *Atmos.Environ.,* **16,** 245-248.

Venkatram, A., 1983: On dispersion in the convective boundary layer. *Atmos.Environ.,* 529-533.

Venkatram, A., 1988: Dispersion in the stable boundary layer. *Lectures on Air Pollution Modeling.* Venkatram, A. and Wyngaard, J. C., American Meteorological Society, 229-265pp.

Venkatram, A., 1992: Vertical dispersion of ground-level releases in the surface boundary layer. *Atmos.Environ.,* **26A,** 947-949.

Venkatram, A., R. Brode, A. Cimorelli, R. Lee, R. Paine, S. Perry, W. Peters, J. Weil, and R. Wilson, 2001: A complex terrain dispersion model for regulatory applications. *Atmospheric Environment,* **35,** 4211-4221.

Venkatram, A., D. G. Strimaitis, and D. Dicristofaro, 1984: A semiemperical model to estimate vertical dispersion of elevated releases in the stable boundary layer. *Atmos.Environ.,* **18,** 923-928.

Venkatram, A. and J. C. Wyngaard, 1988: *Lectures on Air Pollution Modeling.* American Meteorological Society, Boston, 390pp.

Weil, J. C., 1985: Updating applied diffusion models. *J.Climate Appl.Meteor.,* **24(11),** 1111-1130.

Weil, J. C., 1988a: Dispersion in the convective boundary layer. *Lectures on Air Pollution Modeling.* Venkatram, A. and Wyngaard, J. C., American Meteorological Society, 167-227pp.

Weil, J. C., 1988b: Plume rise. *Lectures in Air Pollution Modeling.* Venkatram, A. and Wyngaard, J. C., American Meteorological Society, 119-162pp.

Weil, J. C., 1992: Updating the ISC model through AERMIC. Preprints, *85th Annual Meeting of Air and Waste Management Association,* Air and Waste Management Association, Pittsburgh, PA.

Weil, J. C., 1996: A new dispersion model for stack sources in building wakes. Preprints, *Ninth Joint Conference on Applications of Air Pollution Meteorology with the Air & Waste Management Association,* American Meteorological Society, Boston, MA, 333-337.

Weil, J.C., 1998. The SERDP Open Burn/Open Detonation Dispersion Model (SOBODM), Volume IIa – Technical Description, and Volume IIb – Meteorological Inputs (DRAFT), CIRES, University of Colorado, Boulder, CO.

Weil, J. C. and R. P. Brower, 1983: Estimating convective boundary layer parameters for diffusion applications. PPSP-MD-48, Maryland Power Plant Siting Program, Maryland Department of Natural Resources, Baltimore, MD, 45pp.

Weil, J. C. and R. P. Brower, 1984: An updated Gaussian plume model for tall stacks. *J.Air Poll.Control Assoc.,* **34,** 818-827.

Weil, J.C., B. Templeman, R. Banta, R. Weber, and W. Mitchell, 1996. "Dispersion model development for open burn/open detonation sources," *Preprints 9th Joint Conference on Applications of Air Pollution Meteorology*, American Meteorological Society, Boston, MA, 610-616.

Weil, J. C., L. A. Corio, and R. P. Brower, 1997: A PDF dispersion model for buoyant plumes in the convective boundary layer. *J.Appl.Meteor.,* **36,** 982-1003.

Willis, G. E. and J. W. Deardorff, 1981: A laboratory study of dispersion in the middle of the convectively mixed layer. *Atmos.Environ.,* **15,** 109-117.

Wyngaard, J. C., 1988: Structure of the PBL. *Lectures on Air Pollution Modeling.* Venkatram, A., and Wyngaard, J. C., *eds.*, American Meteorological Society, 9-57pp.

Zilitinkevich, S. S., 1972: On the determination of the height of the Ekman boundary layer. *Bound.Layer Meteor.,* **3,** 141-145.

United States
Environmental Protection
Agency

Office of Air Quality Planning and Standards
Air Quality Assessment Division
Research Triangle Park, NC

Publication No. EPA-454/R-17-001
May, 2017